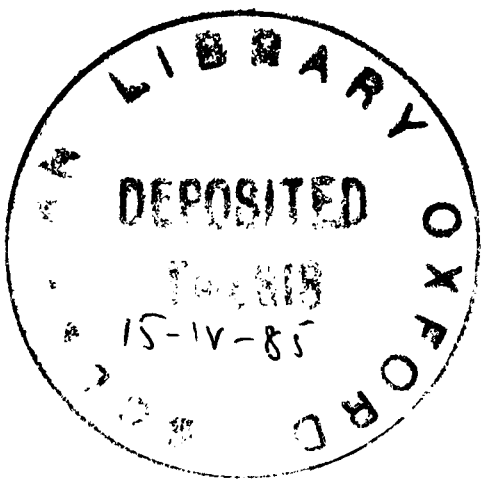
An SEM EBIC Study of the Electronic Properties of Dislocations in Silicon

Dissertation submitted for the degree of
Doctor of Philosophy
Trinity Term 1984.



Peter R. Wilshaw
New College

ABSTRACT

An SEM EBIC Study of the Electronic Properties of Dislocations in Silicon

Dissertation submitted by Peter R. Wilshaw of New College, Oxford for the degree of Doctor of Philosophy, Trinity, 1984.

Individual, well structurally characterised dislocations present in n-type silicon have been studied using the electron beam induced current (EBIC) mode of an SEM.

An EBIC system has been designed and constructed which includes i) phase sensitive detection, ii) computerised control of the experimental equipment and data capture and iii) a variable temperature SEM specimen stage.

With this system measurements have been made of the EBIC contrast of individual segments of deformation induced dislocations produced by two stage compressive deformation at 850°C and 420°C.

An experimental and theoretical analysis of EBIC signal generation in the Schottky barrier specimens used in this work is presented. This shows that the EBIC contrast measurements made may be directly correlated to the dislocation recombination strength.

Contrast measurements have been made at temperatures in the range 120K to 370K and for electron beam currents from 6×10^{-12}A to 2×10^{-9}A. Several new effects have been observed. Minority carrier diffusion length measurements have also been performed in silicon containing dislocations. These show that the value obtained may depend upon experimental parameters used in a hitherto undetected manner.

A new theory describing recombination of carriers at charged dislocations has been developed and this has been extended to provide a description of the variation of the EBIC contrast of dislocations with temperature, electron beam current and also the transient response of the EBIC contrast. Comparison of the theoretical predictions with the results gained experimentally shows full agreement for low temperatures or large beam currents. At high temperatures and small beam currents the theory shows the EBIC contrast will behave differently depending on the density of dislocation states present.

Interpretation of the experimental results in terms of this theory allows some new insight to be gained for recombination at dislocations, and values for some of the parameters controlling recombination have been obtained.

PREFACE

This dissertation is an account of the work carried out by the author in the Department of Metallurgy and Science of Materials, Oxford University, since October 1980. The early stages of the work were supervised by Dr. A. Ourmazd whilst the remainder was supervised by Dr. G.R. Booker. No part of this work has been submitted for a degree at any other University. Any studies carried out by other workers are duly acknowledged and an alphabetical list of references is given at the end of the thesis.

The author wishes to thank Professor Sir Peter Hirsch, F.R.S., for the provision of laboratory facilities. He is especially grateful to both Dr. A. Ourmazd and Dr. G.R. Booker for their helpful supervision, encouragement and invaluable advice. Thanks are also due to:

Prof. H. Alexander and Dr. H. Gottschalk of Cologne University and Dr. E. Weber, now of the University of California, for the low temperature deformation of silicon samples.

Messrs. G. Dixon-Brown and R. Cripps for their maintenance and assistance in the operation of the electron microscopes.

Mr. J. Stead for his expert help and advice concerning the construction of the SEM cold stage.

The author has benefitted from many valuable discussions with colleagues at Oxford University and is particularly indebted to Dr. W. Bergholz, Dr. J. Spence and Dr. P. Pirouz for general discussions on the nature and properties of dislocations in silicon and to Dr. E.D. Boyes for his very

helpful comments on designing an SEM cold stage. Thanks are also due to Mr. K.C. Paus for his help in the later stages of assembling this thesis.

Finally the author wishes to thank all members of the Semiconductor Group, not only for their practical help and advice but also for their encouragement and good humour which have contributed so much to the author's enjoyment whilst working in Oxford.

Some of the results obtained for this D.Phil have been published in the form of articles as follows:

Measurement of contrast from individual dislocations by lock-in EBIC.

Ourmazd A., Wilshaw P.R., Cripps R.M.,

Inst. Phys. Conf. Ser. 61, 519 (1981)

The electrical behaviour of individual dislocations, Shockley partials and stacking faults.

Ourmazd A., Wilshaw P.R., Weber E., Gottschalk H., Booker G.R., Alexander H.,

Proc. 40th Annual EMSA Meeting (1982)

The electrical behaviour of individual dislocations, Schockley partials and stacking fault ribbons in silicon.

Ourmazd A., Wilshaw P.R., Booker G.R.,

Physica 116 B, 600 (1983)

Some aspects of the measurements of electrical effects of dislocations in silicon using a computerised EBIC system.

Wilshaw P.R., Ourmazd A., Booker G.R.,

J. Physique 44, C4-445 (1983)

The temperature dependence of EBIC contrast from individual dislocations in silicon.

Ourmazd A., Wilshaw P.R., Booker G.R.,

J. Physique 44, C4-289 (1983)

CONTENTS

Page

Chapter 1

Introduction and Literature Survey 1

1.1 Introduction 1
1.2 Dislocations in elemental semiconductors 4

1.2.1 Physical structure 5
1.2.2 Electronic structure 9
1.2.3 Non-ideal dislocations 15

1.3 Electrical properties of dislocations 18

1.3.1 Experimental techniques 21
1.3.2 Discussion of results 28
1.3.3 Summary of results and comments on the previous work 37

1.4 Aims of the project 41

1.5 Layout of the thesis 44

Chapter 2

Electron Beam Induced Current Scanning Electron Microscopy 46

2.1 The principles of EBIC microscopy 46

2.1.1 The excitation of semiconductors by energetic electrons 47
2.1.2 The diffusion of carriers generated by an electron beam 51
2.1.3 The collection of injected carriers 54

2.2 The investigation of defects using EBIC 56

2.3 Theory of EBIC contrast of defects in semiconductors 63

Chapter 3

Specimen Preparation and Characterisation of the Deformation Induced Dislocations 72

3.1 Factors influencing specimen selection 72

3.2 Specimen preparation 78

3.2.1 Deformation procedure 78
3.2.2 Fabrication of Schottky Barriers 79

Page

3.3 Characterisation of similar specimens by different authors 83

3.3.1 Structural characterisation 83
3.3.2 Electrical characterisation of the dislocations 84

3.4 Impurities at the core of dislocations 86

Chapter 4

The EBIC System 89

4.1 General requirements for a quantitative EBIC system 89

4.1.1 Spatial resolution 89
4.1.2 Sensitivity 90
4.1.3 Temperature control 90
4.1.4 Reproducibilty 91

4.2 System description 92

4.2.1 The microscope 93
4.2.2 Signal processing 94
4.2.3 System layout 97

4.3 Computerisation of the EBIC system 97

4.4 The cold stage 98

4.4.1 Description 99
4.4.2 Thermal and mechanical performance 101

Chapter 5

Results and Discussion of the Electrial Characterisation of Schottky Barrier EBIC Specimens 103

5.1 I-V characteristics of the Schottky barrier specimens 103

5.2 Measurements of the EBIC signal as a function of series resistance 109

5.3 Measurements of the EBIC signal as a function of the incident beam current 113

5.4 Measurements of the minority carrier diffusion length 115

5.4.1 The method of Wu and Wittry for determining minority carrier diffusion lengths 117
5.4.2 Experimental results 119

5.5 Summary 126

Page

Chapter 6

Experimental Results of the EBIC Investigation of Individual Dislocations 129

6.1 The general form of the EBIC contrast of the dislocations studied 129

6.2 Quantitative measurements of the contrast of dislocations 134

6.3 Comparison of the contrast from screw and 60° dislocations 136

6.3.1 Introduction 136
6.3.2 Results and comments 137

6.4 The dependence of dislocation contrast on the electron beam chopping frequency 140

6.4.1 Introduction 140
6.4.2 Line-scan method 140
6.4.3 Stationary beam method 142

6.5 The dependence of dislocation contrast on temperature 144

6.6 The dependence of dislocation contrast on beam current 147

6.7 Summary 150

Chapter 7

The Theory of Recombination at Dislocations and Discussion of Results 152

7.1 Introduction 152

7.2 Recombination at dislocations 156

7.3 Application of the recombination theory to EBIC measurements 163

7.3.1 General description 165
7.3.2 Temperature and beam current dependence 168
7.3.3 The comparison of EBIC contrast from screw and 60° dislocations 177
7.3.4 The dependence of dislocation contrast on the electron beam chopping frequency 180

Page

7.4 Quantitative analysis and discussion of the EBIC results 185

7.4.1 Calculation of the position of the energy level of screw and 60° dislocations 186
7.4.2 The radius of the space dislocation charge region surrounding the dislocations 192
7.4.3 The dislocation recombination strength 193
7.4.4 The lifetime of minority carriers within the dislocation space charge region 194
7.4.5 Minority and majority carrier capture cross-sections 194

7.5 Discussion 198

7.5.1 The approximation of constant contrast 199
7.5.2 The approximation of 1-f 1 200
7.5.3 The origin of the dislocation levels investigated 204

7.6 Discussion with respect to other EBIC work 204

7.6.1 EBIC work on similar specimens 204
7.6.2 EBIC work on different specimens 209

7.7 Summary 211

Chapter 8

Suggestions For Further Work and Concluding Remarks 214

8.1 Suggestions for further work 214

8.2 Concluding remarks 217

References

Chapter 1

Introduction and Literature Survey

Chapter 1 Introduction and Literature Survey

1.1 Introduction

The use of semiconductor devices has become a fundamental part of a modern technological society and their importance will continue to increase in the forseeable future. The successful manufacture and operation of such devices relies to a large extent on the ability to produce and process semiconductor material in almost perfect crystalline condition. The presence of imperfections produces a region of the device whose properties are often different from those desired and if this occurs in a critical part of the device, failure can result. The effect on the electrical characteristics of a defect present in a small device is in general greater than that for a large device. Thus the presence of defects is more important as the size of components is reduced and their complexity is increased.

Dislocations, being defects which alter the electrical properties of semiconductors, are thus very important from a commercial point of view, and much research is being undertaken to minimise their effect upon devices. By far the most common approach to this problem is to study ways of processing material without introducing dislocations at all. A second way is to "passivate" dislocations when they are present. See for example Pohoryles (1981). However the detailed electrical properties of dislocations are still

largely unknown and so such work is often performed on an empirical basis.

A detailed understanding of the properties of dislocations is therefore likely to be useful to the semiconductor industry by enabling their effect on devices to be reduced. Dislocations are however, even more widely studied because they also provide a means of extending the knowledge of semiconductors themselves and solid state physics generally. They are interesting because they can provide a structure in semiconductors whose behaviour is dependent on the fundamental properties of the semiconductor, whilst still being easy to produce. A study of dislocations may therefore be capable not only of increasing our knowledge of the dislocation but also of the semiconductor itself. In this way we can see the use of "the defect as a laboratory system." (Kimmerling (1983)).

In this work the electrical properties of dislocations have been studied using the electron beam-induced current (EBIC) made of an SEM. The dislocations investigated have been introduced in a controlled way so that their structural properties are well characterised. In this way the data produced may be related directly to specific dislocation types and ideally to their core structures. In this respect the aim of the project has been to increase the detailed understanding of semiconductors rather than to produce results directly relevant to device manufacture.

The experimental work undertaken for this project has been carried out entirely on deformation-induced dislocations in silicon. In order to keep the introduction as short as

possible, discussion in this chapter is confined to the properties of dislocations in silicon and wherever possible is limited to those of straight segments of screw and 60° dislocations which have been studied in this work. Even within these constraints there is much that is relevant to this project.

The electrical properties of dislocations arise directly from their detailed, microscopic physical structure. The precise arrangement of atoms along the dislocation core is thought to play a major role in determining the electronic structure of the dislocation and hence its electrical activity, see for example Shockley (1953) or Teichler and Veth (1983). It is the purpose of section 1.2 to place the measured electrical behaviour of dislocations in context by discussing their physical structure and hence their expected electronic structure. In addition various effects other than those due to the dislocation core are considered.

In section 1.3 the interaction of a dislocation with its surroundings will be discussed in terms of its electronic structure. How the resultant electrical activity of dislocations as measured by various techniques can then be used to deduce the electronic structure is explained together with the principal limitations of these techniques. In section 1.4 a summary of the findings of experimental work on dislocations in silicon so far is given with particular attention being paid to those generated in similar conditions to those investigated in this work.

In this way it is hoped to give a complete picture of what is known so far about the electrical properties of dislocations in the material used and how this knowledge was gained.

Finally the potential advantages of the EBIC technique for elucidating the electronic structure of dislocations over those techniques used in previous investigations are outlined together with the way in which this project has sought to exploit these advantages.

1.2 Dislocations in Elemental Semiconductors

At its simplest a dislocation may be viewed as a linear defect in a crystal lattice characterised by the closing vector of a Burger's circuit around it, the long range topological disorder introduced being described by this Burger's vector. In many situations such a description would be adequate but, as this chapter will show, the electrical properties of dislocations in semiconductors are dependent on the precise atomic configuration of the core of the dislocation. For this reason effects which are sometimes of little or no importance when considering dislocations in other materials become fundamental to the properties of the dislocations in semiconductors. Into this category fall Cottrell atmospheres of impurities or point defect clouds, decoration of the core with impurities, and kinks and jogs along the dislocation line. The discussion in this section will be limited mainly to "pure" dislocations and the secondary effects will be treated in more detail in section 1.2.3.

1.2.1 Physical Structure

Dislocations are generally classified by the angle between their Burgers vector ($\underline{b}$) and the direction of the core of the dislocation. Thus if the Burgers vector is parallel to the dislocation line the dislocation is termed 0° or more usually a screw dislocation. The dislocations most commonly found in silicon are screw, 60° and 90° (the latter is also called an edge dislocation). In this work only those dislocations which are introduced by plastic deformation are considered, these are glissile and their Burger's vectors lie in the slip plane. The dislocations produced are found in the $\{1\bar{1}1\}\langle 110\rangle$ glide system. Dislocations with $\underline{b} = \frac{a}{2}[110]$ and their line direction $\underline{u} = [110]$ are screw dislocations, those with $\underline{u} = [011]$ or $[10\bar{1}]$ are 60° dislocations. With such dislocations two different core structures are possible because the diamond lattice contains two distinct sets of $\{1\bar{1}1\}$ planes. Thus a dislocation formed by shearing one part of the crystal against the other between the closely spaced $\{1\bar{1}1\}$ planes will have a different core structure to a dislocation where the shear takes place between the widely spaced planes. The former is said to be in the glide configuration whilst the latter is in the shuffle configuration. The shuffle arrangement was originally proposed by Shockley (1953) to be the most likely core state because it entails fewer broken bonds and the separation of planes at the core is wider.

It was soon realised that an undissociated perfect dislocation may dissociate into partial dislocations separated by a region of stacking fault. For $\underline{b} = \frac{a}{2}\langle 110 \rangle$ the partials produced have $\underline{b} = \frac{a}{6}\langle 21\bar{1} \rangle$ and $\frac{a}{6}\langle 121 \rangle$. A screw dislocation dissociates into two 30° partials and a 60° dislocation into a 30° and a 90° partial. This splitting is energetically favourable because it reduces the strain energy associated with the dislocation, which is proportional to $\underline{b}^2$. Between the two partials lies a region of stacking fault which in most cases is found to be intrinsic in character. The stacking fault must occur between the narrowly spaced planes if tetrahedral coordination at the fault is to be preserved. This was thought to imply that the glide configuration with its core lying at the closely spaced planes was most likely. However Hornstra (1958) showed that the shuffle configuration was still feasible even for dissociated dislocations. This he showed by proposing that the dislocation might be associated with a stacking fault ribbon on a neighbouring plane. In this way the core of the dislocation lies between the widely spaced planes whilst the stacking fault is in between the narrowly spaced planes. This can be visualised as occurring by the glide configuration partial absorbing a row of print defects (vacancy or interstitial) so that the core moves by one half plane relative to its position in the shuffle configuration. The only difference between the two structures is a column of atoms removed in the shuffle configuration (vacancy type) which is present in the configuration. The overall strain field surrounding the dislocation is the same in each

case leading to identical contrast in conventional TEM. Thus when Cockayne et al in 1969 showed, using weak beam microscopy, that dislocations in silicon were indeed dissociated into partials with few points of constriction, it was still impossible to decide between the two possible core configurations.

Further experiments were performed which gave some indirect evidence as to the nature of the dislocations. In 1975 Gomez et al observed that moving dislocations are still dissociated into partials making the Horstra type configuration unlikely since their mobility should be less and their energies, whilst moving, greater than for the glide type dislocations. Recently more direct evidence has been gained using HREM. Anstis et al (1981) obtained lattice images of 30° partials running perpendicular to the foil surface. The dislocations were introduced by two-stage deformation at 750°C and 420°C in float-zone (FZ) silicon (see section 3.2 for full details of specimens). The images obtained cannot be used to determine the core configuration immediately because the nature of the images is dependent upon various microscope parameters. However the images produced by the glide and shuffle configurations can be simulated for given microscope conditions using a computer.

The computed images showed that for certain experimental conditions the microscope images produced by the glide and associated shuffle configurations would be different. Anstis et al (1981) produced these conditions for several 30° partials and the resulting images all corresponded to those calculated for the glide configuration. This represents the strongest evidence so far that 30° partials in Si FZ material

deformed at 420°C, are indeed in the glide configuration. Unfortunately this has yet to be achieved for a 90° partial in these specimens. It should be mentioned that although the agreement obtained between image and calculation is good it is not perfect. Hutchison (1983) has given a possible explanation of this by including a kink on the dislocation line within the foil which has the effect of "smearing" out the core contrast over two adjacent positions.

Bourret et al (1983) using HREM to study deformation induced dislocations in Czochralski silicon found a large difference between computed and observed images for 30° partials and attributed this to oxygen segregation along their cores. They also obtained images for the 90° partial and this time found no evidence for decoration. The images obtained were in good agreement with those predicted by the glide model. Work performed by Olsen and Spence on Czochralski silicon strained at 800°C shows the 30° partial to be of the glide rather than the shuffle configuration and in these specimens no evidence of oxygen or impurity decoration of any kind was found. In view of these results it seems most likely that both the 30° and 90° partials are indeed of the glide set, though there still remains some uncertainty due to the possible effect of kinks and/or impurities along the dislocation core.

In conclusion, experimental evidence has shown that deformation induced screw and 60° dislocations in silicon are found in the $\{1\bar{1}1\}$ $\langle 110 \rangle$ glide system, are dissociated into partials which are separated by a stacking fault ribbon and are likely to be in the glide configuration.

1.2.2 Electronic Structure

Historically, the theory of the electronic structure of dislocations in plastically deformed semiconductors begins with Shockley (1953). He suggested that the dangling bonds produced at the core of a dislocation should have the properties of a one-dimensional, half-filled band if the dislocation is electrically neutral. The dangling bonds are produced by the breakdown of the standard tetrahedral coordination at the dislocation core where the extra half plane of atoms ends. It is the characteristics of the band or bands produced in the forbidden gap by the dislocation which determine many of its electrical properties and so it is important that their nature should be fully understood.

Two approaches have been used to try to elucidate the band structure produced. The first, which is considered in the following, is to refine the theoretical description of a dislocation in a semiconductor until the models used are sufficiently accurate to predict the physical and electrical structure with some degree of certainty. The second attempts an interpretation of experimental results in terms of a specific band structure associated with specific types of dislocations. This method will be discussed in section 1.3.1. Obviously a full understanding of dislocations in semiconductors will not have been reached until there is agreement between the two approaches.

Theoretical calculation of the electronic states associated with dislocations has proved very difficult, twenty years' work having produced few unambiguous results. The simplest aspect of the effect of dislocations is their long

range strain field. This introduces shallow states into the band gap that may be treated using the effective mass equation. Claesson (1979) and Winter (1978) treating perfect and dissociated 60° dislocations find a small number of states drawn down from the conduction band up to 0.1eV into the gap. However the effect of coupling to the core region is not known and so the precise position of these states is uncertain.

Calculation of the states introduced by the core itself is more difficult for a number of reasons. First, the effective mass approach is inapplicable to the calculation of energy levels for the rapidly varying potentials at the dislocation core. Secondly, the calculation of the atom positions at the core is itself difficult and thirdly, a full solution should be self-consistent. To produce a self-consistent solution the total energy (mechanical and electrical) of the dislocation should be minimised whilst maintaining an electronic structure that is consistent with the atomic coordinates used to describe the physical structure. Hitherto such a solution has proved too complex to be obtained. Most calculations are instead performed by considering only the strain energy and bonding energy of atoms at the core to determine their positions and then using these positions to calculate the electronic states produced. However as the resulting band structure was not taken into account when calculating the atom positions the calculation is clearly not self-consistent and may not even be a good approximation to reality. This is because the energy component contained in the band structure is significant compared with the total energy of the dislocation.

The calculation of atomic positions, even neglecting the electrical energy component, is difficult because in the region of the core the distortion of the crystal is so great that isotropic elasticity theory is no longer valid. Most workers have used some sort of valence force field to determine the atom coordinates but depending on its form different results are obtained. For example Marlkund (1983) has used the parameters due to Keating (1966) and of Baraff et al (1980). Lapiccirella and Lodge (1981) have used a Lifson-Warshel (1968) type force field. Such calculations produce values for the bond angles at the core varying typically by less than 2°, depending on the method used, but this alters the strain energy associated with the dislocation by as much as leV per unit cell. Clearly obtaining an accurate description of the nature of the forces between atoms at the core and deducing their positions is fundamental to resolving the question of the most likely core configuration. In the calculations mentioned the positions of the atoms calculated are then used to calculate the band structures. As mentioned earlier, such calculations are not self-consistent. Most theoretical methods used before 1979 were applied to unreconstructed dislocations (see following), either perfect or dissociated. These produced a variety of different states in the gap, some with partially filled levels. All these calculations predicted that electrons with unpaired spins would occupy theses states, a conclusion which is contrary to the EPR results gained by Weber and Alexander (1979) and Weber (1983). For a full review of the calculations and their results see Teichler and Veth (1983) and Jones (1979).

It was postulated by Jones (1979), Marklund (1979) and independently by Hirsch (1979) that reconstruction of bonds in the core of dislocations may occur. This entails the movement of dangling bonds so that there is overlap between adjacent pairs and a two-electron bond is formed between them. This has the effect of lowering the electrical energy of the dislocation by splitting the half filled band into two giving a full "bonding" state of lower energy and an empty "antibonding" state of higher energy than the original unreconstructed state. Reconstruction may be expected to occur if the extra strain energy introduced into the crystal by the distortion necessary to produce dangling bond overlap is less than the decrease in the electrical energy of the system (that is to say, if the total energy of the dislocation is reduced).

Following the introduction of the notion of reconstruction, calculations have been performed using different methods to determine whether such a process would be energetically favourable. Most workers now believe that the reconstructed configuration of the 30° and 90° glide partials is indeed of lower energy, see for example Hirsch (1979), Lapiccirella and Lodge (1981), Jones (1979), Marklund, Veth and Teichler (1984). The latter three calculations also produced values for the positions of the levels and in all cases found them to lie outside the forbidden band gap. Also they found that reconstruction of the 30° partial was even more likely than for the 90° partial because the strain introduced into the lattice by the 30° is less. However for the 90° partial the most recent calculations by Lodge et al

(1984) whilst showing reconstruction to be most favourable also predicts an empty band 0.4eV below the bottom of the conduction band which extends into the conduction band. However no likely rearrangement of the core atoms seems able to produce the band structure experimentally observed (see for example Schröter et al (1980)). Thus, the theories and core configurations used so far as the basis for calculations predict that 30° and 90° glide partials will reconstruct and with the exception of Lodge et al (1984) that no states will be left in the band gap. This is in good agreement with the EPR results of Weber (1979) who finds few unpaired spins associated with dislocations but it also implies that an "ideal" 30° or 90° glide partial would show little or no electrical activity. This is clearly not the case for the dislocation studied experimentally. (see section 1.3)

To explain the presence of the states which are observed experimentally to lie deep in the band gap, theoreticians have considered special sites that might be present along the line of a reconstructed dislocation and also core configurations different from those predicted by modified isotropic elasticity theory. Jones (1981) considers possible anti-phase defects (APD's) in the reconstruction process along the dislocation core. These APD's, which are the points separating two regions of reconstructed core he calls solitons. They may be neutral, positively or negatively charged depending on whether the unreconstructed dangling bond remains as a single electron, is ionised into the conduction band leaving the APD positively charged or captures another electron to become negatively charged. The presence of an uncharged APD with its unpaired spin would give rise to an EPR

signal which Weber (1983) does not find (but see Kveder et al (1982) who observe substantial signals in different specimens). However Jones calculates that the formation energy for a charged APD would be less than for a neutral APD which would therefore be less likely to occur. A charged APD would give states in the band gap whilst still not contributing to an EPR signal and is therefore consistent with experimental observations. At the moment there is no direct evidence as to the existence of APD's although Jones (1983) uses them to develop a theory for the doping dependence of the mobility of dislocations in silicon. This is essentially a variation of double kink nucleation theory for dislocation mobility of Hirsch (1979,1981).

Marklund (1983) also considers a mechanism whereby energy levels due to 90° glide partials can be produced in the gap but his calculations were of insufficient accuracy to determine whether the core configurations produced are more energetically favourable than those due to reconstruction. The method he used was to calculate the atom coordinates using isotropic elasticity theory and then to modify the results using a valence potential. However rather than using this arrangement to calculate the electronic structure he then considered a further relaxation of the dislocation core. The amount by which he allowed the core atoms to relax into the bulk (either 0.33 Å or alternatively 0.33 Å and 0.165 Å) is similar to that found for relaxed (111) surfaces. Using these different core arrangements he was able to generate one half filled band or, by the 0.33Å and 0.156Å relaxation, two bands one of which is full and the other empty, with the bottom of the empty band lying approximately at the middle of the gap.

As with the anti-phase defect there is no direct evidence to support this structure but unlike the anti-phase defect it cannot be used to explain the electrical activity of the 30° partial, because the relaxation used is specific to the core of the 90° partial. HREM cannot be used to ascertain whether the reconstruction of the core actually takes place because the displacement of the atoms along the core is too small to detect (<0.05Å). Hirsch (1980) has suggested that it may be possible to investigate directly reconstruction by exploiting the periodicity of reconstructed bonds to give some diffracted intensity from an incident electron beam that would not otherwise be present. To the author's knowledge no work of this kind has yet been successfully performed.

In conclusion, theoretical techniques have shown that the electronic structure is critically dependent on the physical structure of the core. If bond angles are changed by ~2° the energy of a dislocation can be changed by 1eV per unit cell. This in turn determines whether the dislocation is likely to be unreconstructed or not, a feature which is fundamental to its electrical activity. A mechanism by which an "ideal" dislocation may introduce the deep levels observed experimentally has yet to be found although various hypotheses, as yet untested, have been put forward.

1.2.3 "Non-Ideal" Dislocations

So far in this chapter only the properties or expected properties of "ideal" dislocation segments have been discussed. In this context "ideal" has been used to mean straight, completely dissociated and of pure character (screw

or 60° in this case). However at present it does not seem likely that it will be possible to describe the great variety of behaviour that dislocations exhibit in terms of such simple models. It thus seems likely that the electrical properties of dislocations may be determined in part or, possibly, even dominated by deviations of the actual dislocation structure away from this "ideal" (Alexander et al (1983)).

Most of the electrical characteristics of dislocations which have been studied experimentally are related to the position of the states introduced into the band gap. The results of such experiments are used to deduce energy level schemes both so that the more fundamental nature of the dislocation is understood and so that the results obtained can be related to and checked against those of other experiments. In describing a band scheme associated with the dislocation it is important to consider the relation between the levels deduced and the actual physical nature of the dislocation. In this way many different factors have to be taken into account other than those met when considering the "ideal" dislocation. In most cases this is not done specifically. For example, Ossipyan (1981) correlates the levels he deduces to "special sites" along the dislocation line where some effect other than that of the "ideal" dislocation is important. He is unable to say what these might be but says that the sites may be associated with jogs or points of intersection with other dislocations or with impurity atoms near the core. Other experimental work (Section 1.3) also indicates that in many cases dislocations do not seem to exhibit a fundamental set of properties but rather that these depend on the way the dislocations were generated. It may be

that one of the reasons for the discrepancies in the results obtained by different workers is that they are in fact studying different systems. For example Bourret (1983) has demonstrated oxygen precipitation at the core of a 30° partial in Czochralski silicon which has not been found in float zone specimens. It is likely that the electrical behaviour of the two specimens would also differ. Alexander et al (1983) investigating the mobility of dislocations in swirl-free FZ silicon at 420°C observed the slowing down of 60° dislocations during movement which is indicative of the interaction of these disclocations with impurities. Etch mounds were also observed suggesting that oxygen may be the impurity present. These effects are not found in conventional float-zone silicon[1] when deformed under the same conditions. Weber (1983) finds the EPR and DLTS response of dislocations to be dependent both on the temperature of predeformation and the temperature of the main deformation in a two-stage process.

Thus the experimental results obtained from dislocations do not seem consistent with a single set of characteristics for all dislocations studied. It therefore seems likely that in most cases the effects observed are not those due to "ideal" dislocations. As yet there is little evidence correlating the observed behaviour to specific effects although Weber (1983) associates an EPR and DLTS line with dopant impurity atoms along the dislocation core for each of n- and p-type silicon. Other possible causes of non-ideal behaviour may be oxygen, nitrogen or other light elements along the dislocation core or a surrounding cloud of point

1. A small number of etch mounds are found after high temperature deformation of float zone silicon but not after deformation at 420°C.

defects (see for example Schröter et al (1980)). The presence of kinks may also alter the observed electrical activity (Hirsch 1980) and jogs and dislocation intersections might be considered although only in highly deformed material. It is noted here for completeness that Kittler and Seifert (1981) have stated that recombination at dislocations showing greater than 1% contrast in EBIC, is necessarily dominated by centres not actually located in the core of the dislocation. Such centres they attribute to impurities. However, the present author believes that the assumptions made in reaching this conclusion are invalid and this will be discussed fully in the light of the present work in Section (7.6.2).

1.3 Electrical Properties of Dislocations

The preceding sections have shown that the presence of dislocations leads to states in the forbidden band gap which can be occupied by electrons. It is these states that determine the elecrical activity of a dislocation and the way in which this happens will be described in the following.

The states introduced into the band gap by a particular type of defect are assumed to occur with a small energy spread. The density of states within this energy range available for occupation is assumed to be continuous and so the individual states merge to form a band or alternatively energy level within the band gap. For a neutral dislocation this band may be empty, full or half filled depending upon the nature of the site generating the level. For example, dangling bonds are expected to produce a half filled band and reconstructed bonds a filled band and an empty band.

In semiconductors the occupation of a level with electrons is given by its position relative to the Fermi level. Thus states below the Fermi level will tend to be mostly occupied, and those above largely empty, the exact occupation being given by the Fermi function. Thus a level which is empty in a neutral dislocation will act as an acceptor level, filling with electrons if below the Fermi level and in the process becoming negatively charged. A level which is full is a donor level which if above the Fermi level will empty becoming positively charged. The half filled band is amphoteric being capable of showing either type of behaviour. In most cases the exact occupation of a level is given by the Fermi function.

The levels introduced into the band gap by dislocations generally have sufficient states that if they were to become fully charged, i.e. acceptor states occupied or donor states empty, the potential barrier surrounding the dislocation would be very large. This would have the effect of bending the conduction and valence bands (fig. 1.1) and so would move the position of the level in the band gap relative to the Fermi level. The equilibrium position actually occurs when the Fermi level runs through the band in the band gap and corresponds to only a few percent of the available states becoming charged. (Assuming 1 state per unit cell). This description of a charged dislocation forms the basis of models formulated to describe most aspects of the electrical activity of dislocations and so it will be discussed in more detail in section 7.2. However it can be seen, even from this brief description, that for a given position of the Fermi level the amount of band bending (size of the potential barrier) is

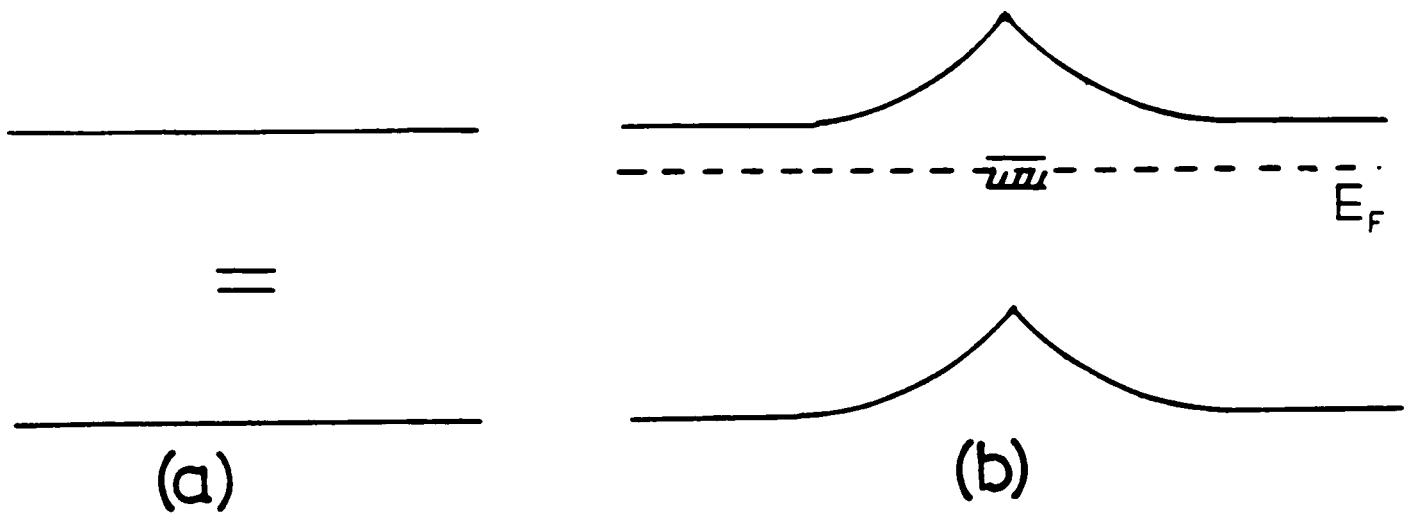


Figure 1.1 Bending of conduction and valence bands around charged dislocation states

a) acceptor states empty, b) acceptor states partially occupied

dependent on the position of the level in the band gap because at equilibrium this will be coincident with the Fermi level. Also that the more the bands are bent the greater the coulomb barrier and hence the greater the charge that must be localised at the dislocation states. It can also be seen that for recombination of an electron with a hole to occur via the dislocation level an electron must be excited over the coulombbarrier (for a negatively charged dislocation). Thus the height of the Coulomb barrier would be expected to determine, at least in part, the dislocation's efficiency as a recombination centre.

It is from these properties that electrical measurements derive their information about the electronic structure of dislocations. The principle of the five major techniques used to study dislocations will now be outlined in terms of the above description.

1.3.1 Experimental Techniques

For a summary of these techniques see table 1.1.

a) Electron Paramagnetic Resonance (EPR)

If the dislocation band introduced into the band gap is half filled in the neutral state then this will generate a number of unpaired spins equal to the total concentration of states singly occupied. For example if the dangling bonds of a dislocation were unreconstructed it is expected that each dangling bond, being unpaired, would give rise to an EPR signal. The density of centres detected in EPR would be the same as the density of centres actually present i.e. dangling bonds in this case. In this way EPR could be used to detect and measure the concentration of dangling bonds at the

TABLE 1.1 Summary of the principal experimental methods used to study the electronic properties of dislocation levels in silicon

Method	Parameter Measured	Direct Correlation to dislocation or surrounding region?	Information gained	Comments
EPR	Presence of unpaired electrons	Yes, through measuring of g-tensor	Concentration of unpaired electrons in different defect states	No spatial resolution. No way of determining energy level of EPR centre.
Hall Effect	Equilibrium concentration of free carriers	No	Generally the temperature dependence of the free carrier concentration, which is used to infer the position of an energy level in the gap	No spatial resolution. If more than one type of dislocation present then the results represent some average of the different types Only sensitive to one level per defect type.
Photoconduction (steady state & transient)	Concentration of non-equilibrium, injected free carriers	No	Temperature dependence of the excess carrier recombination rate	As above plus interpretation of recombination rate in terms of position of energy levels in the gap may be difficult
Spectral-photoconductivity	Concentration of non-equilibrium, injected free carriers	No	Excess carrier concentration as a function of incident photon energy	No spatial resolution. Can detect levels at different dislocation types independently. May be difficult to deduce position of energy levels in the gap.

Method	Parameter Measured	Direct Correlation to dislocation or surrounding region?	Information gained	Comments
Photo-luminescence	Energy of photon liberated by radiative recombination of free carriers	Yes, through the direction of polarisation of the emitted light	Energy difference for transition between two levels. If the temperature dependence of this is known, may give position at levels in the gap, but do not know whether they are measured from the conduction of valence bands	No spatial resolution. Can detect levels at different dislocation types independently. Only radiative recombination centres observed
DLTS	Rate of loading and emptying trap	Yes, through observing filling characteristics for the trap	Time dependence of filling of traps. Temperature dependence of emission from traps which is used to calculate activation energy for emission	No spatial resolution. Not certain that the activation energy measured gives position of level in the gap. Can detect levels at different dislocation types independently.
SDLTS	As above	Yes, through spatial variation	As above	As above but with spatial resolution. Technically very difficult. Not yet achieved for individual undecorated dislocations
EBIC*	Rate of recombination of excess minority carriers	Yes, through spatial variation	Temperature dependence of recombination rate	Spatial resolution Only detect one level per dislocation segment. Difficult to locate position in the gap of level controlling the recombination. Technically difficult.

* - this work.

dislocation core. However if the dislocation possessed an acceptor band, say, that was thus only partly occupied with electrons, then the EPR measurements would detect only that fraction of centres occupied and not the density available for occupation, since the number occupied is determined only by the extent of the coulomb barrier and hence charge on the dislocation. The EPR signal could not, in this case, be used to determine the density of centres produced at the dislocation, but merely to detect the presence of the centre and how this depends upon specimen processing. Because of this limitation in the ability of EPR to measure defect concentrations the technique has been used mainly to investigate specimens deformed at different temperatures and which have undergone different subsequent heat treatments in order that the thermal properties of the different dislocation states may be determined. Although a particular EPR signal cannot be correlated to a given dislocation type or feature on a dislocation, it is possible to determine whether the signal originates from within the strain field associated with the dislocation by observing the symmetry of the EPR response. If this does not occur equally in all the directions allowed by the symmetry of the lattice but rather shows some directionality associated with the Burger's vector of the dislocations, then it is possible to attribute the signal to a region close to the core of the dislocations.

A variation of the EPR technique is photo-EPR. Here EPR is used to measure the occupancy of a state as the specimen is illuminated with monochromatic light of different energies. When the energy of the light is sufficient to promote electrons from the valence band into that dislocation level or

from the level into the conduction band, a change in its occupation will result (for example Mergel and Labusch (1982)). In this way the position of the level relative to the valance and conduction band edges may sometimes be deduced.

b) Hall Measurements

In the following, negatively charged dislocations in n-type material will be considered. Negatively charged dislocations have trapped a certain number of electrons at the dislocation levels which are no longer available for charge transport. In this way the dislocations have reduced the free carrier concentrations and also changed the position of the Fermi level. The degree to which the bands are bent determines the amount of charge which is trapped and so this is dependent upon the position of the Fermi level and on the position of the dislocation level in the band gap. The relation between the amount of trapped charge, temperature, doping and the position of the energy level in the gap has been derived by Schröter and Labusch (1969) by considering the total free energy of the system and minimising this. They use this analysis to determine the position of the dislocation level by monitoring the Fermi level using the Hall technique as a function of temperature for deformed specimens. This treatment remains valid provided the dislocation density is sufficiently low that the space charge regions created by the charge on the dislocation do not overlap and that the approximation of the rigid shift of the band structure of the dislocation as it becomes charged is accurate. However the technique only

measures a bulk characteristic - the density of free carriers - and so relating the dislocations and results gained to specific dislocation types or even distinguishing between dislocations and other defects present in the specimen is difficult. Also the analysis of the data produced does not allow different dislocation states to be determined independently of each other and so ideally specimens should be produced which can be assumed to contain only dislocations of one character, and this is seldom the case.

c) Deep Level Transient Spectroscopy

In DLTS the filling and thermally-excited emptying of deep states within the depletion region of a Schottky barrier or p-n junction is measured. The charge trapped at the states alters the width of the depletion region and so its capacitance. Thus measuring the capacitance of the junction allows the amount of trapped charge to be ascertained. The states are loaded, normally with majority carriers, by changing the bias on the junction so that some states lie in neutral material. If their energy is below that of the Fermi level electrons (n-type material) will be captured. Upon increasing the bias to its previous value these states now find themselves in the depletion region and above the Fermi level, and so the carriers are thermally excited out of the traps. The rate at which this occurs is dependent upon the temperature, energy level position with respect to the conduction band edge, and the capture cross-section for electrons from the conduction band to that state (see Chapter 7).

DLTS spectra are obtained by arranging that only emission processes of a certain rate are detected and this signal is

plotted as a function of temperature (see for example Miller et al(1977)). The temperature dependence of the emission rate for electrons from each state is determined. From this data the activation energy for thermal emission of carriers can be calculated.[1] It should be noted that this is not necessarily the same as the energy difference between the conduction band edge and the dislocation state because the activation energy calculated also includes the temperature dependence of the capture cross-section which is, as yet, unknown. In some cases it is assumed that the effect of the temperature dependence of the capture cross-section is small and that the activation energy measured may be taken as the energy level of the defect, see for example Kveder et al (1982), Mergel and Labusch (1982). This assumption is made throughout this section when discussing the findings of DLTS experiments.

DLTS can thus give details of the occupation and position of energy levels introduced into the band gap by dislocations and other defects. It is possible to distinguish between those states localised at extended defects and those uniformly distributed by studying the loading characteristics of each state. It is a consequence of the coulomb barrier surrounding a charged dislocation that the loading of traps in a DLTS experiment is logarithmic with time rather than exponential which is the case for other defects (such as point defects) not surrounded by a potential barrier. If the filling characteristics of a state are observed to be logarithmic that state can therefore be assumed to be within the coulomb barrier of the dislocations.

1. A T^2 correction is also made to allow for the temperature dependence of the density of states in the conduction band and the variation of thermal velocity.

d) Photoconductivity

In this technique the excess concentration of carriers generated by a light source is obtained by measuring the conductivity of the sample. The number of excess carriers present for a given level of illumination is determined by the rate at which they recombine at dislocations or other defects. The recombination rate and so carrier concentration varies as a function of temperature and depends upon the position of the energy levels in the gap. The theory relating excess carrier concentration to the position of the levels in the band gap is due to Figielski (1978) and as mentioned earlier is dependent on the Coulomb barrier surrounding the dislocation. Measurements are generally made at sufficiently low light intensities that the occupancy of the dislocation states is close to equilibrium throughout an experiment. In this way the photoconductivity response is linear with the intensity of illumination and interpretation of the results is simpler.

There are three main ways in which photoconductivity is used. The first is steady state photoconductivity where the DC conductivity is measured for illumination with light more energetic than the band gap, see for example Makosa (1981). In the second the temperature dependence of the decay of photoconductivity generated by a 'chopped' light beam is measured. From this the activation energy for excitation of carriers over the coulomb potential is found which in turn yields the position of a dislocation energy level. As with the steady state method the energy level in the band gap whose position is deduced is the one in which the Fermi level lies

at equilibrium. This is because it is the position of this level that determines the extent to which the bands are bent and hence the size of the potential barrier surrounding the dislocation. These methods of photoconductivity are similar to the Hall effect measurements in that a bulk parameter is being measured, namely, excess carrier concentration which for a given type of doping responds to only one state in the gap for each type of dislocation present. If there is more than one type of dislocation present the results obtained will be some average of the behaviour of the different types of dislocations as measured independently.

This problem, identical to that inherent in Hall measurements, but not EPR or DLTS, means specimens containing only one type of dislocation should be used if results are to be unambigiuous. This is rarely the case, see for example Mergel (1983) who uses specimens containing screw, 60° and mixed dislocation types.

The third way in which photoconductivity is used does allow the investigation of more than one dislocation type in each specimen and also the independent observation of more than one level for each dislocation. In this case the photoconductivity, either stationary or transient, is measured as a function of the energy of the monochromatic light used to illuminate the specimen. By noting the energies at which "steps" in the photoconductivity occur, it may be possible to deduce a band scheme for the dislocations. Again, however, there is no direct evidence as to which dislocation type produced which energy levels.

e) Photoluminescence

In the photo luminescence technique electron hole pairs are generated by irradiating the specimen with light. Some of these carriers subsequently recombine accompanied by the emission of a photon. The energy of the photon is determined by the difference in energy of the two states between which the transition takes place. Thus by measuring the energies ofthe emitted photons the energy difference between different states in the band gap can be found. However only those states which take part in radiative recombination processes will be detected.

It is found (Drozdov et al (1978)) that dislocated Si specimens produce a photoluminescence spectrum containing four main lines (the D-series) and that this light is strongly polarised along the dislocation line directions thus allowing direct correlation between the light emitted and the dislocations themselves.

1.3.2 Discussion of Results

The electrical techniques outlined in the previous section have been used mainly to study deformation induced dislocations. In the following only work on silicon is considered. The specimens have been compressed, bent or twisted at elevated temperatures in an inert atmosphere. The more recent investigations have been mainly concerned with specimens deformed in compression, see for example Kveder et al (1982), Mergel and Labusch (1983), Weber and Alexander (1983), Kimmerling et al (1981), although Ossipyan performs measurements on specimens prepared by a four point bend. Different directions of compression are employed and different

amounts of strain are produced which will result in different morphologies for the resulting dislocation network.

In most cases no comment is made about the relative proportion of screw to 60° dislocations and the degree to which the dislocations are straight or curved. Thus when different experiments produce different results it may be due at least in part to the nature of the specimens investigated. For example in DLTS measurements different concentrations of the same centres are sometimes found by different groups who have used the same temperature of deformation to produce their specimens. This may be because the detailed morphology of the dislocation networks produced differs from group to group. In studying dislocations generated at different temperatures, three régimes of dislocation behaviour are observed. The first occurs when dislocations are produced by deformation at or above ~750°C or by deformation below this temperature followed by an anneal at 750°C or above. The second régime occurs for temperatures below ~700°C and the third for deformation at or below 420°C. The transition temperature between ranges two and three is not accurately known.

a) <u>High Temperature Deformation or Anneal</u>

These specimens are produced by deformation at $\gtrsim$750°C (>0.6 T melting), or by deformation at a lower temperature followed by an anneal at T$\gtrsim$750°C.

The specimens contain dislocation networks which consist mainly of tangles of curved dislocations. Most dislocations are of mixed character, very few segments being both straight and also parallel to ⟨110⟩.

These specimens have been studied by many workers and there is good agreement in their findings. These are summarised in Table 1.2.

Weber and Alexander (1983), Kveder et al (1982) and Kimmerling et al (1981) have all performed DLTS on such specimens and although the detailed shape of the spectra they obtain differs, the activation energies for each state are broadly similar. They find an electron acceptor state with an activation energy 0.39 eV which, following the convention of Kimmerling and Patel (1978), is written as E(0.39) and a donor state with activation energy $\sim$0.35 eV written as H(0.35). These values have been widely interpreted as the difference in energy between levels in the band gap and the conduction and valence band edges. They are found in nearly all specimens containing deformation induced dislocations.[1] Measurements using the Hall effect (Schröter et al (1980)) on similar specimens also show states at similar positions in the gap.[2] Spectral photoconductivity measurements made by Mergel and Labusch (1982) show an acceptor state at the same energy as DLTS measurements but show two donor states at 0.19eV and 0.5eV above the valence band edge. Mergel and Labusch propose that DLTS experiments may be measuring an activation energy which is the distance between the valence band edge and quasi-Fermi level of these traps. For the 0.19eV and 0.5eV levels detected by spectral photoconductivity the quasi-Fermi level is expected to be 0.35eV from the valence band edge which would then be in agreement with the DLTS results.

1. Kveder does not detect the H(0.35) state after deformation at 680°C.
2. These measurements can also be interpreted to show the splitting of the donor state as observed in spectral photoconductivity.

Author	Weber[1]	Kimmerling[2]	Kveder[3]	Schröter[4]	Mergel[5]
Technique	DLTS	DLTS	DLTS	Hall effect	Spectral photo-conductivity
Deformation temperature	electron trap	electron trap	electron trap	electron trap	electron trap
High or annealed	0.4eV	0.38eV	0.37eV	0.37eV	0.38eV
Intermediate	0.19 0.29 0.40 0.54	0.18* 0.28* 0.41* 0.48* 0.63*	 0.27 0.37 0.51 0.60		
Low	0.19 0.29 plus a broad line				
	hole trap	hole trap	hole trap	hole trap	hole trap
High or annealed	0.35	0.35	0.35	0.21 0.34 0.47	0.19 0.35 0.50
Intermediate		0.09 0.23 0.26 0.29 0.35 0.40 0.60	 0.25 0.39 0.40 0.47 0.67		

Table 1.2 Summary of energy levels observed in deformed silicon
* Levels also observed in 770/450 specimens[6]

1. Weber and Alexander (1983)
2. Kimmerling et al (1981)
3. Kveder et al (1982)
4. Schröter et al (1980)
5. Mergel and Labusch (1982)
6. Patel and Kimmerling (1979)

EPR experiments show few unpaired spins to be present representing only a fraction of those observed after deformation at intermediate temperatures.

b) Intermediate Temperature Deformation

After deformation at temperatures in the range ~600°C to ~750°C with the specimen subsequently cooled under load the dislocation network produced contains mainly straight dislocations aligned along <110> directions. There is, however, still a significant (~20%) proportion of curved dislocation segments.

It is in this range that dislocations show the greatest variety of behaviour. Again they have been extensively studied and the results are summarised in Table 1.1. Around fifteen different DLTS centres have been found including the E(~0.39) and H(0.35) levels most commonly seen. The highest concentration of centres is associated with a level E(~0.52). By comparing the behaviour of the EPR and DLTS spectra on annealing, Weber and Alexander and also Kveder et al deduce that the E(~0.52) level is due to the same centre as the EPR D-line (see below). Weber further attributes E(0.19) and E(0.29) to the Si-K7 centre. Kveder also associates H(0.39) with the D-centre. Kimmerling et al (1981) and Weber and Alexander (1983) postulate that the complicated nature of the DLTS spectrum of these specimens is due to the generation of point defects during non-conservative dislocation motion, possibly due to the movement of jogs. Upon annealing , these point defects are supposed to anneal out. To test this Kimmerling et al performed a slow deformation at low temperature (700°C) such that the rate of point defect

generation was small. In this way any defects generated could recover as the deformation process continued. The DLTS spectrum produced by this specimen was identical to that of a specimen annealed at 900°C as they expected and they further conclude, as do Weber and Alexander, that the electrical activity of dislocationsintroduced in the intermediate temperature range is not directly related to core structure. The intermediate temperature specimens show a strong EPR signal which because of its symmetry can be attributed to centres close to dislocations. These centres have been called D-centres (see chapter 3), but there is some debate as to their concentration. Grazhulis et al (1981) from TEM measurements estimate the dislocation density in the specimens, and then from the concentration of EPR centres calculate their spacing along the dislocation core to be 5Å. This correlates well with the spacing of dangling bonds in a model of an unreconstructed dislocation. From this they infer that the centres are likely to be due to the dangling bonds themselves. However the dislocation density measurements as quoted by Grazhulis are only likely to be accurate to 50%. This is because the deformation used does not produce a uniform distribution of dislocations but rather slip bands where the concentration of dislocations is high and other areas where it is low, the relative densities ranging by at least an order of magnitude, see for example Kimmerling et al (1981). Thus by using TEM, which only allows densities in very small volumes to be measured, accurate measurement of average deformation induced dislocation densities are very difficult to achieve. It is the opinion of this author that

the uncertainty in dislocation density and hence concentration of states at the dislocation core considerably weakens the argument for these states being associated directly with the simple dangling bonds which may be expected along an unreconstructed dislocation core. Weber (1983) and Suezawa (1981) also find a strong EPR signal thought to be associated with the same centre as that found by Grazhulis. Weber estimates its concentration to be equivalent to about 20% or less[1] of atom sites along the core and hence does not ascribe it to dangling bonds at an unreconstructed dislocation core. TEM is again used to measure the dislocation density. Together with this rather broad line in the EPR spectrum other lines are also present termed Si-K1, Si-K2 and Si-K7 (for n-type silicon). The total concentration of centres associated with these lines is however only a few percent of that associated with the D-line.

Upon annealing at 800°C the Si-K1 and Si-K2 lines disappear and the D-line is reduced to a few percent of its former value. Kveder et al account for this behaviour by supposing that the D-centres are due to dangling bonds at the dislocation core which reconstruct upon annealing. It is found that the experimentally observed reduction in the concentration of D-centres may be explained by assuming that the process of reconstruction has an activation energy of 2eV. No comment is made on the behaviour of the Si-K1, K2 centres (Kveder et al (1982)).

Weber and Alexander (see for example Alexander et al (1983)) postulate that the D-centres are not due to dangling bonds at the dislocation core, but rather to a surrounding cloud of point defects. These point defects are

1. As the dislocation density increases so the relative concentration of this centre appears to decrease.

generated by the dislocation motion at $T<0.6T_m$ and are held close to the dislocation by its surrounding strain or electrostatic field. The defects experience various strain fields depending upon their positon relative to the dislocation and thus the D-line is very broad as observed. Upon annealing such a specimen these point defects are removed, so accounting for the observed reduction in the D-line. No change in dislocation density is observed for this anneal. Weber and Alexander attribute the Si-K1 and Si-K2 lines to a single centre containing two dangling bond sites, see chapter 3. This is a "special site", in the same way as Ossipyan proposes, and this special site also anneals out at higher temperature. One possibility suggested, (Weber (1983)), is that these sites occur on unreconstructed segments of dislocation jogs.

Both models for the D-centres predict that a high temperature deformation ($T>0.6T_m$) would yield the simpler energy level structure consistent with that of an annealed specimen because annealing would occur simultaneously with deformation.

c) Low Temperature Deformation

Professor Alexander's group in Cologne has prepared specimens by deformation of FZ silicon under compression along a [213] direction at 420°C with subsequent cooling under load. Generally these specimens are produced by two-stage deformation; the initial stage, predeformation at 850°C, simply nucleates a small number of dislocation loops and these subsequently expand during the main deformation at 420°C. The pre-deformation does not generate any levels in the gap which can be detected by EPR or DLTS that are not produced by a 420°C deformation. The 850°C/420°C specimens

thus show the same spectra as specimens deformed in a single stage at 420°C. The latter are much more difficult to produce and so are not generally studied.

Almost all dislocations in the 850°C/420°C specimens are straight and lie accurately along the <110> directions. TEM shows that they are almost completely dissociated and appear to approximate on a microscopic though not necessarily atomic scale to the "ideal" screw and 60° dislocations considered earlier.

Weber has studied these dislocations using EPR and DLTS. He finds only the Si-K7 EPR centre present in n-type material and can detect no EPR centres at all in undoped material. He concludes that both 30° and 90° partials must be reconstructed and that the Si-K7 centre is due to dopant atoms. Weber explains the difference in activity of these 850°C/420°C specimens compared to the intermediate temperature specimens by postulating that at low temperatures there is insufficient energy available to produce point defects and that the dislocations glide conservatively. If no point defects are present the D-line attributed by Weber to point defects would also disappear as observed.

If the pre-deformation takes place in the intermediate range the EPR and DLTS response remains approximately unchanged throughout the subsequent deformation at lower temperatures (420°C). This Weber (1983) explains by assuming that at this temperature there is insufficient thermal energy for the point defects to anneal and so their concentration remains unchanged. It seems difficult to explain this

1. Less than 0.2% of core sites active for the broad D-line and less than 0.02% of sites active for the other lines which are easier to detect.

behaviour of the EPR and DLTS response in terms of the dangling bond model proposed by Kveder et al (1982). The morphology of the dislocation networks does not change significantly between 650°C and 420°C, both structures containing mostly straight dislocation of pure screw or 60° character. See for example Gottschalk (1983).

DLTS experiments (Weber and Alexander (1983)) show the H(0.35) level common to most specimens and in addition E(0.19) and E(0.29) centres which he associated with the Si-K7 EPR centre. There also exists a broad line ($E \sim 0.4$) for which he is unable to obtain an accurate activation energy.

Weber and Alexander (1983) have also studied 850°C/420°C specimens (cooled under load) which have undergone further heating to 390°C for twelve minutes (no load applied). This causes the dislocation network to relax, the straight segments becoming curved. Rather surprisingly, perhaps, he still finds no EPR signal even though the dislocations should now contain a large number of kinks. This indicates that in these circumstances the kinks contain no unpaired dangling bonds. This may be because kinks are more stable either positively or negatively charged or that they may be associated with some other defect in such a way as to "reconstruct" the kink. It would be interesting to perform DLTS on these specimens to see whether the concentration of E(0.38) increases as would be expected if Kimmerling is correct in assigning this level to kinks, see below.

1.3.3 Summary of Results and Comments on the Previous Work

For a summary of the energy levels that have been determined see table 1.2. The experimental work performed so far has shown three régimes of dislocation behaviour depending upon the thermal history of the specimen. By far the greatest electrical activity (EPR and DLTS) is shown after deformation at intermediate temperatures. Weber and Kimmerling believe that this is due to centres not located in the core of the dislocations whereas Kveder associates it with an unreconstructed core. These suggestions have been discussed in the preceding section. After high temperature deformation or anneal the dislocation morphology does not correspond to that of the "ideal" dislocations discussed earlier. It is only the dislocations generated at low temperatures (~420°C) which show electrical behaviour which does not suggest that it is dominated by effects other than the dislocations themselves and where the dislocation morphology comes closest to the "ideal". In addition investigations of the mobility of these dislocations by Alexander et al (1983) indicate that they are unlikely to be decorated by oxygen and the HREM performed by Anstis (1981) and Hutchinson (1983) does not indicate the presence of any impurities along the dislocation core. Thus it would appear from the research so far that the dislocations produced by two-stage deformation (850°C/420°C) along ⟨213⟩ in FZ silicon approximate closest to the "ideal" dislocation of those currently available for study.

The specimens deformed at low temperature contain the E(0.39) and H(0.35) centres found in nearly all samples containing dislocations regardless of their thermal history.

The concentration, as measured by DLTS, is nearly two orders of magnitude smaller than that of the other centres found after deformation at intermediate temperatures. This leads Kimmerling and Patel (1978) to associate them with special sites. They postulate that the E(0.39) level is due to kinks and the H(0.35) level (or levels according to Mergel and Labusch) is due to defects that arise in the reconstruction process. Neither of these suggestions has yet been verified.

Mergel and Labusch (1982) who detect the E(0.39) level using spectral photoconductivity assign it to a level intrcduced by a 30° reconstructed partial. They also find levels at 0.19eV and 0.50eV above the valence band edge, which they suppose to be equivalent to the H(0.35) level detected in DLTS, and these they associate with a relaxed 90° partial. However recent calculations by Marklund (1983) show the 30° recontructed partial to produce no states in the gap. The interpretation of the levels in this way is dubious because they are also found in the high temperature specimens. Here the approximation to the straight "ideal" dislocation is very poor and it seems unlikely that energy levels introduced into the gap by dislocations of mixed character would be the same as for pure screw and 60° dislocations (30° and 90° partials). Calculations by Marklund (1983) on a 60° partial show its behaviour to be quite different from 30° and 90° partials. It has been suggested that partials of mixed character may form alternate segments of pure 30° and 90° character. However it is not known as yet whether this occurs and if it does whether the segments produced are sufficiently long that the levels they introduce into the gap will approximate to those produced by the straight dislocations

formed at lower temperatures.

In addition to the E(0.39) and H(0.35) DLTS centres, E(0.19) and E(0.29) are also found in the low temperature deformed specimens. These have been correlated with the Si-K7 centre by Weber.

It has been impossible to attribute the majority of levels observed using DLTS, photoconductivity, Hall effect or the centres detected using EPR to any specific type of dislocations or any particular "special site" either at the dislocation or in its immediate vicinity. Without being able to correlate the electrical information gained to specific physical features it is of use only on an empirical basis. Such information does not greatly enhance our knowledge of the structure of dislocations as found in deformed specimens nor does it add greatly to the understanding of dislocations generally.

The reason for the difficulty in assigning the levels measured to particular types of defects is clear. The experimental methods discussed so far all lack spatial resolution. The data gained pertains to a deformed specimen rather than to individual dislocations or segments of dislocations. In some cases the results are some sort of average of the behaviour of the different defects present, e.g. Hall effect and stationary photoconductivity. In others (EPR, DLTS, spectral photoconductivity) different defects can be measured independently, and in some cases attributed directly to the vicinity of a dislocation. However, with none of these methods is it possible to determine the electrical behaviour of a single, well characterised dislocation segment, be it of pure character, or curved. This problem is overcome

to some extent by the experiments performed to measure the mobility of individual dislocation types from which it may be possible to infer the electronic structure of each dislocation type and particularly the properties of kinks present on them. This technique is being used more and more, partly due to the development of a theory by Hirsch (1980) which described dislocation motion in terms of the electrical properties of kinks. As yet the author knows of no results obtained by this technique directly related to the energy levels at dislocations and so the technique will not be discussed here. For a full review of this subject see Lcuchet and George (1983).

The technique which should in principle be capable of accurately determining the position in the band gap of energy levels associated with segments of dislocations with a spatial resolution of ~ 1μm is scanning DLTS (SDLTS) originally proposed by Petroff and Lang (1977). SDLTS works in the same way as ordinary DLTS except that the traps at the dislocation are loaded by irradiating them with an electron beam in a SEM rather than by changing the width of the depletion region across the whole specimen. In this way it should be possible to obtain a DLTS signal only from that volume of material excited by the electron beam. The experimental difficulties associated with processing the small resulting signal have meant that as yet no SDLTS results have been gained from dislocations in silicon. Work has been performed on Cu-doped GaP, by Breitenstein and Heydenreich(1983) although as yet their sensitivity is not sufficient to investigate dislocations nor to achieve a resolution of better than ~5μm. The SDLTS technique is still at an early stage and it may be

some time before it can successfully be applied to individual deformation-induced dislocations in silicon.

A technique which is already available that allows electrical information to be gained with high spatial resolution is the electron beam induced current (EBIC) mode of an SEM. An investigation using EBIC can study the recombination mechanism of minority carriers in a volume of specimen less than $1\mu m^3$ and thus any results gained can be correlated unambiguously to the defects present in that volume. For low dislocation densities (e.g. $\lesssim 10^7$ cm^{-2}) it is possible to investigate single dislocation segments whose character is known. In this way EBIC overcomes the main problems with the electrical techniques discussed so far and is, in principle, capable of clarifying many of the questions arising from the results produced by experiments with no spatial resolution. The EBIC method has been used for many years to obtain qualitative electrical information concerning defects in semiconductors, but has only recently been used in a quantitative manner. A full description of the technique and its use in quantitative investigation is given in chapter 2.

1.4 Aims of the Project

When the EBIC technique is used to image dislocations it relies upon the recombination of carriers at the dislocation to produce contrast and so the technique may be used to investigate recombination at dislocations. It was proposed that the position of the energy level of the defect in the gap might determine the temperature dependence of the recombination and hence EBIC signal (Kimmerling et al (1977)).

In this way an EBIC investigation of defects might yield information as to their energy levels. However the difficulties inherent in the EBIC technique meant that initial temperature measurements were restricted to large decorated stacking faults where changes in the EBIC signal were sufficiently large to be measured easily (Kimmerling et al (1977)).

The first quantitative EBIC work specifically to study individual dislocations was performed at Oxford by Ourmazd et al (1977) on grown-in edge dislocations in silicon bipolar transistors. By using TEM and EBIC on the same dislocations a correlation was found between the EBIC contrast of the dislocations and the proportion of their length over which they were split into 60° partials. The larger the proportion of dissociated segments on a dislocation, the greater the EBIC contrast it produced.

Further work was performed on the same dislocations (Ourmazd and Booker (1979)) to measure the temperature dependence of the EBIC contrast. Different behaviours were found for dissociated and undissociated dislocations. These results were interpreted by Ourmazd (1981a) using a two stage model for deep level capture. Ourmazd et al (1981) continued quantitative EBIC studies of individual dislocations in Oxford by examining the straight deformation induced dislocations in specimens deformed at 850°C and 420°C by the Cologne group, and this thesis represents the further extension of that work on similar specimens. The findings of the earlier work are discussed in chapter 7 in relation to the results presented in this thesis.

It was the purpose of this project:

1) to develop the EBIC technique so that it could be used to improve the accuracy and reproducibility of measurements of EBIC contrast at individual dislocations.

2) to determine whether these EBIC measurements could then be related to the recombination efficiency of the dislocations themselves rather than other factors which also effect the EBIC signal.

3) to deduce values for the rate of recombination at individual, well characterised segments of dislocation as a function of different experimental variables. This data was then to be interpreted in terms of existing theories of recombination of carriers at dislocations so that the energy levels associated with specific defect types could be determined unambiguously for the first time.

It was intended to study specimens containing deformation induced dislocations, produced by Prof. Alexander's group in Cologne. These specimens were chosen because it is believed that the dislocations they contain approximate closest to the "ideal". However the results produced by the EBIC work performed on these specimens showed that the existing theories describing equilibrium recombination of carriers at dislocations are not applicable to the conditions normally arising in an EBIC investigation. The main reason for this is that the increased concentration of minority carriers produced by the electron beam disturbs the charge on the dislocation far from equilibrium, thus changing the temperature dependence of recombination from that which would be expected under equilibrium conditions. In order that information can be

gained about the process of recombination and the electronic properties of dislocations, it was necessary to develop a new theory which described recombination for both equilibrium and non-equilibrium conditions. This provided a good description of the observed variations in EBIC contrast and using this theory, quantitative values for some of the important parameters controlling recombination at dislocations weresuccessfully deduced.

1.5 Layout of the Thesis

The layout of the remainder of this thesis is as follows.

In Chapter 2 a description of the EBIC technique is given and various parameters affecting the EBIC contrast of dislocations are considered. The quantitative relation between the EBIC contrast of a dislocation and its strength as a recombination centre and other specimen parameters is presented.

Chapter 3 gives details of the preparation of the specimens used for this work. Details are given both of the deformation carried out by Prof. Alexander's group in Cologne and subsequent processing by the author to produce specimens suitable for EBIC. Full details are given of experimental work performed by other research groups on similar specimens.

Chapter 4 outlines the experimental requirements for an EBIC investigation of the recombination of carriers at dislocations. The system developed by the author is described including details of the computer control used and the cold stage designed and constructed for this work.

Chapter 5 is the first chapter presenting experimental

results. Here details are given of the characterisation of the electrical behaviour of the Schottky barriers and ohmic contacts used and also of the measurement of minority carrier diffusion length. From these results it is shown that the EBIC contrast may be directly related to the recombination strength of the dislocations.

Chapter 6 gives details of the quantitative measurements taken which show the variation of the dislocation contrast with temperature and with the concentration of excess minority carriers in the vicinity of the dislocation.

In Chapter 7 the problem of recombination of carriers at dislocations is considered. The treatments used by various authors are briefly discussed together with the reasons why they are inapplicable to the interpretation of EBIC experiments. The model produced by the author is presented and is related to EBIC contrast measurements. Details of the properties of screw and 60° dislocations which can then be obtained from the experimental data are given.

In Chapter 8 some of the findings of this work are discussed. Suggestions are made for improving the experimental technique further and for additional areas of study.

Chapter 2

Electron Beam Induced Current Scanning Electron Microscopy

Chapter 2 Electron Beam Induced Current Scanning Electron Microscopy

In the present work the electrical properties of individual dislocations have been studied using the Electron Beam Induced Current (EBIC) mode of a Scanning Electron Microscope (SEM). It is the purpose of this chapter to describe the principles of this technique and the way in which it may be used to study semiconductors in general and dislocations in particular. A brief review is given of work performed by other authors attempting a quantitative investigation of dislocations using EBIC.

2.1 The Principles of EBIC Microscopy

The basis of an SEM is its ability to produce a focussed probe of electrons which can be scanned across a specimen surface. The interaction of the incident electrons with the specimen can be monitored by using a suitable detector. The output from this detector is then most commonly used to control the brightness of a CRT which forms the display screen of microscope. The CRT and the electron probe are scanned in synchrony and so an image of the specimen is built up point by point on the microscope display screen. By using different types of detectors this image may contain different information about the specimen. The workings of the SEM and many of its applications are widely covered in the literature, see for example Thornton (1968) and no further details will be given here except for those pertaining to EBIC. In the EBIC mode of imaging it is the interaction of the electron beam with the specimen to produce electron hole pairs that is exploited. The detector used is a junction (p-n or Schottky barrier) which is present in the specimen together with external circuitry to

measure the current produced. The EBIC mode of the SEM allows the number of holes (or electrons) reaching the collecting junction to be measured as a function of the position of the beam on the specimen surface. The actual number detectd (collected) is dependent upon two factors. Firstly upon the number of carriers generated at the point of incidence of the beam and secondly by the proportion of these which then move through the crystal and are collected at the junction without first recombining.

2.1.1. The Excitation Of Semiconductors By Energetic Electrons

In the SEM's used to perform EBIC experiments the energy of the electrons incident on the specimen is normally in the range 3-40kV. In this range the maximum energy transmitted to an individual atom in the crystal upon scattering is insufficient to displace the atom from its position in the lattice and so modification of the crystal structure whilst under the electron beam does not occur.

A high energy electron penetrating a semiconductor slows down by a series of inelastic, small angle scattering events with valence and core electrons. These events result only in a small deviation in the path of an electron and so result in the continuous slowing down of the electrons whilst they travel in approximately straight lines. When a core or valence electron takes part in such a scattering event it aquires sufficient energy to make a transition into the conduction band leaving behind a hole in the valence bond. Thus this type of scattering event generates an electron hole pair.

Less frequently the energetic electrons undergo large angle scattering from the nucleus of an atom in the crystal. This is essentially Rutherford scattering which is elastic and caused by the Coulombic interaction between the electron and the nucleus.

These two types of scattering events result in a collimated electron beam incident on the specimen surface spreading out as the electrons penetrate the specimen and slow down. Each high energy electron leaves a trail of low energy electron hole pairs along its path. The path periodically deviating through a large angle due to an elastic scattering event.

The incident electrons acquire a velocity distribution characteristic of the lattice temperature in typically 10^{-12}s and in this time are able to travel distances of up to microns in directions determined by large angle scattering. This gives rise to the spatial distribution of the resulting electron hole pairs.

The spatial variation of the rate of generation of electron hole pairs has been widely investigated both experimentally (see for example Everhart and Hoff (1971) who use an EBIC technique) and theoretically by performing Monte Carlo calculations (see for example Shimizu and Murata (1971)). The results obtained are in good agreement and show that the distribution of carrier generation by a focussed electron beam is well described by a universal curve for electrons whose energy is in the range 5-50 kV and materials whose atomic numbers are in the range $10<Z<15$. For elements outside this range a correction must be made before the curve will apply. Figure 2.1 shows this curve.

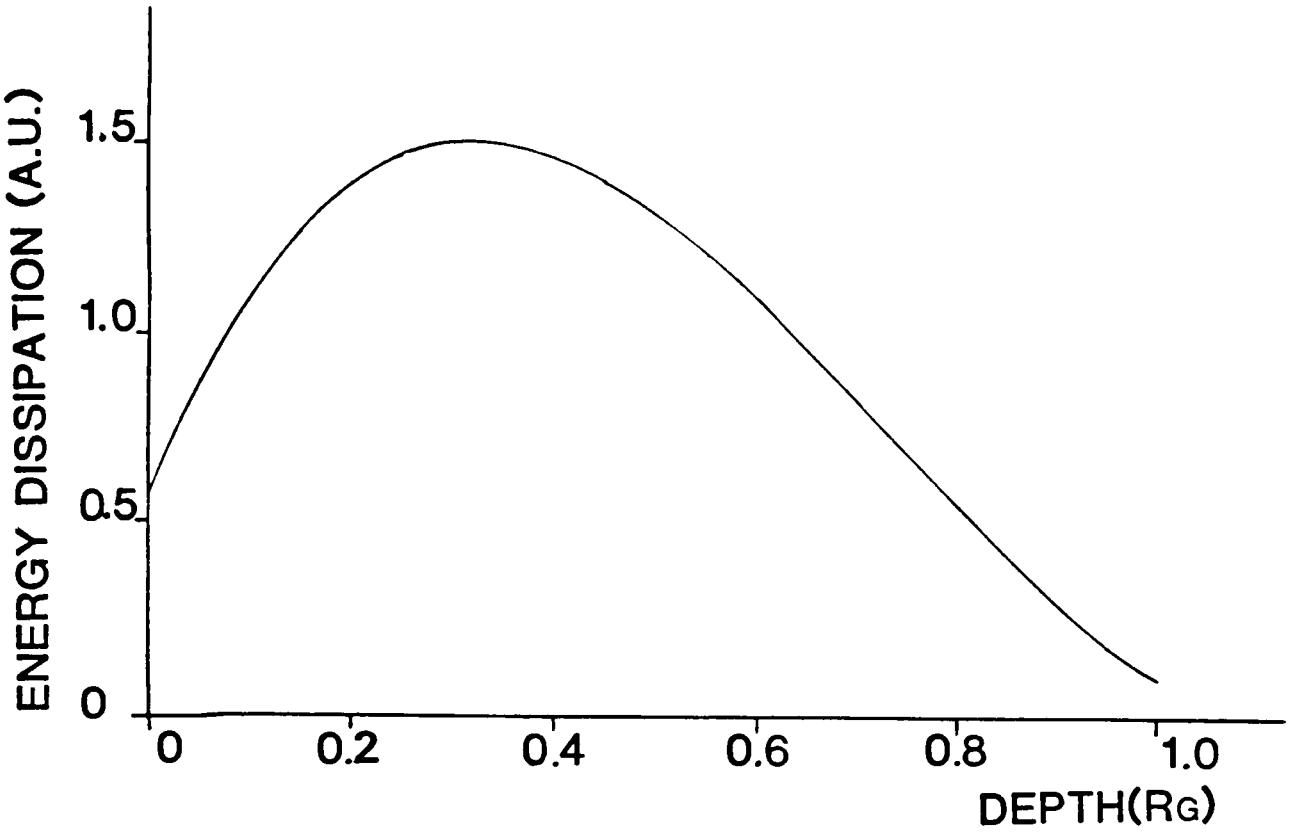


Figure 2.1 Experimentally determined generation of carriers below specimen surface

To convert distance below surface to microns multiply by $\frac{4.28 \times 10^{-6}}{\rho} \cdot E_B^{1.75}$ (After Everhart and Hoff (1971))

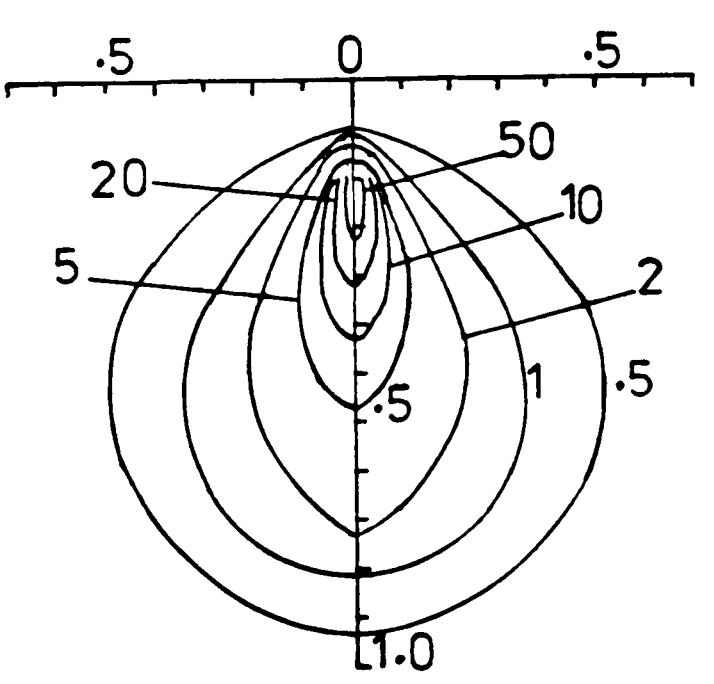


Figure 2.2 Lateral variation of the generation of carriers

Scales normalised to the Gruen range of the incident electrons. Generation rate shown by contours of equal ionisation rate. (After Cohn and Caledonia (1970)).

In order to calculate the same curve for different elements it is noted that the depth distribution varies with specimen density and also that the range, R_G, and consequently depth distribution of the generation of carriers is given by $R_G \propto E^{1.75}$. Here R_G is the Gruen range defined as the extrapolation of the linear portion of the depth generation curve to the x-axis. Thus to determine the depth distribution in microns for different beam energies and specimen densities the x-axis should be multiplied by $R_G = \frac{4.28 \times 10^{-6}}{\rho} E^{1.75}$. Everhart and Hoff (1971) have found that the depth distribution curve is well approximated by $g(Z) = 0.6 + 6.21Z - 12.40Z^2 + 5.69Z^3$ where the normalised depth Z is equal to the actual depth divided by R_G.

Figure 2.2 shows the lateral spreading of the beam which again is a universal function. This curve should also be scaled according to the beam energy used and the specimen density in order to find the actual spatial distribution of the generation of carriers in a given semiconductor.

From these curves it can be seen that carrier generation is confined to a region whose size, for the beam energies used in an SEM, is of the order of microns. This region of the crystal is termed the generation volume. Approximations are made because of the complex nature of the algebra associated with calculating the EBIC signal produced for given specimen geometry using an exact formulation of the spatial distribution of the generation of carriers. The simplest and most widely used is that generation takes place at a single point on the crystal surface where the beam is incident. This is valid

when the parameters investigated are large compared with the generation volume for example in experiments to measure long diffusion lengths, (see for example (Fuyuki and Matsunami, (1981)), or where the defect studied lies far from the edge of the generation volume, see for example the theoretical work of Pasemann (1981). A better approximation is that generation takes place uniformly within a spherical generation volume whose radius is $R_G/2$. This sphere may or may not be tangential with the specimen surface. This approximation has been used by Fuyuki et al (1980) to investigate the effect of the surface recombination velocity on the EBIC signal collected by a junction perpendicular to a surface and also by Donolato (1978). Donolato uses this approximation to calculate the contrast produced by point defects for different experimental parameters. A full description of this will be given in the following section. The total number of carrier pairs generated, per second, G is given by $G = \frac{E_{beam} I_{beam} (1-f_b)}{E_{eh}\, q}$

Where E_{beam}, I_{beam} are the beam energy and current respectively, f_b is the fraction of beam energy reflected back off the specimen and E_{eh} is the average energy required to generate an electron hole pair. This equation may be written

$$G = \frac{\eta I_{beam}}{q} \qquad [2.1]$$

where η is the number of electron hole pairs generated per incident energetic electron. For 15 kV electrons in silicon $\eta \simeq 4000$. To obtain the generation rate at a particular point in the specimen g(r), the total generation rate G, should be

multiplied by the appropriate normalised value taken from the distribution curves shown in Figure 2.2.. The fraction of beam energy reflected from the sample (f_b) is approximately 0.08 for silicon and arises mainly from the energy carried away by back scattered electrons. This energy is unavilable for pair production. The energy E_{eh} to create an electron hole pair is, in general, approximately three times the band gap energy for the semiconductor considered and is found to be 3.6 eV for silicon (Klein 1968). This value is larger than the band gap energy itself because not all the energy of the beam is dissipated in electron hole pair production. Rather some produces phonon heating and the electron hole pairs may themselves possess large amounts of kinetic energy upon creation which they subsequently lose as they come into thermal equilibrium with the lattice.

2.1.2. The Diffusion of Carriers Generated by an Electron Beam

Having considered the spatial distribution of the generation of carriers it is now required to determine their subsequent motion in order that the relation between the EBIC signal collected and the electrical properties of the specimen studied may be deduced.

The movement of electrons and holes in semiconductors is described by their diffusion coefficient D_e or D_h. In the experiments performed in this work n-type material was used and the injected carrier concentrations were small such that $\Delta p = \Delta n \ll n_o$. In this case the minority carriers diffuse as a result of any minority carrier concentration gradients and the majority carriers follow their motion such that charge

neutrality is maintained throughout the specimen with the exception of those regions of the crystal which would normally support a field (e.g. the depletion region). Momentary lack of cancellation of excess minority and majority carrier charge distribution results in a field being produced within the crystal E, and the majority carriers then drift with a velocity $v=\mu E$ in such a way as to eliminate this field. μ is the mobility of the carriers and is different for electrons and holes. In this way the majority carriers follow the motion of the minority carriers whose movement is determined by their diffusion coefficient D. Thus in the experiments performed here it is sufficient to consider only the hole concentration and diffusion coefficient.

During motion recombination of the excess carriers can occur. In n-type material where the concentration of injected minority carriers (holes) is much smaller than the concentration of majority carriers the recombination rate is, in general, proportional to the minority carrier concentration. Recombination of carriers in silicon may occur directly between the conduction and valence bands (Auger recombination) or via an intermediate state within the band gap. The probability of Auger recombination for minority carriers depends upon the square of the majority carrier concentration and is not significant except at high majority carrier concentrations. This is because there are normally sufficient deep levels present in the silicon that the recombination rate via these levels is dominant. Direct

recombination from band to band accompanied by the emission of a photon is important in direct gap semiconductors but is not normally significant in indirect material such as silicon.

In considering the mechanism by which recombination occurs via a level in the band gap it is usual to associate with the level a finite region in space such that a carrier incident on this region, called the capture cross-section σ, becomes trapped. Once the carrier is trapped a carrier of opposite type will then also make the transition to the level and recombination is complete. The rate R, at which minority carriers are trapped is given by $R = \sigma_h . N_T . v_{th} . p$ where vth is the thermal velocity of the carriers. Thus the average time a hole is free to move before trapping takes place, called the free life time τ_h, is $\tau_h = (\sigma_h N_T v_{th})^{-1}$.

In this time the carrier can move a distance $L_h = \sqrt{D_h \tau_h}$. Here D_h is called the diffusion length for holes. For high purity, low doped silicon L_h=1 cm and D_h= 12 $cm^2 s^{-1}$ at room temperature.

It is now possible to completely describe the motion of the injected carriers in the semiconduc tor specimen by using the diffusion equation. Here it is assumed that n-type material is used and that the steady state, in the bulk, is reached in a time much shorter than the length of time for which the system is observed so allowing the steady state diffusion equation to be employed. This gives for neutral material and p < n:

$$D_h \nabla^2 p(r) - \frac{1}{\tau_{(h)}} p(r) = -g(r) \qquad [2.2]$$

Where D_h is the minority carrier diffusion coefficient assumed to be independent of position.

$p(r)$ is the concentration of holes

$\tau(r)$ is the hole life time

$g(r)$ is the rate of generation of carriers

r is a vector denoting position within the specimen.

A solution of this equation with the appropriate boundary conditions would thus describe the motion of minority carriers and predict the EBIC signal collected for any specific specimen geometry. Unfortunately such solutions are difficult to obtain for all but the simplest experimental configurations and so in practice approximations must be used.

The approximations employed depend upon the specific nature of the experiment undertaken.

2.1.3. The Collection Of Injected Carriers

The EBIC signal obtained is given by the number of carriers diffusing to the collecting junction according to equation (2.2). Once they have diffused to the edge of the depletion region they experience the electric field due to the junction and the minority carriers then drift with velocity $V = \mu E$ towards the other side of the junction or towards the metal contact in the case of a Schottky barrier. The separation of holes from electrons which results gives rise to a potential at the metallic contact or across the p-n junction. This is termed the barrier electron voltaic effect (b.e.v.e) and under open circuit conditions will be such that there is no net flux of holes across the junction. The voltage so produced is termed the Electron Beam Induced Voltage

(EBIV). If however both sides of the Schottky barrier or p-n junction are joined to each other by a zero resistance connection then no potential can be sustained across the junction. In this case for every hole collected at the junction an equivalent charge will flow through the external connection and the current so produced in this circuit is the Electron Beam Induced Current (EBIC). This should not be confused with the charge in conductivity that results from the increase in free carriers due to the action of the electron beam in a manner analagous with photoconductivity. This effect now generally known as β - conductivity has been described in some of the earlier literature as Electron Beam Induced Conductivity (EBIC).

The number of holes diffusing into the depletion region in determined by the gradient of the hole concentration at the edge of the depletion region. Thus, if all the carriers reaching the edge of the depletion region are subsequently collected, the EBIC signal produced at the junction will be given by:-

$$I_{EBIC} = qD_h \iint_{z=0} \frac{\partial p(r)}{\partial z}\, dxdy \qquad [2.3]$$

Where Z = 0 at the edge of the depletion region and $\frac{\partial p(r)}{\partial z}$ is given by a solution of [2.2]. The assumption that all minority carriers reaching the edge of the depletion region will be collected is normally valid because the length of time taken for a carrier to traverse the depletion region is short. In 10^{15} cm^3 silicon it takes only 4×10^{-11}s. This is much shorter than the minority carrier lifetime as limited by most recombination processes and so recombination within the depletion region is, in most cases, highly unlikely. An

exception which has been found in the present work is that dislocations are sufficiently efficient recombination centres that carrier recombination at dislocations in the depletion region is significant. This indicates that the lifetime of a minority carrier at a dislocation is very short indeed (see Chapters 6 and 7).

2.2 The Investigation Of Defects Using EBIC

The preceeding section has shown that the EBIC signal produced by a specimen will be dependent on D_h, $\gamma(r)$, $g(r)$ and the position of the beam relative to the collecting junction according to equations [2.2] and [2.3]. The EBIC technique has been used to perform experimental investigations of all these parameters but a detailed description will only be given of those experiments directly relevant to this work. For details of other experiments the reader is referred to the review by Leamy (1982).

The investigation of defects is usually performed using a specimen of the geometry shown in Figure 2.3. In this configuration the electron beam penetrates the surface metallisation and generates carriers both in the depletion region and the neutral material underneath. Some of the minority carriers generated in the neutral material then diffuse towards the edge of the depletion region and are subsequently captured. Minority carriers initially generated in the depletion region immediately drift towards the metallic contact and are collected. The speed with which the carriers drift within the depletion region compared with that with which they diffuse in the neutral material is sufficiently large that the

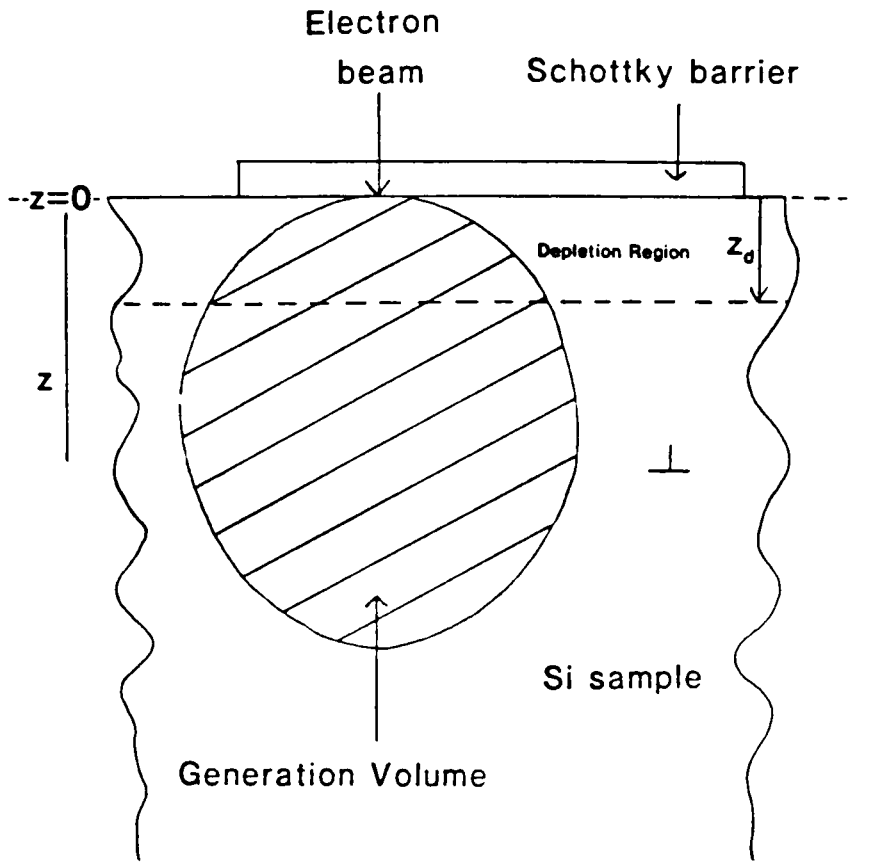


Figure 2.3 Specimen geometry for EBIC signal generation

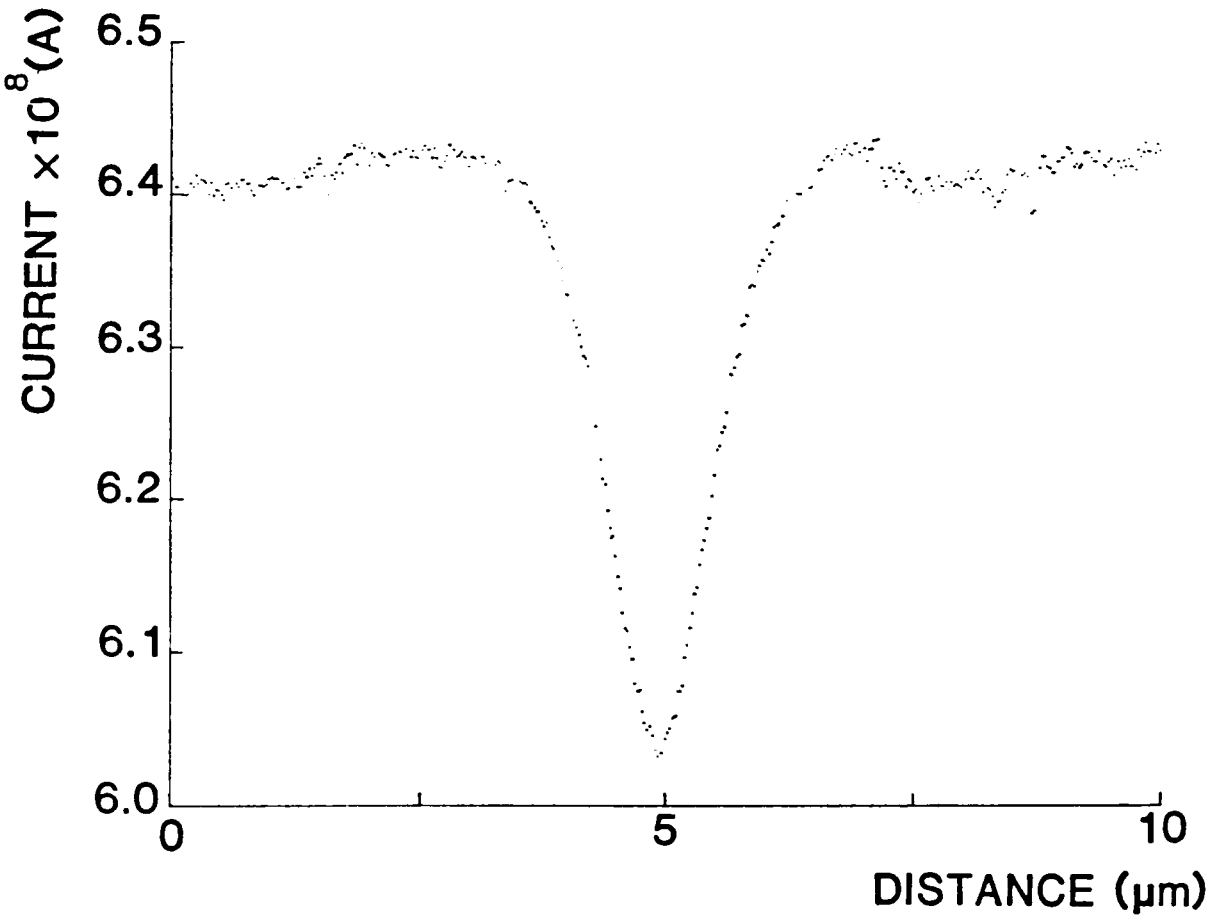


Figure 2.4 EBIC line-scan across a defect

EBIC contrast $C = \frac{I_b - I_d}{I_b}$

concentration of carriers in the depletion region is assumed to be zero when compared with the concentration in the bulk. The continuity condition that $\frac{dp(r)}{dr}$ is finite for all r then implies that $p(r)\Big|_{z=0} \simeq 0$ and this provides one of the boundary conditions used for solutions of [2.2].

When the generation volume is at or close to a region of reduced carrier lifetime the recombination of carriers is increased and so their concentration is reduced. This in turn leads to a reduction in the number diffusing to the depletion region and hence collected. Thus as the electron beam of an SEM is scanned across a defect which acts as a recombination centre the EBIC signal produced at the collecting junction (for a specimen of geometry shown in fig 2.3) will be reduced. If this signal is used to modulate the brightness of a CRT an image is produced in which the dark areas represent regions of reduced carrier lifetime . Most of the EBIC investigations of defects to date have been performed in this way. The images obtained showing the extent and distribution of defects behaving as recombination centres.

A review by Heydenreich et al (1981) gives details of work performed which correlates EBIC activity to defects present as determined by TEM and other techniques. It also includes work which relates EBIC contrast to the presence of impurities decorating defects. Briefly, the investigations performed to date indicate that all dislocations observed in low and moderately doped n-type silicon act as recombination centres and are thus imaged in EBIC. (See for example Ourmazd et al (1977), Ourmazd et al (1979), Blumtritt et al (1979)).

They also indicate that stacking faults decorated with impurities act as recombination centres (see for example Kimmerling et al (1977), Marcus et al (1977)) and that in general the greater the concentration of impurities at a defect the more efficient recombination centre it will become regardless of defect type (Menninger et al (1981) , Kittler et al (1983)).

Recently, EBIC investigations of defects have tended to become more quantitative in approach. Improvements in the SEM's available have led to microscopes which provide good resolution at low kV's with stable beam currents and electron optics which are easier to adjust for optimum imaging conditions. Advancements in external circuitry have also facilitated quantitative measurements rather than simply the production of images, for example lock-in detection, digital store, numerical analysis, are now more commonly employed. The second reason for a more quantitative aproach is the formulation of better models for EBIC signal collection so that the EBIC contrast of a defect may now be related to its strength, as a recombination centre if various other experimental parameters are known for the defect studied. This enables different defects in the same specimen and in some cases in different specimens to be compared quantitatively. The quantitative work performed can be split broadly into three sorts. In the first, quantitative measurements of the defects are made under different experimental conditions and the results then compared with the theories describing EBIC contrast of defects developed by Donolato (1978) and Pasemann

(1981). In the second set of experiments the theoretical descriptions of Donolato or Pasemann are assumed and used to determine the relative recombination efficiencies of different types of defects. The third set of measurements have been made with a view to gaining information concerning the mechanism of recombination at a dislocation and details of its electronic structure. All three types of experiments are briefly reviewed in the following.

i) Toth (1981) has performed EBIC line scans across a dislocation running perpendicular to the surface of a specimen of the geometry shown in Fig. 2.3. The signal was stored and processed digitally. The contrast and width of the dislocation line observed in EBIC was measured as a function of incident beam energy and the diffusion length in the specimen was measured using the method of Wu and Wittry (1978). The dislocation image width and contrast produced were compared with those predicted by Donolato for a specimen of similar diffusion length and were found to be in good agreement.

Sieber and Dupuy (1983) have investigated the dependence of the contrast of defects in CdTe as a function of the incident beam energy and find that defects at different depths show different variations in EBIC contrast consistent with Donolato's theory. However they record the linescans taken on a chart recorder and their accuracy is limited. As a consequence they are unable to comment on the accuracy of Donolato's theory rather only that it predicts trends which are experimentally observed.

Castaldini et al (1983) record the EBIC profile of a dislocation running parallel to the specimen surface averaging the signal over repeated scans. They compare the measured profile with that predicted theoretically and obtain an estimate of 20um for the diffusion length of the surrounding material. However the depletion region width in the specimen they investigated is ~3μm and the dislocation image width (FWHM) is ~1μm thus implying from Donolato's theory that if the dislocation lies in neutral material then it is less than 1.5μm below the specimen surface. Therefore it is likely that the dislocation investigated lies in the depletion region. This indicates that the analysis used for the exact shape of the profile is inappropriate and the subsequent estimation of a diffusion length, for a dislocation within the depletion region, ambiguous.

ii) Experiments to compare the efficiencies of recombination at various different types of defects have been performed by Kimmerling et al (1981), Ourmazd et al (1981), Ourmazd and Booker (1979), Heydenreich et al (1981) and Kittler et al (1983).

Kimmerling et al (1981) find no difference in the EBIC contrast of screw and 60° dislocations at the same depth in n-type material ($n_d=3.10^{15}cm^{-3}$) whereas Ourmazd et al (1981) studying n-type material ($n_d=10^{16}cm^{-3}$) find the ratio of the EBIC contrast of screw and 60° dislocations to be 0.81 ± 0.03 in specimens deformed at 850°C/420°C and 1.09 ± 0.01 in specimens deformed at 650°C. In addition a dependence on the chopping frequency of the electron beam which is employed for

phase sensitive detection was found (see section 1.4). These results will be discussed in more detail in Chapter 7. Ourmazd et al (1983) also investigated specimens produced by two stage deformation with the second stage stress applied along the [2 1 11] axis. This deformation produces dissociated dislocations whose constituent partials may be separated by as much as 1μm. This is sufficient to allow the individual partials to be resolved in EBIC images. An important result of this investigation is that no contrast was observed from the stacking fault between the two partials indicating that the stacking fault ribbon shows no significant activity in the n-type specimens studied.

The remaining works, Ourmazd and Booker (1979), Heydenreich et al (1981) and Kittler (1983), are all investigations correlating the EBIC contrast of individual dislocations with their type as deduced from subsequent TEM examination. Ourmazd and Booker study grown in, edge type, misfit dislocations in a silicon transistor structure and found that their efficiency as recombination centres increased with increasing dissociation into partials along their length. Here EBIC contrast was measured using a chart recorder. Kittler studied a variety of different types of grown in dislocations in epitaxial silicon and found that their contrast increased with increasing magnitude of their Burger's vector which he attributed to greater gettering capability of impurities to the dislocation core. EBIC contrast was measured photometrically from photographed EBIC images. In these experiments by Ourmazd and Booker and by Kittler et al it was a consequence of the

specimens studied that all the dislocations investigated were at the same depth and so no correction had to be made when different dislocations were compared quantitatively. However in the work of Heydenreich et al (1981) studies of dislocations at different depths is made. Their position is determined from stereoscopic analysis of HVEM images. The theory of Pasemann (1981) is then used to correct for this and so it was possible to compare dislocations at different depths. He found recombination efficiencies varying by more than a factor of two for dislocations of similar types and so concluded that in this case the recombination efficiency of the dislocations studied was mainly determined by the concentration of impurities at the dislocation rather than by the properties of the core itself (but see section 7.6.2).

iii) The remaining quantitative EBIC experiments have been performed mainly to study the mechanism of recombination and the electrical properties of defects themselves. In order to do this the EBIC contrast has been investigated as a function of the specimen temperature and in one case, Ourmazd et al (1981a), a preliminary observation of the time constant of the recombination process at dislocations has been attempted.

Kimmerling et al (1977) successfully measured the temperature dependence of an oxygen induced staking fault some 50μm in diameter and also measured the contrast from the boundary of the stacking fault. They found the latter remained constant from ~80K to ~240K; however this is unlikely to represent the behaviour of the bounding partial but rather of the large impurity concentration likely to be present there.

Ourmazd and Booker (1979) give details of the temperature dependence of grown in dislocations and Ourmazd et al (1981b) report preliminary investigations of the temperature dependence of deformation induced dislocations performed on the same specimens as those used for this work. These investigations form the basis of the present work which has produced more accurate and complete measurements. This earlier work will be discussed in chapter 7.

In summary the quantitative EBIC performed so far has shown the general features of the predictions of Donolato and Pasemann's theories to be correct without providing the sensitivity to produce a rigorous test of the accuracy of these theories. Initial work has been able to detect differences in the activity of dislocations depending both on the degree of decoration and the proportion of their length which is split into partials. There is conflicting evidence for differences between supposedly undecorated 0° and 60° dislocations. Although the temperature dependence of the EBIC contrast of defects has been measured the present work represents the most accurate investigation of clean dislocations to date.

2.3 Theory of EBIC Contrast of Defects in Semiconductors

The mechanism by which EBIC contrast arises as an electron beam is scanned across a defect which acts as a recombination centre is easy to understand (section 2.2.1) and the formulation of a mathematical description of the problem in terms of the diffusion equation [2.2] and [2.3] is also staight forward. However the solution of these equations is difficult because of the complex 3-D relation between the generation

volume, defect position and collecting junction. The most complete solution published to date for the specimen geometry of Fig 2.3 is that due to Donolato (1978) who considers a point defect recombination centre and the theory due to Pasemann (1981) who considers a defect of finite size but with slightly different specimen geometry. The results of the analysis of the mechanism of formation of EBIC contrast are important in considering the interpretation of quantitative EBIC measurements of dislocations in terms of their electrical activity. In the following the results of the theoretical treatment by Donolato and by Pasemann are considered.

Donolato (1978) produces an approximate analytical solution for equations [2.2] and [2.3] in such a way that the EBIC signal produced by a point defect is given as a function of the position of the electron beam relative to the defect, its normalised depth[1] and its recombination efficiency. The EBIC signal collected is also dependent on the minority carrier diffusion length in the bulk of the material. Subject to the approximations used the resulting solution will quantitatively describe the image of a point defect positioned arbitrarily in a specimen. By considering a dislocation to be a row of point defects this treatment may easily be extended to the case of a dislocation. In applying this analysis to the experimental results of the present work two sets of factors have to be considered. The first is the degree to which the approximations employed render the solution applicable to the experimental configuration used in these EBIC experiments and the second is the accuracy required from the detailed

1. normalised depth is the ratio of the depth of the defect to the diameter of the generation volume.

quantitative predictions to produce a useful interpretation of the results obtained.

In obtaining an analytical solution Donolato makes approximations both in the physical configuration of the specimen and the subsequent mathematical analysis. He approximates the actual experimental conditions used by assuming:

1. Semi-infinite specimen of the configuration shown in Fig. 2.3
2. The surface Schottky barrier is electron transparent.
3. The concentration of excess minority carriers is zero at the specimen surface i.e. the surface recombination velocity $v_s = \infty$.
4. The minority carrier lifetime is uniform except at the defect.
5. The generation volume is tangential to the specimen surface.
6. The depletion region width is negligible.
7. The generation of carriers takes place uniformly within a spherical generation volume.
8. The recombination centre is vanishingly small.
9. Recombination at the point defect produces only a weak perturbation of the excess minority carrier distribution.

Of these approximations 1, 2 and 3 are valid for specimens with Schottky barriers $\sim 100\text{Å}$ thick and accelerating voltages $\gtrsim 10\text{kV}$ as with the experiments performed here. Approximation 4 is also valid because the background EBIC signal from around the dislocations studied was found to be uniform indicating a uniform bulk diffusion length within that region.

The main source of the errors arising in applying the treatment due to Donolato to the experimental configuration used, is the poor approximation of the spatial generation of carriers. As can be seen from fig. 2.2, generation is not uniformly distributed within a sphere but rather the rate of generation of carriers varies by a factor of ~100 from the top of the generation volume to the bottom and by a factor of ~10 from its centre to its edges. Also the $10^{15}cm^{-3}$ specimens used contained a depletion region extending 1um below the surface. The approximation that the edge of the depletion region which defines the plane of zero excess carrier concentration is at the surface of the crystal is clearly a poor approximation for the 15kv electrons typically used whose Gruen range is 2um. Thus approximations 5, 6 and 7 are very poor and will lead to errors in the calculated EBIC signal. In particular the variation of the EBIC signal as a function of defect depth and also the profile of a defect as the electron beam is scanned across it will be inaccurate.

To overcome these difficulties Donolato (1982) has extended his calculation to include a modified Gaussian generation function. However no analytical form of the solution is available and the numerical processing required to simulate an EBIC image of a dislocation with a resolution 4k by 4k takes approximately one hour. Donolato has compared the resulting images to those obtained experimentally and finds better agreement than for calculations using a uniform, spherical generation volume. However the fit is still imperfect because the finite size of the depletion region is ignored.

Approximations 8 and 9 relate to the recombination at the defect. Here Donolato assumes the defect to have a recombination strength γ such that

$$\gamma = \frac{1}{D}\left[\frac{1}{\tau'} + \frac{1}{\tau}\right] \cdot V_d$$

where τ' is the reduced lifetime at the defect and V_d is the volume of the defect. V_d and τ' are reduced together to give a point defect recombination centre described by a delta-function of strength γ.

The approximation 9, that the recombination centre only weakly perturbs the minority carrier distribution, is valid if the dimensions of the defect are much smaller than the diffusion length of the minority carriers within it. This approximation allows Donolato to simplify the calculation of the recombination current at the defect by taking the recombination rate to be the same as that which would occur if the concentration of carriers had been undisturbed by the defect's presence. In other words, it does not allow for the actual depression in the carrier concentration around the defect caused by the recombination of carriers there. This is a first order approximation of the minority carrier distribution around the defect and yields a linear dependence of recombination rate on the defect strength γ. If this approximation, that the defect is only a weak recombination centre, is valid then approximation 8, that a defect of finite size can be represented by a point defect of equivalent strength is also valid provided that the dimensions of the real defect are sufficiently small that the carrier concentration is uniform throughout its volume. In practice approximation 9 represents conditions less likely to be met in an experiment. The validity of approximation 9 has been considered by Pasemann (1981) and will be discussed later in this section.

Subject to the approximations so far discussed Donolato solves the problem of the EBIC signal produced from a specimen containing a point defect by a Greens function solution of the relevant integral equations. The solution obtained shows the contrast to be proportional to γ and only a function of γ, L, R_G and depth d. In Donolato's calculation it is assumed that charge collection takes place at the specimen surface from which the depth of the dislocation is measured. As mentioned before there exists a finite width depletion region whose edge defines the plane of zero excess minority carrier concentration. Thus a change in the depletion region width is equivalent to a change in d in the analysis used by Donolato. For the remainder of the chapter it is assumed that maintaining d constant requires the width of the depletion region to remain constant also.

The result that the contrast is only a function of γ, L, d and R_G is central to the interpretation of the EBIC measurements made in this work. This is because it shows that if in a given experiment L, d and R_G are constant any change in the contrast of a defect in an EBIC image will be proportional to the change in the recombination efficiency of that defect. Similarly if the recombination efficiency of different defects is to be directly compared this will only be valid if the defects are observed in material of the same bulk diffusion length, at the same depth and with the same electron beam energy.

In principle the theory also accounts for variations in experimental parameters and so if these were known a number of interesting quantitative experiments could be performed by

directly comparing the EBIC contrast of different dislocations in different specimens. However it is this author's view that the errors introduced by the approximation of the spatial distribution of the generation of carriers make the exact image profile and depth dependence of the predicted contrast too unreliable to make exact quantitative comparisons worthwhile.

A comparison of dislocations in samples with different doping is particularly prone to error because the depletion region width changes from specimen to specimen thus changing the geometry of the collecting junction relative to the generation volume and defect position. However, as stated earlier, although measurements of the absolute strength of the dislocations are likely to be inaccurate the variation of the EBIC contrast for an individual dislocation will demonstrate the actual variation in its recombination efficiency provided other experimental parameters (L, d and R_G) remain constant. It is in this way that the quantitative EBIC contrast measurements obtained here have been interpreted, and in this respect the accuracy of Donolato's theory is sufficient.

Pasemann (1981) performs a similar analysis to Donolato (1978) except that he takes into account the finite size of the dislocation and its effect on the minority carrier distribution. The geometry he uses is that of a dislocation running parallel to the specimen surface much deeper than the generation volume so that the generation volume may be considered a point source. Clearly this is not directly applicable to the experiments performed here but the work does indicate the effect of approximation 9 made by Donolato.

Pasemann finds that the calculated contrast of a dislocation is reduced when higher order approximations of the minority carrier distribution are made. The exact amount of the reduction in contrast relative to that obtained by the first order approximation (as used by Donolato) is dependent both on the depth of the defect and on its strength as a recombination centre. Unfortunately Pasemann's analysis does not extend to the geometry used in this work. However it does show that the correction for a dislocation close to the collecting junction is less than that for one further away and that the correction increases with increasing recombination strength. Using his calculated data the contrast C can be written approximately as $C \propto \gamma^n$ where $n<1$ and depends on depth. For the dislocations he considered $n \simeq 0.9$. (Actually Pasemann calculated values for various normalised dislocation depths the smallest of which is equivalent to 0.7μm in the specimens studied here and it is from this data that $n \simeq 0.9$ is obtained.)

In the analysis of the results produced in this thesis the linear dependence of contrast on recombination strength is assumed because the error this introduces (compared to taking n=0.9) is small when investigating how the EBIC contrast changes with respect to experimental variables, see for example figure 6.8.

In many semiconductors plane and line defects acting as recombination centres are so efficient that the change in excess minority carrier concentration due to recombination at the defect is very large. Under such conditions the recombination rate is dependent mainly on the rate at which the

carriers can diffuse to the defects and is only weakly dependent on their recombination strength. This behaviour, which represents the limit of Pasemann's consideration of non-linear effects, is found in GaP and has been extensively studied by Wight et al (1981). In silicon the dislocations investigated act only as weak recombination centres, see above, and so the case where the contrast of dislocations is mainly diffusion limited will not be discussed.

In summary, the previous two sections have analysed the way in which EBIC contrast is produced by dislocations. The theoretical treatments of Donolato and Pasemann have been used to show that, in silicon where dislocations act as weak recombination centres, changes in their EBIC contrast are very closely proportional to changes in their recombination efficiency provided that minority carrier diffusion length, beam energy and the depth of the dislocation (including its position relative to the edge of the depletion region) remain constant.

Chapter 3

Specimen Preparation and Characterisation of the Deformation Induced Dislocations

Chapter 3 Specimen Preparation and Characterisation of the Deformation Induced Dislocations

In this chapter a description is given of the method used to fabricate the specimens examined throughout this work together with details of the dislocation structure produced. Similar specimens have been studied by other workers using different techniques and a summary of their findings is given.

3.1 Factors Influencing Specimen Selection

As chapter 1 demonstrated, there has been a great deal of effort devoted to the study of dislocations in silicon. Many different research groups have used a variety of techniques to investigate dislocations that have been produced under a variety of different experimental conditions. A large amount of data has thus been produced and there is now general agreement as to how dislocations generated at a particular temperature might respond in a given experiment. However, there has been little success in attributing the electrical activity observed to specific physical defects. It has in general been impossible to relate the results obtained to dislocations of a given character or even to a specific form of "special site," whether the "special site" be at the dislocation core (e.g. kink, jog, impurity) or in its immediate vicinity (e.g. point defect cloud, Cottrell atmosphere). The principal reason for this is that the techniques used have lacked spatial resolution. In this project the EBIC technique is used to investigate carrier recombination at dislocations with a spatial resolution of $< 1\mu m$. The EBIC technique thus has

the potential for greatly clarifying the relationship between the electrical activity of dislocations and their physical structure. The specimens investigated have been chosen because they contain dislocations which allow this potential to be realised as far as possible.

The dislocations investigated were the straight screw and 60° dislocations introduced by the two stage deformation process (850°C/420°C) described later in this chapter. The reasons why they were chosen are given below.

1. It is important that the dislocations investigated are well structurally characterised so that there can be no ambiguity as to the type of dislocation studied. The straight screw and 60° dislocations are ideal for this purpose.

2. Because the straight dislocations are so well characterised the reproducibility of the measurements can be checked quantitatively by studying different dislocations which are known to have, very closely, the same line direction and identical Burger's vectors. This process would be more difficult with curved dislocations or those of mixed character.

3. Because the quantitative use of the EBIC technique is new it is advantageous to begin with dislocations whose electrical activity is thought to be uncomplicated. This should therefore make the interpretation of the data gained as simple as possible.

4. Similar dislocations have been studied by different techniques and so it is possible to compare the results obtained using EBIC with those of other experiments.

5. The straight dislocations chosen appear to come closest

to the concept of the "ideal" dislocation considered by theoreticians (see chapter 1). Thus the results may provide an interesting test of existing theories and would ideally result in a more detailed knowledge of the core structure of dislocations.

The straight dislocations actually studied may differ from the "ideal" dislocation considered by theorists for two distinct types of reason. The first is that the "ideal" dislocation is not physically attainable because of effects which are intrinsic to the stability of or generation of dislocations. Into this category fall effects such as a surrounding point defect cloud generated by movement of the dislocation, or decoration of the core by dopant atoms during dislocation glide. The activity of kinks may be so large that the equilibrium concentration during glide which remains "frozen in" on cooling may dominate the electrical activity.[1] Into the second category fall effects which could be eliminated through better specimen preparation and experimental technique, for example contamination from the processing apparatus, curved dislocations or those which contain a large number of jogs.

Specimen preparation was such that it is believed that problems of the latter type were overcome. This means that a full programme of experiments on these dislocations would, ideally, increase our understanding of the core structure of dislocations and/or show why the "ideal" dislocation is as yet unobtainable. In either case the results obtained would be of great interest.

1. For reasons why this is not believed to be the case in specimens studied for this project see section 3.3.2.

In addition to the characteristics of the dislocations themselves there are other criteria which have to be fulfilled in order to make a useful quantitative EBIC investigation of individual dislocations possible. These are outlined below:

1. The specimen should be doped to a level which allows production of a satisfactory Schottky barrier.

2. The dislocation density should be sufficiently low so that the EBIC contrast of an individual dislocation segment can be accurately measured without being influenced by the effect of adjacent dislocations.

3. The host material should be sufficiently clean and uniform to ensure that its properties do not interfere with those of the defect being studied.

4. It should be possible to structurally characterise each dislocation studied.

5. Wherever possible extended defects should run parallel to the specimen surface.

These requirements and the way in which they were met by the specimens used is discussed below. The specimens used throughout this work were float zone, phosphorus doped Si containing networks of deformation induced dislocations.

Two different doping levels, $10^{15}Pcm^{-3}$ and $10^{16}Pcm^{-3}$ were used, both allowing satisfactory Schottky barriers to be made. if the doping level is high (greater than $\sim 10^{17}Pcm^{-3}$) then the fabrication of good Schottky barriers becomes more difficult and an increase in the level of noise in the EBIC signal is produced thus making quantitative measurements more difficult. Also at higher dopant concentrations there is more likely to be segregation of dopant atoms towards a dislocation which may mask or alter the true behaviour of the defect.

It is not possible to use low doping levels either. For example if the dopant concentration is $\sim 5.10^{13} Pcm^{-3}$ then the depletion region produced under an unbiased Schottky barrier is 5um wide making it necessary to use accelerating voltages greater than 30kV to image defects in the neutral material. At these accelerating voltages the spatial resolution of the EBIC technique is seriously reduced thus making very low defect densities necessary if individual defects are to be resolved. If the doping level is reduced below $\sim 10^{13} Pcm^{-3}$ then the depletion region width becomes too large (>10μm) to be penetrated by the accelerating voltages available on most SEM's. This imposes a lower limit to the doping level in Si on which a Schottky barrier may be fabricated which has the properties which would allow an EBIC study of dislocations in neutral material to be made.

It is this author's view that wherever material constraints allow, surface Schottky barriers should be used in preference to p-n junctions for the EBIC investigation of dislocations. The reason for this is that the preparation of a p-n junction requires higher temperatures than those for producing Schottky barriers. Thus if a p-n junction is fabricated on material already containing defects it is more likely that processing will induce segregation of dopant to the dislocations. If on the other hand the defects are introduced after the fabrication of the junction, which will be at the surface of the specimen, then the defects studied will be introduced into that region of material whose cleanliness is most in doubt. These difficulties can be overcome by Schottky barriers as will be shown later.

The defects studied in this work are screw and 60° dislocations which were produced by plastic deformation of a Si ingot. The total strain produced was kept small (<0.3%) so that the resulting dislocation density is low. There are thus areas in each crystal, between slip bands, where the distance between neighbouring dislocations is greater than ~5μm. Accelerating voltages of 15kV or less were used to study the dislocations giving an EBIC resolution of approxima tely 2μm (see description of EBIC method given in chapter 2) and this allowed individual defects to be studied in accordance with criterion 2.

The starting material was high quality Wacker, float zone, Si and every attempt was made to maintain cleanliness throughout all stages of specimen production. The extent to which this was achieved is discussed in section 3.4.

Criteria 4 and 5 require that the structural properties of the individual defects studied be known and that extended defects, such as dislocations, lie parallel to the surface of the crystal. TEM studies by Wessel and Alexander (1977) have shown that the dislocations produced in Si by the deformation treatment used for this work lie accurately on only one set of (111) planes. Thus it is possible to ensure that the dislocations lie parallel to the specimen surface by cutting the deformed ingot into slices whose surfaces are parallel to the (111) planes. The Schottky barrier is then prepared on one of these surfaces. It is advantageous for the defects to run parallel to the surface because, as Chapter 2 has shown, EBIC contrast is a function of the distance beneath the barrier of the dislocation being studied. Thus the contrast of an inclined dislocation will vary along its length making accurate reproducibility of results difficult.

The work by Wessel and Alexander (1977) and others e.g. Ourmazd et al (1983a) shows that in these specimens structural information can be reliably obtained simply by inspection of the line direction of a dislocation (see section 3.3.1). Thus criterion 4 is met without the need for an independent TEM examination of each dislocation investigated.

3.2 Specimen Preparation

Specimens are prepared in two stages, the first step, which is the deformation, is kindly carried out by Prof. H. Alexander's group at Cologne University. In the second, performed by the author, EBIC specimens suitable for study in an SEM are fabricated from the deformed Si.

3.2.1 Deformation Procedure

The as-received, phosphorus doped, float zone Si[1] is cut into square based prisms elongated along a [213] direction. All faces are polished to a mirror finish and aligned parallel to within ½° of the crystal planes $(5\bar{4}\bar{1})$, (111), $(\bar{1}\bar{2}3)$. Any surface irregularity or faces which are non-parallel give rise to stress concentrators which result in the crystal shattering during deformation. The specimens are deformed in compression along the [213] axis in a specially prepared jig. The earlier specimens were deformed in a jig using stainless steel chucks and the other using quartz chucks. No difference in the EBIC behaviour of the different specimens was evident when studied using the same EBIC system.

1. Wacker Chemitronic oxygen and carbon below IR detection limit.

The deformation is carried out as a two stage process in an argon atmosphere. Initially the sample is heated to 850°C and a low stress (15MPa) is applied to nucleate a number of dislocations. Only one slip system is activated, that with the highest Schmidt factor. The dislocations virtually all lie in the (111) plane and have Burger's vector $a/2[1\bar{1}0]$. Only a small amount of strain is introduced at this stage to keep the resulting dislocation density low. For the next part of the process the specimens are cooled to 420°C and the stress is increased to 300MPa and held for approximately 45 minutes. Under these conditions few new dislocations are nucleated but the existing loops grow outward along the (111) planes relieving the stress and in turn becoming accurately aligned along the $\langle 1\bar{1}0 \rangle$ directions. This produces hexagonal loops with diameters of up to 100μm. The specimens are then cooled to 50°C under load so retaining the dislocation morphology. The deformed ingots are sliced along (111) planes into wafers measuring approximately 3 x 4 x .5mm, one side of which is cut parallel to the Burgers vector of the induced dislocations as a reference.

3.2.2 Fabrication of Schottky Barriers

The remaining procedures required to fabricate EBIC specimens were carried out by the author in Oxford.

The wafers were mechanically polished using diamond pastes until a 1μm finish was achieved. Mechanical damage at the surface of the specimen was then removed by chemical polishing with "Syton" (colloidal silica). The specimen surface was periodically checked under an optical microscope and polishing was continued for at least one hour after all

traces of the 1μm scratches had disappeared. The specimen surface was then cleaned before the application of the Schottky barrier. Throughout the following procedure the utmost care was taken to maintain cleanliness of all the equipment used if satisfactory barriers were to be produced.

The following steps, which were devised by Dr. A. Ourmazd and the author were taken:

1. Boil in methanol for 10 minutes
2. Boil in trichloroethylene for 10 minutes
3. Repeat steps 1 and 2
4. Rinse for 10 minutes in $6H_2O:1H_2O_2:1HCl$
5. Rinse in deionised water
6. Rinse for 10 minutes in $6H_2O:1H_2O:1NH_3$
7. Rinse in deionised water
8. Leave under methanol until ready for metallisation; this should be less than 10 minutes
9. Rinse for 20 seconds in $15H_2O:1HF$
10. Rinse for 5 seconds in methanol
11. Place in the evaporator and evacuate chamber immediately

The filament and metal wire used for evaporation, tweezers and the glass disc on which the specimen is placed during evaporation undergo steps 1 to 3. In addition the filament was heated to white heat under vacuum before being loaded. The wire for metallisation was rinsed in 40% HF for 20s before being placed in the filament. $\sim$ 5mg of wire are evaporated from $\sim$ 4cm above the specimen surface (see fig. 3.1) For the n-type Si used in this work, Au-20% Pd was used to make the barriers. The evaporator used was able to pump down to 4.10^{-5} Torr in approximately 10 minutes and once this pressure

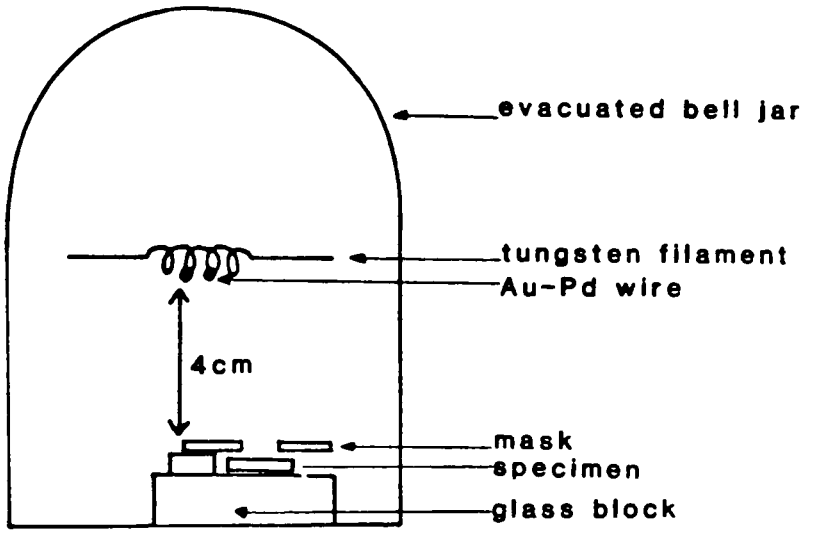


Figure 3.1 The arrangement for evaporating the Schottky barrier metallisation

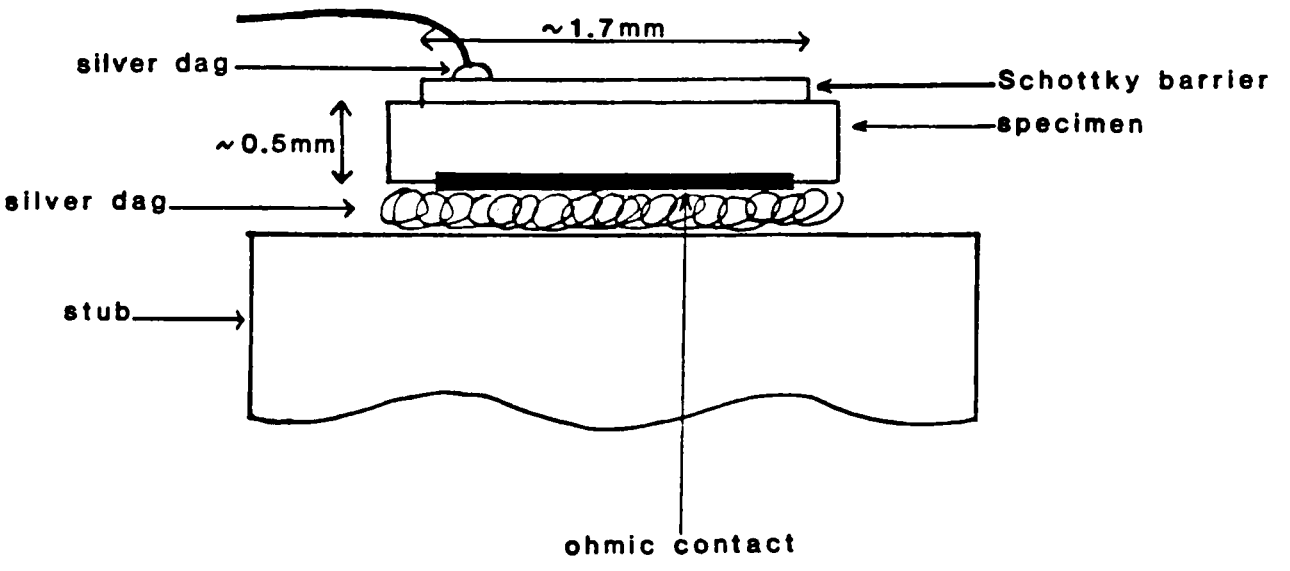


Figure 3.2 Schematic diagram of a completed Schottky barrier EBIC specimen

was attained the Au-Pd was evaporated on to the surface of the Si through a mask positioned above the specimen. This produced a square Schottky barrier of ~3mm^2 and ~100Å thick. During evaporation, which lasted ~10s, the specimen temperature did not rise above 100°C. The mask was positioned so that the Schottky barrier produced was in the middle of the specimen surface. In this way the dislocations examined are those which were close to the centre of the ingot during deformation. This together with the minimal temperature rise during evaporation helps to ensure that the dislocations examined are uncontaminated.

To provide an EBIC specimen suitable for examination in an SEM it is necessary to prepare an ohmic contact on the rear face of the specimen and to mount it on an SEM stub making the required electrical connections. Details of the microscope stub and connections may be found in section 4.4.1. To make the ohmic contact, the rear face of the specimen was roughened and on to it a mixture of gold and antimony was evaporated. This was performed in a different evaporator to that used for Schottky barrier production, so eliminating any risk of contamination. Evaporation was again through a mask, this time touching the specimen surface, which thus reduces the possibility of antimony reaching the Schottky barrier.

A diagram of the completed EBIC specimen may be found in fig. 3.2.

Table 3.1 gives details of the experiments which were performed on each specimen. All specimens having the same first four digits originate from the same ingot as deformed in

Cologne. All specimens were produced using the techniques described in this chapter. Data from experiments marked with an asterisk is presented in this thesis.

Table 3.1

Specimen	Doping, cm^{-3}	Experiments
3509/2	10^{15}	* Temperature dependence of contrast (T-dependence) * Beam current dependence of contrast (I_{beam}-dependence) * Frequency dependence of contrast (F-dependence) * Screw/60° comparison * Ratio of measured signal to beam current I_m/I_{beam}) * Diffusion length measurements
3502/3	10^{15}	* Diffusion length measurements T-dependence F-dependence
3502/2	10^{15}	T-dependence
2722/1	10^{16}	* F-dependence * Screw/60° comparison * Series resistance dependence of measured current
2711/4	10^{16}	F-dependence
2711/3	10^{16}	* F-dependence * I-V characteristics using the computer T-dependence
2711/2	10^{16}	T-dependence F-dependence

Table 3.1 Summary of specimens used for each experiment. Those marked with an asterisk appear in this thesis.

3.3 Characterisation of similar specimens by different authors

The network of dislocations produced by the deformation procedure outlined in section 3.2.1 is well suited for investigation in several ways. Many workers have therefore undertaken investigations on identical specimens and their findings are relevant to this work and will be outlined below.

3.3.1 Structural Characterisation

Wessel and Alexander (1977) using TEM showed the dislocation network produced by the compressive deformation procedure to consist of planar hexagonal loops lying on parallel (111) planes. The separation between loops perpendicular to the (111) planes being 0.3μm. All dislocations are characterised by a single Burgers vector $a/2[1\bar{1}0]$ and are accurately aligned along the $\langle 1\bar{1}0\rangle$ directions. Thus as a dislocation changes its line direction from $[1\bar{1}0]$ to $[01\bar{1}]$ or $[10\bar{1}]$ it changes its character from screw to 60°. This is very important for the EBIC work undertaken because it means that the dislocation type can be deduced simply by observing on the EBIC image whether the dislocation runs parallel to the side of the specimen cut along the $[1\bar{1}0]$ direction. By this means dislocation type can be inferred whilst the specimen is in the SEM without recourse to other techniques.

Weak beam TEM work by Gottshalk (1979) showed the dislocations to be dissociated into Schockley partials $(a/6\langle 121\rangle)$ with very few points of constriction. This work

also demonstrated that the spacing of the partials is different from that at equilibrium (~50Å). The partial spacing measured are those assumed during the motion of the dislocation on deformation which are then held as the specimen is cooled under load. The partial separation can be increased further by deforming along [2 1 11] and in these specimens, not studied here, Gottshalk has recorded separations of ~2000A.

3.3.2 Electrical Characterisation of the Dislocations

Some of the results of the experiments to determine the electrical properties of dislocations were given in chapter 1. In that chapter much of the work performed on the deformed (850°C/420°C) specimens studied for this project was described and so only a brief summary will be given here. However a more detailed discussion of points relevant specifically to the 850°C/420°C specimens will be given.

EPR studies by Weber and Alexander (1983) show that undoped (850°C/420°C) specimens contain no EPR centres and when doped with phosphorus only the Si-K7 centre. DLTS measurements also made by Weber and Alexander (1983) show the existence of four DLTS lines E(0.19), E(0.29), H(0.35) and a very broad line E(~0.4). The latter two lines are found in all specimens containing deformation induced dislocations.

Weber correlates the E(0.19) and E(0.29) DLTS lines with the Si-K7 EPR centre because both the EPR and DLTS centres are found in n-type specimens that have been deformed at 650°C or at 850°C and then 420°C. He further attributes the Si-K7 EPR centre to phosphorus atoms at the dislocation core. His

reasons for this are as follows. The centre has been observed in all n-type material (phosphorus doped), containing dislocations, it disappears in p-type or undoped material. The form of the g-tensor is similar to that of the Si-G24 centre which is known to be a vacancy-antimony complex.

The ~0.4eV trap detected by DLTS in all specimens has been tentatively ascribed by Patel and Kimmerling (1981) to kinks on the dislocation line. Although there is no direct evidence to support or disprove this suggestion, the photoluminescence results of Suezawa et al (1983) indicate that kinks may not be the cause. Suezawa has shown that specimens deformed at 650°C produce the characteristic D-series of lines. Specimens deformed at 850°C and 420°C show the D1 and D2 lines to be absent. These lines reappear only on annealing. Upon annealing the straight dislocations become curved and this together with the behaviour of the lines at low temperature under the application of stress has led Suezawa to postulate that the D1 and D2 lines may be due to kinks on the dislocation. If Suezawa is correct then this would indicate that kinks on dislocations in the 850°C/420°C specimens contribute very little to their electrical activity in comparison with kinks on dislocations in the 650°C specimens. The E(0.4) DLTS centre is however found in both types of specimens.

Suezawa et al (1983) also find a photoluminescence line at 1.01eV in the 850°C/420°C specimens. This line becomes stronger in specimens deformed along a [2 1 11] axis which then contain a high density of wide stacking faults and so it

is attributed to the stacking fault between partial dislocations. This suggests that the stacking fault introduces a level into the gap either 0.15eV above the valence band or 0.15eV below the conduction band.

3.4 Impurities at the Core of Dislocations

It is clear that to be sure the electrical properties of the dislocations studied are due to the properties of the dislocations themselves every effort must be made to ensure that impurities are not introduced which may decorate them.[1] Instrumental neutron activation analysis has been used to test the concentration of 44 elements present as impurities in the FZ silicon both before and after deformation (Riotte et al (1977)). The results showed no significant increase in the concentration of impurities after deformation. In the subsequent processing, used to prepare a Schottky barrier, the specimen is kept meticulously clean and the temperature is never higher than 100°C. With these conditions it is highly unlikely that any impurities will be introduced into the Si. It is possible however that during the deformation process the dislocation accumulates oxygen or other light elements. There is not firm evidence as yet that this is the case and it will not be discussed further.

Once the EBIC specimen has been made, the dislocations which are studied are those which lie close to the surface, i.e. outside the depletion region, and within the range of the electron beam at 15kV. It is important to establish whether gold diffusing from the Schottky barrier might, within the

1. For a discussion of the evidence for dopant atoms at the core of dislocations, see previous section.

lifetime of a specimen, decorate the dislocations studied. Unfortunately there is very little data available for the room temperature diffusion coefficient of gold because it is so small that it is difficult to measure directly. However Pearton et al (1982) have studied the diffusion of gold by the interstitial controlled dissociative mechanism. This proceeds via an (Au_i V_{si}) complex which is negatively charged in p-type material and neutral in n-type. They have looked at the motion of the charged centre in the presence of an electric field by monitoring the concentration profile of gold in a reverse biased diode using DLTS over a period of days. From this data they calculate a diffusion coefficient for gold in silicon where no field is present.

This analysis gives a value for D, the diffusion coefficient, of $2.0 \pm 0.8 \times 10^{-16} cm^2 s^{-1}$. The extrapolated value from conventional data is within an order of magnitude of this ($D \sim 6 \times 10^{-17} cm^2 s^{-1}$). Obviously if this result is to be applied to the situation in the EBIC specimens, a number of assumptions must be made. Firstly, as Pearson notes, the high fields used in his experiments are assumed not to change the charge state of the defect or its mechanism of diffusion. If they do not then his results may be applied to the interstitial controlled dissociative mechanism in neutral p-type material. Second it must be assumed that the diffusion coefficient is the same for the charged centre in p-type material as for the uncharged centre in n-type and finally that this mechanism is in fact controlling diffusion of gold in n-type material at room temperature.

In the absence of other data the value of $D=2.8 \times 10^{-16}$ cm^2s^{-1} will be taken as an upper estimate. Using this and substituting into the equation $x^2 \simeq Dt$ with $x=1.0\mu m$ gives a value for t of 350 days, which is applicable to the $10^{15}cm^{-3}$ material. Taking $x \simeq 0.3\mu m$ gives $t \sim 35$ days which is applicable for 10^{16} material with the narrower depletion region. The $10^{15}cm^{-3}$ specimens were used for measurements over a period of about 100 days and the 10^{16} cm^{-3} over a period of about 10 days, so given that the assumptions used above are valid, bulk diffusion of gold does not give rise to decoration of the dislocations.

It has been noted, however, that diffusion along a dislocation core may be much faster than through the bulk. Mimkes (1979) for example states that pipe diffusion may be as much as 1000 times greater, so it is also necessary to consider the situation where gold diffusing along the dislocations is responsible for their decoration.

The dislocations examined in the present work are inclined to the specimen surface at an angle of at most a few degrees. Thus the gold would have to diffuse a distance of $\sim 10\mu m$ along the dislocation in 10^{15} cm^{-3} material and $\sim 3\mu m$ in 10^{16} cm^{-3} before it reached a depth where the dislocation is studied. Fitting these values and $D=3 \times 10^{-13}$ cm^2s^{-1} into $x^2 \simeq Dt$ gives $t \sim 35$ days for the 10^{15} cm^{-3} specimens and $t \sim 3.5$ days for the 10^{16} cm^{-3} doped specimens. These values are well within the time during which the dislocations were studied.

Rough calculation has shown, therefore, that it is possible that gold may be decorating the dislocations but the accuracy of the data available makes it impossible to say with any certainty. The EBIC results that were obtained show no change in the level of EBIC contrast from the defects studied during the period of their examination. This effect indicates that if any gold is present it is not electrically active unless the diffusion process is so quick that the dislocations are completely decorated prior to initial observation and thereafter no change takes place.

The surface Au-Schottky barrier geometry is also used in DLTS studies of similar specimens. In this technique it is possible to study the behaviour of dislocations up to a depth of 5μm. To the author's knowledge no work has been performed which shows the dislocations to have different defect states at different depths. This again indicates that gold is unlikely to be decorating the dislocations. It is, however, the author's view that further studies should be made to be completely certain about this question.

Chapter 4

The EBIC System

Chapter 4 The EBIC System

Initial work on this project was performed using an EBIC system installed on a J.S.M. 35-X SEM. This system underwent various stages of development; however it was only with the introduction of the more sophisticated system based around a Philips 505, which is described in this chapter, that the accuracy and reproducibility of results was such that the correct variation of EBIC contrast with beam current and temperature could be established. The results presented in Chapters 5 and 6 were gained using this equipment. It is believed that this system provides better sensistivity, accuracy and flexibility than any used hitherto.

4.1 General Requirements for a Quantitative EBIC System

4.1.1 Spatial Resolution

In EBIC the spatial resolution is principally determined by the size of the generation volume (Chi and Gatos (1979)) and the incident electron probe diameter. In the standard operating conditions of accelerating voltage and beam current used when the microscope is operating in the secondary electron mode, the generation volume is much larger than the probe size which therefore does not limit resolution. However to improve EBIC resolution it may be necessary to lower the accelerating voltage to as little as 4 or 5kV in order that the generation volume is sufficiently small. In addition, if the EBIC sensitivity is low or an experiment is being performed which requires large beam currents, then the probe current may have to be of the order of 10^{-9}A.

The Philips 505 possesed excellent electron optics and used a high brightness LaB_6 gun. When properly adjusted the probe diameter was found not to significantly effect the EBIC resolution at 5kV.

4.1.2 Sensitivity

For many EBIC experiments it is necessary to use very small incident electron beam currents if a full description of the behaviour of a defect is to be obtained. (see Chapter 7) In practice this requires using beam currents of a few 10^{-12}A or less which result in a total EBIC current of 10^{-8}A. This small signal is usually generated at a very noisy Schottky barrier and it is the poor signal-to-noise ratio that chiefly limits sensitivity. The barrier itself produces large amounts of noise because, by the nature of the investigation, the depletion region is threaded by a large concentration of dislocations which act as generation-recombination centres and surface states are present at the metal silicon interface which also produce noise.

4.1.3 Temperature Control

To study the behaviour of dislocations fully it is necessary to monitor their recombination efficiency as a function of temperature. The cold stage developed for this work, had a working range of 115-400K. Obviously if the range were extended other phenomena of recombination at dislocations may be detected, but this range was found sufficient to gain some understanding of the process of recombination at dislocations.

A problem with performing EBIC experiments at low temperatures is that residual gases and organic material will tend to condense onto the surface of the specimen. Under the action of the electron beam it is thought that the organic molecules polymerise and consequently do not re-evaporate. An EBIC experiment entails repeated line scans on the same part of the specimen surface and if the vacuum is not "clean" contamination will form along the scanned area. Measuring the induced current with ~0.1% accuracy and using relatively low accelerating voltages means EBIC is particulary susceptible to this problem and so great care was taken not to introduce materials into the vacuum that may induce this behaviour.

4.1.4 Reproducibility

In practice the contrast produced by a dislocation is not totally uniform along its length. This may be due to the dislocation not running exactly parallel to the surface, or variations in the thickness of the metalisation or depletion region.

This spatial variation of EBIC contrast means that when performing an experiment it is necessary to scan the same region of the dislocation for each measurement. This presents no difficulty if measurements are to be made at a constant temperature, however during some experiments the specimen temperature is changed by ~250K. Drift both parallel and perpendicular to the plane of the specimen is inevitable as parts of the stage expand and contract. Thus the mechanical stability of the stage plays an important role in achieving reproducible measurements. With the cold stage used for this work it was possible to scan the required section of dislocation to within 0.5μm after 1 min at the required

temperature.

To obtain reproducible results the performance of the microscope should be such that a stable electron probe is produced. Obviously any change in focus or astigmatism between readings would introduce inaccuracy into a contrast measurement and for this reason the beam was refocussed immediately prior to each scan. Drift of focus in the course of a measurement, usually 30s, was negligible. More difficult to control, and in the case of these experiments a limit to the ultimate sensitivity, was drift in the beam current due to filament instability. As the beam current is reduced so is the signal-to-noise ratio. If the signal is to be extracted from the noise, by whatever technique, the integration time for each data point must be increased to reduce the noise. For a given number of data points on each scan this implies that each scan takes longer. If the beam current drifts between measuring the induced current at the dislocation and the background, from which the contrast is calculated, then the meaurement will be in error. It was found that with the LaB_6 filament used in the Philips 505, the maximum duration of scan before drift significantly reduced reproducibility was ~4 seconds. This in turn imposed an upper limit on the amount of signal averaging that could be used to reduce noise and so improve sensitivity.

4.2 System Description

The EBIC system developed for this work is distinguished from those more commonly used (Leamy 1982) by the method employed for signal processing and by on-line computer control

and data collection. Full details of the system are given below.

4.2.1 The Microscope

The SEM used for this work was a Philips 505 that had undergone various modifications. The electron-optics were very stable and the design was such that accelerating voltages and beam currents could be altered with a minimum of realignment and adjustment of the microscope controls. The resolution of the microscope in secondary electron mode was better than 20nm. The electron source was a high brightness LaB_6 gun enabling beam currents of 2.10^{-9}A into a 0.1μm probe at 15kV to be achieved.

The main specimen chamber was evacuated using an Edwards "Diffstack" diffusion pump and periodically it was "baked" under vacuum so producing a very clean vacuum at the specimen of 4.10^{-7}Torr. Contamination, which had been a problem on an earlier system using a standard diffusion pump, was virtually eliminated for the experimental conditions used. This led to a great improvement in the efficiency with which microscope time could be used and was crucial to the success of the high beam current, low temperature experiments.

The microscope was modified to have a beam chopping unit installed. The Lintech system used had a risetime, measured at the specimen, of 0.5nS which was much faster than that necessary for signal processing. A cold stage was installed - see section 4.4.

The scan system used on the microscope was found to have insufficient flexibility and so was modified to give a variable selected area scan facility. This could also be used

to generate variable length line scans whose position could be easily adjusted to make an EBIC contrast measurement of a particular dislocation segment.

4.2.2 Signal Processing

As mentioned earlier, the generation of high spatial resolution, low excitation regime EBIC data generally implies very low EBIC signal intensities. In order that the EBIC signal could be recovered from the noise present in the system a process of phase sensitive detection was used.

The phase sensitive (or lock-in) detection technique, which is widely used in a variety of systems, relies on encoding the signal, which can then be distinguished from the background noise by the so-called phase-sensitive detector (PSD). The signal is encoded by the modulation of the source intensity; thus in the case of EBIC, the incident electron beam is repetitively chopped. The PSD is given the chopping or modulation frequency as a reference and is thus able to select the encoded signal from the background noise. It does this by behaving as a variable gain amplifier controlled by the reference signal so that only that part of the signal in phase with the reference is amplified whilst the out of phase noise component is rejected.

If the bandwidth of the amplifier response is defined in terms of an equivalent flat topped, vertical sided bandpass filter centred at the reference frequency, then its width f is given by $f \simeq \frac{1}{4T}$ Hz where T is the time constant of the low pass filter used to average the output of the modulated gain amplifier. The bandwidth is independent of reference frequency and for white noise it can be seen that output noise

is determined by the time constant of the signal averaging.

A normal amplifier also has a certain bandwidth which is determined by its risetime but, in contrast to a lock-in amplifier, this is centred near zero frequency. In the EBIC set-up used the low frequency noise component is very large, thus requiring the risetime of a normal amplifier to be prohibitively large for small signal EBIC experiments. The low frequency noise is caused principally by mains interference and the imperfect nature of the Schottky barriers which have an area of several square millimetres containing a high density of surface states which contribute to "1/f" noise. (Fraser (1979)). Generation-recombination and leakage currents due to dislocations throughout the entire depletion region of the barrier also generate large noise signals. The noise present falls considerably from ~10Hz to 1kHz and then reduces more slowly up to 20kHz. Best results are achieved by using a reference frequency for phase sensitive detection at a point in the noise spectrum where the noise present is small. For most experiments 10kHz was used providing excellent filtering of the dominant low frequency noise components, whilst not requiring too large a bandwidth for the preamplifier.

As mentioned earlier it is the electrical and mechanical stability of the microscope which determine the maximum length of time which may be taken for a single line scan of a dislocation whilst producing accurate measurements. The actual duration of each scan used in most experiments was 2s thus allowing an integration time of 30ms to be employed without the risetime of the amplifier affecting the

value of the EBIC contrast measurements. This gave a bandwidth of ~8Hz thus reducing noise to a level far below that obtainable by normal amplifiers. If the risetime was increased above 30mS then in some cases the EBIC contrast, was noticeably "smoothed" by the signal averaging so reducing the value of contrast that would be measured. For each dislocation measured it was checked that the risetime of the amplifier was not affecting the contrast recorded. The use of a Keithley 427A, current amplifier of similar risetime was found to reduce the signal-to-noise ratio by more than 15dB, compared with a phase sensitive detector.

In addition to the improvement in the accuracy of EBIC measurements produced by reducing the level of noise present in the signal, further improvements were gained by averaging the measurements obtained. This was achieved by recording under the same conditions three consecutive scans and averaging the contrast calculated from each one. Obviously the more scans used the better the accuracy of measurement that would have been obtained. However, there was insufficient computer memory available to allow more than three scans to be made for each measurement.

Initial amplification of the EBIC signal was performed using a preamplifier placed inside the microscope close to the specimen. In this way the length of leads carrying the small unamplified EBIC signal was kept short and wholly contained within the microscope, thus reducing pick up of noise from external sources.

The current preamplifier used a single, low noise, high gain-bandwidth product op-amp to provide a gain of 10^5 in a single stage with a bandwidth of 100kHz. See diagram 4.1. The preamplifier could be switched out of circuit using a reed relay if accurate measurements of absolute signal level were to be made.

4.2.3 System Layout

The overall layout of the system is shown in diagram 4.2. In order that the lock-in amplifier could be interfaced to the microscope and computer two modifications were made. The first provided an auxilliary output, buffered to match the input impedance of the video channel on the microscope. The second provided an output voltage proportional to the offset applied to the input signal within the amplifier; this was then read by the computer to enable it to calculate contrast values from the signal produced by the PSD.

4.3 Computerisation Of The EBIC System

Computerisation of the EBIC system, which was originally suggested by Ourmazd, allowed high accuracy EBIC contrast measurements to be produced with relative ease and gave a good deal of flexibility to the operater as to which experiments to perform and how. It is arguable that the results produced here could have been obtained without the use of the computer. But it is this author's view that the time and effort required to achieve the optimum conditions necessary to gain data of the same accuracy using, for example, a chart recorder, whilst

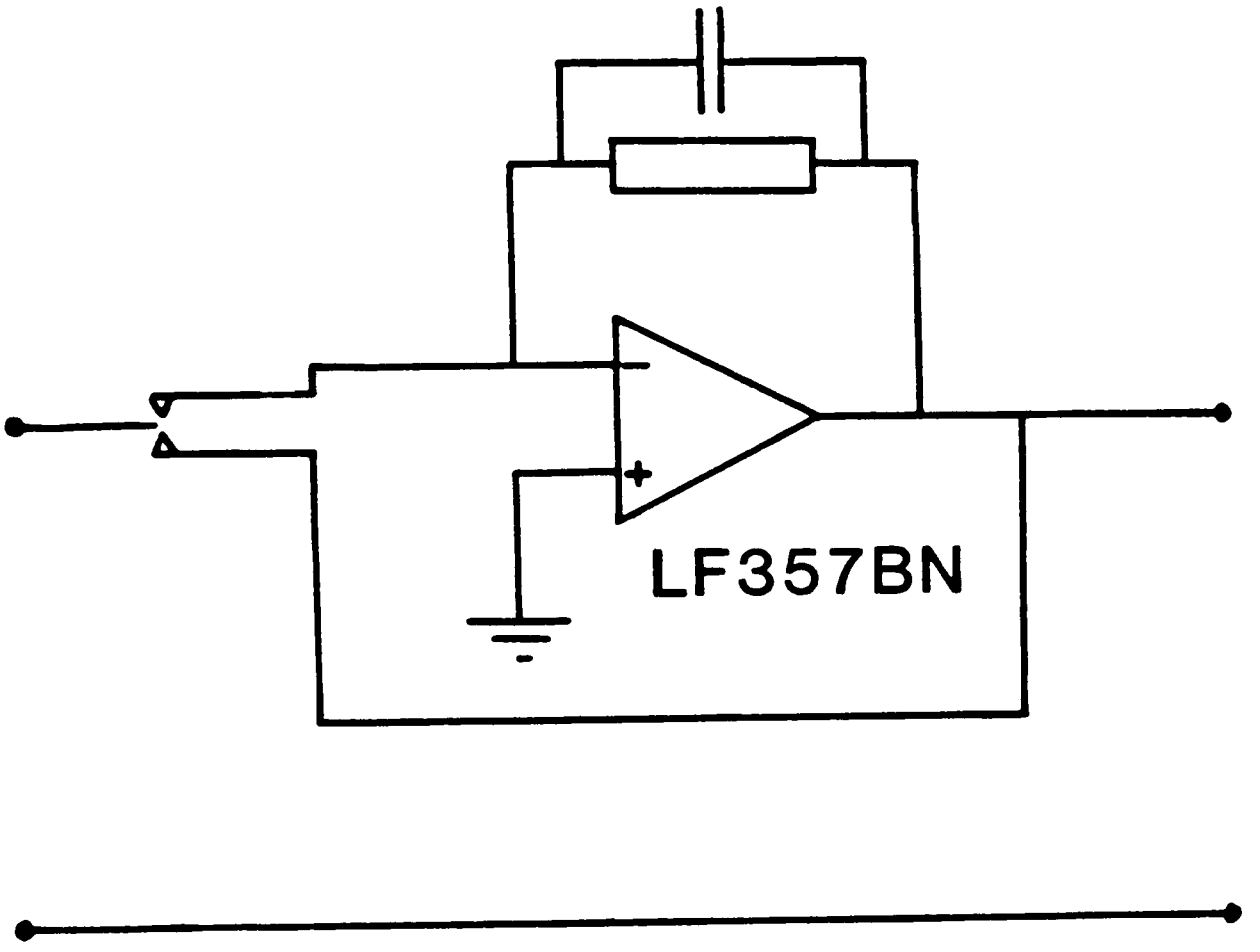


Figure 4.1 Circuit diagram of head amplifier used

Gain of $10^5 VA^{-1}$

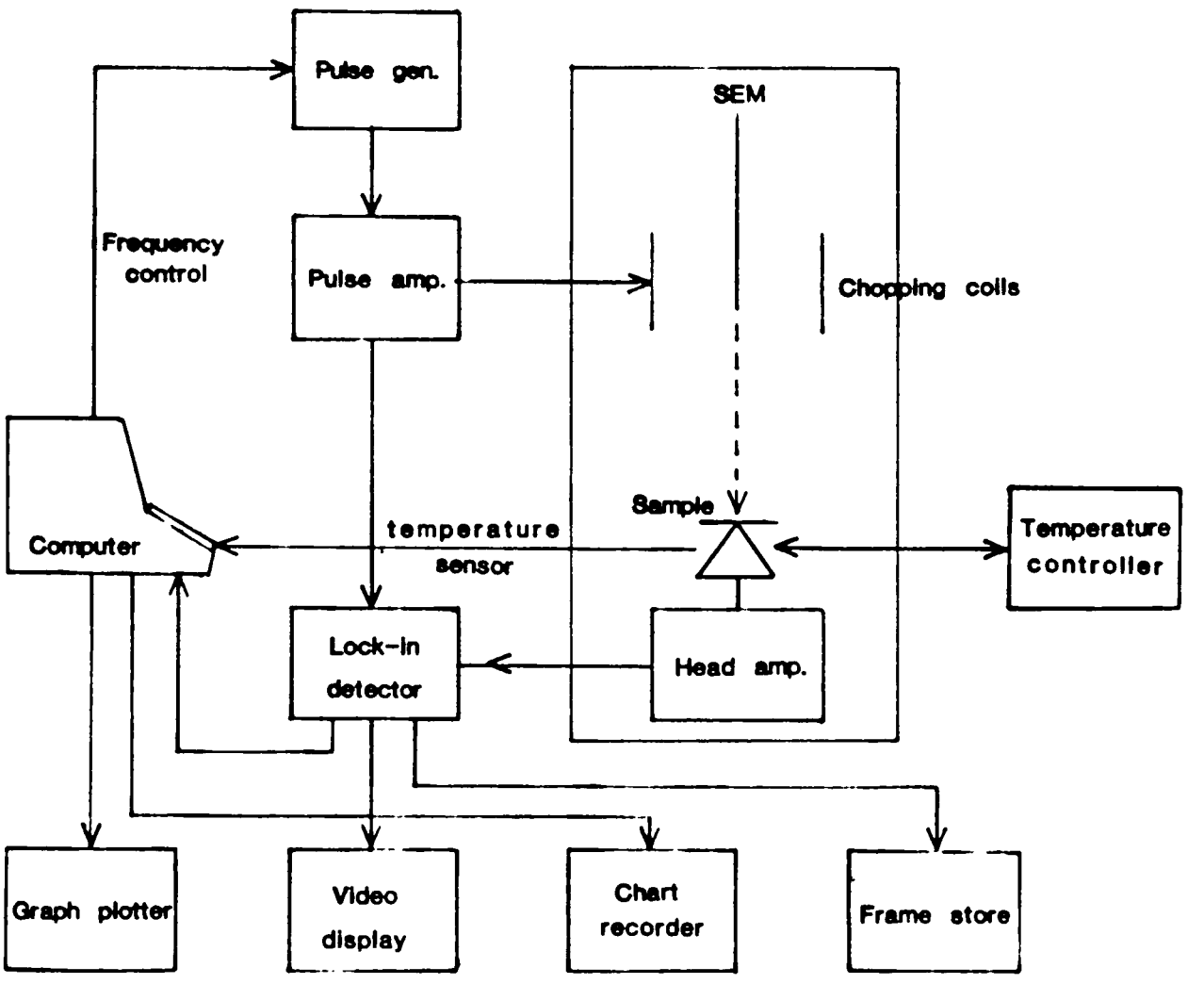


Figure 4.2 Block diagram of the EBIC system

the system was under manual control, would result in the experiments being too difficult to be performed, by a single operator. In addition the prolonged electron irradiation of the specimen that such an experiment would entail would result in prohibitive contamination in all but the cleanest vacuums. Because of this it is considered essential to have computer control and data collection if routine, accurate EBIC measurements are to be made of individual defects under various different experimental conditions.

In the EBIC system developed the computer, a PDP11/03 minicomputer, served three purposes. It controlled the experiment by prompting the user for information, setting and reading values off other equipment and ensuring that each set of measurements corresponding to a particular dislocation was accompanied by the relevant data concerning that experiment. Secondly it collected and re-displayed the EBIC line scans and if these were found satisfactory stored them on disk for future access and processing. Finally it was used to perform data analysis and numerical calculation and to produce hard copy of the data obtained.

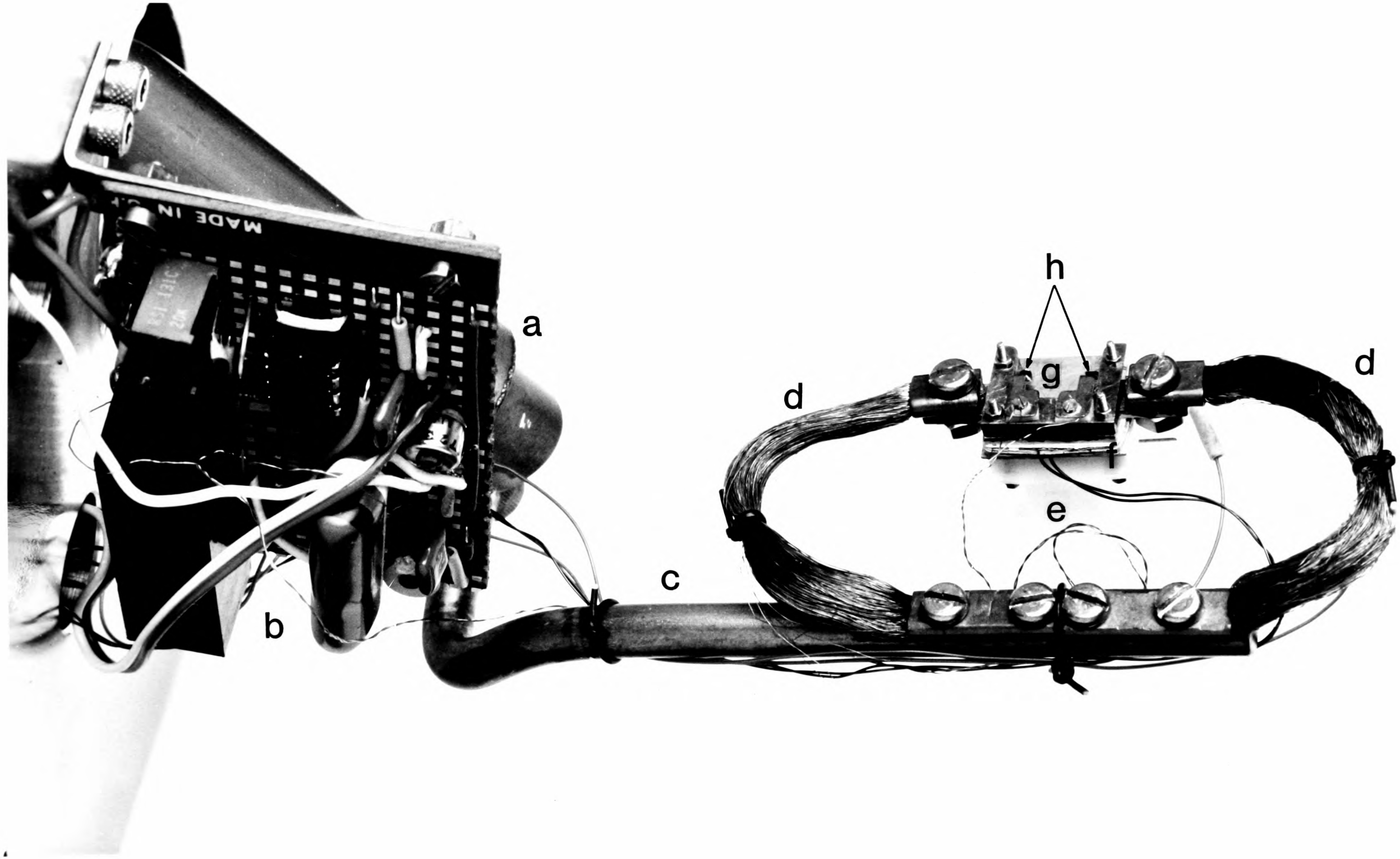
4.4 The Cold Stage

To gain information about the recombination processes taking place at dislocations it is desirable to study them at different temperatures. To do this using EBIC it is necessary to have a microscope stage which does not interfere with the SEM operation and is able to alter the temperature over a large range. In particular it should be possible to position the specimen to better than 0.5μm and drift due to expansion and contraction should be kept to a minimum. Such a stage

Figure 4.3 Photograph of the SEM cold stage

The various parts of the cold stage are labelled as follows

(a) bottom of the LN_2 cryostat
(b) pre-amplifier
(c) copper rod for heat transfer to the cryostat
(d) flexible copper braids
(e) teflon pillar
(f) heater coil
(g) main copper block
(h) spring clips to hold specimen in place and to make electrical connections to the specimen


a
b
c
d
d
e
f
g
h

was designed and constructed by the author in collaboration with Dr. E.D. Boyes. In principle this stage is similar to that used for EBIC work on the JSM 35-X microscope (Boyes et al 1981). The stage developed for the present work is however superior in that the temperature range available is larger (by 100K) and the time taken to reach a set temperature is shorter by approximately a factor of two.

4.4.1 Description

Figure 4.3 shows a photograph of the coldstage. The design is such that the "cold" copper block part of the cold stage on which the specimen is mounted is screwed onto the top of a rigid teflon pillar. The bottom end of this pillar is fixed to the standard microscope stage. In this way the high precision specimen translates can still be used to move the specimen whilst the microscope stage itself remains at room temperature, being thermally isolated from the cold stage by the teflon pillar.

For the EBIC experiments performed in this work a temperature range of 100 to 400K was used. The lower limit was set by using a liquid nitrogen cold stage and the upper limit was imposed by the deterioration in the electrical characteristics of the Schottky barriers used above 350K making accurate EBIC measurements difficult. In order that the specimen temperature could be set in this range it was necessary to have a high thermal conductivity link with a liquid nitrogen cryostat and to have a heater. The design employed was a copper rod leading from the LN_2 cryostat to a point close to the copper block on which the specimen is mounted and to have flexible copper braids joining the rod to

the copper block, thus allowing the stage to be moved to the required specimen's position.

The cryostat was constructed using a near vertical twin walled tube attached to a plate mounted on the side of the microscope.

The design of the specimen holder and the stubs used is such that they have as low a thermal mass as possible whilst allowing easy specimen insertion through a microscope port. This is done by sliding the specimen stub, a piece of copper sheet, approximately 1cm square and 0.5mm thick, under two spring clips on the stage which then hold it firmly in place. Electrical connections are made via the spring clips which rest on two thin brass runners at either side of the stub. The runners are insulated from the stub by a thin layer of glue. The main part of the stage is the copper block on which the specimen stub rests. This is square, of dimensions 13x13x4mm, and has the heater wire wrapped around it and the copper braids, which withdraw heat, attached to the sides, see Figure 4.3. The thermocouple is sandwiched between the bottom of the copper block and the top of the teflon pillar on which it is mounted.

Temperature measurement was made by a Au-0.03%Fe v Chromel thermocouple connected to an Oxford Instruments DTC2 temperature controller whose accuracy, according to the manufacturers specifications, is better than 1K in the range 4.2K to 500K. Calibration of the temperature measured by the thermocouple with that at the point where the specimen is placed during an experiment was made using a Cryogestic Linear

Temperature Sensor (CLTS) device obtainable from Oxford Instruments. This planar device was mounted on a stub in the same way as a specimen.

The thermocouple voltage serves as the input to the three term (PID) temperature controller which adjusts the heater current to produce the set temperature at the specimen. The heater consisted of ~20 turns of insulated resistance wire wound around the main part of the stage. Design of the cold stage was such that the heater, thermocouple and specimen are as close together as possible so allowing rapid stabilisation of the specimen of the temperature set on the controller. To ensure good thermal contact between the wire and the stage the windings were painted with a silver paint.

4.4.2 Thermal and Mechanical Performance

The temperature at the thermocouple takes 35 minutes to reach 115K after the addition of liquid nitrogen to the cryostat. The highest temperature available is 400K.

Typically upon changing the "set" temperature of the controller 20K it takes 30s for the thermocouple to stabilise, within 0.1K, of the desired temperature and a further 90s for the specimen temperature as measured by the CLTS device to stabilise. At low temperatures, i.e. less than 130K, stabilisation of the specimen temperature when cooling took significantly longer, eg. ~10 minutes for 140K to 120K. At high temperatures heating took longer, for example 320K to 340K took ~ 4 minutes. Once the set temperature had been reached this was held to within 0.1K.

Mechanical drift was less than 0.5μm per minute in the x-y plane (for a 20K temperature change) 2 minutes after the temperature reading had stabilised. Drift in the vertical direction could not be readily measured but on changing the temperature by 200K the total movement was 0.8 mm.

Chapter 5

Results and Discussion of the Electrical Characterisation of Schottky Barrier Specimens

Chapter 5 Results and Discussion of the Electrical Characterisation of Schottky Barrier EBIC Specimens

In order that the quantitative measurement of the EBIC contrast from dislocations in the specimens investigated could be related to their electrical activity it was necessary to establish various aspects of the electrical behaviour of the specimens themselves. In particular it was necessary to determine the way in which the practical limitations of specimen behaviour altered the measured EBIC signal from that which would be obtained from an "ideal" specimen. A description of how this was done, together with details of the measurements made of the minority carrier diffusion length, are presented here and it is shown that for nearly all the experimental conditions used in this work the EBIC contrast measured may be simply related to that which would be produced by an "ideal" specimen.

5.1 I-V Characteristics of the Schottky Barrier Specimens

I-V measurements of the specimens used were made on a curve tracer. The curves produced by both specimen 3509/2 and 2722/1 (10^{15} and 10^{16} cm^{-3} respectively) see chapter 3 for details, showed that their maximum differential reverse bias resistance was approximately 50kΩ and this occurred at ~1V. The minimum forward differential resistance was ~300Ω for 3509/2 and ~400Ω for 2722/1. For reverse bias voltages of greater than ~2V the diode characteristics showed "soft" breakdown. Both specimens had Schottky barriers and ohmic contacts of area ~3mm. The ideal behaviour of such specimens would be a very small forward bias resistance and very large

reverse bias resistance, however the characteristics actually observed may be easily explained as follows. The Schottky barrier specimens include an ohmic contact to the substrate and although this contact is not rectifying[1], it is of fairly high resistance and so introduces a series resistance into the measuring circuit of the diode junction itself. The ohmic contact resistance in series with the junction is shown in figure 5.1.

When the forward bias voltage on the specimen is increased so the resistance of the diode R_D is reduced as the current through it increases. Thus for high applied forward voltages the current flowing is sufficiently great that R_D is much smaller than R_S and so nearly all the voltage applied is dropped across R_S. Under these conditions the slope of the I-V curve will be approximately the series resistance of the ohmic contact and not that due to the diode itself, as in an ideal specimen. It was in this way that approximate values for R_S were obtained for specimens 3509/2 and 2722/1.

In reverse bias the characteristics are again far from ideal. This is because within the depletion region the defects present such as dislocations act as generation centres for carrier pairs which are subsequently separated in the depletion region field and so form the reverse bias current. At higher voltages it is possible that plasmas also occur leading to further increased leakage currents.

1. This was tested by fabricating two ohmic contacts on a specimen and observing the I-V characteristics for current passed between them.

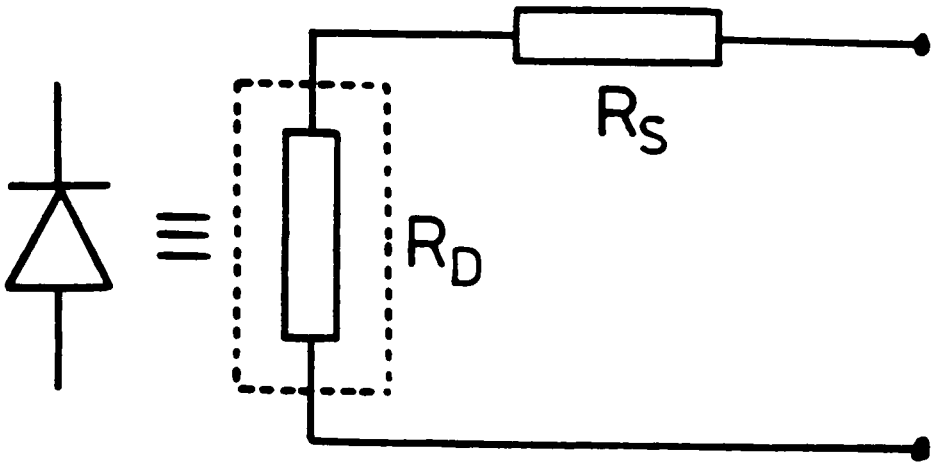


Figure 5.1 Resistances present in a Schottky barrier specimen

R_S is the series resistance due to the ohmic contact and R_D is the resistance of the diode junction for which;

$$I = I_O \exp \frac{qV_O}{KT} - 1$$

V_S and V_D are the voltages dropped across the series and diode resistance respectively.

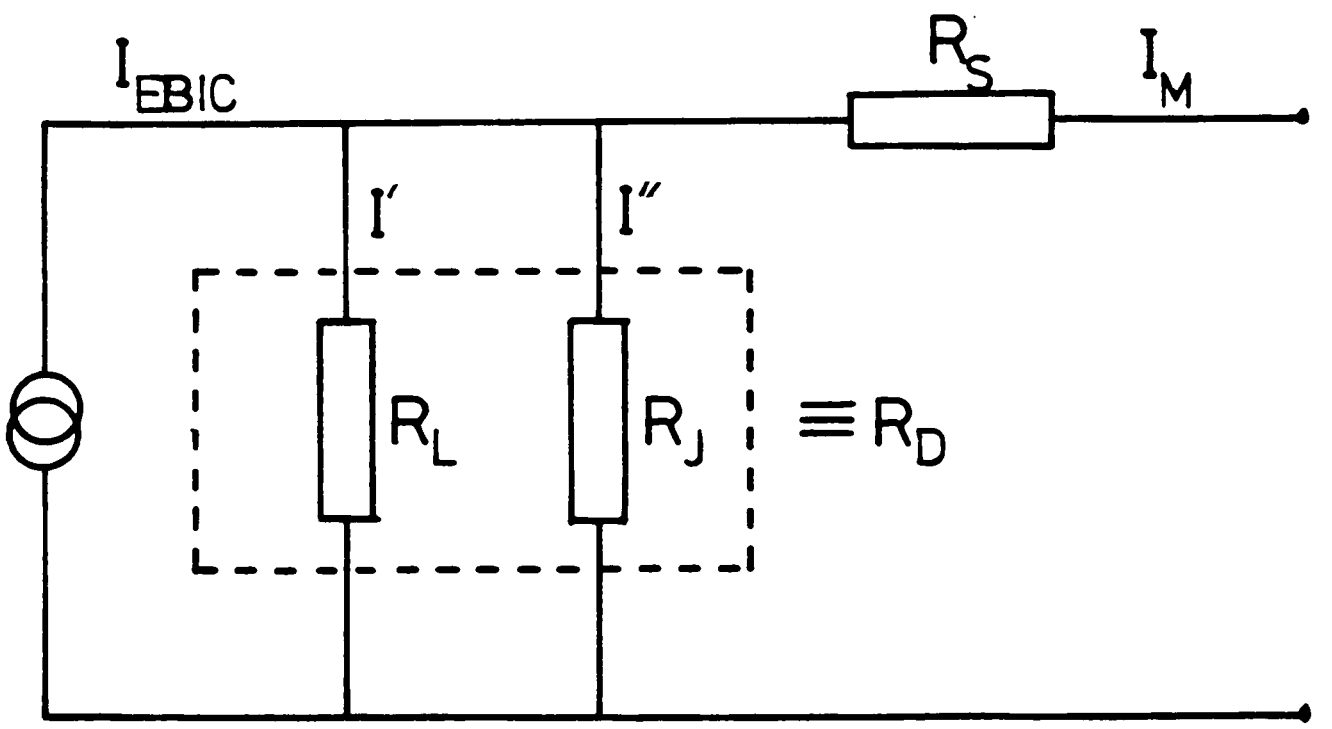


Figure 5.2 Equivalent circuit for the Schottky barrier specimens

I_{EBIC} is the induced current in an ideal specimen

I_m is the current measured

I is the current flowing forward through the forward biased junction $I_{EBIC} = I_m + I$

$I = I' + I''$

R_L is the "leakage resistance" of the diode

$$R_L = \frac{KT}{qI_O}$$

R_J is the non-ohmic part of the junction resistance whose value depends on I

R_S is the series resistance due to the ohmic contact

When the specimen is being used to generate an EBIC signal with no external bias voltage applied it can be considered to be a current generator in parallel with the diode resistance and in series with the ohmic contact, see figure 5.2. The current generated will flow either through the series resistance due to the ohmic contact and any external series resistance, or through R_D the forward bias resistance of the diode, the relative proportion depending upon the ratio of the two resistances. Thus the signal measured I_m which is that flowing through the series resistance, is dependent both on the series resistance and the diode resistance. The series resistance during most EBIC measurements was almost entirely due to the ohmic contact since the resistance of the amplifier used was $< 5\Omega$.

To investigate the forward bias characteristics of the diode and the series resistance of the ohmic contact more fully the following experiments were performed.

A circuit was built so that the voltage set by an analogue output of the computer was applied to the specimen and the current produced amplified and fed into the computer. This allowed the computer to control measurements in such a way that a large number of individual voltage and current measurements could be taken quickly and stored digitally. The forward bias characteristics of specimen 2711/3 measured in this way are shown in Fig 5.3. A program was written to model the specimen by a diode and resistance in series. In this way the series resistance used for the model could be varied until the data produced a straight line on a ln(I) vs V plot corresponding to an ideal diode (Fig 5.4). The value of the

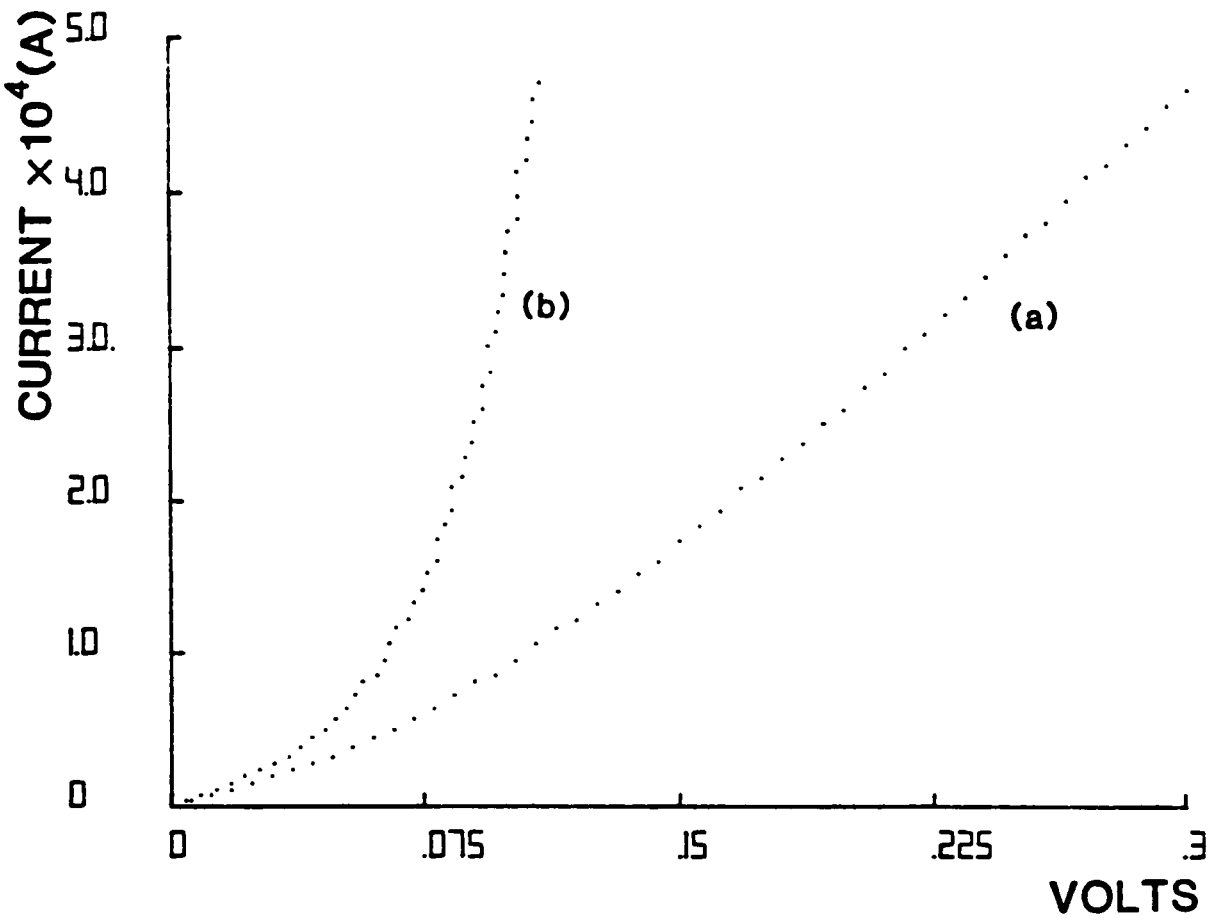


Figure 5.3 Plot of forward biased I-V characteristics

Deformed, n-type, 10^{16} cm^{-3} silicon, ~3mm^2 Schottky barrier. Curve (a) shows the measured valued, curve (b) the values calculated from curve (a) by taking R_S= 405 .

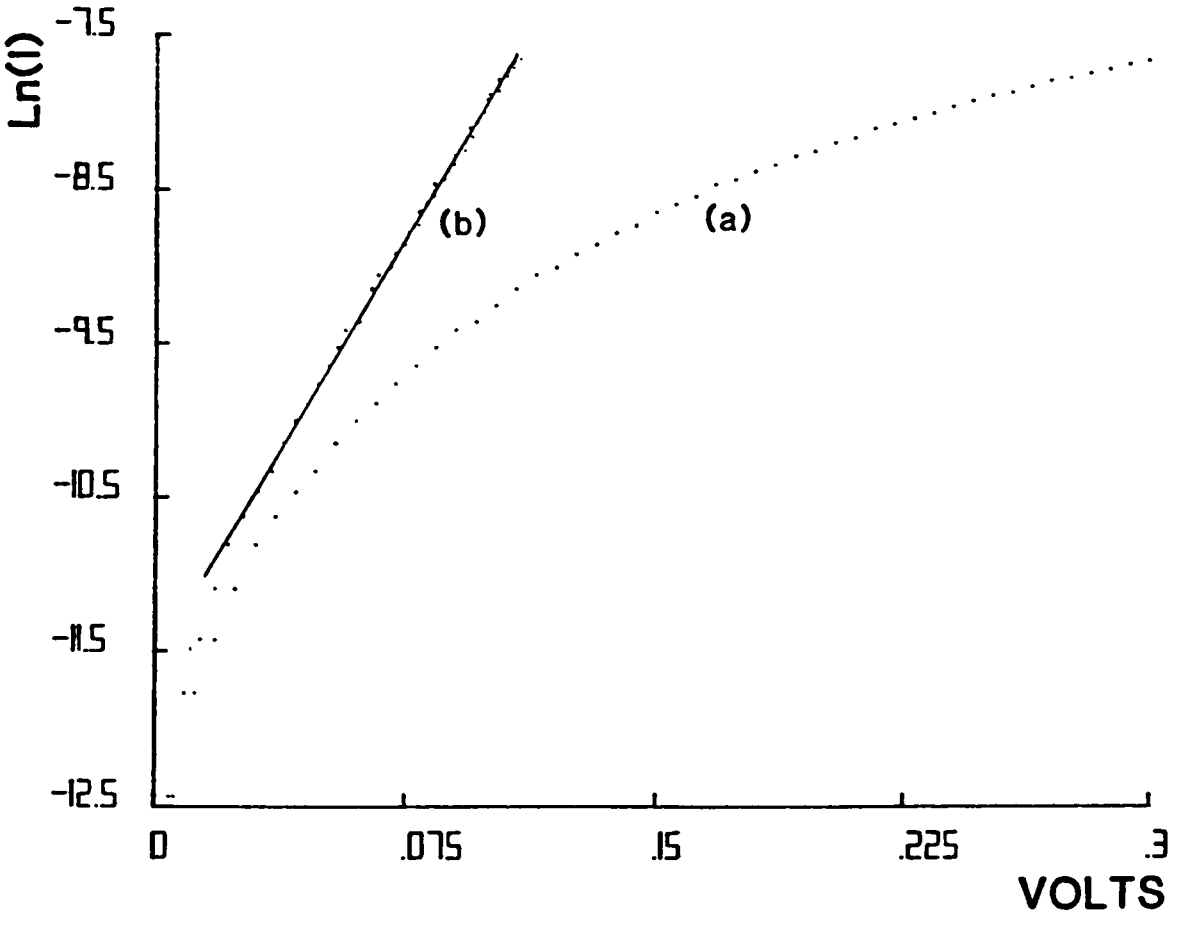


Figure 5.4 Plot of ln(I) versus V for forward biased diode.

Experimental details as figure 5.3

series resistance used to obtain the straight line on this plot was assumed to be the series resistance of the specimen. Using this method the series resistance, R_s could be found more accurately than by using the curve tracer. However, the slope of the straight line produced and the y-axis intercept on the log plot, which can be used to calculate β and I_o in the equation

$$I = I_o\left(\exp\left(\frac{qV}{\beta KT}\right) - 1\right) \qquad [5.1]$$

were very sensitive to changes in the value of R_s. Equation [5.1] is the theoretical equation for an ideal diode where β is the ideality factor , usually between 1 and 2. Plots such as Fig 5.4 could not therefore be used to measure I_o and β accurately. Figure 5.4 shows $I_o \sim 10^{-5}$A (although the accuracy of this value is poor) whereas measurements by Chang and Sze (1970) for a better Schottky diode, (i.e. one not containing a high density of dislocations), gave results which are equivalent to $I_o \sim 10^{-8}$A for a diode of similar area to that of specimen 2722/1. This very large value of I_o for the specimen studied here indicates that the forward characteristics are dominated, at low injection, by recombination centres. This implies that the value of β in equation [5.1] should be close to 2 (Sze (1981)), however the gradient of the line in figure 5.3 shows $\beta = 1.1$, thus illustrating the inaccuracy of this method.

In considering the behaviour of the junction it is useful to note that because I_o is so large, the condition $I \ll I_o$ is true for a large range of values of I, a situation which does not normally arise in many investigations. Equation 5.1 may be rewritten,

$$1 + \frac{I}{I_o} = \exp\left(\frac{qV}{\beta kT}\right)$$

which for $I \ll I_o$ gives,

$$\frac{I}{I_o} \simeq \frac{qV}{\beta kT}$$

or

$$R \simeq \frac{\beta kT}{qI_o}$$

This resistance is dependent on the leakage current I_o and so will be termed R_L the "leakage resistance". This is the resistance of the diode for $I \ll I_o$. For $I \gg I_o$ equation [5.1] may be simplified to its more usual form,

$$I \simeq I_o \exp \frac{qV}{\beta kT}$$

and for these conditions the resistance of the diode will be much smaller than the leakage resistance R_L and will show the more usual forward biased junction characteristics. This resistance which is dependent upon I, will be termed R_J the "junction resistance". Thus in the specimens used in this work where I_o is so large, it is useful to approximate the diode resistance R_D by two resistors R_J and R_L in parallel, with the value of R_J decreasing as the current through the diode increases. An equivalent circuit may thus be drawn as in Figure 5.2. This equivalent circuit was first proposed by Pfann and van Roosbroek (1954).

For $I \ll I_o$ (I is the current flowing forward through the forward biased junction) $R_L \ll R_J$ and the specimen behaves approximately as a network of ohmic resistors, whereas for $I \gg I_o$ $R_J \ll R_L$ and the specimen behaves as an ideal forward biased junction and a series resistance. From this equivalent

circuit it can be seen that there are three régimes of behaviour for the measured EBIC signal.

i) For $R_S \ll R_L$ and $R_S \ll R_J$ the EBIC signal measured I_m, is equal to the ideal EBIC signal, I_{EBIC}.

ii) For $R_L \ll R_J$ (i.e. $I \ll I_O$) and $R_L \lesssim R_S$ the current measured

$$I_m \simeq \frac{R_L}{R_L + R_S} \cdot I_{EBIC} \qquad [5.3]$$

This implies that although the measured signal does not have the same absolute value as the ideal EBIC signal, it is always directly proportioned to I_{EBIC} and any variation in the measured signal will accurately reflect the variation in the ideal EBIC signal. Thus, as in the previous case, the measured contrast of a defect is equal to the contrast that would be produced by the same defect in an ideal EBIC specimen.

iii) For $R_J \ll R_L$ (i.e. $I \gg I_O$) and $R_J \lesssim R_S$ the current measured

$$I_m \simeq \frac{R_J}{R_J + R_s} \cdot I_{EBIC}$$

and is no longer proportional to I_{EBIC} because R_J varies with I, the current flowing through the forward biased junction. The experiments performed to measure open circuit voltage, EBIV, where R_S is effectively infinite, are usually performed in the régime. By writing $I_{EBIC} = I + I_m$ and noting $I_m \ll I$ for $R_S \gg R_L$ equation [5.1] can be rearranged to give $V = \frac{\beta kT}{q} \ln\left(\frac{I_{EBIC}}{I_O}\right)$ and by applying Ohm's law to R_S this gives

$$I_m \simeq \frac{kT}{qR_s} \ln\left(\frac{I_{EBIC}}{I_o}\right) \qquad [5.4]$$

The measured signal will vary as the log of the ideal signal and the measured contrast of a defect,

$$\frac{I_m - I_m'}{I_m} = \frac{\ln\left(\frac{I_{EBIC}}{I'_{EBIC}}\right)}{\ln I_{EBIC}} \qquad [5.5]$$

where the prime denotes the current produced whilst the electron whole pairs are generated at the defect. Thus in this, the third régime, not only is the measured contrast different to the ideal EBIC contrast but the measured contrast is also dependent on the EBIC current, changing as $\ln(I_{EBIC})^{-1}$ with increasing I_{EBIC}.

Clearly in this régime the contrast and any changes in it cannot be easily related to the ideal contrast.

The régime in which the EBIC measurements are made depends upon I_{EBIC} , I_o and R_s and so other experiments were performed to check the analysis given above and to determine I_o for a typical specimen. These experiments are described in the following section.

5.2 Measurements of the EBIC Signal as a Function of Series Resistance

In this experiment an EBIC signal was generated by a 10kV electron beam of known current incident on specimen 2722/1 and the collected EBIC current was measured as different values of external series resistances were inserted in the circuit. This was performed for different beam

currents. The results are summarised in Table 5.1. The diode resistance R_D is the parallel resistance in figure 5.2 and was calculated as follows. It is assumed that the measured current I_m for the 400Ω series resistance is almost exactly the same as the ideal EBIC current I_{EBIC}. Thus the current flowing through R_D is $I = I_{EBIC} - I_m$. The voltage across the diode V_D, is simply $I_m \times R_s$ and so $R_D = V_D / I$. The reason for the unexpectedly low value of I_m and hence R_D, for $R_s = 70k\Omega$ and $I_{beam} \simeq 2 \times 10^{-8}A$ is not known. The experiment was not repeated to check this value.

The results produced verify the validity of the description of the EBIC specimen given above. In particular it can be seen that there are indeed three régimes of behaviour. In the first, which occurs for low beam currents and small series resistance, the collected current is independent of the series resistance in the circuit and will be closely equal to the ideal EBIC current, I_{EBIC}.

In the second régime when the series resistance is of the same order or greater than the leakage resistance of the diode the measured current falls with increasing series resistance and the calculated diode resistance shows ohmic behaviour, being roughly constant at 37kΩ for this particular specimen.

In the third régime at very large beam currents, the resistance of the forward biased junction becomes dependent on the current flowing through it and the signal now detected is equivalent to EBIV as commonly measured. The change from the seond to the third régime according to equation [5.1] occurs when $I \simeq I_o$ and from the table this can be seen to happen for a

	I_b= $1x10^{-11}$A		I_b= $5x10^{-11}$A		I_b= $2x10^{-10}$A		I_b= $2x10^{-8}$A	
$R = R_{ser} + R_{ohmic}$	Measured current(A)	Calculated resistance(Ω)	Measured current(A)	Calculated resistance(Ω)	Measured current(A)	Calculated resistance(Ω)	Measured current(A)	Calculated resistance(Ω)
400	$2.5x10^{-8}$		$1.3x10^{-7}$		$4.0x10^{-7}$		$3.9x10^{-5}$	
870	$2.5x10^{-8}$		$1.3x10^{-7}$		$3.9x10^{-7}$		$3.8x10^{-5}$	
1.4K	$2.5x10^{-8}$		$1.3x10^{-7}$		$3.9x10^{-7}$		$3.6x10^{-5}$	
5.0K	$2.4x10^{-8}$		$1.1x10^{-7}$		$3.4x10^{-7}$		$3.0x10^{-5}$	
8.8K	$2.0x10^{-8}$		$1.1x10^{-7}$		$3.2x10^{-7}$		$2.8x10^{-5}$	22.4K
28K	$1.4x10^{-8}$	35.6K	$7.5x10^{-8}$	38.2K	$2.2x10^{-7}$	34.2K	$1.6x10^{-5}$	19.5K
41K	$1.2x10^{-8}$	37.8K	$6.3x10^{-8}$	38.5K	$1.9x10^{-7}$	37.1K	$1.3x10^{-5}$	13K
70K	$8.6x10^{-9}$	36.7K	$4.3x10^{-8}$	34.6K	$1.4x10^{-7}$	37.7K	$8.3x10^{-5}$	1.5K

Table 5.1 Measured EBIC current I_m, for various series resistances and beam currents. The resistance calculated is the diode resistance, R_D of Fig. 5.2 and is equal to $\frac{R_L.R_J}{R_L+R_J}$. R_D is calculated by assuming $I_m=I_{EBIC}$ for the 400Ω series resistance, see text for details. The beam voltage used was 10kV.

current greater than the largest in the third column of the table (2.5×10^{-7}A) and a current smaller than the smallest in the fourth column (1×10^{-5}A). This provides a check for equation [5.2] which, rearranged, gives:

$$I_o \simeq \frac{\beta kT}{qR_L}$$

Inserting $R_L = 37k\Omega$ and taking $\beta = 2$ (due to the non-ideal nature of the junctions containing dislocations) yields $I_o \simeq 1.5 \times 10^{-6}$A, in agreement with the observed behaviour mentioned above. The forward biased junction will have a slightly narrower depletion region than the unbiased junction. However, the size of this effect is negligible because the values of V_D generated in régimes one and two are so small ($< 10^{-2}$V, see table 5.1) and so it is not expected to alter the EBIC contrast of the dislocations. This was checked by measuring the contrast of individual dislocations for a series resistance of 400Ω and $41k\Omega$ with a beam current of 2.4×10^{-10}A. No change in the contrast was found.

These experiments have thus shown that the analysis given for the measured EBIC current from a non-ideal specimen is correct. In particular they show that contrary to popular belief, accurate quantitative EBIC measurements of the contrast of defects may be made even when large series resistances are present provided that the current induced is smaller than I_o for the specimen studied. This also implies that the "poorer" the Schottky barrier, i.e. the larger I_o, the larger the beam currents and series resistances that may be used whilst still ensuring that the contrast measured is equal to the true EBIC contrast of the defect.

Having established the behaviour of a typical specimen at room temperature it was necessary to determine the characteristics of the specimen as a function of temperature. This was done by measuring the series resistance of the ohmic contact to the specimen using the computer controlled measuring circuit and the method of fitting the collected data described earlier. The specimen was mounted in the SEM cold stage to allow temperature control. It was found that the series resistance increased with decreasing temperature reaching 8kΩ at 200K; below this temperature measurements could not be made with accuracy because the linear portion of the log I vs V curve was too small. However, at 200K measurements of the collected current showed that it started to decrease having been approximately constant at higher temperatures. At 120K the collected current was only 40% of the signal measured at 300K for the same beam current. If this effect is attributed to an extrapolation of the increasing series resistance with decreasing temperature it can then be explained by the collection of the measured EBIC signal moving into the second of the three régimes discussed earlier. Thus below 200K the absolute level of the signal collected is no longer the same as the ideal EBIC signal. However, provided that I remains less than I_o, it will still give an accurate measure of the EBIC contrast of a defect.

As was stated earlier in this chapter, it was the intention of this part of the work to determine whether the measured EBIC contrast of dislocations could be attributed, unambiguously, to the behaviour of the defects themselves and so to this end it was necessary to determine the range of beam

currents for which, at low temperature, the collection of the EBIC signal remained in the second régime, that is to say for which $I \ll I_o$. Unfortunately the large and difficult to measure series resistance of the ohmic contact precluded the measurement of I_o by changing the series resistance present in the circuit in the same way that was used at 300K and so measurements were made of the efficiency of collection of the EBIC signal as a function of I_{EBIC} the ideal EBIC current. This was done by changing the beam current incident on the specimen and is described in the following section.

5.3 Measurements of the EBIC Signal as a Function of the Incident Beam Current

Recalling equation [2.1] which shows I_{EBIC} is proportional to the electron beam current I_{beam}, and that

$$I_m \simeq \frac{R_L}{R_L + R_S} \cdot I_{EBIC}$$

in collection régime two, it can be seen that in this régime $\frac{I_m}{I_{beam}}$ is constant. However for régime three where equation [5.4] is valid the ratio is

$$\frac{I_m}{I_{beam}} \simeq \frac{A}{I_{beam}} \ln\left(\frac{I_{beam}}{I_o}\right)$$

where A is constant. Thus measurement of the ratio I_m/I_{beam} as a function of I_{beam} will determine whether signal collection is in régime two or three and consequently whether the EBIC contrast measurements can be related to the efficiency of the defect studied.

The EBIC signal was produced by injecting carriers in an area of the crystal where no dislocations could be imaged and the EBIC signal was uniform (for at least 4μm laterally) indicating that the collected current was independent of the short range effects of dislocations. The specimen was mounted on the cold stage to provide temperature control and the beam energy used was 15kV, the column preamplifier was used to amplify the EBIC signal before measurement. For this experiment specimen 3509/2 was used (see chapter 3 for details). This is the same specimen as that used for the investigation of the temperature and beam current dependence of dislocation contrast presented in chapter 6 and so the findings given here are directly applicable to those results.

The results of measurements at 300K, 225K, 200K and 131K, are shown in Figures 5.5 and 5.6. The arbitrary units used for the ratio of I_m/I_{beam} are the same for both figures.

From figures 5.5 and 5.6 it can be seen that with decreasing temperature, I_m/I_{beam} decreases indicating that R_S is increasing. The reduction begins to occur before 225K in this specimen indicating that R_L is lower or R_S higher at this temperature, than for specimen 2722/1 which was studied in the previous section. This deduction is supported by noting that I_m falls to ~30% of its room temperature value by 131K which is lower than for specimen 2722/1.

It is evident that at temperatures at or above 225k and for I_{beam} 10^{-9}A the measured EBIC signal-beam current ratio is independent of beam current showing that signal collection is in régime one or two. At lower temperatures (131K and 200K) the transition between régimes two and three is detected

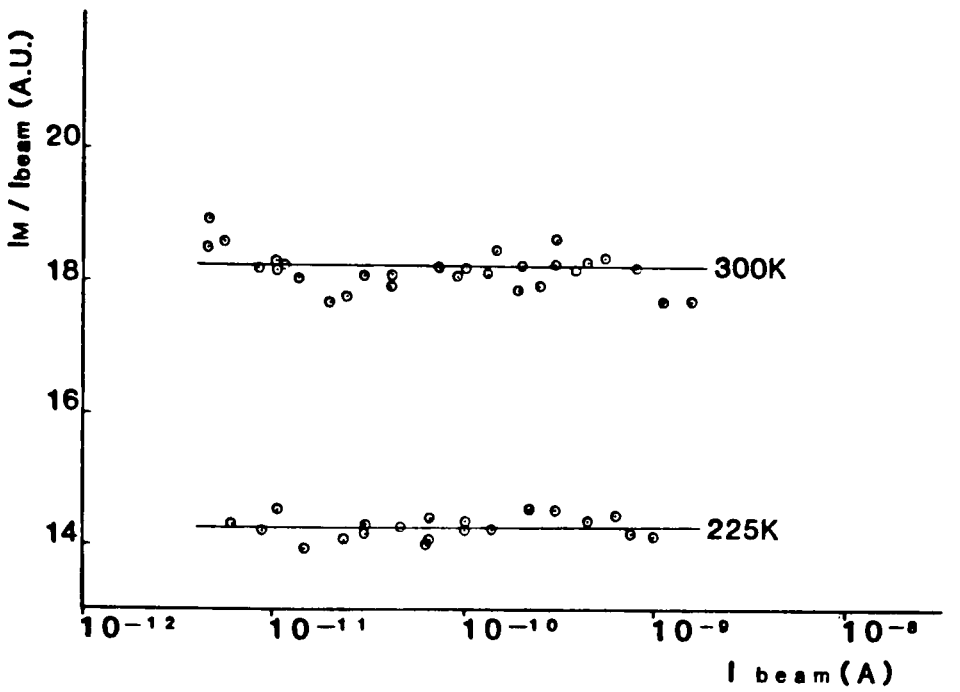


Figure 5.5 Plots of the ratio I_m/I_{beam} against I_{beam} for measurements at 300K and 225K

No variation of I_m/I_{beam} is detected indicating that signal collection is occuring according to régimes 1 or 2. Specimen 3509/2, n-type 10^{15} cm^{-3}, beam voltage 15kV.

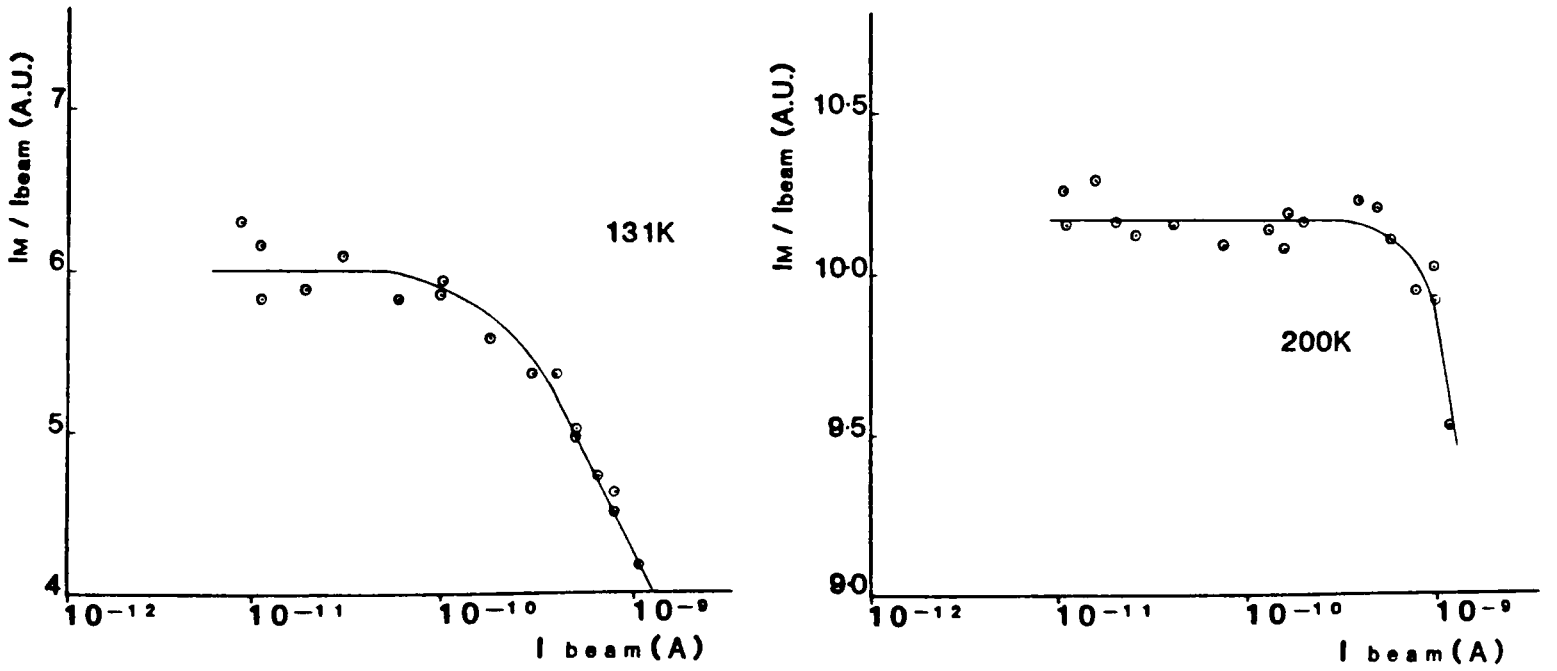


Figure 5.6 Plots of the ratio I_m/I_{beam} against I_{beam} for measurements at 200K and 131K

Other experimental details as figure 5.5. The arbitrary units are the same for each figure. The high beam current portion of the curves shows I_m/I_{beam} to decrease according to régime 3.

when the ratio begins to decrease as the beam current is raised fulfilling the condition that $I > I_o$. At 200K this occurs for $I_{beam} = 7x10^{-10}A$ and at 131K for I_{beam} $2.4x10^{-10}A$. Thus at these low temperatures, régime 3 for this specimen is entered at beam currents easily attainable in the SEM. The next chapter will show that the contrast produced in this régime departs from the ideal contrast as expected and consequently does not then provide a direct measure of the recombination strength of the dislocation.

5.4 Measurements of the Minority Carrier Diffusion Length

The experimental work presented in the preceding section has established the range of temperatures and beam currents for which the measured contrast of a defect is equal to its ideal contrast. In this section it is shown that, for specimen 3509/2 the ideal EBIC contrast may be related directly to the recombination strength, γ of the defect.

In chapter 2 it was shown that:

$$C = \gamma^n f(L,d,R)$$

where C is the EBIC defect contrast,

L is the minority carrier diffusion length,

d is the defect depth,

R_G the Gruen range of the incident electrons.

In the analysis due to Donolato (1978), n=1, and for that due to Pasemann (1981), n=0.9. Thus provided R_G, d and L remain constant throughout an experiment, any changes in C can be directly related to changes in γ. The Gruen range R_G, of the incident electrons is independent of temperature over the

temperature range for which the specimens were studied and so maintaining a constant accelerating voltage throughout an experiment ensured that R_G remained constant. The actual position of a dislocation did not change during an experiment but a change in the depletion region width W would alter the effective depth of the dislocation in relation to the plane of carrier collection. The width, W of the depletion region due to a Schottky barrier is

$$W = \frac{2\epsilon_s}{qn_o}\left(V - 2kT/q\right)^{\frac{1}{2}} \qquad \text{(Sze (1981))}$$

where ϵ_s is the permittivity of silicon

n_o is the density of majority carriers (n-type)

V is the potential of the junction

In the temperature range 110K to 400K, ϵ_s is a constant and the shallow donors are completely ionised throughout, yielding n_o constant (see for example Sze (1981)). For doping levels greater than 5.10^{13} cm^{-3} the intrinsic contribution is also negligible in this range. The potential across the junction $V = V_{bi} + V_{bias}$, where V_{bi} is the built-in potential which for a Au/Pd Schottky barrier on silicon is 0.77V (Sze (1981)). The maximum value of V_{bias} is 10^{-2}V for current collection in régimes one and two and the maximum change in $\frac{2kT}{q}$ is $5x10^{-2}$V. Thus, the maximum possible fluctuation in W throughout an experiment is $\sim 4\%$, which would induce a negligible change in the EBIC contrast of the defects measured, see section 5.4.1.

In order to determine whether the contrast C, may be directly related to γ, it now only remains to determine the variation of L the minority carrier diffusion length with temperature.

5.4.1 The Method of Wu and Wittry for Determining Minority Carrier Diffusion Lengths

The method developed by Wu and Wittry (1978) is particularly suited to the measurement of relatively short (<15μm) diffusion lengths and was found to be appropriate for the specimens studied here. A brief description of the technique is given in the following.

In this method a standard barrier specimen is illuminated with a defocused electron beam so that the generation and subsequent diffusion of carriers is uniform over an area large compared to the depth to which the electrons penetrate. In this way solution of the equations for generation and collection of carriers is reduced to a one dimensional problem. A modified Gaussian approximation of the depth distribution of the generation of carriers is used and a solution for the collected current is produced. This consists of two parts, the first due to carriers generated within the depletion region where all carriers generated are assumed to be collected, and the second for carriers generated within the neutral material for which the proportion collected depends upon the minority carrier diffusion length. Account is taken of the finite thickness of the Schottky barrier metallisation.

The current collected is compared with the total number of carriers generated in the specimen so that the efficiency of collection, e is obtained. In order to measure diffusion lengths it is usual to plot ln(e) vs V_{beam} the beam voltage. A typical plot is shown in Figure 5.7. The shape of the curve is dependent on:

i) the thickness of the barrier metalisation, d. The rising edge of the curve is particularly sensitive to d which has little effect on the remainder of the curve. d can thus be measured to ± 10%.

ii) the depletion layer width, W. The thicker the depletion layer the higher e for values of V_{beam} when R_G is sufficient for electrons to penetrate into the bulk. The centre portion of the curve is sensitive to W.

iii) the minority carrier diffusion length L. This affects the efficiency when electrons have sufficient energy to penetrate into the bulk. In particular the value of the gradient of the ln(e) vs V_{beam} plot is almost entirely due to the value of the diffusion length. It is only weakly dependent on the metal and depletion layer thicknesses.

An experimental determination of L is performed by measuring e for different values of V_{beam} and adjusting the values of d, W, and L used to generate the theoretical ln(e) vs V_{beam} plot until the best fit to the experimental data is obtained. As mentioned above values of d and L are largely independent of each other and so can be obtained quite accurately. The shape of the curve is only weakly dependent on W which is thus difficult to measure and whose value is thus normally taken to be the calculated value. Altering the

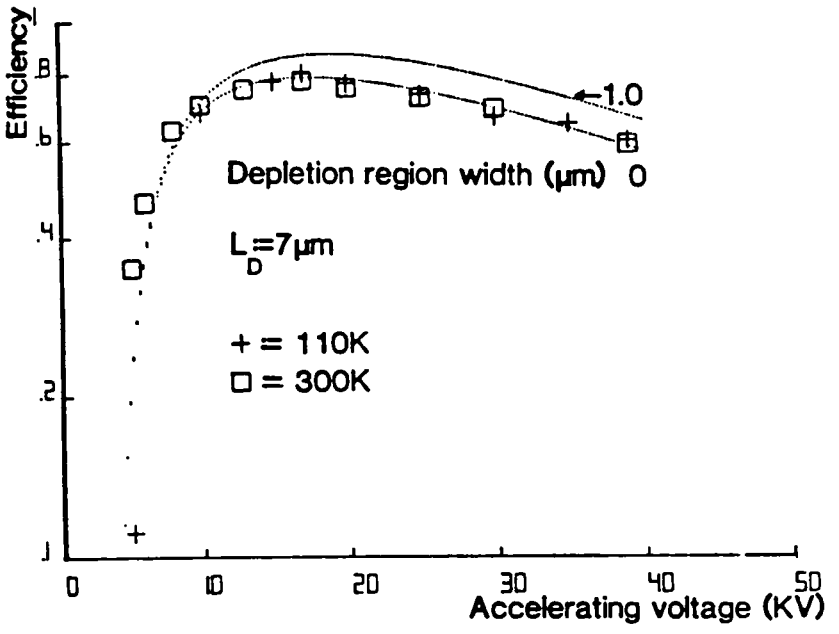


Figure 5.7 EBIC collection efficiency versus accelerating voltage

Low dislocation density region. The curves correspond to L_D = 7um.

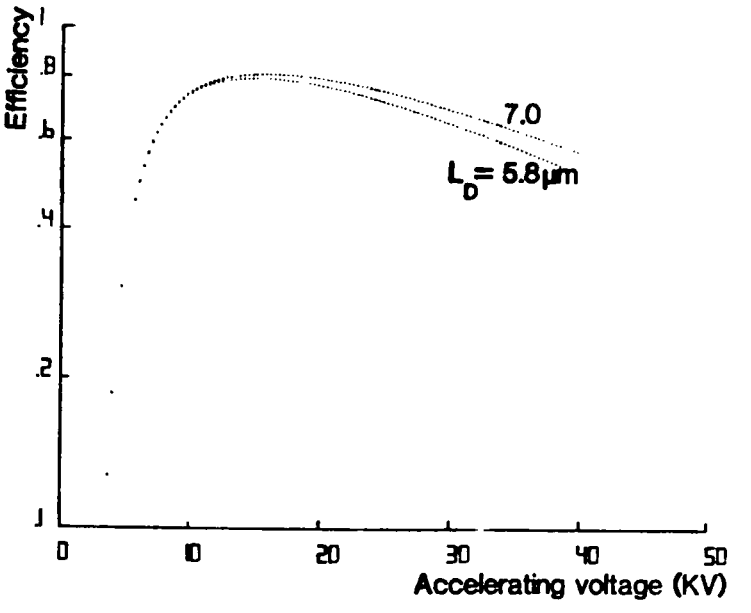


Figure 5.8 Curves showing the effect of a 15% change in L on the EBIC collection efficiency

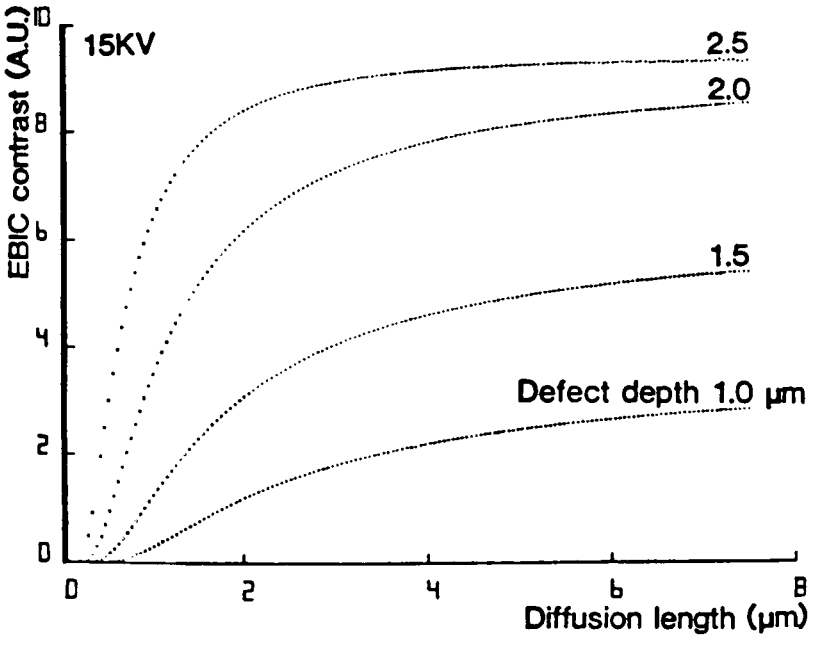


Figure 5.9 Theoretical curves for EBIC contrast versus diffusion length for a point defect

Curves calculated for different defect depths.

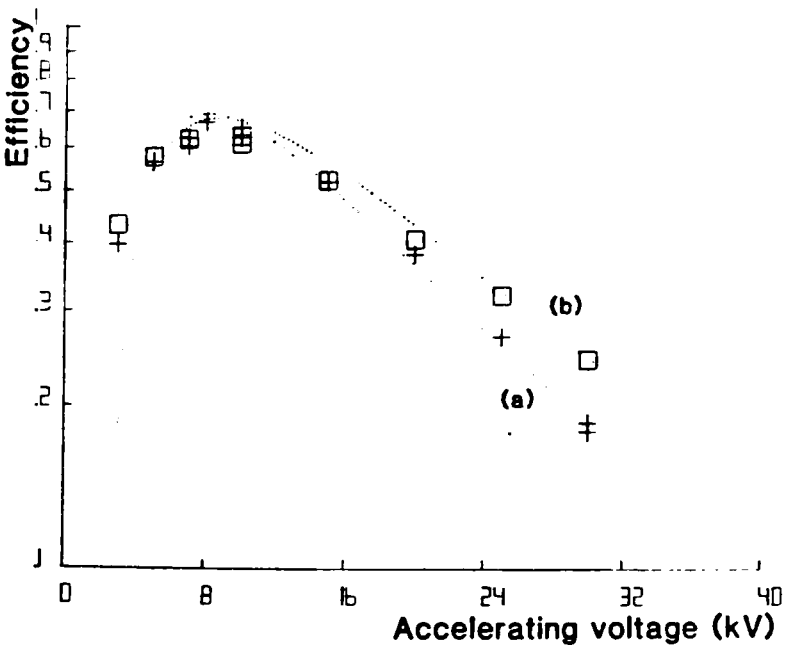


Figure 5.10 EBIC collection efficiency versus accelerating voltage

High dislocation density region.
Curve (a) obtained with
$I_{beam}=1x10^{-9}A$
Curve (b) with
$I_{beam}=8x10^{-11}A$

value of the depletion region width by 4%, the maximum amount by which it may change during an experiment, makes no significant difference in the efficiency e. Thus for dislocations not immediately adjacent to the depletion region, a change in W of 4% will not alter the EBIC contrast measured.

5.4.2 Experimental Results

Initial measurements of the minority carrier diffusion length were made for beam powers of less than 10^{-5} watts. For each diffusion length experiment the beam power was kept constant as the accelerating voltage was changed so that the number of carriers generated also remained constant. In this way the excess carrier concentration remained roughly constant throughout. The electron beam was defocused to 40μm diameter. The required amount of defocus was obtained by scanning the beam across a sharp edge and adjusting the defocus until the image width (10%-90%) as observed in y-modulation was 40μm. The beam current was measured using a Faraday cup. Both the beam current and the EBIC signal generated were measured using a Keithly 602 electrometer.

a) Low Dislocation Density Region

The first measurements made were of the diffusion length on specimen 3502/3 in a region of the crystal where no dislocation could be imaged at 39kV over an area approximately 70μm across. The central 40μm area was used to make the diffusion length measurement. The experimental data together with the corresponding computer plot of efficiency vs beam voltage are shown in Figure 5.7. From this it can be seen that the data is not in good agreement with the theoretically

predicted efficiency values when the depletion region thickness is taken to be 1μm, its calculated value. There are two possible explanations for this. The first is that the approximation that all carriers generated in the depletion region are captured may be incorrect thus reducing the effective width of the depletion region. The limiting case of this would be when recombination inside the depletion region was the same as in the bulk. This is shown on the diagram by the curve with depletion region width zero.

An alternative explanation may be that the current measured is not the ideal EBIC signal and that a significant proportion (~ 10%) of the current is flowing forwards across the forward biased junction. From the results of the previous sections this seems unlikely at room temperature. Despite the non-ideal behaviour of the Schottky barrier, a value for the diffusion length can be obtained by considering the higher accelerating voltage portion of the current where the effect, on the gradient of the line, of recombination within the depletion region is much less significant. However, in view of the nature of the collecting junction it is possible that the error in the diffusion length measurement may be as high as 25%. No dependency of the efficiency of the Schottky barrier on the beam current was found indicating the diffusion length measurement to be independent of the beam current at which it was made.

Measurement of the same area was also made at 120K. In this case the large series resistance of the ohmic contact at 120K meant that the actual signal collected was small and hence the calculated efficiency of the barrier reduced. The

effect of the series resistance, on measurements in régime two, was shown in the previous sections, to merely reduce the collected current I_m by a constant amount $\frac{R_L}{R_L + R_s}$ independent of the value of I_m. Thus to compensate for this effect, all the measured values of current were scaled by a constant amount, in this case 3.6 so that the values recorded at 15kV at 300K and 120K were approximately the same. The resultant data is plotted on Figure 5.7. From this it can be seen that the data obtained at 120K is very close to that obtained at 300K and values of L=7μm and d=130Å for the thickness of the metallisation are obtained. Although, as mentioned earlier, the error in the absolute size of the diffusion length may be quite large the error introduced in comparing the relative values of two similar curves is much smaller in each case. Figure 5.8 shows theoretical curves generated for L=7μm and 5.8μm which illustrate the change introduced by a 15% reduction in L. From Figures 5.7 and 5.8 it is reasonable to conclude that the change in diffusion length for the area measured, where no dislocations were visible in EBIC, was less than 15% over the temperature range 120K to 300K.

To determine whether a 15% change in L would produce a significant change in the measured EBIC contrast of a defect, independent of any change in γ, it is reasonable to apply Donolato's model of contrast for a point defect. The value of L is close to 7μm in the low dislocation density region investigated, which is similar to the uniform, dislocation-free regions surrounding the dislocations which have been studied in detail, and so this value is applicable to an analysis of their contrast. According to the model a change of 15% in L would produce a change in the EBIC contrast of from, say, 10% to 8% for the imaging conditions used. This is demonstrated in Figure 5.9 which shows the computer calculated contrast of defects at different depths as a function of the bulk diffusion length.

The implications of this for the EBIC contrast measurements made on dislocations in these specimens, as a function of temperature is that the changes in contrast detected, $\sim$50%, are very large compared with any possible variation caused by a change in bulk diffusion length. This result together with those presented earlier in this chapter shows that for the specimens and experimental conditions used in this work, changes in the EBIC contrast, C, may indeed be directly related to changes in the recombination strength γ, of the dislocation studied.

b) High Dislocation Density Region

Measurements of the diffusion length of minority carriers in regions of the specimen (3509/2) containing high densities of dislocations were also made. Although these measurements do not directly relate to the measurement of the recombination efficiency of individual, well-characterised dislocations, such results are interesting and important in view of the extensive use of diffusion length measurements to investigate and characterise most semiconductor materials and devices. In general the techniques used rely on the injection of excess carriers using either an electron beam or a light source and measure the decay of the carrier distribution either as a function of time or position away from the point of generation. The findings of this section are applicable to all such techniques when investigating material for which the diffusion length is limited by dislocations and possibly other extended defects.

Measurements were made at 300K using the technique described above on a region containing a high density of dislocations. The density was difficult to measure accurately

but was estimated from an EBIC image of the examined area, to be 10^7 to 10^8 cm^{-2}. The electron beam was defocussed to 5μm, a smaller area than that used for the previous experiment, thus generating a higher density of carriers. However because the distribution of dislocations is not uniform on a 5μm scale, the diffusion length measured using a stationary beam would have been very sensitive to small movements in the beam position. To overcome this problem the spot was scanned at a TV-rate over an area 100μm square so that the signal collected and "smoothed" by the electrometer, represented an average over this area. Two sets of measurements were made (figure 5.10), the first for a beam current $I_{beam} = 8.0 \times 10^{-11}$A and the second for $I_{beam} = 1 \times 10^{-9}$A. Figure 5.10 shows that the diffusion length is much smaller than that measured in the region of lower dislocation density as might be expected. The figure also shows that the measured diffusion length is dependent on the beam current used for the measurements, other parameters remaining constant. The deduced value of L increases with increasing I_{beam} from 0.8μm to 1.2μm. If the size of the electron probe was reduced by bringing the beam into focus (for constant I_{beam}) the measured efficiency, and hence value of diffusion length deduced, increased. This indicates that it was the density of excess carriers that was the cause of this effect and not simply the number generated. This effect has been investigated in detail for individual dislocations and the results and interpretation are presented in chapters 6 and 7 respectively. Briefly, the results show that when the excess minority carrier concentration Δp, is above a certain threshold level the minority carrier capture cross-section decreases with increasing Δp. Thus if the

diffusion length of minority carriers is controlled by recombination at dislocations then the diffusion length will also be dependent upon the excess minority carrier concentration. The threshold density of excess minority carriers required to produce this effect is quite large at room temperature although it occurs for concentrations which are still much smaller than the concentration of majority carriers. It was to obtain concentrations greater than the threshold level that a spot size of 5μm rather than 40μm was chosen for the diffusion length measurements which demonstrate the dependence on beam current. As the spot size is reduced so the beam current at which the threshold density of carriers is reached is also reduced. Chapter 6 shows that with a focussed beam[1] at 300K, beam currents greater than 10^{-11}A lead to a dependence of dislocation capture cross-section, for the dislocations measured, and hence diffusion length, on beam current. Since beam currents of 10^{-11}A and larger are almost always used in SEM measurements of semiconductors, care must be taken when analysing results made on specimens containing dislocations when such beam currents have been used.

The threshold density of carriers at which the dislocation capture cross-section deviates from its equilibrium value decreases exponentially with decreasing temperature. The beam current into a focussed probe which is required to produce this concentration is estimated in chapter 7 to be of the order of only 10^{-17}A at 131K for the dislocations studied. Clearly accurate measurements of the

1. The focussed beam used produced a roughly spherical generation volume of radius 1μm.

equilibrium minority carrier diffusion length at low temperatures would be very difficult to achieve even when using large spot sizes.

Unless such small beam currents or very large spot sizes are used, the measured diffusion length will be many times larger than the equilibrium value. At 131K the dislocation capture cross-section decreases by ~15% for every increase by a factor of 20 in the excess minority carrier concentration above the threshold level. For these conditions the measured value of the diffusion length, which is not the equilibrium value, is sensitive both to the beam current used and the spot size employed.

The non-linearity of the relation between the EBIC signal produced from a specimen containing dislocations and the beam current used, has also been observed by Sieber (private communication, 1983) for CdTe but no explanation was given.

The effect also invalidates a previous result reported by the present author (Wilshaw et al (1983)) that the diffusion length in a highly dislocated region of a specimen did not vary with the temperature. This result was obtained by using a beam current very much smaller at 120K than at 300K. However both beam currents used were above the threshold level and so neither diffusion length was the equilibrium value. The reduction in beam current at 120K had the effect of decreasing the diffusion length, measured relative to the value which would have been obtained using the beam current employed for the 300K measurement. The smaller beam current was used because the author, at that time, mistakenly believed that the

effect of the increased series resistance of the ohmic contact at 120K could be reduced by reducing the EBIC singal and hence voltage across this resistance. In view of the dependence on minority carrier concentration of the diffusion length in highly dislocated material it is not possible to draw reliable conclusions of its variation with temperature from the results produced in the above work. Further, because of the very small beam currents and large spot sizes required it has not been possible to repeat the work to obtain a value of the equilibrium diffusion length in a highly dislocated region of a specimen at 120K. Such difficulties illustrate the need for caution, particularly at low temperatures, when using excess carrier techniques to measure diffusion lengths in specimens containing dislocations and also the problems in relating the results gained to equilibrium values.

5.5 Summary

The main results of this chapter are summarised below.

1. Analysis has been performed of the way in which the measured EBIC signal from a specimen is produced in relation to the leakage current I_O, of the diode and the series resistance R_S of the ohmic contact. This analysis is especially relevant to diodes contining a high concentration of defects and with ohmic contacts that may have a high resistance at low temperatures.

2. This analysis shows, for the first time, that the EBIC response of the specimen may be split into three régimes. In the first, for small series resistance R_S, the signal measured is the ideal EBIC signal. In the second, when

$R_S \gtrsim R_L$ (R_L is the diode "leakage resistance") and for small EBIC signals such that $I_{EBIC} \ll I_o$, the measured current is reduced but the EBIC contrast of defects remains unaffected independent of how large the series resistance is. For example in the specimens studied $R_S > 8k\Omega$ was observed for some EBIC experiments performed. This is contrary to the widely held view that accurate EBIC contrast measurements may only be obtained from specimens containing a low series resistance. The response in the third régime is similar to that for EBIV as described in the literature and is unsuitable for quantitative experiments. The transition to this régime is shown to depend not only on the value of the series resistance and on the value of R_L but just as importantly, on the magnitude of the EBIC signal generated.

3. Experiments have been described which verify the above analysis and demonstrate that the EBIC contrast measurements made may be related directly to the activity of the dislocations studied.

4. Minority carrier diffusion length measurements have been made which show that the value measured using an excess minority carrier technique on the specimens containing dislocations, described in chapter 3, is dependent upon the excess minority carrier concentration. Results for individual dislocations presented in chapter 6 show that at low temperatures very small excess carrier concentrations are required if the equilibrium diffusion length is to be measured. These concentrations are so low that such experiments may prove difficult to perform.

5. Minority carrier diffusion length measurements in areas free of dislocations, in the specimens used for the work described in chapter 6, show the diffusion length to be independent (within experimental error) of temperature (and beam current) in the range 120K to 300K. From this result it can be deduced that the observed changes in the EBIC contrast of dislocations are due to genuine changes in their recombination strength.

Chapter 6

Experimental Results of the EBIC Investigations of Individual Dislocations

Chapter 6 Experimental Results of the EBIC Investigation of Individual Dislocations

In this chapter details are given of the experiments performed to investigate the recombination strength of well structurally characterised segments of individual dislocations by measuring their EBIC contrast as a function of various experimental parameters. Full details of the specimens used are given in chapter 3.

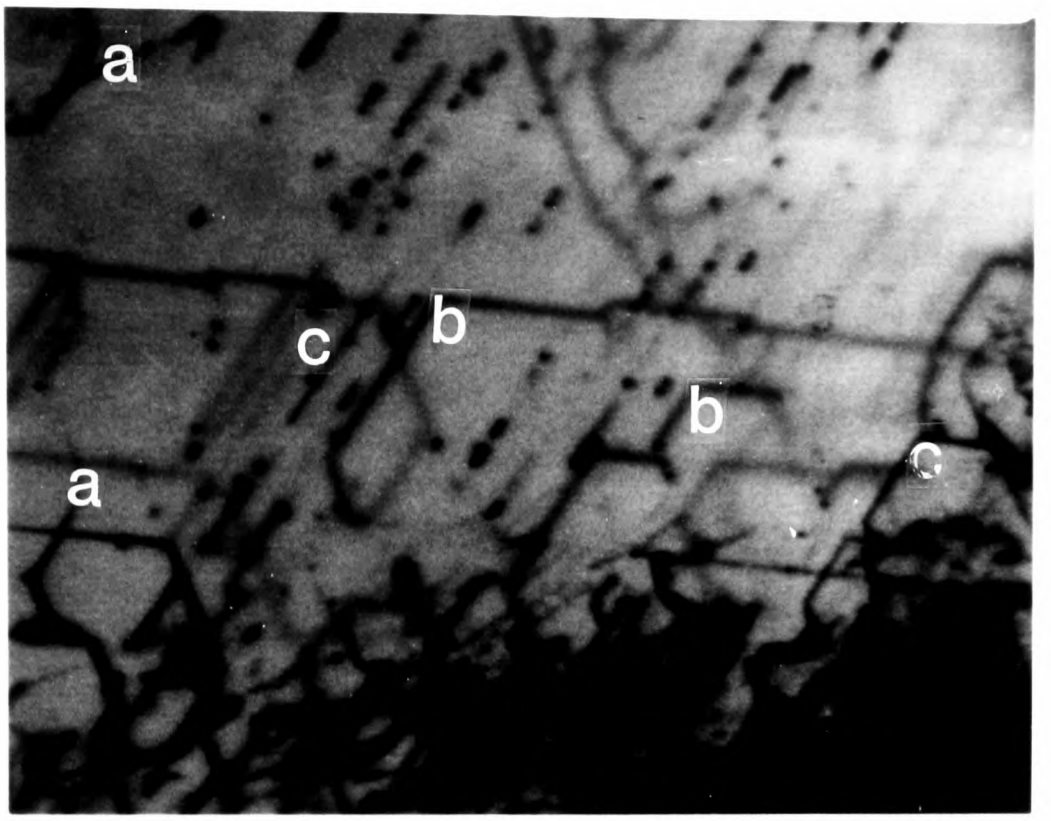
6.1 The General Form of the EBIC Contrast of the Dislocations Studied

Figure 6.1 shows EBIC images of a typical low dislocation density ($\sim 3 \times 10^5$ cm^{-2}) area of specimen 3509/2 taken at 300K. At the bottom of the images the edge of a slip can be seen where the density of dislocations is much higher. These images were taken using the lock-in amplifier with the electron beam chopped at 10kHz as described in chapter 4. The EBIC signal produced as the electron beam is scanned across a dislocaton consists of a small reduction in a large background signal. Thus to increase the contrast of the dislocations on the photograph a DC signal is subtracted from the amplified EBIC signal after phase sensitive detection and before it is fed to the display unit. The maximum EBIC contrast of the dislocations present in Figure 6.1a is ~10% although because of the DC offset applied, the contrast appears greater on the photograph. To enable comparisons to be made the DC offset, magnification, brightness and contrast setting of the camera are the same for figures 6.1 and 6.2a. The pictures were recorded on Polaroid "Land" film at 512ms per line and 500 lines per frame. The lock-in amplifier risetime was 1ms.

Figure 6.1 EBIC micrographs of deformed n-type silicon

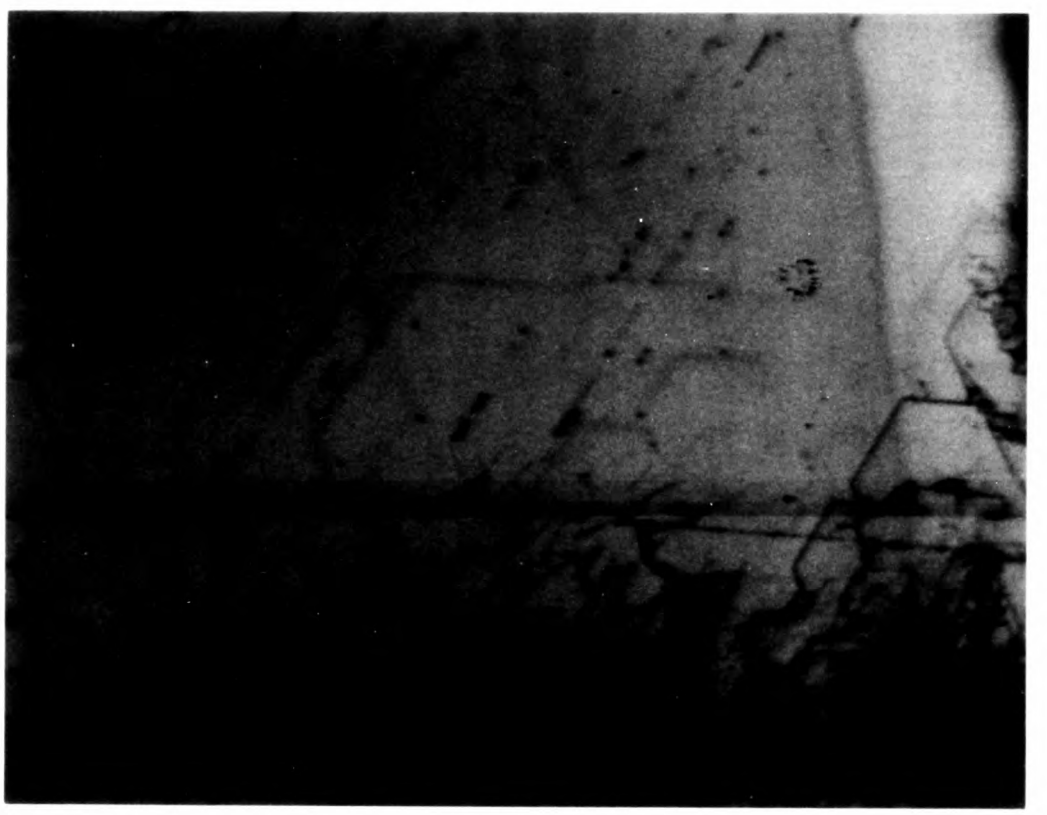
10^{15} cm^{-3}, specimen 3509/2. All micrographs are obtained from the same area at 300K, for accelerating voltages of 15kV, 10kV and 8kV in figures (a), (b) and (c) respectively. The dislocations labelled (a) show a reduction in contrast as the accelerating voltage is reduced, whilst those labelled (b) disappear at 8kV. The contrast of dislocations labelled (c) increases as the voltage is reduced from 15kV to 10kV.

(a)



100μm

(b)



b

(c)

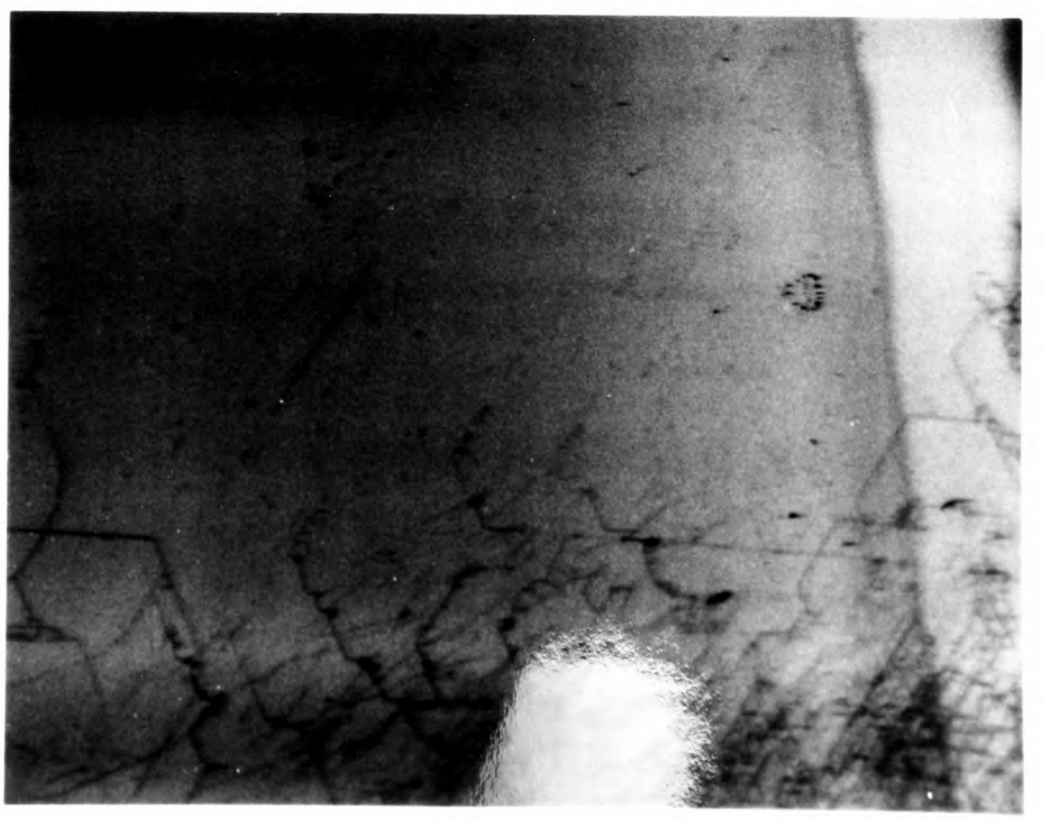


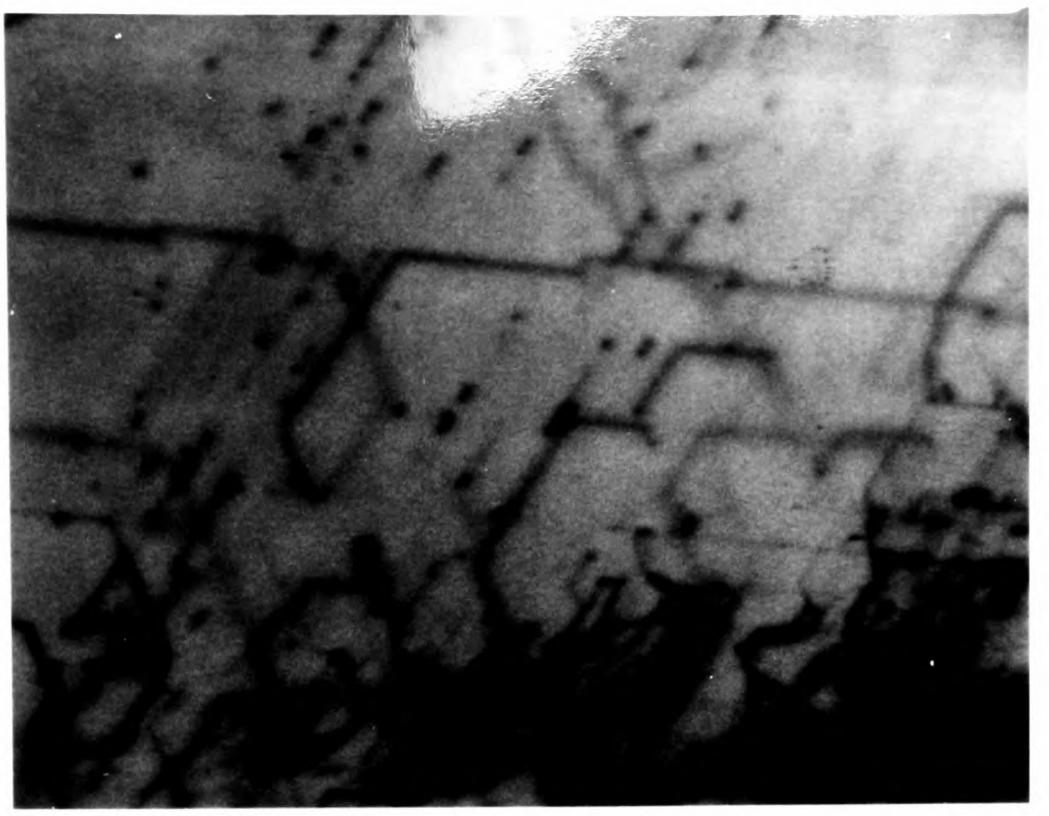
Figure 6.2 EBIC micrographs of deformed n-type silicon

Figure (a) is the same as figure 6.1(a) except that the specimen temperature has been reduced to 120K. Figures (b) and (c) show images obtained from 10^{16} cm^{-3} material (specimen 2722/1) at 4kV. The dislocations observed lie in the depletion region.

(a)

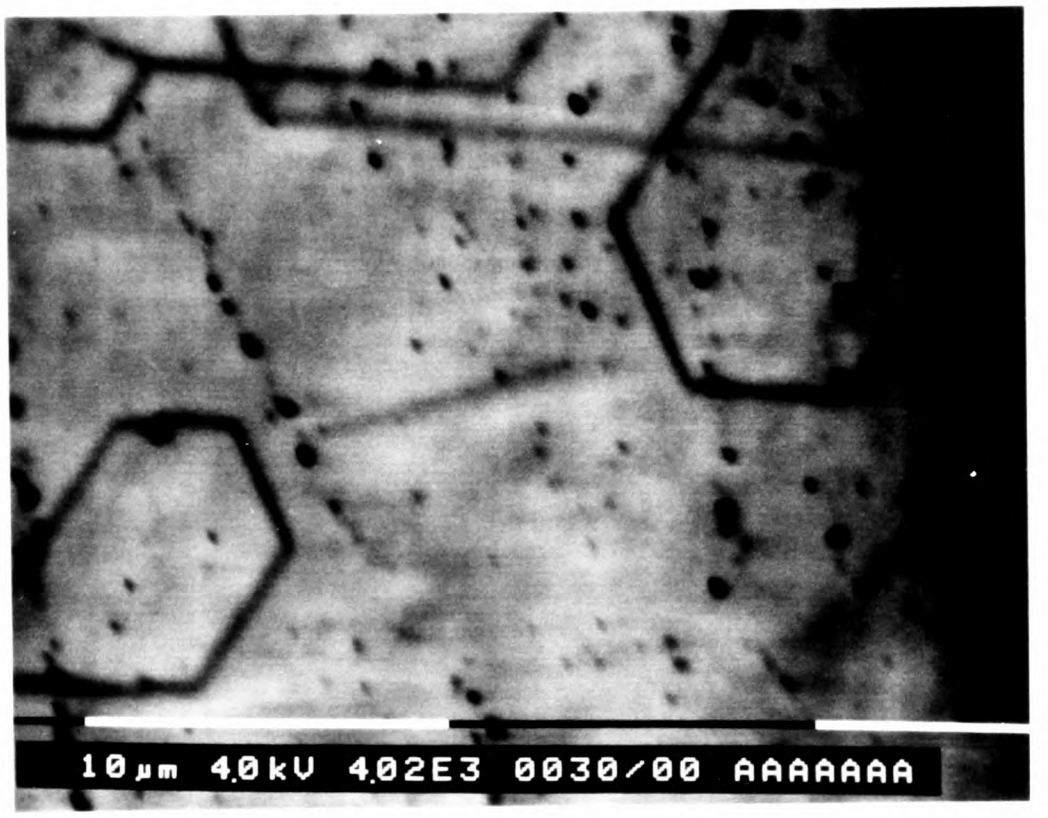
100μm

b



(b)

b



(c)

b



Figure 6.1a was recorded using a 15kV beam at 280X and illustrates the straight deformation-induced dislocations running along the ⟨110⟩ directions on a {111} plane parallel to the surface. The uniformity of the contrast, which is depth dependent, along the length of the dislocations indicates how closely parallel the surface is to {111}. The direction of the Burger's vector $\underline{b}$ is marked. The "dots" visible are thought to be small dislocation loops which were nucleated at 850°C but which did not expand during the 420°C stage of the deformation. They are not the traces of dislocations induced on other {111} planes because most of them are seen to disappear as the beam voltage is reduced (fig. 6.1c) and hence they do not run up to the specimen surface (see below).

The images of different dislocations in figure 6.1a vary both in width and contrast. This is in agreement with the general trends predicted by Donolato's model for a point defect, the results of which are shown in figure 6.3 (see chapter 2 for details of the model used to generate fig. 6.3). The dislocations with weak contrast have image widths either broader than average or, apparently, narrower than average. The broad images are of dislocations deep in the specimen and the narrow ones are of dislocations close to the surface according to the results of Donolato's theory. Thus the qualitative agreement between the images in figure 6.1a and the predictions in figure 6.3 is good.

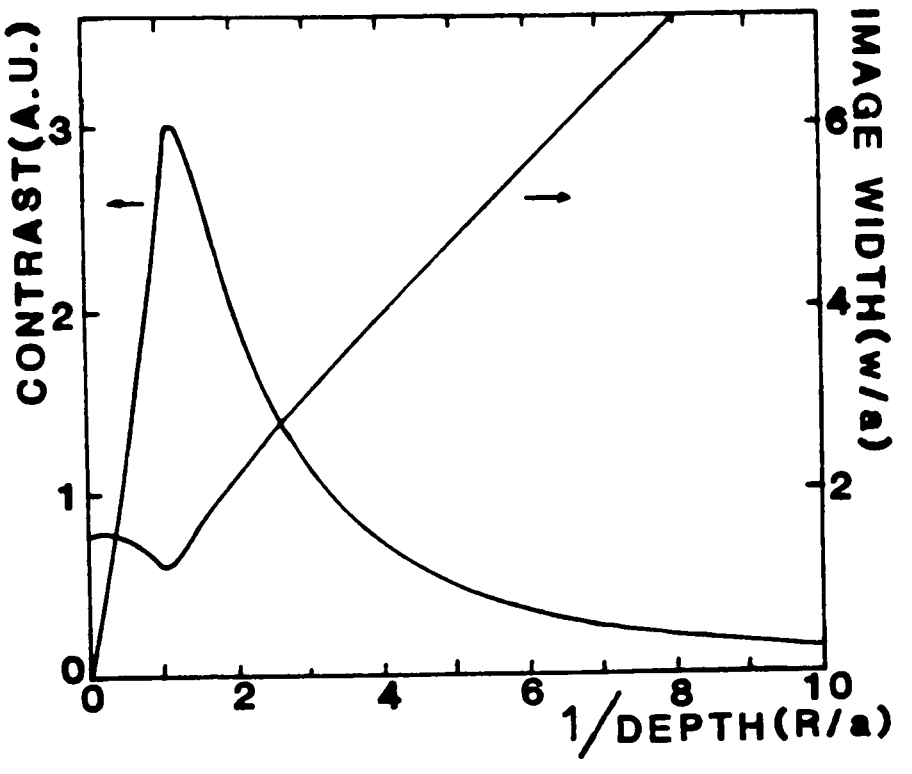


Figure 6.3 Contrast and resolution of the image of a point defect versus normalised electron range

Calculated for an infinite minority carrier diffusion length. After Donolato (1978).

Figures 6.1b and 6.1c show the same area as figure 6.1a but imaged using 10kV and 8kV electrons respectively. The images change in two ways:

i) the contrast of the dislocations changes. This is because the Gruen range of electrons at 15kV, 10kV and 8kV is 2.0μm 1.0μm and 0.7μm respectively. Thus as the beam voltage and hence size of the generation volume is reduced, the depth of the dislocations relative to the generation volume increases. For those dislocations deeper than the point at which maximum contrast occurs, reducing the beam voltage will decrease their contrast by making them effectively deeper still. This is true for the majority of dislocations whose contrast is reduced (some of which are labelled "a" in the figure) or which disappear (labelled "b") as the accelerating voltage is decreased from 15kV to 10kV to 8kV. For those

dislocations just shallower than the point of maximum contrast a reduction in contrast will also occur because the size of the generation volume is made so much smaller at each step. However the contrast of the very shallowest dislocations, labelled "c" in Figure 6.1 is seen to increase on going from 15kV to 10kV as Donolato's theory would predict for dislocations as their relative depth approaches that for maximum contrast. At 8kV only the shallowest dislocations are imaged, these being the ones that gave the weak, narrow images at 15kV. Thus, it can be seen that the general trends predicted by Donolato are substantiated, the observations reported here being similar to those reported by Sieber and Dupuy (1983) for CdTe.

ii) The image width of the dislocations is also seen to decrease with decreasing accelerating voltage. This is because the image width of a dislocation is approximately given by the width of the generation volume. The more accurate treatment given by Donolato (Figure 6.3) shows that although the image width for most dislocation depths will increase for the shallowest dislocations the image width should actually increase slightly with decreasing voltage. However from Figure 6.1 it is not possible to say whether or not this is the case. The depth dependence of the contrast of the dislocations was used to determine whether or not they lay within the depletion region before they were investigated. If, in 10^{15} cm^{-3} material, a dislocation was imaged at 15kV but disappeared for 10kV electrons, the dislocation was assumed to be in the bulk. If a dislocation could be imaged with 6 or 7kV electrons it was assumed to lie in the depletion region.

Figure 6.2a shows the same area as Figure 6.1 at 120K and 15kV. From this it can be seen that the level of contrast of dislocations is reduced with decreasing temperature. For those within the depletion region some of which are labelled "c", the reduction is much greater and some actually disappear. This qualitative observation has been studied in more detail and the results are presented in section 6.4.

The general morphology of the dislocation networks and the EBIC images obtained from 10^{16} cm^{-3} samples are similar to those for the 10^{15} cm^{-3} samples. However in 10^{16} cm^{-3} material the depletion region is only 0.3μm wide and so it is possible to image dislocations in neutral material using a smaller accelerating voltage and hence higher resolution for dislocations in neutral material is possible. For the highest resolution pictures it is necessary to reduce the accelerating voltage as much as possible until the electron probe size becomes the limiting factor in EBIC resolution. Under these conditions it is likely that the dislocations imaged, even in 10^{16} cm^{-3} material, will lie within the depletion region. Figures 6.2b and 6.2c show dislocations in the depletion region imaged using 4kV electrons giving an image width of ~ 0.2μm. The specimen was prepared having a Schottky metallisation 40Å thick so facilitating the use of low accelerating voltages. These images represent the highest resolution EBIC images that have been obtained to date. Unfortunately adjusting the electron optics of an SEM to produce a high current, small diameter probe at 4kV is difficult and figure 6.2b shows clearly the effects of the astigmatism present in the probe

that was too large to be fully corrected. This results in the dislocations running top left to bottom right showing stronger contrast than the other dislocations. This is not due to any fundamental property of the dislocation.

The high resolution obtained when using low accelerating voltages is useful for studying closely-spaced defects and has been used by Ourmazd et al (1983a) to image individual partials comprising a widely separated ($\sim 0.7\mu m$) pair.

6.2 Quantitative Measurement of the Contrast of Dislocations

This section describes the method by which quantitative measurements of the contrast of dislocations were made. The same method was used for the studies of EBIC contrast as a function of the lock-in detection frequency (section 6.4) as a function of temperature (section 6.5) and for the comparison of screw and 60°. In no case was an external bias voltage applied to the specimen and with the exception of the measurements made in section 6.4 the lock-in detection frequency was 10kHz throughout.

In order that an accurate measurement could be made the dislocations studied had to fulfil certain criteria. In general many dislocations would be examined before one suitable for detailed study was found. Wherever possible a pair of screw and 60° dislocations close to each other ($\sim 10\mu m$ apart) would be studied simultaneously so that information about screw and 60° dislocations in the same environment and for exactly the same experimental conditions was obtained. This ensured that a direct comparison of any

changes in their contrast was valid. The background EBIC signal used to calculate contrast was measured at the same point for each dislocation. For the experiment comparing the absolute values of EBIC contrast between screw and 60° dislocations, members of the same loop were chosen to ensure that they were at the same depth. In no case was there any evidence for the formation of beam induced plasmas for the conditions used to make a contrast measurement. The dislocations chosen for study fulfilled the following conditions:

i) They appeared straight within the resolution of the EBIC technique.

ii) No other dislocations were present around the dislocations studied and the background EBIC signal was uniform.

iii) The contrast along the length of the dislocation was uniform in the region where the measurements were to be made. This enabled reproducible results to be achieved for scans across the dislocation varying in position by about 0.5μm, this amount being determined by experimental constraints (see chapter 4).

iv) The dislocation depths were checked by varying the accelerating voltage to ensure they were in either the neutral material or the depletion region as required.

Having selected a dislocation or pair of dislocations the scan direction was rotated to make a suitable angle with the dislocation and the position and length of the line scan adjusted as appropriate. The position of the dislocations or other noticeable features was then marked on the display screen

so that the specimen could be repositioned. If a series of measurements on the same segment of a dislocation was required in general the focus, astimatism and specimen position were checked before each measurement and the beam current recorded. Line scan measurements were generally made at a magnification of 2000 to 4000X with a 2s line time and a lock-in amplification time constant of 30ms. Pre-amplification by the head amplifier was used. Data collection was at 330Hz, 2000 points being collected from 3 sweeps of the beam across the selected region. These three sweeps were measured individually using the computer to calculate the contrast from the data which was smoothed by taking a rolling average of typically, 10 data points. This smoothing removed any noise pick-up introduced after lock-in amplification had taken place. The contrast measurement C, was obtained by averaging the results of each of the three sweeps. Both the raw data and the resultant contrast measurements were stored on a floppy disk for subsequent use. For further details of the computerisation and noise reduction see section 4.2.2.

6.3 Comparison of the EBIC Contrast from Screw and 60° Dislocations

6.3.1 Introduction

It was shown in chapter 2 that the EBIC contrast of a dislocation is dependent upon its depth in the specimen. Thus if the recombination strength of two dislocations is to be directly compared they must lie at the same depth. The specimens studied are ideal for such work because the dislocations lie accurately in (111) planes parallel to the surface. All the dislocations are characterised by the same Burger's vector and thus when a particular dislocation changes

its line direction it may also change its character but will still remain at the same depth. Any change in contrast upon changing its direction may thus be directly related to a change in its recombination efficiency. The photographs in Figure 6.1 and 6.2a show that there is no large difference in EBIC contrast between the two types of dislocations for the conditions used. The beam current used for figure 6.1a is $6x10^{-11}$A and for 6.2, $1x10^{-10}$A. However, to determine whether there are small differences it is necessary to make more accurate quantitative measurements. Many pairs of screw and 60° dislocations which were members of the same loop were studied using the method described in section 6.2.

6.3.2 Results and Comments

A total of 20 different dislocation pairs were studied in 10^{15} cm^{-3} and 10^{16} cm^{-3} material at 300K, both in neutral material and in the depletion region. The results are summarised in table 6.1. From these results it can be seen that, for the conditions used, there is no systematic variation of EBIC contrast between screw and 60° dislocations.

The large scatter in the ratios of the dislocation contrast up to ±20%, is not caused by errors in the actual measurement but might be caused by non-uniformity of the specimen. For example fluctuations in the thickness of the Schottky metallisation or slight undulations of the specimen surface or even changes in the dopant concentration (and hence depletion region width) on a scale of a few microns laterally would all contribute to changes in the measured contrast of dislocations lying in the same (111) plane. In addition to these possible changes due to geometry effects the differences

may also represent actual differences in the recombination strength of the dislocations. These variations however only affect measurements of the absolute level of EBIC contrast and errors are much smaller when looking at how the EBIC contrast of a particular dislocation segment changes during the course of an experiment, see for example sections 6.4 and 6.5.

Apparent systematic differences between the screw and 60° dislocations could have been introduced in two ways and great care was taken to ensure that this was not the case in the present work. The first way would have been if the generation volume had not been circularly symmetric due to astigmatism in the electron beam. For the large generation volume produced by 15kV electrons it is unlikely that the electron beam would be sufficiently astigmatic to have an effect, but at 8kv or lower the effect may have been important and so great care was taken to remove astigmatism from the electron probe. The other way systematic differences could have been produced would have been if the specimen surface had been polished a few degrees off the (111) plane resulting in the dislocations being inclined to the surface. Figure 6.1 shows this was not the case because the dislocation contrast appears to be uniform for dislocations in all directions for distances up to 50μm.

In chapter 7 it is described how the results of contrast vs temperature measurements at different beam currents may be interpreted to show that at high temperatures and low beam currents a systematic difference in the levels of contrast of screw and 60° dislocations is expected. The data presented in this section is however obtained at higher beam currents and lower temperatures where this is no longer the case.

Doping cm^{-3}	Depletion Region	kV	I_{beam}(amps)	Contrast 0°	Contrast 60°	Ratio 0°/60°
10^{15}	No	15kV	3.6×10^{-11}	4.36	4.55	0.96
"	"	"	"	8.43	7.98	1.06
"	"	"	"	8.84	8.25	1.07
"	"	"	"	9.03	7.41	1.22
"	"	"	"	2.92	3.59	0.81
					Average =	1.02
						σ = 0.14
"	"	"			10.94	0.99
			1.2×10^{-11}	10.89		
"	"	"	6×10^{-11}	2.30	2.40	0.96
"	"	"	"	3.14	2.89	1.09
"	"	"	"	3.44	3.62	0.95
"	"	"	"	2.88	2.58	1.12
"	"	"	"	2.30	2.67	0.86
					Average =	1.00
						σ = 0.10
10^{16}	No	8kV	7×10^{-11}	5.10	4.58	1.11
"	"	"	"	6.84	7.12	0.96
"	"	"	"	7.70	7.85	0.98
"	"	"	"	5.43	5.82	0.93
					Average =	1.00
						σ = 0.07
"	Yes	"	"	10.07	9.30	1.08
"	"	"	"	6.84	7.67	0.89
"	"	"	"	6.82	7.05	0.97
"	"	"	"	10.00	9.36	1.07
"	"	"	"	10.58	10.32	1.03
					Average =	1.01
						σ = 0.07

Table 6.1 Contrast Measurements for Screw and 60° Dislocation Pairs at the Same Depth at 300K. σ is the standard deviation of the measurements obtained.

6.4 The Dependence of Dislocation Contrast on the Electron Beam Chopping Frequency

6.4.1 Introduction

In section 7.3.5 full details are given of how the EBIC contrast would vary if the recombination efficiency of the dislocation varied with time after the electron beam was switched on. Preliminary results obtained at Oxford earlier by Ourmazd et al (1981a) indicated a variation of the EBIC contrast of dislocations with the electron beam chopping frequency which was attributed to this effect and so an investigation was undertaken in this work with the more sophisticated system that had been developed here.

6.4.2. Line-Scan Method

The frequency dependence of the EBIC contrast was first measured using the line-scan technique, described in section 6.2, to measure the contrast of a particular dislocation segment at different frequencies of the chopped beam. The frequency was varied in the range 31Hz to 10kHz. The rise time of the lock-in amplifier was increased from 30ms to 300ms so that the increased noise present at low frequencies was sufficiently attenuated to allow accurate EBIC measurements to be made. The amount of noise remaining depended on the size of the EBIC signal and the exact frequency used. The scan speed across the dislocation was reduced so that the line-time was 10s. This ensured that the dislocation profile was not affected by the increased risetime of the amplifier. However,

the longer line-time also resulted in an increase in the scatter of the measurements due to other errors introduced by fluctuations in the beam current over the 10s period. The frequency measurements were only performed at 300K and so possible contamination by the slowly moving beam was not a problem.

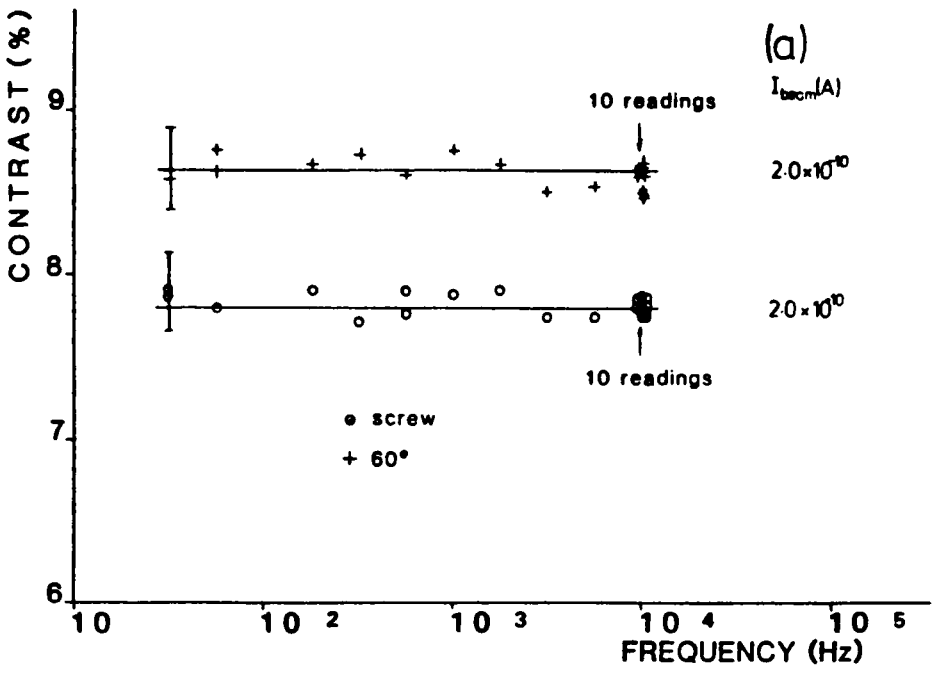
The measurements presented were performed mostly on 10^{16} cm^{-3} material (2722/1 and 2711/3) but some also on 10^{15} cm^{-3} material (3509/2) with a variety of beam currents and accelerating voltages. Screw and 60° dislocations in both the depletion region and neutral material were studied. The results are shown in figure 6.5. The errors are larger for measurements at low frequency than for those at 10kHz because of the increased noise in the signal. Also because the contrast is calculated by the computer which searches for the maximum and minimum present on each sweep, any noise present will tend to increase the measured level of contrast. This effect was kept to a minimum by the noise reduction and averaging techniques applied. In addition to the results presented in Fig. 6.5 two sets of screw and 60° dislocations were measured alternately at 31Hz and 10kHz four times and the ratio of the contrasts at these frequencies calculated. It was from these repeated measurements at 31Hz that the scatter in results, shown by the error bars on the graphs was calculated. The results of these measurements are shown in table 6.2.

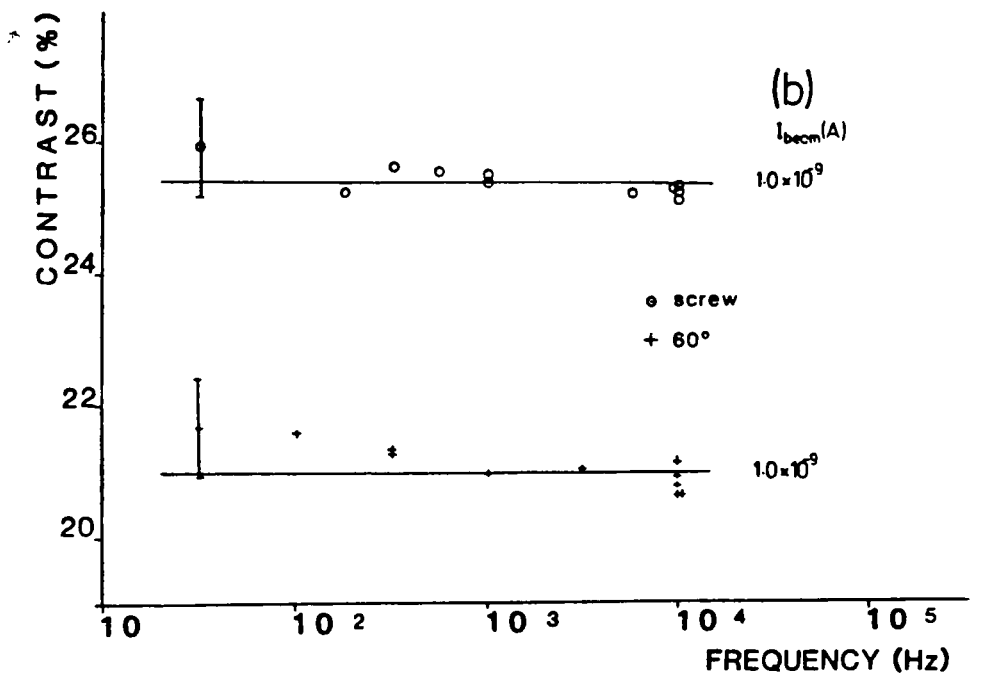
Figure 6.5 EBIC contrast of screw and 60° dislocations as a function of the electron beam chopping frequency. Line-scan method.

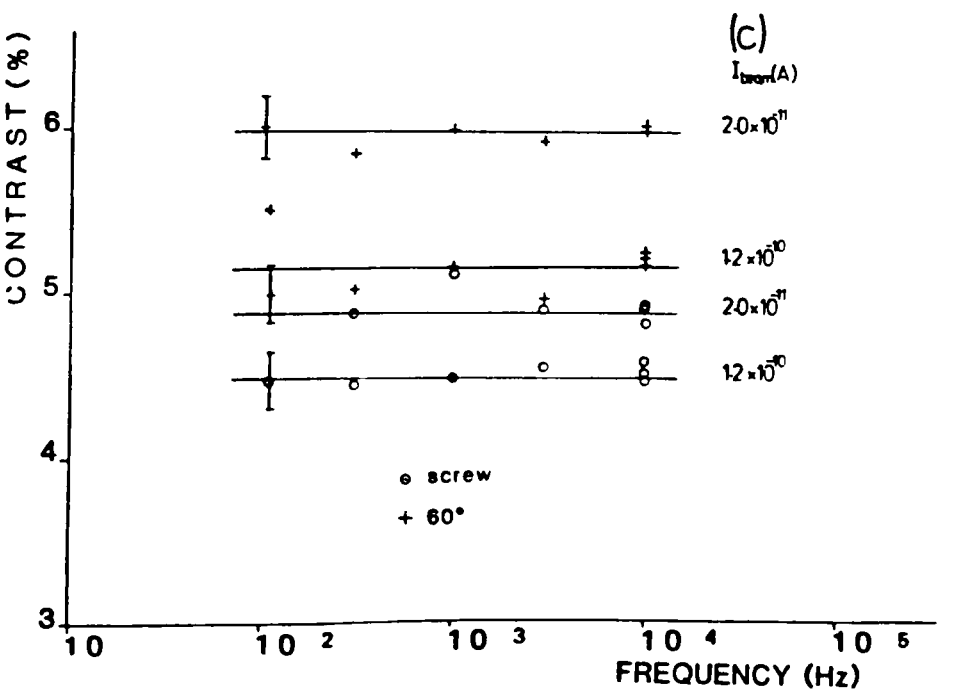
Figure (a) n-type, 10^{15} cm^{-3}, specimen 3509/2 accelerating voltage 15kV, neutral material, beam current 2×10^{-10}A.

Figure (b) n-type, 10^{16} cm^{-3}, specimen 2722/1 accelerating voltage 15kV, neutral material, beam current 10^{-9}A.

Figure (c) n-type, 10^{16} cm^{-3}, specimen 2722/1, accelerating voltage 6kV, depletion region, beam current 1.2×10^{-10}A and 2×10^{-11}A.


(a)
I_{beam}(A)
10 readings
2.0×10^{-10}
2.0×10^{-10}
10 readings
CONTRAST (%)
9
8
7
6
• screw
+ 60°
10
10^2
10^3
10^4
10^5
FREQUENCY (Hz)


(b)
I_{beam}(A)
1.0×10^{-9}
CONTRAST (%)
26
24
22
20
• screw
+ 60°
1.0×10^{-9}
10
10^2
10^3
10^4
10^5
FREQUENCY (Hz)


(c)
I_{beam}(A)
2.0×10^{-11}
1.2×10^{-10}
2.0×10^{-11}
1.2×10^{-10}
CONTRAST (%)
6
5
4
3
• screw
+ 60°
10
10^2
10^3
10^4
10^5
FREQUENCY (Hz)

	$10^{16}cm^{-3}$ 10kV, $I_{beam} = 10^{-9}A$		$10^{16}cm^{-3}$ 8kV, I_{beam} $10^{-10}A$	
	screw	60°	screw	60°
Average Contrast 10kHz	10.97	11.19	14.22	11.38
Average Contrast 31Hz	11.16	11.24	14.32	11.66
Ratio 10kHz/31Hz	0.989	0.979	0.993	0.989
Standard Deviation	0.008	0.014	0.007	0.006

Table 6.2 Ratio of EBIC contrast of dislocations measured at 10kHz and 31Hz for specimen 2711/3.

Thus from figure 6.5 and the results in table 6.2 it can be seen that the relative change in the EBIC contrast of dislocations as a function of chopping frequency is less than ±2% at the particular frequencies measured.

6.4.3 Stationary Beam Method

In this method the beam was positioned first at the dislocation and then nearby in the bulk. At each position the frequency of the chopped beam was ramped from 30Hz to 10kHz on a log scale in ∿10s under computer control, thus enabling the entire frequency range to be sampled. The EBIC signal produced at the specimen was pre-amplified using the head amplifier and the resulting signal was fed into the phase sensitive detector operating in auto-correlation mode with a 100ms rise time. For each of 500 frequencies the output of the phase sensitive detector was read and stored by the computer. The contrast of the dislocation was then calculated for each frequency from the

EBIC values obtained at and away from the dislocation of that particular frequency. The signal processing inthis method results in the EBIC signal obtained being the average from adjacent freqencies whereas in the line-scan method averages are obtained from spatially adjacent signals.

The advantages of this technique are that it allows data to be collected for a much larger number of frequencies thus allowing the entire frequency dependence of the contrast of a dislocation to be measured in ~5 mins rather than a day as with the line-scan method. Also an increase in noise does not artifici ally increase the measured EBIC contrast, only the scatter of the measurements. Its disadvantages are that it does not give an accurate value of the absolute level of EBIC contrast because it is difficult to position the beam exactly at the centre of the dislocation. Also it cannot be used at temperatures other than room temperature because stage drift then results in movement of the beam relative to the dislocation during the 10s duration of a measurement.

Several dislocations were measured in specimen 3509/2 (10^{15} cm^{-3}) using this method at 15kV and typical results are shown in figure 6.6. The large scatter of data points at 50Hz is due to mains pick-up. The small dip at 700 Hz for the screw dislocation shown in figure 6.5a was not reproducible. The contrast measurements performed using this technique show that any frequency dependence of the dislocation contrast is less than ±15% over the complete range of frequencies 30Hz to 10kHz.

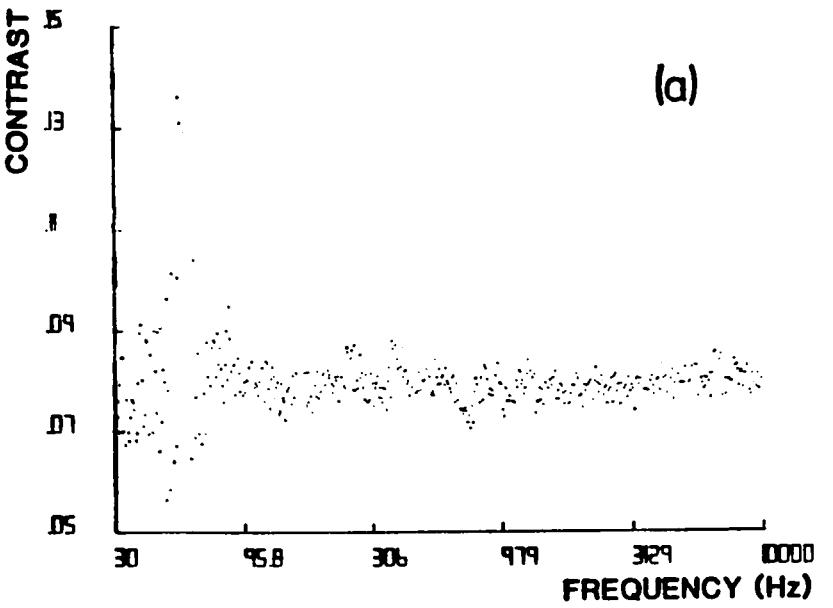


Figure 6.6 EBIC contrast of screw and 60° dislocations as a function of electron beam chopping frequency. Stationary beam method.

n-type, 10^{15} cm^{-3}, specimen 3509/2, accelerating voltage 15kV, neutral material, beam current 5×10^{-11}A.
Figure (a) a screw dislocation
(b) a 60° dislocation

6.5 The Dependence of Dislocation Contrast on Temperature

The contrast of straight screw and 60° dislocation segments was measured, using the line-scan method described in section 6.2 for a range of temperatures. 10^{16} cm^{-3} specimenswere studied using 10kV electrons for temperatures 120K to 300K, whilst 10^{15} cm^{-3} specimens were studied using 15kV electrons over the same range. Initial investigations showed the behaviour of the dislocation contrast for both dopant concentrations to show similar trends in this range and so due to time constraints a detailed investigation was only performed on 10^{15} cm^{-3} specimens. These specimens were chosen because they contained a lower dislocation density and consequently more dislocations suitable for study. The temperature range of the investigation was subsequently increased to 370K and the detailed study of the 10^{15} cm^{-3} specimens was thus extended into this region.

In 10^{15} cm^{-3} specimens, screw and 60° dislocations were investigated both in neutral material and in the depletion region for a range of beam currents. The temperature was controlled using the cold stage and controller described in chapter 4. During an experiment the temperature of the specimen was cycled from room temperature to 120K and then to 370K before returning to room temperature. Measurements were made, typically, at 20K intervals throughout and due to the temperature cycle used were thus measured both on heating and cooling. In all cases the contrast obtained at a particular temperature was independent of whether the specimen was being heated or cooled. This provided evidence that any contamination present on the specimen surface was not affecting

measurements and that impurity segregation towards dislocations or other effects which might occur during the higher temperature part of an experiment were not altering the dislocation contrast on re-cooling, thus providing evidence that such segregation was unlikely. In addition, in some cases, the same dislocation segments were re-measured using identical conditions after a period of some months without any significant change ($\lesssim 0.2\%$) in their EBIC contrast being detected. This provided evidence that long term migration of impurities was also unlikely to be an important factor in determining the level of contrast. The reproducibility of EBIC measurements at 300K was typically $\pm 0.1\%$ for measurements made within a single experiment and $\pm 0.2\%$ for those made in different experiments.

Figure 6.7 shows the temperature dependence of the EBIC contrast of screw and 60° dislocations in neutral 10^{15} cm^{-3} material in specimen 3509/2. These dislocations were not members of the same loop and so were unlikely to be at the same depth. It can be seen that the EBIC contrast decreases with decreasing temperature and that for low temperatures this variation is linear. The variation of the contrast of both screw and 60° dislocations is similar in the linear region and so figure 6.7 shows quantitatively the differences observed qualitatively between the images shown in figure 6.1a and figure 6.2a. At higher temperatures ($\gtrsim 260K$) the variation with temperature becomes sublinear and here a difference in the behaviour of the screw and 60° is observed. The contrast of the 60° dislocation increases faster with temperature than does that of the screw. The difference in the absolute measurement

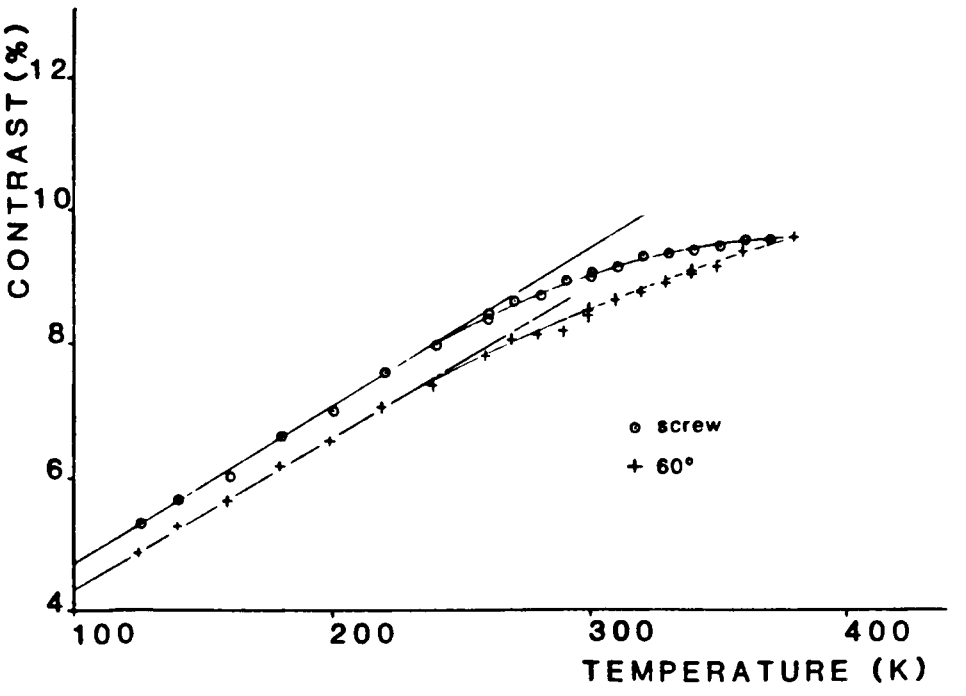


Figure 6.7 Plot of contrast versus temperature for a screw and 60° dislocation

n-type, 10^{15} cm^{-3}, specimen 3509/2, accelerating voltage 15KV, neutral material, beam current≈1.1×10^{-10}A.

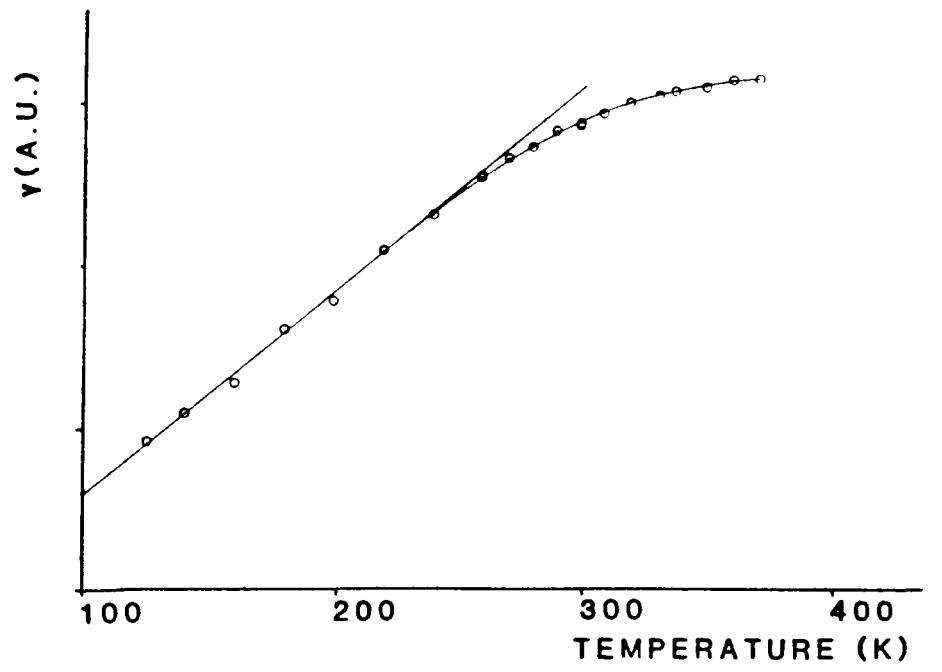


Figure 6.8 Plot of dislocation recombination strength versus T

Contrast measurements used are those of the screw dislocation in figure 6.7. γ is calculated by assuming the relation $C = \gamma^{0.9}$.

(not the percentage change) between the deviation from a linear dependence for the screw and the 60° dislocations is 0.5% at 370K. This implies that had the two dislocations been at the same depth and hence shown the same constrast for large beam currents, the 60° dislocation would now show 0.5% greater contrast than the screw.

Figure 6.8 shows the same data as figure 6.7 but recalculated to show the temperature dependence of γ by assuming the relation $C \propto \gamma^{0.9}$ due to Pasemann (1981), see chapter 2. From figure 6.8 it can be seen that the effect of this correction is approximately the same as scaling the y-coordinates by a constant factor. No significant change in the form of the curve is introduced and so this correction is not applied to any other data.

The temperature dependence of screw and 60° dislocations lying at different depths was investigated, typical results are given in figure 6.9. From these curves it can be seen that the behaviour of all the dislocations studied was similar in that at low temperatures the contrast varies linearly with temperature but begins to level off at higher temperatures (250K). All dislocations lying in neutral material give a positive intercept when extrapolated to the C-axis whilst the screw and 60° dislocations in the depletion region which were measured gave a negative intercept. The value of the intercepts shown is only approximate due to the large errors introduced by extrapolation from 120K to 0K. The magnitude of the contrast of the individual dislocations varies, depending mainly on the depth in the specimen at which they lie. For the screw and 60° dislocations lying in neutral material the

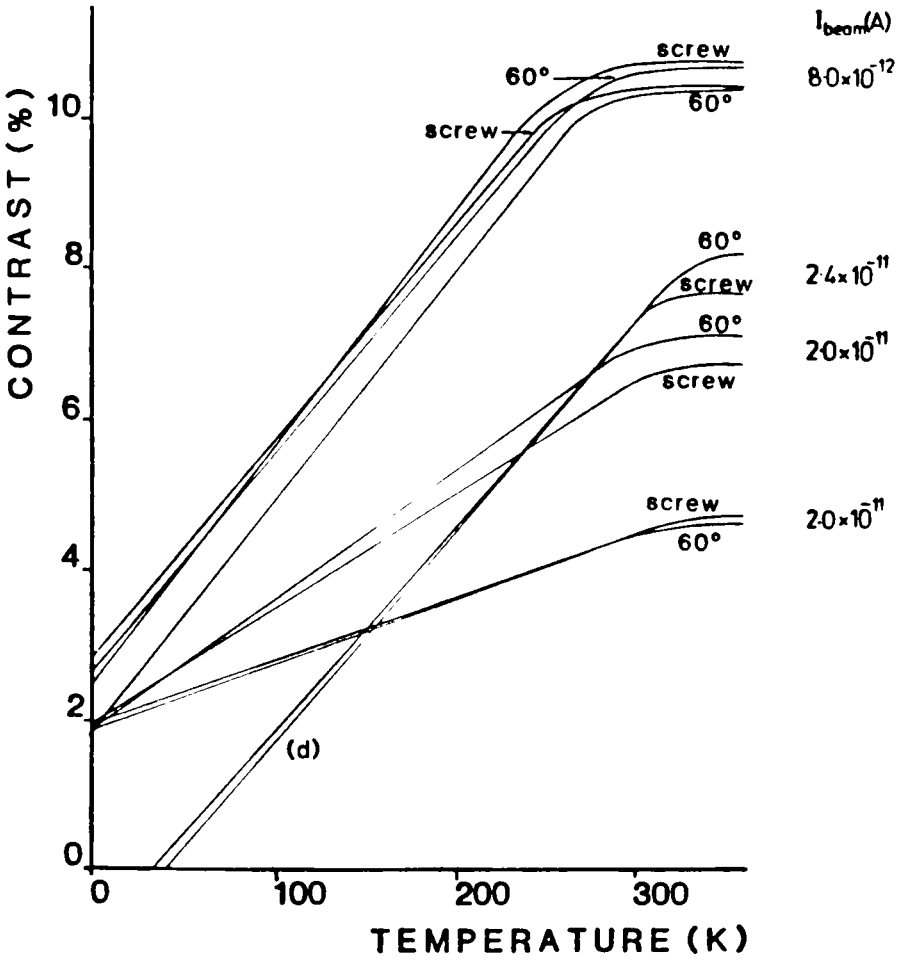


Figure 6.9 Plot of contrast versus temperature for screw and 60° dislocations at different depths

Experimental details as figure 6.7. The beam current is marked against each curve. The curves marked (d) show contrast for dislocations in the depletion region.

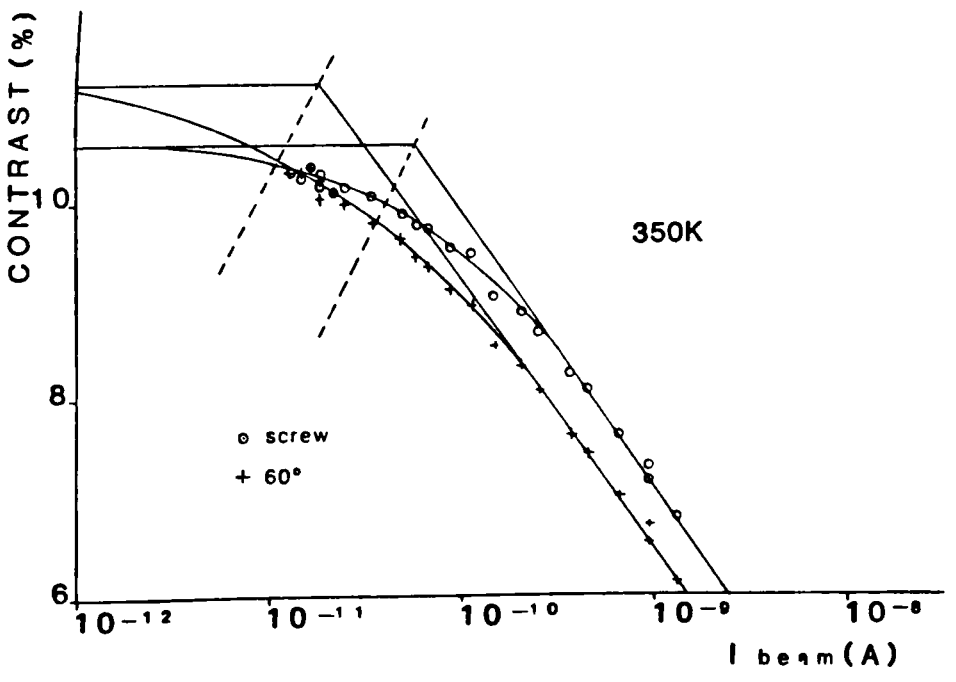


Figure 6.10 Plot of contrast versus beam current at 350K for the screw and 60° dislocation of figure 6.7

The extrapolation of the C versus $\ln(I_{beam})$ data is shown. See chapter 7 for details.

gradient of the linear portion is seen to increase with increasing contrast of the dislocations at any particular temperature, whilst the intercept on the C-axis remains closely the same. The gradient of the C vs T curve for the dislocations in the depletion region is higher than would be expected for dislocations in neutral material giving similar contrast.

Another feature of the curves shown in figure 6.9 is that the temperature at which the transition from a linear to sublinear dependence of contrast on temperature takes place occurs at higher temperatures for larger beam currents.

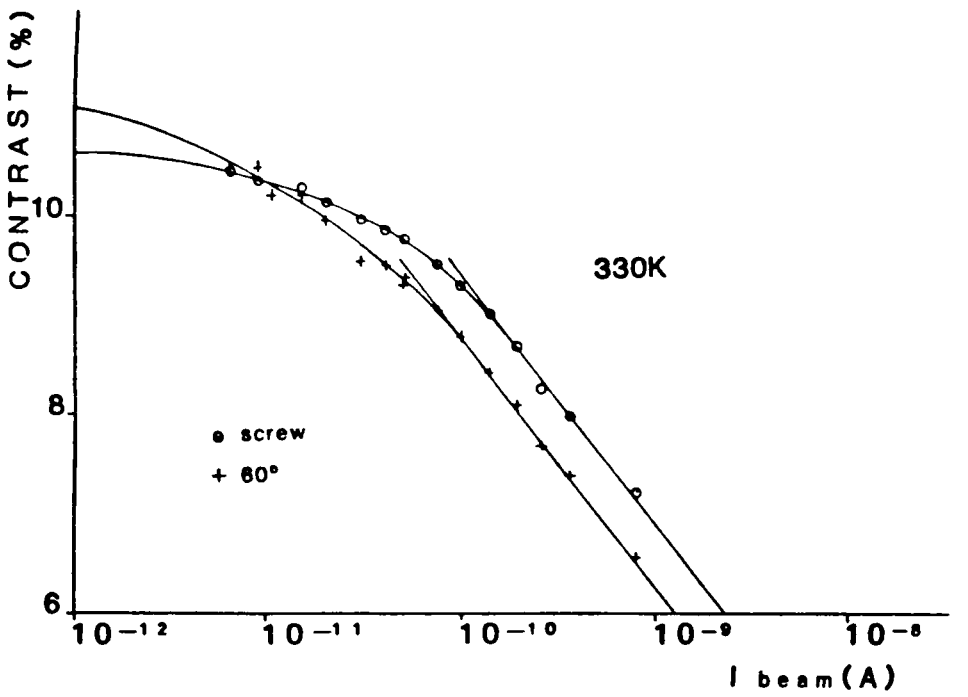
6.6 The Dependence of Dislocation Contrast on Beam Current

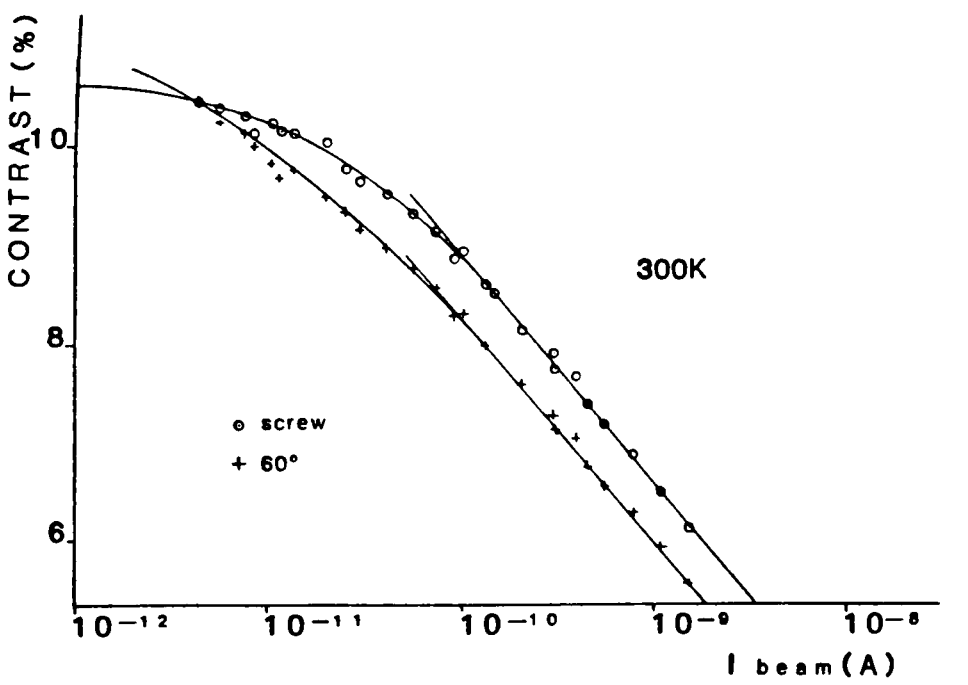
The behaviour of the EBIC dislocation contrast as a function of beam current was investigated for the screw and 60° dislocations in neutral 10^{15} cm-3 material whose temperature dependence is shown in figure 6.7. Their contrast was mesured using the line-scan method described in section 6.2. The beam currents used were varied in the range 6×10^{-12}A to 2×10^{-9}A at specimen temperatures in the range 130K to 350K. The beam current was altered by adjusting the filament heater current and the condenser lens setting. Even at the highest beam currents the probe size was maintained <100nm and hence was much smaller than the generation volume. The results are presented in figures 6.10, 6.11 and 6.12.

In section 5.3 the experimentally observed relation between the measured EBIC signal and beam current was used to establish that, in general, the contrast measured is directly related to the recombination efficiency of the dislocation. However for low temperatures and large beam currents the signal

Figure 6.11 Plots of contrast versus beam current at different temperatures

Same screw and 60° dislocation as in figure 6.7.


CONTRAST (%)
10
8
6
330K
o screw
+ 60°
10−12
10−11
10−10
10−9
10−8
I beam (A)


CONTRAST (%)
10
8
6
300K
o screw
+ 60°
10−12
10−11
10−10
10−9
10−8
I beam (A)

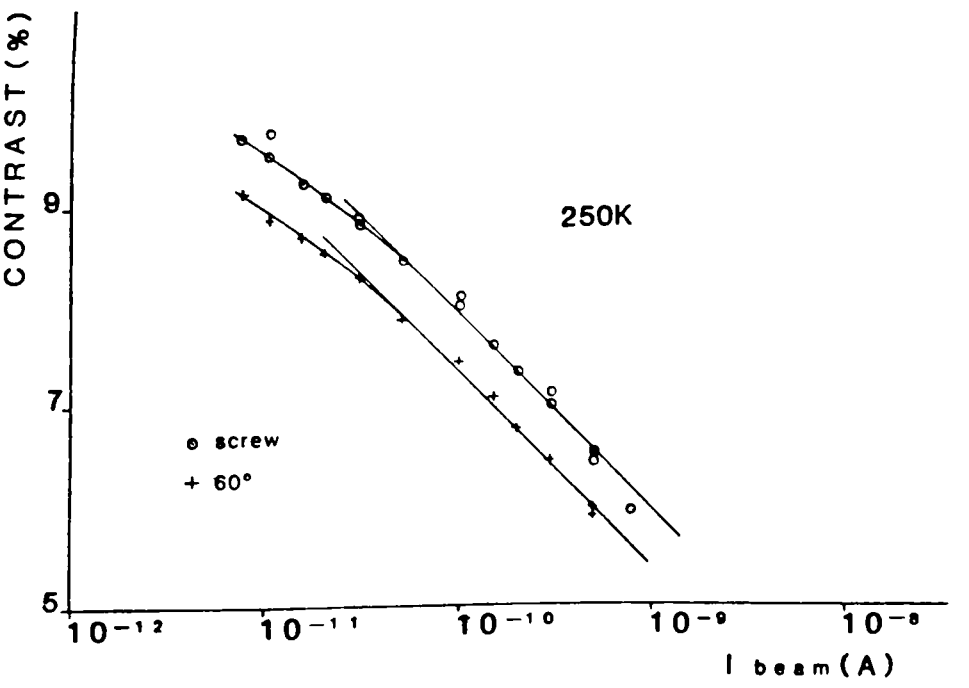
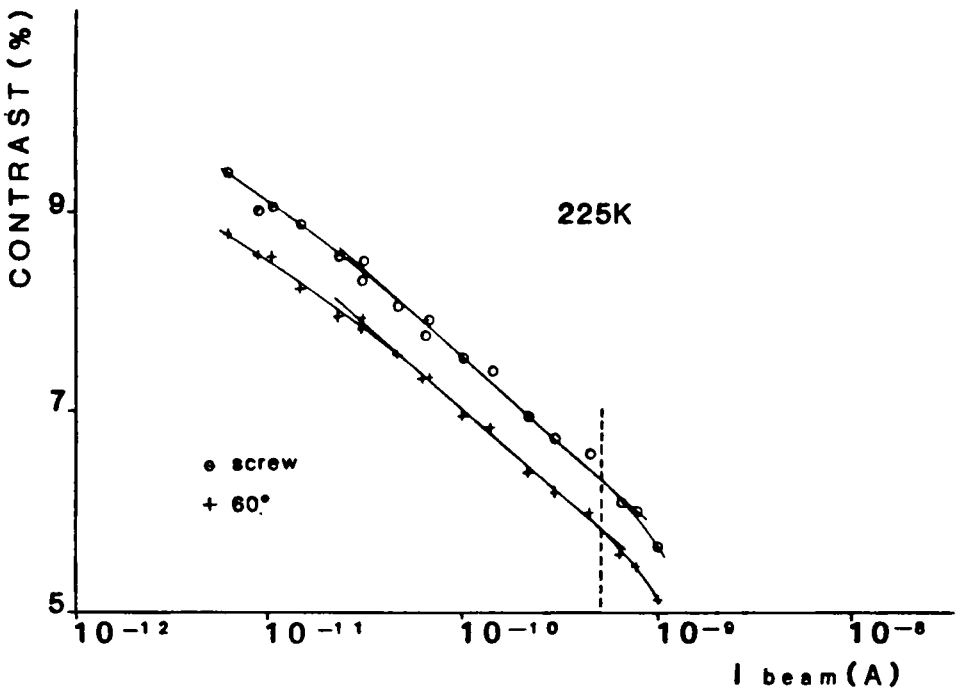
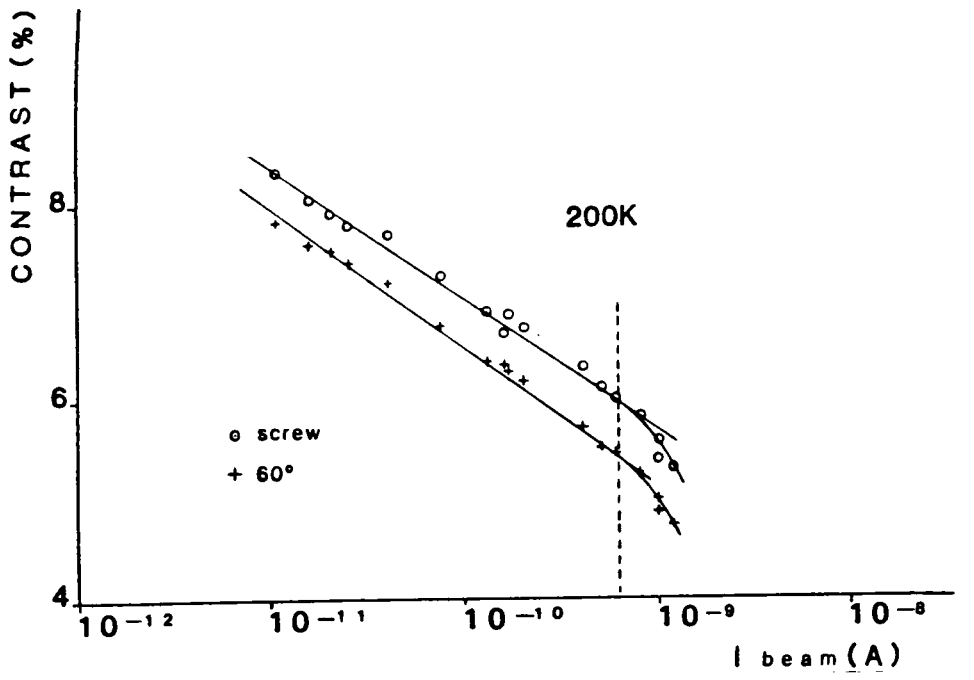
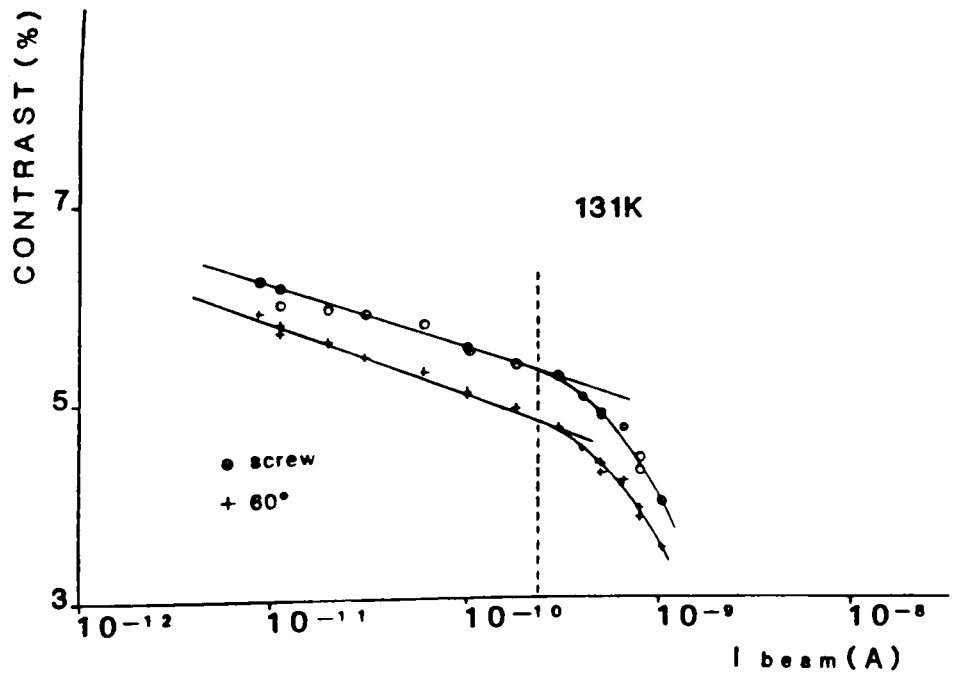

CONTRAST (%)
9
7
5
250K
o screw
+ 60°
10−12
10−11
10−10
10−9
10−8
I beam (A)

Figure 6.12 Plots of contrast versus beam current at different temperatures

Same screw and 60° dislocations as in figure 6.7. See chapter 5 for details of signal collection which result in the rapid decrease of contrast shown for large beam currents at 200K and 131K.


CONTRAST (%)
9
7
5
225K
e screw
+ 60°
10 −12
10 −11
10 −10
10−9
10−8
I beam (A)


CONTRAST (%)
8
6
4
200K
e screw
+ 60°
10 −12
10 −11
10 −10
10−9
10−8
I beam (A)


CONTRAST (%)
7
5
3
131K
e screw
+ 60°
10 −12
10 −11
10 −10
10−9
10−8
I beam (A)

collection became non-linear, this was termed régime 3 of signal collection, and the contrast of a dislocation was then expected to decrease with increasing beam current according to equation [5.5]. The transition to régime 3 was found to occur at I_{beam} 2 x 10^{-10}A and 7 x 10^{-10}A at 131K and 200K respectively for this specimen (3509/2). The measurements of dislcoation contrast presented in figure 6.12 show that their contrast shows a rapid decrease at 1.2 x 10^{-10}A and 5 x 10^{-10}A and 131K and 200K respectively. Thus this decrease in contrast is consistent with the analysis presented in chapter 5 and hence it is not thought to be due to a real change in the recombination efficiencies of the dislocations studied. This effect, which supports the analysis presented in chapter 5 will be excluded from the remaining discussion in this chapter and chapter 7.

These results demonstrate that for each temperature studied there is a major portion of the C vs $\ln(I_{beam})$ curve which is straight. In this region and for the range of beam currents studied, the behaviour of the contrast at constant temperature may be described empirically by

$$C = A - B \ln(I_{beam}) \qquad [6.1]$$

where A and B are constants which may vary with temperature (and from dislocation to dislocation) and I_{beam} is here taken to be the numerical value of the beam current when measured in amps. For small beam currents at high temperatures the curve begins to level off with decreasing I_{beam}. These results are the first reported observation of any variation in the EBIC contrast of dislocations, or indeed any defects, with the beam current with which they are measured. This is a large effect,

for example, the contrast of the dislocations studied has been observed to change from 10% to 5% on changing the beam current from 10^{-11}A to 10^{-9}A.

At high temperatures, 330K and above, and for very small beam currents, 6 x 10^{-12}A, the contrast of the screw dislocation becomes independent of beam current. For these conditions the contrast appears to be constant with increasing temperature. This effect is thought likely to occur at higher temperatures for the 60° dislocation because the rate at which the contrast levels off is smaller . However, in this case, it was not possible to take measurements at sufficiently high temperatures to directly detect the expected constant contrast with increasing temperature, see figures 6.10 and 6.11. The data used in chapter 7 showing this constant contrast region are obtained by extrapolating the contrast vs current curves to sufficiently small values of current.

The beam current at which the contrast begins to deviate from a linear relationship with $\ln(I_{beam})$ is seen to be larger at higher temperatures. The curves showing the beam current dependence presented in figures 6.10, 6.11 and 6.12 may be related to the curve showing the temperature dependence of the same dislocation segments. The temperature dependence measurements were recorded using a beam current of 1.1 x 10^{-10}A. It can be seen that data points lying on the linear portion of the temperature dependence curve also lie in the linear region of the beam dependence curves. The curved portion of the temperature dependence curve corresponds to the high temperature, small beam current region of the beam dependence curves.

A full set of contrast vs temperature curves at different beam currents are produced by replotting the data shown in figures 6.10, 6.11 and 6.12 on contrast vs temperature axes. This is shown for screw and 60° dislocations in figures 6.12 and 6.13 respectively. The temperature at which the variation of contrast with temperature begins to become sublinear is seen to increase with increasing beam current (Figures 6.13 and 6.14). Empirically the straight portions of the curves may be described by

$$C \simeq \alpha - \beta T \ln (I_{beam}) \qquad [6.2]$$

which show s that the constant B in equation 6.1 does vary with temperature. This relation is only approximate because the extrapolation of the straight lines to the C-axis, i.e. absolute zero, shows that they do not meet at a single point (β) but instead over a range of C values varying by ~1.5%. However the maximum error introduced by approximating the behaviour observed to equation 6.2 is only ~0.25% (absolute not percentage error in contrast measurement) for the range of temperatures and beam current investigated experimentally, see figures 6.13 and 6.14.

6.7 Summary

This work represents the first detailed investigation using EBIC of the temperature and beam current dependence of the recombination activity of individual dislocations in any semiconductor. It has confirmed the general trends predicted by Donolato's theory of EBIC image formation. The quantitative measurements made on straight screw and 60° dislocations in the silicon specimens used here have shown:

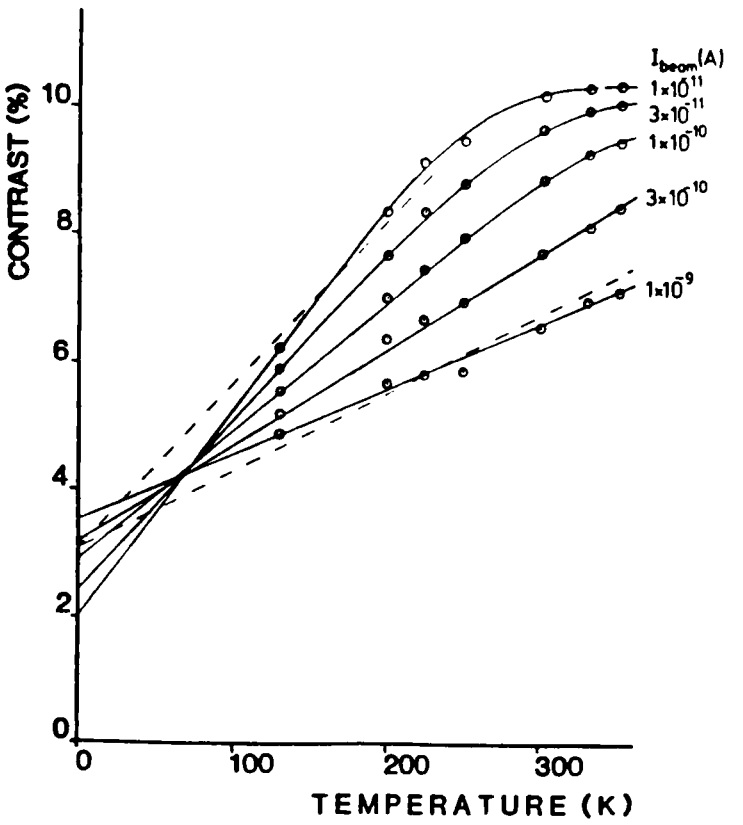


Figure 6.13 Plot of contrast versus temperature at different beam currents for the screw dislocation of figure 6.7

This data is taken from figures 6.10, 6.11 and 6.12. The dotted lines show curves fitting equation [6.2] of the text.

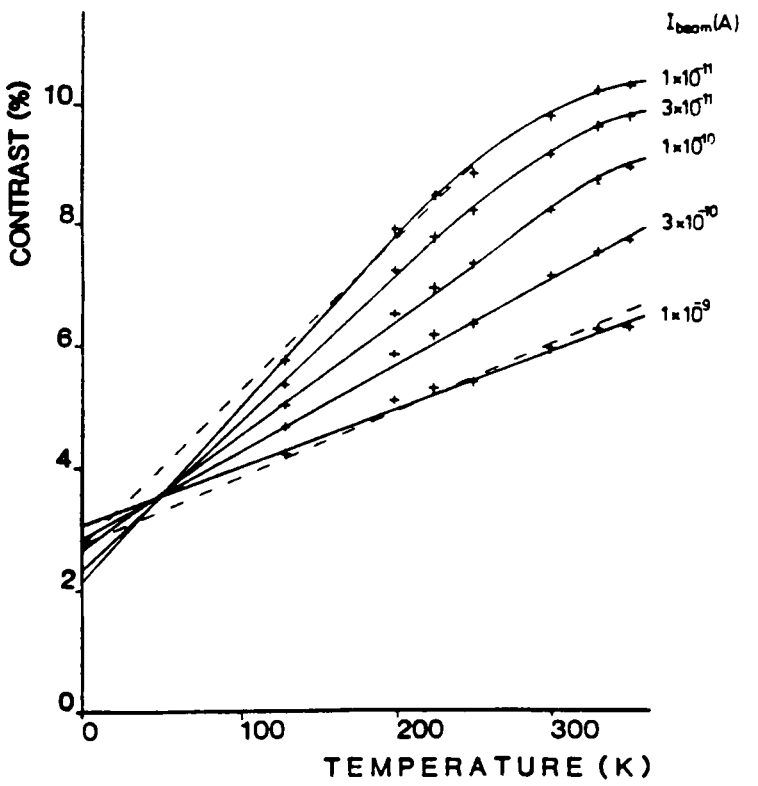


Figure 6.14 Plot of contrast versus temperature at different beam currents for the 60° dislocation of figure 6.7

Details as figure 6.13.

1. That the EBIC contrast of screw and 60° dislocations at the same depth are equal for high levels of minority carrier injection and that the 60° shows higher contrast at low levels of injection and high temperatures for members of the same loop. The carrier concentration at which the transition occurs depends on the specimen temperature.

2. The contrast of screw and 60° dislocations is independent of the frequency with which the electron beam is chopped in the range 30Hz to 10kHz.

3. At low temperatures and for large beam currents the variation of dislocation contrast is linear with temperature.

4. At low temperatures and for large beam currents the change in dislocation contrast is proportional to $-\ln(I_{beam})$, where I_{beam} is the numerical value of the beam current measured in amps.

5. At high temperatures and small beam currents the contrast begins to become independent of beam current and levels off with increasing temperature. In this régime differences are seen between the behaviour of screw and 60° dislocations.

Chapter 7

The Theory of Recombination at Dislocations and Discussion of Results

CHAPTER 7: The Theory of Recombination at Dislocation and Discussion of Results

7.1 Introduction

The previous chapters have described the design and construction of an EBIC system which allows high accuracy measurements of the EBIC contrast of individual dislocations to be made and it has been shown that these measurements may be directly related to the electrical activity of the dislocation itself. Details of the experimentally observed behaviour of the EBIC contrast have been given. It is the purpose of this chapter to formulate a model for the physical processes taking place at the dislocation in such a way that the theory describes the experimental results obtained. This model leads to a better understanding of how recombination at dislocations occurs and gives some insight into the values of the physical parameters involved. Finally the work of others is discussed in relation to this theory together with the implications for EBIC measurements generally.

The following discussion is restricted to n-type silicon in which dislocations introduce acceptor states into the band gap. These states form a band normally below the position of the Fermi level. Some of the states are occupied and so the dislocation becomes negatively charged. This negative charge increases the energy of electrons in the vicinity of the dislocation and is represented on a band diagram by the conduction and valence bands bending up.

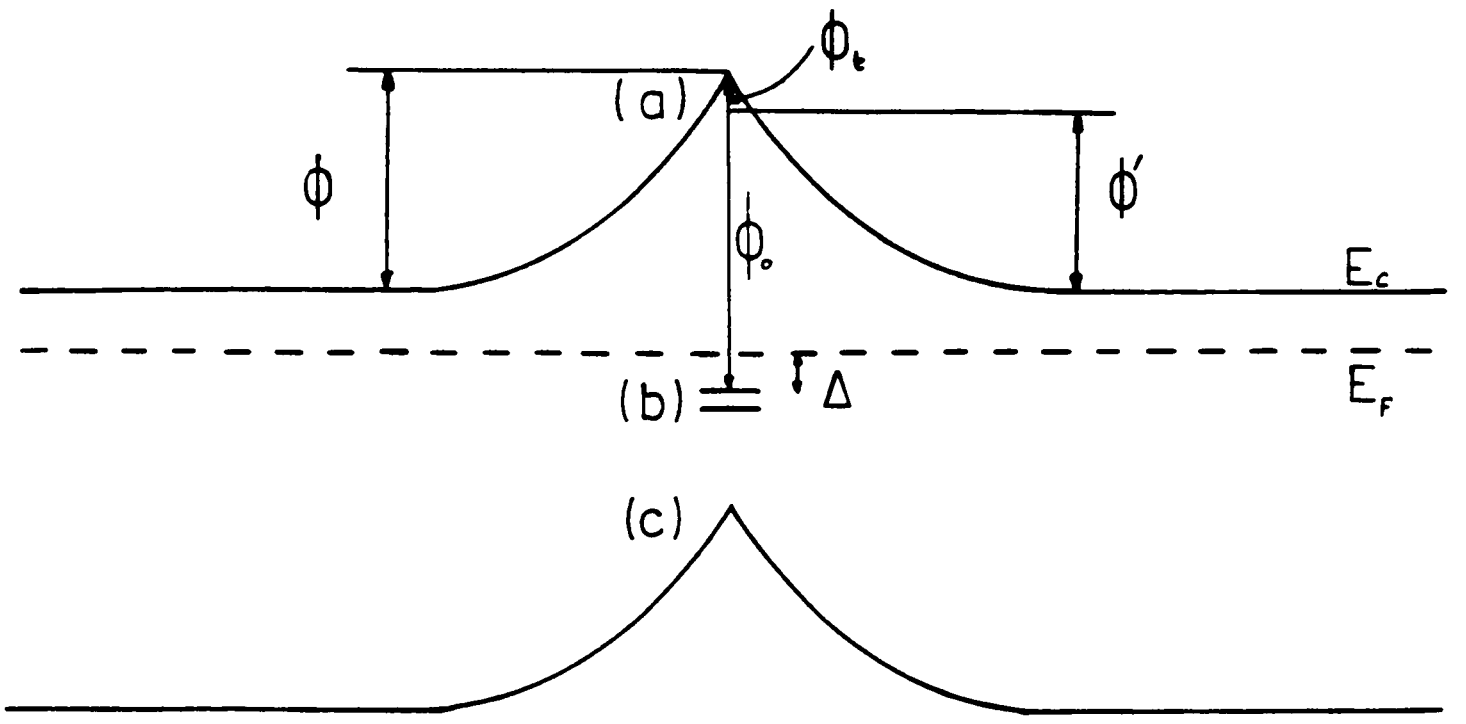


Figure 7.1 Diagram of a charged dislocation
(a) is the "tunnelling level" (Labusch (1979))
(b) is the dislocation level
(c) is the bound hole level

ϕ_o, is the distance below the conduction band of the dislocation level
ϕ', is the effective barrier height for electron capture
ϕ_t, is the reduction for barrier height due to tunnelling
ϕ, is the barrier height
Δ, is the difference between the dislocation level and the Fermi level

It is normally assumed that the addition of electrons to the dislocation energy level does not alter its position relative to the band edges and so as the charge on the dislocation is increased the dislocation level will rise by the same amount. Mergel and Labusch (1982), however, consider the case of variable core reconstruction where this will not be true, but

this possibility will not be included in the following discussion. The equilibrium charge state is usually reached when the Fermi level runs through the bottom part of the dislocation band and this results in a few percent of the available states[1] along the dislocation core being occupied. The spatial extent of the wave functions associated with the dislocation states (~10Å) is small compared to the long range electrostatic potential which normally extends for greater than 0.1μm and so the entire dislocation level can be considered to be rigidly shifted by the electrostatic potential of its charge.

Recombination of carriers proceeds via the capture of minority carriers, a process which is aided by the attraction of the charge on the dislocation. Majority carriers make the transition to the dislocation level after excitation over the repulsive potential due to the negative dislocation charge. It is the detailed processes of recombination and the effect these will have on the measured electrical properties that different authors have treated in different ways. For example Labusch (1979) considers an arbitrary system of energy levels induced by a dislocation and shows that in most cases recombination will be limited by a single rate-determining step provided that the recombination rate is sufficiently low. He assumes that the holes in the

1. Assuming one state per dangling bond or two per reconstructed electron pair.

bound hole state are in thermal equilibrium with the valence band and then deduces an exponential dependence for minority carrier lifetime with reciprocal temperature, the activation energy depending upon which dislocation levels form the rate determining step. This analysis is extended to treat the decay of an excess concentration of majority carriers and so is applicable to low excitation photoconductivity experiments.

Figielski (1978) considers higher excitation[1] for which the charge on the dislocation changes both as a function of excitation and temperature. He derives equations which predict the steady-state excess free carrier concentration for a given injection level and then uses these to describe photoconductivity experiments at both high and low injection levels. For all but the highest temperatures he assumes virtually all the minority carriers to be trapped at the dislocation bound hole level and that the capture cross-section for this process is independent of the temperature and the degree of excitation. The observed changes in photo-conductivity are then entirely due to changes in the majority carrier recombination because the concentration of free excess majority carriers is many orders of magnitude higher than that of the free minority carriers. Thus Figielski's work, which concentrates on majority carrier lifetime, assumes the capture of minority carriers to be constant except at very high temperatures.

Ourmazd (1981) modifies the two-stage model for deep level capture postulated by Gibb et al. (1977) to describe recombination at dislocations in order to explain the EBIC

1. i.e. a larger concentration of injected carriers.

results presented by Ourmazd and Booker (1974). He considers two temperature régimes for dislocations in heavily doped material for which the position of the Fermi level is assumed constant. At low temperatures he assumes no thermal re-emission of holes from the bound hole state and for lightly charged dislocations he then deduces a constant capture cross-section. For heavily charged dislocations he postulates that excitation of electrons over the potential barrier would become rate determining leading to an exponential dependence on inverse temperature. At high temperatures Ourmazd assumes thermal re-emission of bound holes and this leads to an exponential temperature dependence for both lightly and heavily charged dislocations in this régime. Thus Ourmazd also finds the capture of minority carriers to be constant or exponentially dependent on temperature.

In the following a new theory is proposed which is also based upon the barrier model fundamental to the other theories discussed here.

7.2 Recombination at Dislocations

In n-type material the capture of holes is very fast because the dislocations are negatively charged. However, at steady state the rate of capture of electrons and all subsequent transitions must equal the rate of capture of free holes by the bound hole state. Thus a full description of the capture of holes will result in a full description of the recombination rate of both minority and majority carriers at dislocations and should be applicable to any semiconductor where recombination is not diffusion-limited provided the

assumptions used remain valid. In the following it is assumed that the number of excess electrons $\Delta n \ll n_o$, the majority carrier concentration, and that n_o remains constant throughout. It is also assumed that $\Delta p \gg p_o$ and that bound holes are not thermally re-emitted into the valence band. This is also assumed in the theories of Figielski, and Ourmazd for low temperatures, but here it is assumed for all temperatures and experimental conditions for which $\Delta p \gg p_o$ in the excited n-type material. For doping levels of $10^{15} cm^{-3}$ and greater and temperatures of 350 K or less this condition will certainly be met in all EBIC and photoconductivity experiments. The justification of this assumption is given in section 7.3.2.

The capture of free holes by the bound hole band takes place in the space charge region surrounding the dislocation. Capture occurs as the hole cascades through a series of excited states, a process which has been studied theoretically by Sokolova (1970). She finds that the lifetime of holes within this region varies as $T^{1.5}$ and is independent of the charge on the dislocation. γ, the strength of the dislocation as a recombination centre is defined as:

$$\gamma = \frac{\pi r_d^2}{D_h} \left(\frac{1}{\tau'} + \frac{1}{\tau} \right)$$

where r_d is the radius of the space charge region surrounding the dislocation, τ' is the lifetime governed by cascade capture and D_h is the diffusion constant for holes.

For $\gamma' \ll \gamma$ this gives:

$$\gamma = \frac{\pi r_d^2}{D_h} \quad \frac{1}{\gamma'} \qquad [7.1]$$

where γ is a dimensionless quantity. The rate of capture of holes per unit dislocation length J_h (cm^{-1} s^{-1}),

becomes $J_h = \Delta p D_h \gamma$ [7.2]

where Δp is the excess hole concentration at the dislocation. The dislocation strength γ, is related to the capture cross-section σ_h, of the defect states whose concentration along the dislocation is N_d (cm^{-1}), by

$$\sigma_h = \frac{D_h \gamma}{V_{th} N_d} \qquad [7.3]$$

where V_{th} is the thermal velocity of holes. It will be assumed that the dislocation acts only as a weak recombination centre so that Δp at the dislocation is the same as Δp in the bulk. This ensures that the recombination flux is directly proportional to γ. D_h and γ' are taken to be independent of Δp.

From [7.1] it can be seen that the recombination strength of the dislocation depends upon r_d, the radius of the space charge region. r_d is given by the condition of charge neutrality:

$$\pi r_d^2 = \frac{Q}{n_o q} \qquad [7.4]$$

Where Q is the net excess negative charge per unit dislocation length. Equation [7.4] is accurate provided that the barrier height is large compared with KT. This is because the edge of

the space charge region is not entirely depleted of carriers, until the bands have bent up by more than KT. For the experimental conditions encountered in the present work the barrier height is approximately ten times greater than the thermal voltage and so equation [7.4] is accurate. The relation between Q and the amount of band bending ϕ, has been calculated by Read (1954):

$$\phi = \frac{Q}{2\pi\epsilon\epsilon_o}\left[\frac{3}{2}\ln\left(\frac{Q}{(\pi n_o)^{\frac{1}{3}}q}\right) - 0.616\right] \qquad [7.5]$$

where ϕ has units of volts.

This is valid when the following conditions have been met:

i) The space charge cylinder contains ionised donors and the electrons have been expelled. This condition is the same as that required for the accuracy of equation [7.4].

ii) The spacing of charged sites along the core is much less than the radius of the space charge region, thus allowing the line charged to be treated as uniform.

The value of ϕ can be obtained by considering the electron flux over the potential barrier. Labusch (1979) has pointed out that the electrons will tunnel through the barrier a distance ϕ_t from the top where ϕ_t may be a few hundredths of a volt, see figure 7.1. Thus the potential barrier for the transition to the dislocation level via the tunnelling level is:

$$\phi' = \phi - \phi_t$$

however in the following ϕ_t will be assumed much smaller than ϕ

and hence $\phi \simeq \phi'$. Now by detailed balance the net electron flux J_e, i.e. the number of electrons per unit dislocation length, making the transition to the dislocation state is:

$$J_e = C_e N_d \left(n_o \exp \frac{-q\phi}{KT} \; (1-f) - f \, N_c \exp \frac{-q\,\phi_o}{KT} \right) \qquad [7.6]$$

where C_e ($cm^3 s^{-1}$) is the probability of transition between a dislocation state and the conduction band,

N_d (cm^{-1}) is the number of states in the dislocation level per unit length,

f is the fraction of dislocation states occupied,

N_c (cm^{-3}) is the effective density of states in the conduction band.

ϕ_o (V) is the difference in potential of the occupation limit of the dislocation level and the bottom of the conduction band.

Rearranging the above expression for J_e gives:

$$\phi = - \frac{KT}{q} \left(\ln \frac{J_e + C_e N_d f N_c \exp \frac{-q\,\phi_o}{KT}}{(1-f)\, C_e N_d n_o} \right) \qquad [7.7]$$

At steady state $J_e = J_h = J$, the recombination rate per unit length, thus equations [7.4] to [7.7] describe the dependence of the extent of the space charge region on temperature and recombination rate. Equation [7.1] can then be used to obtain, implicitly, the dislocation recombination strength γ.

The resulting expression is rather long and instead a simplified form will be used. This is obtained by using the following approximations:

i) The number of dislocation states per unit length N_d, is not known because the nature of the defect responsible for this state is itself unknown. In the following the value for N_d will be assumed to be $\gtrsim 2\times10^{7}cm^{-1}$. For the values of ϕ deduced experimentally in this work, ($\lesssim 0.2$ V), this results in $f \lesssim 0.1$ for $10^{15}cm^{-5}$ and 10^{16} cm^{-3} material, allowing the approximation $1-f \simeq 1$ to be made in the following. It is stressed that taking $N_d \gtrsim 2\times10^{7}cm^{-1}$ is only an assumption. However, other workers (for example Figielski (1978), Kittler (1981)) also make the same assumption and it seems likely to be true if the dislocation states are due to dangling bonds or a large concentration of impurities. Possible implications of taking $N_d < 2\times10^{7}cm^{-1}$ are discussed in section 7.5.3.

ii) Equation [7.5] is plotted in figure 7.2 from which it can be seen that for 0.05 V $< \phi <$ 0.2 V, (1.5×10^{-13} $Ccm^{-1} < Q < 3.8 \times 10^{-13} Ccm^{-1}$) the expression may be approximated by $\phi = \beta Q - \delta$. This simple relation can then be used instead of [7.5].

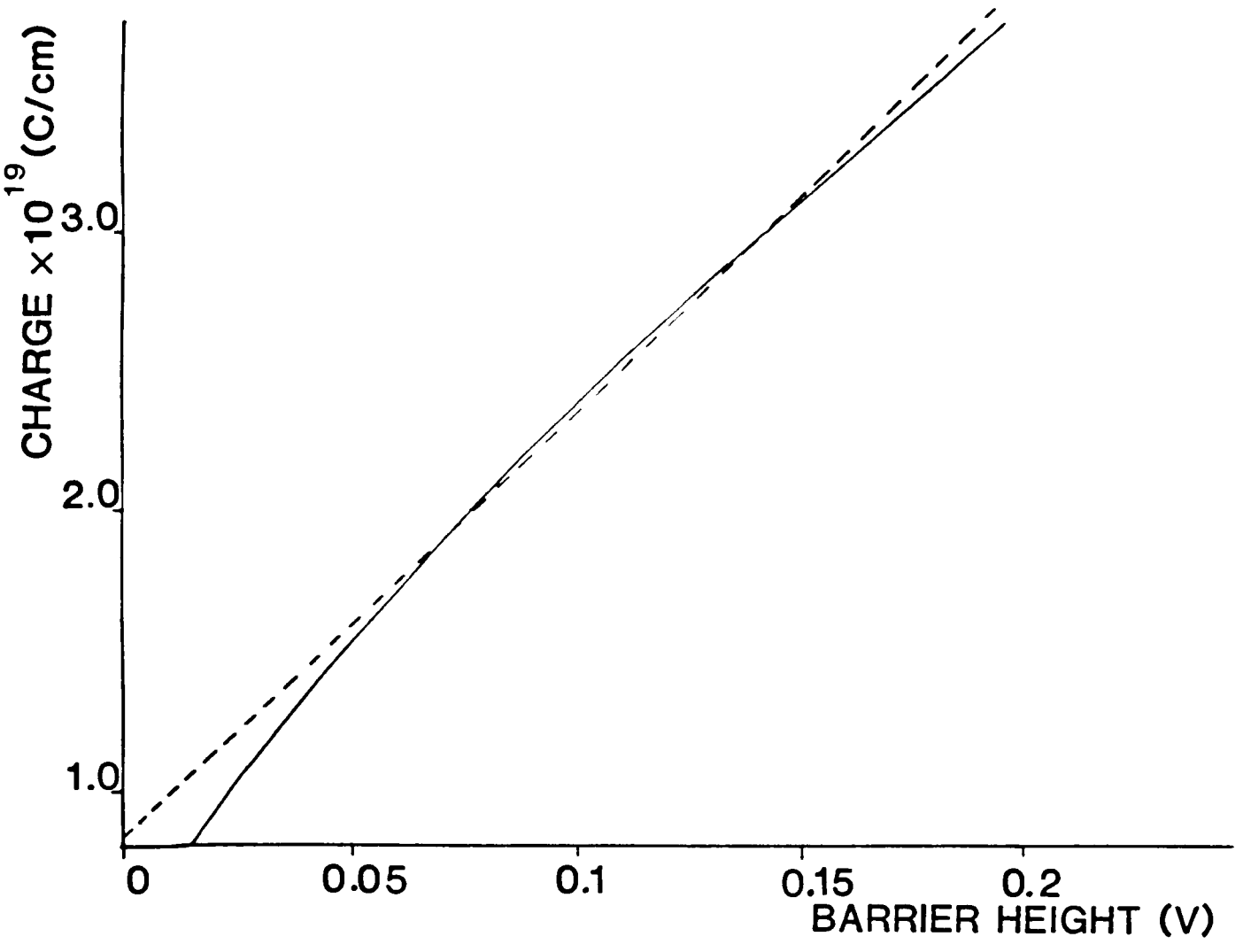


Figure 7.2 Plot of dislocation charge Q, versus barrier height ϕ

The dotted line shows a curve of form $\phi = \beta Q - \delta$.

An approximate expression for γ is now obtained:

$$\gamma \simeq \frac{-1}{n_o q \beta r' D_h} \left[\frac{KT}{q} \ln\left(\frac{\Delta p \gamma D_h + C_e N_d f N_c \exp\left(\frac{-q\phi_o}{KT}\right)}{C_e N_d \, n_o} \right) - \delta \right] \qquad [7.8]$$

γ appears in the log term of this equation, however in most cases the change in γ produced by changes in other parameters will be sufficiently small that the value of γ in the log term can be considered to a first approximation, constant. To determine the temperature dependence of γ it is necessary to examine each of the variables in the above equation in turn.

The temperature dependence of D_h is given by Jacoboni et al. (1977) as $D_h \propto T^{-1.4}$ for the temperature and doping ranges used in this work. Sokolova (1970) finds the temperature variation of γ' to be $\gamma' \propto T^{1.5}$ and thus the $D_h \gamma'$ product is essentially temperature independent. β and δ are constants. The actual temperature variation of C_e is not known but initially it will be assumed constant or only weakly dependent on temperature so that the log term in which it appears is also constant. The $T^{1.5}$ variation of N_c is small compared to the variation with temperature of the following exponential. Thus a further simplified relation is:

$$\gamma \simeq - AT \ln \left(B \Delta p D_h \gamma + Df \exp \frac{-q\phi_o}{KT} \right) + E$$

where A, B, D and E are constants. As mentioned earlier the behaviour of f will be discussed in more detail in section 7.3.2.

7.3 Application of the Recombination Theory to EBIC Measurements

In EBIC measurements on dislocations their contrast is measured as a function of temperature and beam current. Chapters 2, 5 and 6 show that the EBIC contrast C of the dislocations measured in this work is directly proportional to γ their recombination strength except at very high beam currents and low temperatures.

Before using the full theory to describe the EBIC experiments it is important to note that since C is directly proportional to γ equations [7.1] and [7.4] give:

$$C = A'' Q \qquad [7.9]$$

where A'' is a constant whose value is effectively independent of temperature (actually varying as $T^{-0.1}$). Furthermore, the earlier relationship $\phi \simeq \beta Q - \delta$ can be rewritten as $Q = \beta' \phi + \delta'$ and so the contrast is also approximately linearly dependent on ϕ .

In equation [7.8] $\Delta p \gamma D_h$ represents the recombination flux per unit dislocation length, J. In an EBIC experiment the recombination flux J is: $J \simeq \frac{G\ C}{l}$ where G is the total number of electron hole pairs generated by the beam each second, and l is the length of the dislocation at which recombination occurs.

G is given by; $G = \frac{\eta I_{beam}}{q}$ (see chapter 2) where η is the number of electron hole pairs generated per incident electron. Thus for EBIC contrast equation [7.8] may be written:

$$C \simeq - \frac{A' T}{n_o} \left[\ln \left(\frac{\eta I_{beam} C q^{-1} l^{-1} + C_e N_d f N_c \exp \frac{-q\phi_o}{KT}}{C_e N_d\ n_o} \right) \right] + B' \qquad [7.10]$$

where A and B are constants. This equation will now be used to interpret the EBIC contrast measurements that are presented in chapter 6. It is noted that the application of this theory

to cathodoluminescence (CL) contrast measurements of charged dislocations should also be valid with two provisions, 1) the dislocation acts as a non-radiative recombination centre and 2) the dislocation acts as a 'weak' defect. If these conditions are met CL contrast will give a measure of the recombination flux at dislocations in exactly the same way as the EBIC contrast.

7.3.1. General Description

It can be seen that the behaviour of the EBIC contrast as described by [7.10] is dependent on the ratio of two terms. The first is equal to the total recombination flux, J:

$$J = \frac{\eta I_{beam} C}{q l}$$

and the second is the flux due to the thermal emission of electrons from the dislocation level, J_{te}:

$$J_{te} = C_e N_d \, f N_c \exp \frac{-q\phi_o}{KT} \qquad [7.11]$$

Provided f is close to its equilibrium value, J_{te} will be close to the equilibrium rate of capture and emission of electrons, which occurs when $\Delta p = 0$.

In order to describe the behaviour of the contrast three régimes will be defined although the change over between régimes is continuous and cannot be said to occur at any particular value of J and Jte·

In the first régime $J \gg J_{te}$, i.e. the rate of electron capture is much greater than the equilibrium rate of capture (or re-emission).This is achieved by a substantial lowering of the potential barrier as the occupation f, of the dislocation level and hence its charge is reduced. Equation [7.10] in régime 1 reduces to;

$$C \simeq - \frac{A' T}{n_o} \left[\ln \left(\frac{\eta I_{beam} C}{q 1 C_e N_d n_o} \right) \right] + B' \qquad [7.12]$$

which will therefore describe the contrast in this régime. The contrast is then linearly dependent both on T and $\ln(I_{beam})$ for small changes in C. For a large change in C, caused by changes in either T or I_{beam}, the relationship will not be strictly linear because the changing contrast also appears in the log term. The consequences of this are described in section 7.5.2.

In the second régime $J \simeq J_{te}$ and so the full form of [7.10] is required to describe the contrast. Inspection shows that the variation of C with $\ln (I_{beam})$ is now sub-linear because as J is reduced J_{te} becomes more significant in determining the contrast level. Also it can be seen that the variation of C with temperature is also sub-linear. This is because as T is increased J_{te} increases exponentially and thus increases the value of the log term so resulting in the deviation away from the linear T dependence of C.

Régime 3 occurs when I_{beam} has been reduced still further so that $J \ll J_{te}$. For these conditions the barrier height and hence charge on the dislocation are close to their

equilibrium levels. The position of the Fermi level relative to the dislocation level at equilibrium has been calculated by Read (1954). He finds that the dislocation energy level is then shifted by an amount Δ below the position predicted by the usual Fermi statistics, where $\Delta = \frac{Q}{4\pi\epsilon\epsilon_o}$.

According to Read, $q\Delta$ represents the energy of interaction of an electron with its neighbours. As the charge on the dislocation Q, is reduced so the distance between charges increases and hence their interaction becomes smaller. From figure 7.1 it can be seen that (at OK);

$$q\phi_o = E_c - E_f + q\phi + q\Delta$$

Recalling equation [7.5] this gives

$$q\phi_o = E_c - E_f + \frac{q\,Q}{2\pi\epsilon\epsilon_o}\left(\frac{3}{2}\ln\left(\frac{Q}{(\pi n_o)^{\frac{1}{3}}\,q}\right) - 0.116\right) \quad [7.13]$$

at OK. At higher temperatures the entropy of the different arrangements has to be included when finding the minimum free energy. This requires a term $KT \ln\frac{f}{1-f}$ to be added to the right hand side of equation [7.13]. This results in the equation used by Schröter (1979) to analyse various Hall measurements. Schröter however only considers a very small line charge for which the interaction term $q\Delta \ll KT$. Now Read also treats the case where $q\Delta \gg KT$ which occurs for large Q. He suggests that the minimum energy arrangement, which is equally spaced charges, will nearly always be found because

the repulsion between charges is such that only a very small displacement from the uniform spacing will increase the electrostatic energy of the system by much more than KT. The approximation of the actual configuration to this uniform distribution results in a zero entropy contribution to the free energy equation and $q\phi_o$ is then described by equation [7.13]. For simplicity this approximation will be made throughout this work although here $q\Delta \simeq KT$. From equation [7.13] it is now possible to determine the value of ϕ_o from the value of the EBIC contrast of a dislocation in régime 3, i.e. when the charge on the dislocation is close to equilibrium. It has been shown above that $C = A'' Q$ thus if A'' is known, a value for Q can be obtained. Substituting this value into equation [7.13] then yields ϕ_o since all the other parameters are known.

As the temperature is raised E_f is reduced, and equation [7.13] shows Q decreases and hence the contrast C also decreases. The contrast in this régime will however be independent of the beam current.

7.3.2. Temperature and Beam Current Dependence

In chapter 6 an extensive set of measurements was presented of the contrast of two individual dislocation segments, one screw and the other 60°, both as a function of temperature and beam current. These were summarised in figures 6.13 and 6.14. At low temperatures or high beam currents a linear dependence on T and $\ln (I_{beam})$[1] was found, as predicted by equation [7.12] which is valid for $J \gg J_{te}$. Thus it appears that the theory derived here to

1. Here I_{beam} is the value of the beam current when measured in amps and is thus a dimensionless quantity. Throughout the remainder of this work it is assumed that if I_{beam} appears in $\ln(I_{beam})$ this dimensionless quantity is implied whereas if it appears as $\ln \frac{\eta I_{beam} C}{q l C_e N_d n_o}$ it has dimensions of current.

describe régime 1 is a very good description of the observed EBIC contrast provided I_{beam} is large and T is small for which $J \gg J_{te}$ is expected. The observation that the contrast in this range is very accurately linear with temperature verifies the assumption that C_e is a constant or only weakly temperature dependent. This is the assumption often made when interpreting DLTS data which allows the activation energy for emission of carriers from the dislocation level to be correlated with ϕ_o, the position of the dislocation level. Unfortunately insufficient parameters are known in equation [7.12] to determine quantitatively the minimum change in C_e that could be detected.

At higher temperatures and for small beam currents the contrast curves break away from the linear dependence on T and on ln (I_{beam}) This is in agreement with the theory for $J \simeq J_{te}$. Finally at still higher temperatures and lower beam currents the theory predicts a third régime should be entered where the dislocation contrast is independent of beam current.

Figures 6.10, 6.13 and 6.14 show measurements that indicate this to be the case for the screw dislocation but insufficient data is available to show this for the 60°. It appears that if the 60° dislocation follows the same trends as the screw, then recombination at the 60° will enter régime 3 for temperatures higher and beam currents lower than those that were available experimentally.

For most of the experimental conditions used the contrast is independent of, or only weakly related to, the position of the defect state within the band gap. The theory then allows the process of recombination at dislocations to be visualised as follows. Upon injection of an excess of minority carriers the dislocation, initially at equilibrium, will capture holes into the surrounding space charge region much faster than the corresponding capture of electrons. These trapped holes will reduce the negative charge on the dislocation. The charge will continue to decrease until the rate of capture of electrons over the reduced potential barrier is equal to the rate of capture of holes. The resulting steady state barrier height in this régime and hence recombination efficiency, is thus due to the excess minority carrier concentration and is independent of the position of the dislocation level. Clearly once steady state has been reached the net rate of transition of carriers between all levels will be equal to the rate of capture of holes.

The above description of recombination together with the experimental results relating EBIC contrast to beam current allow the nature of the variation in dislocation occupancy f, and the degree of thermal re-emission of bound holes to the valence band to be better understood. The dislocation parameter which is most widely accessible to experimental measurements is the dislocation charge. However the charge on the dislocation is determined by the difference in the amount of excess negative charge given by qfN_d, and any positive charge which may also be present at the dislocation due to

excess holes. Thus although in most cases the dislocation line charge can be determined this does not lead to a value for fN_d since the concentration of bound holes is unknown. The excess concentration of holes trapped at the dislocation may be stored either in the bound hole state or in the dislocation band itself. The latter case will also result in a reduction of f. The level in which the holes are stored will depend upon which of the transitions in the recombination path is rate limiting. This may be determined by considering the following.

If a particular recombination step is rate limiting then the transition rate between the two relevant levels will be proportional to the product of the concentration of electrons in one and the concentration of states available for the electrons to move into in the other. This is because for the rate determining step the proportion of electrons making the transition in the "opposite" direction is negligible. Thus if the transition of electrons from the dislocation level to the bound hole band (see figure 7.1) is rate limiting then

$$J \propto fN_d . p_{HB} \qquad [7.14]$$

where p_{HB} is the concentration of holes in the bound hole band per unit dislocation length. In addition the charge on the dislocation

$$Q = q.(fN_d - p_{HB}) \qquad [7.15]$$

and experimentally Q is known to be approximately constant since C varies at most by 50%. Thus

$$fN_d - p_{HB} \simeq \text{constant} \qquad [7.16]$$

Equations [7.14] and [7.16] describe how the occupation of the dislocation states f, depends on recombination rate J, for the case where the transition from the dislocation level to the bound hole level is rate limiting. Unfortunately, the constant of proportionality in equation [7.14] is not known and so the exact variation of f with J cannot be calculated. However, inspection of the above equations shows that if p_{HB} is of the same order as fN_d then f is approximately proportional to $J^{\frac{1}{2}}$. However, if p_{HB} is much smaller than fN_d equation [7.16] shows p_{HB} may increase many times with little resulting change in f and so p_{HB} is approximately proportional to J. Thus the way in which f changes with J depends on whether or not $fN_d \simeq p_{HB}$.

In figure 6.11 experimental data is presented for dislocations at 300K for which the beam current changes by a factor of $\sim$ 400 times. Since in this range the contrast is observed to decrease by a factor of two, this represents a change of $\sim$ 200 times in the recombination rate. Also, taking the 60° dislocation as an example, at 10^{-11}A the contrast and hence net charge on the dislocation has been reduced by $\sim$10% from its equilibrium value and so the above analysis indicates that at $I_{beam} = 10^{-11}$A, $p_{HB} \gtrsim 0.1\ f_o N_d$ where f_o is

the equilibrium occupation of defect states. Clearly as the beam current is further increased, to 2×10^{-9}A it is expected that P_{HB} would quickly become of the same order as $f_o N_d$ and that f would then vary as $J^{\frac{1}{2}}$. Thus for $I_{beam} = 2 \times 10^{-9}$A, f would be $\sim 10 f_o$. If this resulted in a

value of f close to 1 then the approximations $f \ll 1$ and $1-f \simeq 1$ would no longer be valid when deducing equation [7.10]. Consequently a deviation of contrast from the predicted $\ln(I_{beam})$ dependence at high currents would be expected and this was not observed. Thus it is deduced that $f \ll 1$ at high beam currents and $f_o \ll 0.1$ at 300K.This result is in agreement with the value of f deduced for the expected values of barrier height (a few tenths of a volt) and the assumed concentration of states N_d ($\gtrsim 2 \times 10^7$) for the dislocations studied, see section 7.2. Thus a scheme of recombination for which the transition from the dislocation level to the bound hole level is rate limiting is compatible with the experimental results obtained at 300K.

However at lower temperatures this no longer appears to be the case as is shown in the following. It is noted that although the beam current was only changed by a factor of ~ 400; at low temperatures the transition rate to the dislocation level J was increased from its equilibrium value J_{te}, by many orders of magnitude, even for the lowest beam currents used. For example, if it is assumed that the equilibrium contrast value at 131K is approximately the same as its value in the range 300K to 350K i.e. ~10%, then extrapolation of the C versus ln (I_{beam}) curves shows this value of contrast would be obtained with beam currents of 10^{-17}A (see figure 6.12). Thus it is reasonable to assume that I_{beam} and hence J have been increased by 10^8 over their values for equilibrium conditions in the experiment performed at 131K. Since no deviation from the ln (I_{beam}) dependence is observed and if the transition considered here is rate limiting over the entire temperature range, it is deduced

using the same reasoning as above, that $f_o \lesssim 10^{-4}$ at 131K. The charge on the dislocation Q, required to give a contrast of 10% is calculated in section 7.4.4 to be $3.5 \times 10^{-13} Ccm^{-1}$. Now $Q = fN_d q$ thus $f_o \lesssim 10^{-4}$ implies $N_d \gtrsim 2 \times 10^{10}$ cm^{-1} for the dislocations studied. Such a high value for N_d seems unlikely unless the dislocation states are due to a very high concentration of impurity atoms surrounding the dislocation core and this is contrary to the evidence of other workers on the same specimens (see chapter 1). Thus the experimental data obtained at low temperatures is incompatible with the transition from the dislocation level to the bound hole level being rate limiting and it is deduced that a different scheme of recombination is required.

An alternative scheme for recombination is that it is the transition from the tunnelling level to the dislocation level that is rate limiting. In this case the occupancy f <u>decreases</u> with increasing recombination rate in a manner exactly the opposite of that described above. Virtually no holes are now stored in the bound hole level, see below, and so as f is reduced the charge on the dislocation is reduced accordingly. For example a reduction in f of a half also halves the band bending ϕ, surrounding the dislocation. Since the concentration of electrons in the tunnelling state varies approximately as $n_o \exp\left(-\frac{q\phi}{KT}\right)$ this will result in an increase in the concentration of electrons in the tunnelling level, and hence an increase in recombination rate by many orders of magnitude for the values of T and ϕ (see section 7.4.1) encountered in this work. Thus if the transition from the tunnelling level to the dislocation level is rate

limiting, the experimentally observed data can be described, at all temperatures, without postulating a very large value of N_d for the dislocation. Since a large value of N_d is thought unlikely, this analysis indicates that it is the transition from the tunnelling level to the dislocation level and not the transition from the dislocation level to the bound hole level which is rate limiting.

That the transition from the tunnelling level to the dislocation level is rate limiting has a number of important consequences. Firstly it implies that the hole concentration in the dislocation level and the bound hole band are described by the same quasi-Fermi level (see for example Labusch (1979)) and hence the concentration of holes on the former is many orders of magnitude higher than on the latter because of the energy difference between them. This means that when the charge of a dislocation is reduced from its equilibrium level, the excess holes occupy the dislocation level and not the bound hole level. This is contrary to the assumption of Figielski (1978) and Mergel (1983). It also implies that the occupancy f, is proportional to the charge on the dislocation Q. In this work Q varies by ~50%, as deduced from the observed changes in contrast, and so the value of f in equation [7.11]

$$J_{te} = C_e N_d f N_C \exp \frac{-q\phi_o}{KT}$$

may be taken as constant in comparison to the exponential term when examining the temperature variation of J_{te}.

Finally, since the hole concentration on the dislocation level changes at most by a few percent (for $f_o \lesssim 0.1$) the concentration of holes on the bound hole level will also change at most by a few percent since both are described by the same quasi-Fermi level. At equilibrium, by detailed balance, the rate of capture of holes, J_c, to the bound hole band from the valence band is equal to the thermal re-emission back into the valence band, J_{th}. The bound hole concentration is increased at most by a few percent during an experiment and so the thermal re-emission of holes is itself increased by the same amount and so is always very nearly equal to the equilibrium capture rate at any given temperature. Since the capture rate is proportional to p the concentration of holes in the valence band, the ratio of the re-emitted holes to those captured is $\frac{Jth}{Jc} = \frac{p_o}{p}$. Thus thermally re-emitted holes are negligible for p more than a few times p_o, the equilibrium hole concentration. This justifies the assumption made in section 7.2 that thermally re-emitted holes can be neglected for $\Delta p \gg p_o$ (provided $f_o \lesssim 0.1$).

It is interesting to note that when the charge on the dislocation is significantly reduced from its equilibrium value the overall recombination path appears to have two rate limiting steps. These are capture of holes to the bound hole level and capture of electrons to the dislocation level. Both these transitions appear to behave as a 'bottleneck' in a manner characteristic of a rate limiting step. This is because for each, the rate of transition in one direction is

many orders of magnitude greater than in the opposite direction. For lower injection levels and hence smaller recombination rates, the thermally re-emitted electron flux J_{te} becomes significant and consequently the transition of electrons to the dislocation level ceases to behave as a 'bottleneck'.

7.3.3 The Comparison Of EBIC Contrast From Screw And 60° Dislocations

In chapter 6 results were presented that showed that the EBIC contrast of screw and 60° dislocations at the same depth are equal. These measurements were all made under experimental conditions of temperature and beam current for which $J >> J_{te}$ and consequently the contrast was independent of the position of the dislocation energy level. In this régime the contrast is given by [7.12];

$$C \underset{\sim}{\nu} - \frac{AT}{n_o}\left(\ln \frac{\eta I_{beam} C}{q l C_e N_d n_o}\right) + B$$

In this equation the only variables which may be dependent upon dislocation type are C_e and N_d. Thus the experimental observation of similar recombination efficiencies (±1%) for screw and 60° dislocations when $J >> J_{te}$ indicates that the $C_e N_d$ product is the same (±6%)[1] for the screw and 60° dislocations studied in this work.

1. This value calculated by taking ϕ = 0.15 eV which is the value calculated in section 7.4.1 for the two dislocations studied and for a 9% contrast level. See section 7.4.1 for details.

For lower beam currents the electrons thermally re-emitted from the dislocation level to the conduction band begin to affect the dislocation contrast. At the beam currents for which this happens differences appear between the contrast of the screw and 60° dislocations. These are evident both when the beam current is varied and when the temperature is varied and can be seen in figures 6.7, 6.10, 6.11 and 6.12. These plots show that the position on the curve where contrast measurements break away from the linear dependence occurs at lower temperatures and higher beam currents for screw dislocations than for 60° dislocations. From the theory presented here, the deviation occurs when $J_{te} \simeq J$ i.e. when

$$C_e N_d N_c f \exp\left(\frac{-q\phi_o}{KT}\right) \simeq \frac{\eta I_{beam} C.}{q l}$$

It has already been shown that $C_e.N_d$ is likely to be independent of dislocation type and that f is proportional to Q and hence C. Thus the curves show that ϕ_o screw $< \phi_o 60°$.

Once the beam current has been reduced sufficiently so that the linear dependence no longer holds, the exact ratio of the contrast of the two dislocation types will depend upon the beam current and temperature at which the measurement is made. With decreasing beam current the ratio $C_{60°}$ to C_{screw} will increase with $C_{60°}/C_{screw} > 1$ for dislocations of the same depth. In section 6.5 the temperature dependence of a screw and a 60° dislocation segment was presented. These dislocations are not part of the same loop and so are not likely to be at the same depth. However, if the contrast of the dislocations is normalised to remove the different depth

effects, i.e. so that both screw and 60° show the same contrast in régime 1, then the 60° dislocation shows progressively larger contrast than the screw in régime 2. The largest 60°/screw ratio measured was 1.08 at 370K and I_{beam}= $1x10^{-10}$A. This measurement was made with the lowest beam current and highest temperature combination available experimentally in the present work.

After reducing the beam current still further régime 3 would be entered when $J \ll J_{te}$ for both types of dislocations and the contrast is then expected to be independent of the beam current yielding $C_{60°}/C_{screw}$ constant at constant temperature. As described earlier this régime was not accessible experimentally with the present set-up and so this behaviour was not observed.

In the above, it has been assumed that the deviation from a linear dependence of C on temperature and $\ln(I_{beam})$ occurs when $J \simeq J_{te}$. In section 7.5.3 an alternative explanation is proposed which, if correct, would mean that no information can be gained concerning the relative values of ϕ_o screw and ϕ_o sixty.

7.3.4 The Dependence Of Dislocation Contrast On The Electron Beam Chopping Frequency

It has been shown in this chapter for experimental conditions where $J \gg J_{te}$ that the charge on the dislocation and hence its efficiency as a recombination centre can differ markedly from the equilibrium value obtained as $\Delta p \rightarrow 0$. If the charge on the dislocation is at its equilibrium value when the minority carrier concentration is increased by switching on the electron beam, then the recombination efficiency , will decrease with time as the charge on the dislocation is reduced. The rate of reduction of the dislocation charge and hence contrast is determined by the difference between the rate of hole capture and the rate of electron capture. Once steady state has been reached these two rates are equal and the charge on the dislocation remains constant.

In the experiments performed in this work phase sensitive detection was used to improve the signal noise ratio and as a consequence the electron beam was chopped repetitively, typically at 10kHz, although also at different rates in the frequency dependence experiments (section 6.4.). If the 'on' time of the beam in each cycle is much longer than the time in which recombination at the dislocation comes to steady state then the recombination efficiency measured will be the steady state value and will be independent of the beam chopping frequency. However, if the 'on' time is sufficiently short, then the transient variation in the contrast at the beginning of each cycle will significantly affect the contrast. The

contrast would then differ from the steady state value and increase with increasing beam chopping frequency. The actual variation in contrast will depend both on the proportion of the cycle for which the transient is significant and the magnitude of the transient itself. The magnitude of the transient will depend on the deviation of the final charge state of the dislocation from its equilibrium value and also how close to the equilibrium value the dislocation is at the start of each cycle. For example if the charge on the dislocation is reduced significantly whilst the beam is 'on', and during the 'off' period the dislocation captures insufficient electrons to return the dislocation to its equilibrium state, then the size of the transient at the beginning of each cycle would be reduced and the value of contrast measured would be closer to the steady state value. In the following a simple calculation is made to estimate the maximum duration of the contrast transient and hence whether this would be detected by the experiments performed.

The specimens used can be represented at 300K by a capacitor of ~ 5 pF and resistance of $\sim 500\Omega$ in series. The RC time constant of such a specimen is ~ 3ns and is much shorter than the rise time (5%-95%) of the amplifier used which was $\sim 10^{-5}$s. At 10kHz, the maximum chopping frequency used, the rise time of the specimen and amplifier thus do not significantly affect the signal measured.

To estimate the maximum possible length of the contrast transient at the beginning of each cycle two approximations will be used that may both over estimate the size of

the transient. In the first it will be assumed that at the beginning of each cycle the dislocation is in its equilibrium state though this is not necessarily the case, as described above. The rate of capture of holes, according to the theory presented earlier, is

$$J_h = A\,\phi \qquad [7.17]$$

where A is a constant, and of electrons

$$J_e = C_e N_d \left(n_o \exp \frac{-q\phi}{KT} (1-f) - f\, N_c . \exp \frac{-q\phi_o}{KT} \right)$$

To simplify the calculation J_e will be approximated by

$$J_e = B\,(\phi_e - \phi) \qquad [7.18]$$

where B is a constant (see below) and ϕ_e is the equilibrium value of ϕ. This is the second approximation and gives a value of J_e greater than or equal to the true value. The rate of change of charge, and hence ϕ is determined by the difference in the rate of capture of holes and electrons thus

$$\frac{d\phi}{dt} = -D\,(J_h - J_e) \qquad [7.19]$$

where D is also a constant.

At steady state $\frac{d\phi}{dt} = 0$ and thus a value for B can be obtained:

$$B = \frac{A\,\phi_s}{\phi_e - \phi_s} \qquad [7.20]$$

where ϕ_s is the steady state value of ϕ. Solving equations [7.17] to [7.20] and using $\phi = \phi_e$ at t = 0 gives

$$\phi = \phi_s + (\phi_e - \phi_s) \exp \left(-AD . \frac{\phi_e}{\phi_e - \phi_s} . t\right) \qquad [7.21]$$

which thus approximately describes the change in ϕ with time.

Since the contrast C is approximately proportional to ϕ (section 7.3), equation [7.21] also describes the variation of contrast with time. The time constant for the transient change in contrast γ_c, is

$$\gamma_c = \frac{\phi_e - \phi_s}{AD.\phi_e}$$

and so

$$\gamma_c = \frac{C_e - C_s}{AD.C_e} \qquad [7.22]$$

where C_e and C_s are the equilibrium and steady state values of contrast respectively.

In order to determine whether the effect of the contrast transient would be detected in the present experiments it is necessary to calculate approximate values for A and D. A value of 0.15 V is used for ϕ since this is approximately the value deduced in section 7.4.1. It will also be assumed that the dislocations are at such a depth that their equilibrium contrast is 10%. In this way the results apply to typical dislocations studied. Now $J_h \simeq \frac{\eta I_{beam} C}{ql}$ (from section 7.3) and for 15kV electrons, $\eta = 4 \times 10^3$ and $l \simeq 2 \times 10^{-4}$ cm using $J_h = A\phi$ gives

$$A \simeq 8 \times 10^{25} \times I_{beam} \ (cm^{-1}s^{-1}\ V^{-1}).$$

From equation [7.5] $\phi \simeq 1 \times 10^{-7} \times N$ (V) for $\phi \simeq 0.15$V, where N is the number of electrons per unit dislocation length.

Thus

$$\frac{d\phi}{dt} = 1 \times 10^{-7} \frac{dN}{dt}$$

and hence from equation [7.19], since $J_h - J_e = -\frac{dN}{dt}$

$$D = 1 \times 10^{-7} \quad (Vcm)$$

Thus the value of D is constant and A depends on the beam current used to investigate the dislocation. The time constant of the transient τ_c is now calculated at 300K for two representative values of beam current for the particular dislocations whose contrast as a function of beam current is presented in figure 6.11.

i) For $I_{beam} = 10^{-11}$ A

$A = 8 \times 10^{14}$ $cm^{-1}s^{-1}V^{-1}$

$D = 10^{-7}$ Vcm

$C_e = 0.11$

$C_s = 0.10$*

Substituting into equation [7.22] gives $\tau_c = 1 \times 10^{-9}$s

ii) For $I_{beam} = 10^{-9}$ A

$A = 8 \times 10^{16}$ $cm^{-1}s^{-1}$ V^{-1}

$D = 10^{-7}$ Vcm

$C_e = 0.11$

$C_s = 0.065$*

Substituting into equation [7.22] gives $\tau_c = 6 \times 10^{-11}$s

This calculation demonstrates that for the two beam currents used in this calculation the duration of the contrast transient at the beginning of each 'on' period is many orders

* obtained at a beam chopping frequency of 10KHz and assumed to be the steady state value.

of magnitude smaller than that which could be detected ($\sim 10^{-5}$S) with the EBIC system used here. For lower beam currents Figure 6.11 shows that the contrast does not deviate significantly from its equilibrium value and therefore the transient would be negligible independent of its duration. Further this calculation shows that the dislocation contrast measured will be independent of frequency in the range 0-10kHz, in agreement with the experimental findings presented in section 6. Consequently the contrast measured is the steady state contrast that would be obtained without beam chopping. Indeed, the duration of the contrast transient for large beam currents is probably shorter than the time required for the electron hole pair distribution to reach steady state after the beam is switched on and thus for these conditions, experimentally τ_c is so short as to become impossible to detect.

7.4 Quantitative Analysis and Discussion of the EBIC Results

In the previous sections the theory developed has been shown to predict the general form of the experimental observations of EBIC contrast. In this section quantitative values for some of the physical parameters involved will be determined. Unfortunately the EBIC technique does not lend itself to accurate measurement of many parameters, chiefly due to the non-uniform distribution of the excess carriers. Consequently with the exception of the values obtained for the dislocation energy levels and the extent of the dislocation space charge region, the results in the following section are only approximate.

7.4.1 Calculation of the Position of the Energy Level of Screw and 60% Dislocations.

It has been described earlier how for most of the beam currents and temperatures used experimentally the dislocation contrast is independent of the position of the dislocation energy level ϕ_o. It is only at high temperatures and very low beam currents that the contrast deviates from a linear relationship with temperature and $\ln(I_{beam})$.

In the following a method for calculating ϕ_o is given. It was shown in section 7.3 that $C = A'' Q$ where A'' is a constant which does not change with temperature and equation [7.5] gave the relation between ϕ and Q. These may be used to give,

$$\phi = \frac{C}{2\pi\epsilon\epsilon_o A''} \left(\frac{3}{2} \ln \left(\frac{C}{(\pi n_o)^{\frac{1}{3}} A'' q} \right) - 0.616 \right) \quad [7.23]$$

Thus every value of measured contrast represents a particular dislocation charge and hence barrier height, the relation between C and ϕ being independent of temperature. Now in the linear régime thermal re-emission is negligible and so

$$J = C_e N_d n_o \exp \frac{-q\phi}{KT}$$

and $J = \frac{\eta I_{beam} C}{q\ l}$. It has also been shown in this chapter that $C_e N_d$ is approximately independent of temperature. Thus

for constant C

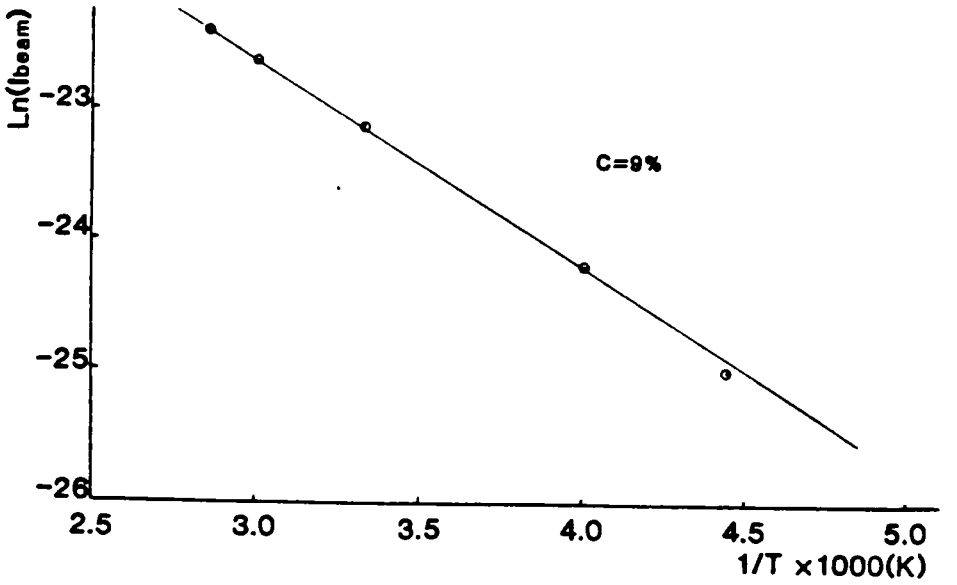
$$I_{beam} = B\exp\ \frac{-q\phi}{KT}$$

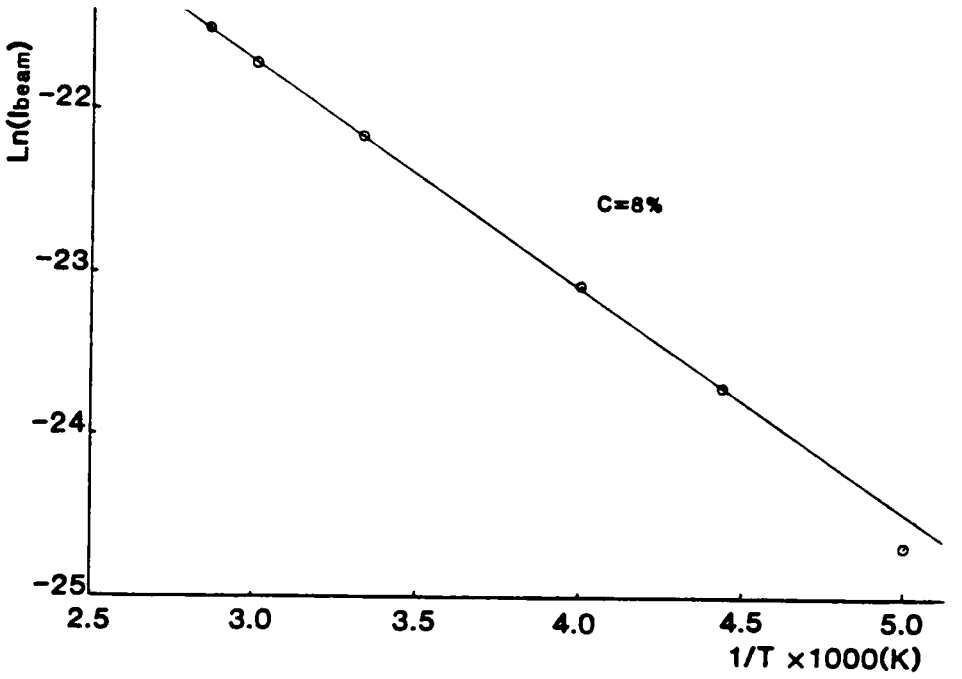
where B is a constant. A plot of ln (I_{beam}) vs T^{-1} will then yield ϕ for that value of C.

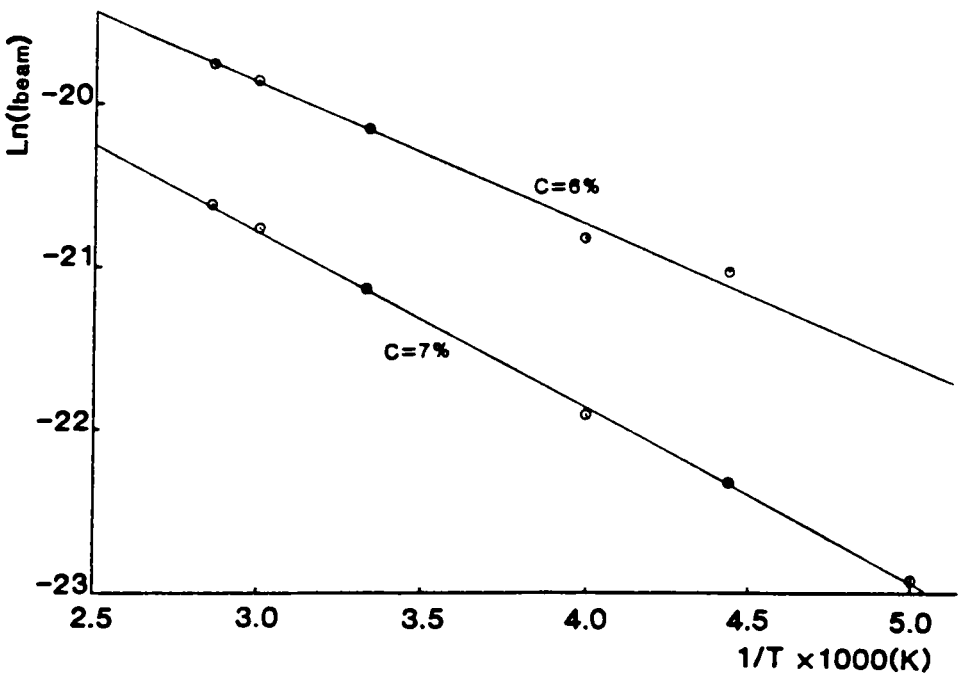
Figure 7.3 shows such plots for the screw dislocation whose beam current dependence at different temperatures is shown in figures 6.10, 6.11 and 6.12. It is from these figures that the data for these plots are taken. Plots are made for contrast values of 6, 7, 8 and 9% and yield values of 0.08eV, 0.093eV, 0.120eV and 0.135eV respectively. A similar procedure may be followed for the 60° dislocation investigated. The activation energies in this case are 0.076eV, 0.088eV, 0.112eV, 0.131eV and 0.141eV for contrast values of 6%, 6½%, 7½%, 8% and 8½% respectively. These contrast ranges were chosen so that measurements were only made on the linear portion of the curves so ensuring that thermal re-emission could be neglected. Thus the range of temperatures used depends on the contrast value used. In this way values of ϕ have been obtained for each value of C. These values should fit equation [7.23]. Figure 7.4 shows the contrast plotted against barrier height together with the theoretical equation [7.23]. The constant of proportionality A'' in equation [7.23] is not known and will, in general, vary with the depth of the dislocation and accelerating voltage. In plotting figure 7.4 a value for this constant has been used, for each of the two dislocations, which gives the best fit to the theoretical curve. The contrast axis is different

Figure 7.3 Plot of ln (I_{beam}) vs 1/T for different values of C

These plots, which are for the screw dislocation of figure 6.7, give the activation energy for the capture of electrons over the potential barrier ϕ at different values of contrast.


Ln(Ibeam)
-23
-24
-25
-26
C=9%
2.5
3.0
3.5
4.0
4.5
5.0
1/T ×1000(K)


Ln(Ibeam)
-22
-23
-24
-25
C=8%
2.5
3.0
3.5
4.0
4.5
5.0
1/T ×1000(K)


Ln(Ibeam)
-20
-21
-22
-23
C=6%
C=7%
2.5
3.0
3.5
4.0
4.5
5.0
1/T ×1000(K)

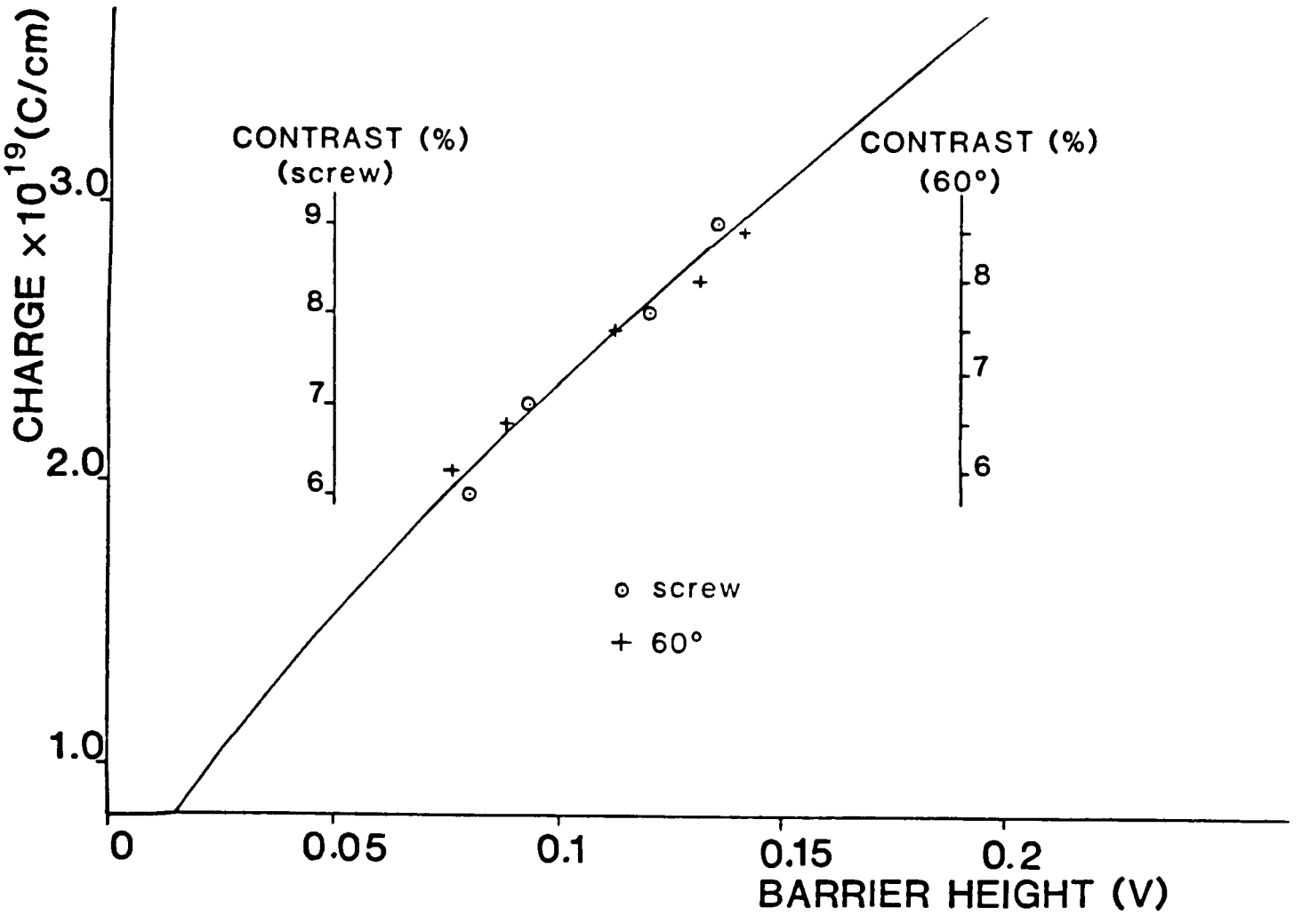


Figure 7.4. Theoretical curve showing the relationship between the dislocation charge and the potential barrier for electron capture

Superimposed are the experimentally determined values of the dislocation barrier height for different levels of contrast for the screw and 60° dislocation of figure 6.7. The values of contrast have been plotted so that $C=A''Q$ where A'' is different for the screw and 60° dislocations. From this it can be seen that the agreement between the experimentally obtained values and the curve describing the theoretical relation between charge and barrier height is good.

for the dislocations because they lie at different depths. It was shown in section 7.3.3 that C_eN_d is equal for both screw and 60° dislocations within experimental error (±6%). For the same beam current both the screw and 60° dislocations, whose temperature and beam current dependences were presented in sections 6.5 and 6.6, have nearly the same recombination flux J because both show approximately the same contrast. Now from section 7.3.1 in régime 1,

$\phi = \frac{-KT}{q} \ln \frac{J}{C_eN_dn_o}$, thus for the same beam current

both screw and 60° dislocations should have the same barrier height. This is because the small differences in J and possibly $C_e.N_d$ for the two dislocations are negligible because they appear in the log term. Thus the different values of contrast measured at the same beam current for the screw and 60° dislocations should arise from the same value of barrier height. From figure 7.4 it is seen that the same barrier height does indeed give rise to different levels of contrast for screw and 60° dislocations and the difference is indeed that observed between the contrast of screw and 60° at the same beam current. This provides a check for the accuracy of the deduced values of ϕ .

The fit to equation [7.23] of the values for ϕ and C is very good for both the screw and 60° dislocation and so it can be assumed that the barrier height for each value of contrast on the curve is known quite accurately (±4%).

It was shown in section 7.3.1 that for sufficiently low beam currents or high temperatures régime 3 is reached where $q\phi = q\phi_o - (E_c-E_f) - q\Delta$. Under these conditions the dislocation contrast is independent of beam current.

For the screw dislocation inspection of figure 6.10 and 6.11 shows these conditions are very nearly reached at the lowest beam current for the data obtained at 300K, 330K and 350K. On figure 6.10 is shown the extrapolation of the contrast curve until it becomes independent of beam current. The extrapolation is obtained by making the shape of the extrapolated curve as it approaches the equilibrium value identical to the experimental curve as it deviates from the straight line ln (I_{beam}) dependence. Thus the extrapolation of the data for small beam currents is symmetrical about an axis (shown on the 350K plot in figure 6.10) with the data obtained on the high beam current side of this axis. Clearly this method of extrapolation is rather arbitrary but it does give a very good fit to the available data for all the curves, and 6.11 even at the lowest beam currents used. From figures 6.10, it can be seen that the shape of this curve is identical[1] at 300K, 330K and 350K and all measurements tend, within experimental error, to give the same equilibrium value of contrast. This value being 10.6 ± 0.3% for the screw dislocation. Using figure 7.4 the barrier height ϕ is deduced to be 0.178eV ± 0.01eV. Thus Q the dislocation line charge is 3.45 ± 0.10 x 10^{-13}Ccm^{-1}. This value when substituted into equation [7.13] yields values of ϕ_o for the screw dislocation of 0.46eV, 0.50eV, 0.52eV ± 0.01eV at 300K, 330K and 350K respectively. This change in the

1. Indeed if all three sets of data are superimposed on the same graph it is not possible to distinguish the separate curves within experimental error (0.2%).

deduced value of ϕ_o with temperature is very large compared with the accuracy of the technique. For example if the value of ϕ_o at 300K was the same as its value at 350K, 0.52eV, then the equilibrium contrast level at 300K would be $\simeq$ 13.5%, a very large change over the actual value of 10.6% ± 0.3% (i.e. in the range 10.3% to 10.9%) and too large to be accounted for by errors in the extrapolation of data.

The same procedure may be followed for the 60° dislocation although here the accuracy is not as good because the data has to be extrapolated further to reach the equilibrium value of contrast. Once again the equilibrium contrast is found to be the same at 300K, 330K and 350K within the accuracy of the technique and is estimated to be 11.2% ± 0.6% yielding a barrier height of 0.21 ± 0.02eV and a line charge of $3.8 \pm 0.25 \times 10^{-13} Ccm^{-1}$. This gives values of ϕ_o for the 60° dislocation of 0.49eV, 0.53eV, 0.55eV ± 0.02eV at 300K, 330K, and 350K respectively.

In the above the errors quoted are due simply to errors in the measurement of experimental data and subsequent manipulation. Errors which may be due to approximations in the theory itself are not analysed. However, there are several factors which indicate that these effects may be small, at least as regards the correlation of specific values of contrast to specific barrier heights. The first is how closely the ln (I_{beam}) vs T^{-1} curves fit straight lines. The second is that the gradients of these lines fit the theoretical curve (figure 7.4) - a process which has required manipulation of the EBIC contrast measurements twice, each manipulation

resulting from the model for recombination in régime 1. And lastly that the independent check of the C vs ϕ curves shows that they accurately account for the difference in depth of the two dislocations. Thus the author believes it is reasonable to have confidence in the deduced values of barrier height as a function of contrast and also believes that the theory describing recombination at dislocations in régime 1 is correct. It is, however, very surprising that the energy levels deduced from the foregoing theory vary with temperature to such a large extent, i.e. by 0.06eV on changing the temperature from 300K to 350K. Moreover it seems somewhat of a coincidence that the change in position of the energy level exactly matches the movement of the Fermi level with temperature, so as to render the equilibrium contrast value constant. In section 7.5.3 suggestions are made which may account for these observations.

Despite the ambiguities of the exact position of the energy level it is deduced that the barrier height for the screw and 60° dislocation is $\sim$0.18 eV and $\sim$0.21eV respectively at 350K when the Fermi level is 0.31eV below the conduction band edge. Thus for the dislocation to be charged $q\phi_o > q\phi + E_c - E_f$ i.e. ϕ_o is greater than $\sim$0.49 eV and $\sim$0.52eV for the screw and 60° dislocation respectively at 350K.

7.4.2 The Radius of the Space Charge Region Surrounding the Dislocations

As stated earlier in this chapter the charge on the dislocation and hence its space charge region are determined by the conditions under which the dislocation is observed. However, in the following calculation only the radius of the space charge region of a dislocation at equilibrium at 300K will be calculated. To obtain the radius for these dislocations under any other experimental conditions the following expression should be used:[1]

$$r = r_o \left(\frac{C}{C_o} \right)^{\frac{1}{2}}$$

where C_o is the equilibrium contrast at 300K and r_o is the corresponding radius of the space charge region which is calculated here. Section 7.4.1 shows that the equilibrium barrier height at 300K is 0.18 and 0.21eV for the screw and 60° dislocation respectively. Equation [7.5] can be used to calculate the excess charge per unit dislocation length, Q and gives values of 3.45×10^{-13} and 3.80×10^{-13} Ccm^{-1} respectively which correspond to an extra electron every ~40Å along the dislocation line.

The excess electrons on the dislocation result in the expulsion of an equal number of majority carriers from the depletion region. Thus equation [7.4]; $r_d^2 = Q\ (n_o q)^{-1}$ may be used to calculate r_d which is found to be 0.26 μm and 0.27μm for the screw and 60° dislocations respectively.

1. $C = A'' Q$ and $Q = n_o q \pi r_d^2$ thus $C \propto r_d^2$.

7.4.3. The Dislocation Recombination Strength, γ

From equation [7.2] $J_h = \Delta p . \gamma . D_h$ and $J_h = \frac{4}{3} \cdot \frac{\pi R^3}{l} \cdot g_o C$

where R is the radius of generation volume, g_o is the rate of generation of carriers per unit volume and l is the segment of the dislocation along which recombination takes place. Using Donolato's approximation (Donolato (1978)), for the generation and distribution of minority carriers the maximum excess carrier concentration is:

$$\Delta p = \frac{g_o R^2}{3 D_h}$$

Using these equations and taking $l = 2R$ gives

$$\gamma = 2\pi C$$

This equation is derived for dislocations lying at the depth for maximum contrast and is only approximate since it assumes the maximum concentration of minority carriers along the entire length of the dislocation intersecting the generation volume whereas in practice this will only be true at the centre.

The screw and 60° dislocations studied gave close to the maximum contrast observed with values for C in the range 6% to 11% at 300K, the exact value depending on the beam current used. These values indicate γ ranging from 0.4 to 0.7. Pasemann et al. (1982), using a different specimen geometry, find values of γ in the range 0.3 to 0.7 for EBIC measurements of process induced 60° dislocations in n-type, $10^{15} cm^{-3}$, Czochralski silicon at room temperature. Although no value for beam current is quoted for these results it is likely that

beam currents greater than $\sim 10^{-10}$A were used since the noise suppression employed in their EBIC system is less sophisticated than in the present work. Thus, within the accuracy of the approximations used to deduce the values for γ, both the dislocations studied in this work and those studied by Pasemann et al (1982) show similar recombination strengths.

7.4.4 The Lifetime of Minority Carriers Within the Dislocation Space Charge Region

It was shown in section 7.4.3 that for a dislocation lying at the depth required to give maximum EBIC contrast, $\gamma = 2\pi C$ and in section 7.2 γ was defined as $\gamma = \frac{\pi r_d^2}{D_h \tau'}$. Thus the life-time of carriers within the space charge region τ', is $\tau' = \frac{r_d^2}{2CD_h}$. For a dislocation giving an EBIC contrast of $\sim 10\%$ with $r_d \simeq 0.25\mu m$ and $D_h = 11.7 cm^2 s^{-1}$ at 300K, $\tau' = 2.7 \times 10^{-10}$s.

The time taken for a minority carrier to traverse the depletion region in $10^{15} cm^{-3}$ material is $\sim 4 \times 10^{-11}$s. Thus the value of τ' obtained is compatible with a dislocation showing a contrast of a few per cent in the depletion region, provided r_d for the dislocation is the same order or larger than in the bulk.

7.4.5 Minority and Majority Carrier Capture Cross-Sections.

The minority carrier capture cross-section σ_h, is a parameter sometimes quoted to help characterise recombination at dislocations. The equation used to calculate a value is

$\sigma_h = \frac{J}{\Delta p . V_{th} . N_d}$, where J is the recombination flux,

V_{th} the thermal velocity of holes and N_d the density of recombination centres per unit dislocation length. σ_h is then understood to be the capture cross-section for the recombination centre whose concentration along the dislocation line is N_d. However, the physical significance of such a definition seems somewhat arbitrary in view of the fact that the rate of capture of holes and hence recombination is determined by the extent of the space charge region, see section 7.2, and not directly by the number of centres N_d. Also, to the author's knowledge, a value for N_d is not known but assumed in calculations of σ_h. For example Kittler and Seifert (1981) take N_d to be the concentration of hypothetical dangling bonds or impurity centres. In this work a value for $\sigma_h . N_d$ rather than σ_h is obtained.

From section 7.4.3, $\Delta p = \frac{g_o R^2}{3D_h}$ and $J = \frac{4}{3} \frac{\pi R^3}{1} g_o C$.

Taking 1 as 2R gives:

$$\sigma_h N_d = \frac{2\pi . D_h . C}{V_{th}} \quad .$$

Thus at 300K, C = 0.1, D_h = 12 $cm^2 s^{-1}$ and V_{th} $\sim 2 \times 10^7 cm\ s^{-1}$ giving $\sigma_h N_d \simeq 4 \times 10^{-7} cm$ for the screw and 60° dislocations studied. This value is the equilibrium value and will decrease as the charge on the dislocation is reduced by using large beam currents or by reducing the temperature, see section 7.3. Kittler and Seifert (1981) perform a similar calculation and also arrive at values for σ_h and N_d which

give $\sigma_h N_d \simeq 4 \times 10^{-7}$cm for a dislocation giving 10% contrast in a similar geometry specimen.

The majority carrier capture cross-section σ_e is defined by[1]

$$\sigma_e = \frac{J_e}{N_d \; n \; V_{th}}$$

where n is the majority carrier (electron) concentration and J_e is the capture rate of electrons, excluding thermal re-emission. Using $J = \frac{\eta I_{beam} C}{q l}$ and $J = J_e$ in régime 1 where thermal re-emission is negligible, allows $\sigma_e N_d$ to be calculated from C in this régime. For example taking $l = 2 \times 10^{-4}$cm for 15 kV electrons, V_{th} (for electrons) $= 3 \times 10^{7}$cm s^{-1} and $I_{beam} = 2 \times 10^{-10}$A and C = 8% at 300K for both the screw and 60° dislocations in figure 6.11 then $\sigma_h N_d \simeq 7 \times 10^{-8}$cm.

The value for $\sigma_h N_d$ may be obtained when the dislocation charge is close to its equilibrium value, by extrapolating the portion of the C vs ln (I_{beam}) curves in régime 1 to the equilibrium value of contrast. The value of beam current so obtained is that which represents the equilibrium capture rate of electrons neglecting thermal re-emission. From this value of I_{beam}, J_e may be calculated and hence $\sigma_e N_d$ at equilibrium. At 300K, from figure 6.11, the beam current

1. Sometimes a capture cross-section $\sigma_e^{l} = C_e V_{th}^{-1}$ is defined, see for example Kveder et al. (1982)

required to give the equilibrium contrast, neglecting thermal re-emission, is $\sim 2.2 \times 10^{-11}$A and $\sim 6.5 \times 10^{-12}$A for the screw and 60° dislocations respectively. Thus J_e is $\sim 3 \times 10^{14}$cm^{-1} s^{-1} and $\sim 9 \times 10^{13}$cm^{-1} s^{-1} and hence $\sigma_e N_d$ is $\sim 1 \times 10^{-8}$cm and $\sim 3 \times 10^{-9}$cm for the screw and 60° dislocations respectively.

Other measurements of σ_e in the literature have mainly used the DLTS technique. For example, Patel and Kimmerling (1979) investigate the length of time it takes to load the dislocation traps detected by DLTS and so deduce a value for σ_e of 3.10^{-16}cm^2 for the acceptor level ~ 0.6eV deep. There are, however, two errors in the analysis. The first is that they assume N_d to be the concentration of defect states as measured by DLTS, whereas in fact DLTS gives the number of occupied states, i.e. fN_d , where a value for f is not known. Secondly, as the electron traps fill, so the barrier height increases, thus the value they obtain pertains to some 'average' barrier height during the process of filling empty traps to their equilibrium level. Since the capture cross-section varies exponentially with barrier height the errors introduced into the measurement of σ_e by using an 'average' value of barrier height will be very large indeed.

Kveder et al. (1982) interpret DLTS data in such a way that they obtain values for σ_e' which may then be related to σ_e, see above. The values they obtain are true capture cross-sections for each of the N_d centres along the dislocation line. However, again the value of N_d is unknown

and so their results cannot be directly related to those deduced above where only the quantity $\sigma_e N_d$ has been deduced. The results Kveder et al. obtain for σ_e differ by a factor of more than 10^5 for the different defect levels they investigate.

7.5 Discussion

In this section some points arising from the theory and interpretation of results presented here are given. Discussion of the work in terms of other workers' results is given in section 7.6.

It is briefly noted that in the above treatment the possibility of conduction along the dislocation core was neglected. If such an effect exists it would increase the length of the dislocation whose charge was altered from its equilibrium value and so allow electron capture to take place over a longer length of dislocation. This would alter the effective value of the minority and majority carrier capture cross-sections. However, unless the conductivity of the dislocation changed with temperature and with an activation energy large compared to the barrier height, it seems unlikely that the effect of conduction would be detected and hence will not be discussed further.

Two approximations made in developing the theory have important consequences and are discussed in the following.

7.5.1 The Approximation of Constant Contrast

Equation [7.12] was derived to describe the variation of contrast in régime 1.

$$C \simeq \frac{-A\ T}{n_o}\left(\ln \frac{I_{beam}C}{q l C_e N_d n_o}\right) + B$$

When using this equation to describe the observed EBIC results the change in C is assumed small so that the log term can be assumed independent of C over the range investigated experimentally. Figure 7.5 shows the true variation in the log term when plotted against C for values in the range 10% to 2%. At low contrasts the gradient of a C vs ln (I_{beam}) curve would clearly be less than that expected from a linear extrapolation of the curve from high values of C. The assumption that the log term was independent of C in equation [7.12] satisfactorily described all the observed EBIC results in régime 1 with just one exception. That was that plots of contrast vs temperature at different beam currents intersected at a finite temperature rather than at OK, see figures 6.13 and 6.14. This effect may be expressed in a different way by plotting the gradient of the C vs ln (I_{beam}) curve against temperature. That is by plotting dC/d (ln(I_{beam})) vs T.
If the variation of C in the log term is neglected

$$dC/d\ (\ln(I_{beam})) = \frac{A\ T}{n_o}$$ which would thus result in a

straight line passing through the origin and is equivalent to the C vs T curves intersecting at OK. This is shown in figure 7.6 by the dotted line. The experimental data obtained for

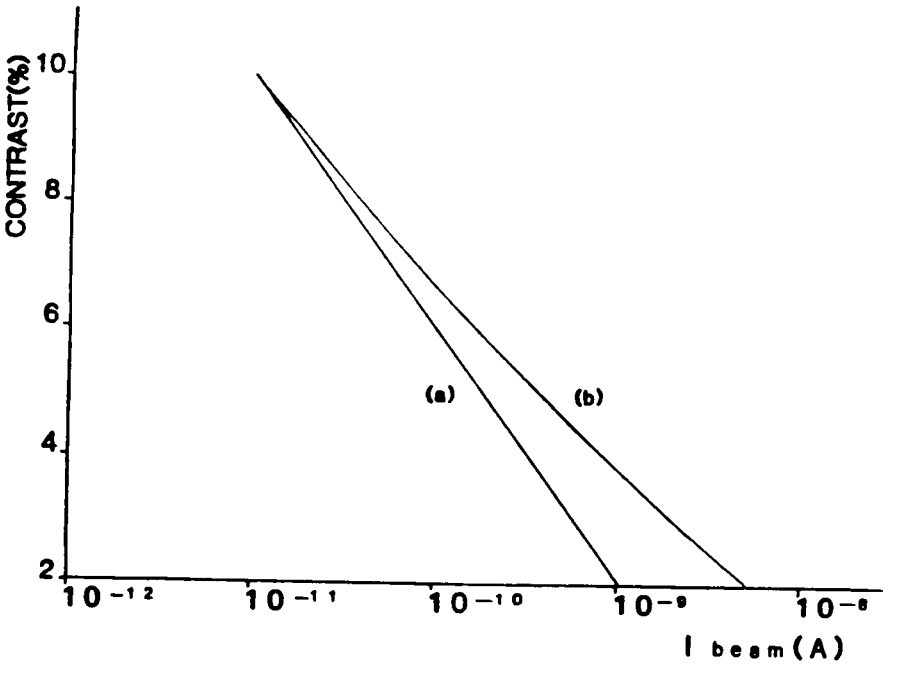


Figure 7.5 Plot of C = Aln (I_{beam}), curve (a) and C = Aln (I_{beam}.C), curve (b).

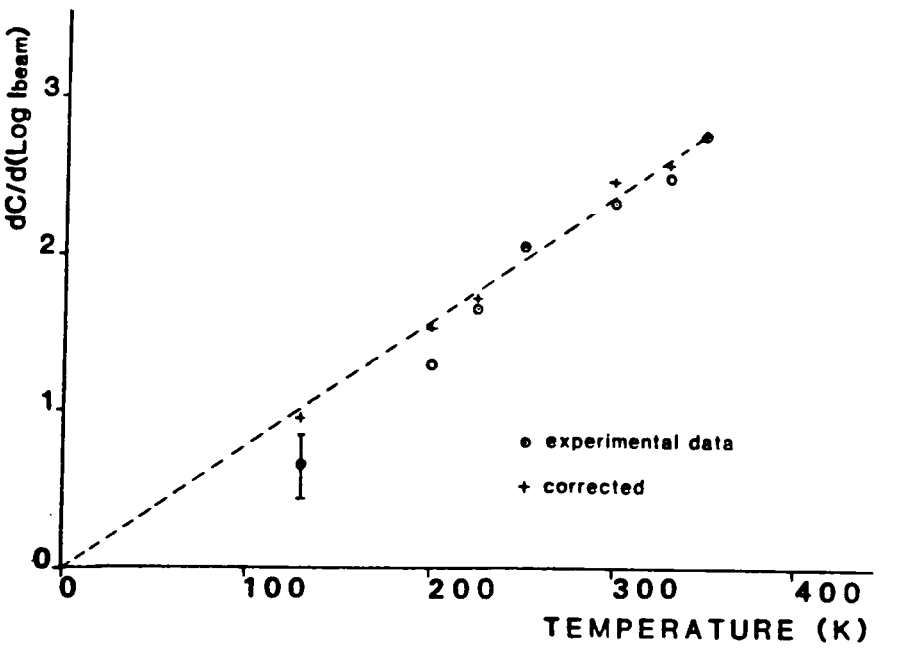


Figure 7.6 Plot of dc/d ln(I_{beam})

The circles show the data obtained experimentally and the crosses the same data corrected for the variation of C in ln(I_{beam}.C).

the screw dislocation[1] is also plotted on figure 7.6 and this is seen to lie on a curve better described by $dC/d(\ln(I_{beam})) = \delta T - \epsilon$ where δ and ϵ are constants. This is due to the different C vs T curves intersecting at a finite temperature (in this case ϵ/δ). Clearly at low temperatures and hence for small C the measured values of $dC/d(\ln(I_{beam}))$ are lower than that predicted when the effect of C in the log term is neglected. The crosses on figure 7.6 show the experimentally determined values of $dC/d(\ln(I_{beam}))$ corrected to account for the variation of C in the log term. It can be seen that the fit to the straight line passing through the origin is good. The value of C used for this correction is taken from the middle portion of each of the C vs $\ln(I_{beam})$ curves.

From the above it is clear that if the effect of C in the log term is included, the theory derived in this chapter accurately describes all aspects of the variation of EBIC contrast in régime 1.

7.5.2 The Approximation $1-f \simeq 1$

For the last thirty years it has been usual to assume that f, the occupation factor of a dislocation, is small for a dislocation at equilibrium. The value of f being such that the dislocation level lies close to the Fermi level. As the position of the Fermi level is moved so the barrier height is changed and to achieve this f itself will change, increasing

1. Similar curves may be obtained for the 60° dislocation but are not included here for brevity.

as the Fermi level approaches the conduction band . This model has been used by, for example, Read (1954), Figielski (1975) and Labusch (1979) and indeed by many other workers. The assumption was considered physically reasonable because the first models of dislocations in semiconductors included a row of dangling bonds which introduced into the gap a high density of states N_d, for the dislocation level. Even a small occupation factor ($f \lesssim 10\%$) of these states could produce sufficient band bending to ensure that for all temperatures and positions of the dislocation levels in the band gap equilibrium would be obtained with the dislocation level at or close to the Fermi level. However, recent theoretical work by many authors on dissociated dislocations indicates that dangling bonds are unlikely to exist at the core of either 30° or 90° partials in silicon, see chapter 1. Clearly the wealth of experimental data shows that levels are introduced into the gap but it is no longer clear what type of defect is responsible for their presence. Under such circumstances there is no longer any physical basis for the assumption that N_d is sufficiently large that $f \ll 1$. In the following the implications of taking a much smaller value for N_d are considered.

The first implication of taking a small value for N_d is that f may equal 1, i.e. all the dislocation states are occupied, without the charge on the dislocation being sufficient to produce enough band bending to bring the dislocation level close to the Fermi level. In this situation the dislocation level will lie below the Fermi level and the

amount of band bending is given solely by N_d. The band bending is effectively independent of the position of the Fermi level and ϕ_o provided that the Fermi level is more than $\sim$KT above the dislocation level. As the temperature is increased the charge on the dislocation and hence the barrier height surrounding it will remain constant until the Fermi level moves within $\sim$KT of the dislocation level. Then as the temperature is increased further, f starts to decrease and the charge on the dislocation is reduced so that the barrier height changes as the position of the Fermi level changes. This situation can now be described in the usual way for a dislocation at equilibrium and recombination will be approximately described by the equations given earlier in this chapter pertaining to régime 3.

In considering recombination it is still valid to write:

$$J_e = C_e N_d \left(n_o \exp \frac{-q\phi}{KT} (1-f) - f N_c \exp \frac{-q\phi_o}{KT}\right)$$

for the net electron flux over the potential barrier, see section 7.3. And indeed at high beam currents the charge on the dislocation will be reduced so that, in régime 1, the occupation f will be much less than one and so the theory derived earlier will still apply. However, as the beam current, and hence J_e is reduced, the barrier height is increased and this is achieved by an increase in f. For sufficiently small beam currents $f \rightarrow 1$ and so the dislocation barrier height becomes constant and thus independent of beam current. This was termed régime 3 in section 7.3. It should be noted that it is this increase in f which now results in

constant ϕ and not that $J \ll J_{te}$ as was deduced earlier in the chapter for different assumptions. No information may now be gained about J_{te} from the observation of régime 3. This régime now has a different physical significance.

In section 7.3 it was shown that $C = A'' Q$ and that $Q = qfN_d$ thus the above model very simply predicts all the features experimentally observed in this work for the EBIC contrast of dislocations. Summarising: in régime 1 the behaviour is exactly the same as that described earlier. In régime 2, f is significant such that 1-f is no longer approximately 1. In régime 3 $f \simeq 1$, all the available dislocation states are occupied by electrons and the contrast is now independent of both beam current and temperature.

In section 7.4.1 it was calculated that Q, the dislocation line charge in régime 3 is $3.45 \pm 0.1 \times 10^{-13} Ccm^{-1}$ and $3.8 \pm 0.25 \times 10^{-13} Ccm^{-1}$ for the screw and 60° dislocation segments measured. Assuming f = 1 this gives $N_d = 2.16 \pm 0.06 \times 10^{6} cm^{-1}$ and $2.4 \pm 0.14 \times 10^{6} cm^{-1}$ for the screw and 60° dislocation respectively. It is the author's belief that the observation of constant contrast in régime 3 as the temperature is changed strongly suggests that N_d is small and that the behaviour of the dislocations studied is better described by the model presented in this section than by the one presented earlier in the chapter. However, for many dislocations, for example those introduced during device processing, the concentration of electrically active impurities and hence N_d may be sufficiently large that the treatment given earlier in the chapter will be more appropriate.

7.5.3 The Origin Of The Dislocation Levels Investigated

If recombination at dislocations is correctly described by the model proposed in the previous section then the experimental EBIC results may be used to deduce the following:

1. The dislocation level is further from the conduction band edge than 0.49eV for the screw and 0.52eV for the 60° dislocation.
2. $N_d \simeq 2.16 \times 10^6 cm^{-1}$ and $2.4 \times 10^6 cm^{-1}$ for the screw and 60° measured.
3. N_d is independent of temperature for the range 300K to 350K.
4. The $C_e N_d$ product is the same within experimental error for the screw and 60° dislocations measured.
5. From 2 and 4 above C_e is approximately the same for screw and 60° dislocations.

From 2 it is clear that dangling bonds are not responsible for the dislocation levels as their concentration would be of the order $3 \times 10^7 cm^{-1}$ or higher. Also from 2 it can be seen that the active level is not limited to the 30° partial or else N_d-screw would be twice N_d-sixty. From 3 it seems that the antiphase defects (solitons) postulated by Jones are unlikely to be the cause since their concentration is predicted to be temperature dependent (Heggie and Jones (1983)). Thus it would appear that the levels are due to impurities or point defects or to kinks along both partials of the dislocation line. The concentration of states N_d, seems rather high for kinks since measurements so far, Hirsch et al. (1981), seem to indicate a value of $N_d \sim 5 \times 10^4 cm^{-1}$ for a single 90° partial at 420°C in silicon (10^{12} Bcm^{-3}).

7.6 Discussion With Respect To Other EBIC Work

7.6.1 EBIC Work On Similar Specimens

This work represents the continuation of a similar EBIC project by Ourmazd and co-workers. The specimens used here are similar in doping and deformation to the ones used in the previous work and in a very few cases exactly the same specimen has been used. However, the equipment available for the early work was less sophisticated and so did not give results as reproducible as those in the present work. In view of the equipment used, Ourmazd and co-workers always stressed that the results obtained were preliminary. In one case markedly different results were obtained when changes were made to an earlier EBIC system. This is shown in Ourmazd et al. (1981) where the temperature dependence of contrast is totally different to that presented later by Ourmazd et al. (1983a) even though the work was performed on the same specimens. With hindsight it appears that contamination of the specimens whilst in the microscope may well have been the cause of the problem in the early work. Modifications to the system have not altered the general form of the EBIC contrast since the work published by Ourmazd et al. (1983a). The changes made in the system during the present work, finally resulting in the system described here, have however greatly improved the accuracy, reproducibility and the range of temperatures of the measurements made.

In the first experiments by Ourmazd and co-workers evidence was found for a dependence of the dislocation

contrast on the frequency at which the electron beam was chopped, see for example Ourmazd et al. (1981b). Here again it was stressed that the results were preliminary. The results of the present work, both theoretical and experimental, on exactly the same specimens and others similar, show no variation and it is thus likely that the effect measured was some artefact of the earlier system and that the results should now be discounted. The same factors apply to the measurements of the ratio of screw and 60° dislocation contrast presented in the same paper. These too were not repeated until the present work, for which the latest version of the EBIC system was used. Again different results were found from similar specimens.

The most recent paper which has been published on the samples used in this work, Ourmazd et al. (1983b) reports results obtained by the present author using a fairly sophisticated system but one still not as accurate as that described here. The results obtained are not presented in this work because the temperature range used is only 120K - 300K and the accuracy of the results is not as good. However, the results will be discussed briefly in relation to the present work.

The results were obtained from two pairs of screw and 60° dislocations which were each measured at one or more different places. In all eight separate C vs T curves were obtained each for a different segment of dislocation. It was only possible to measure the straight line parts of the C vs T curve and this gave a set of lines which when extrapolated are like those shown schematically in figure 7.7.

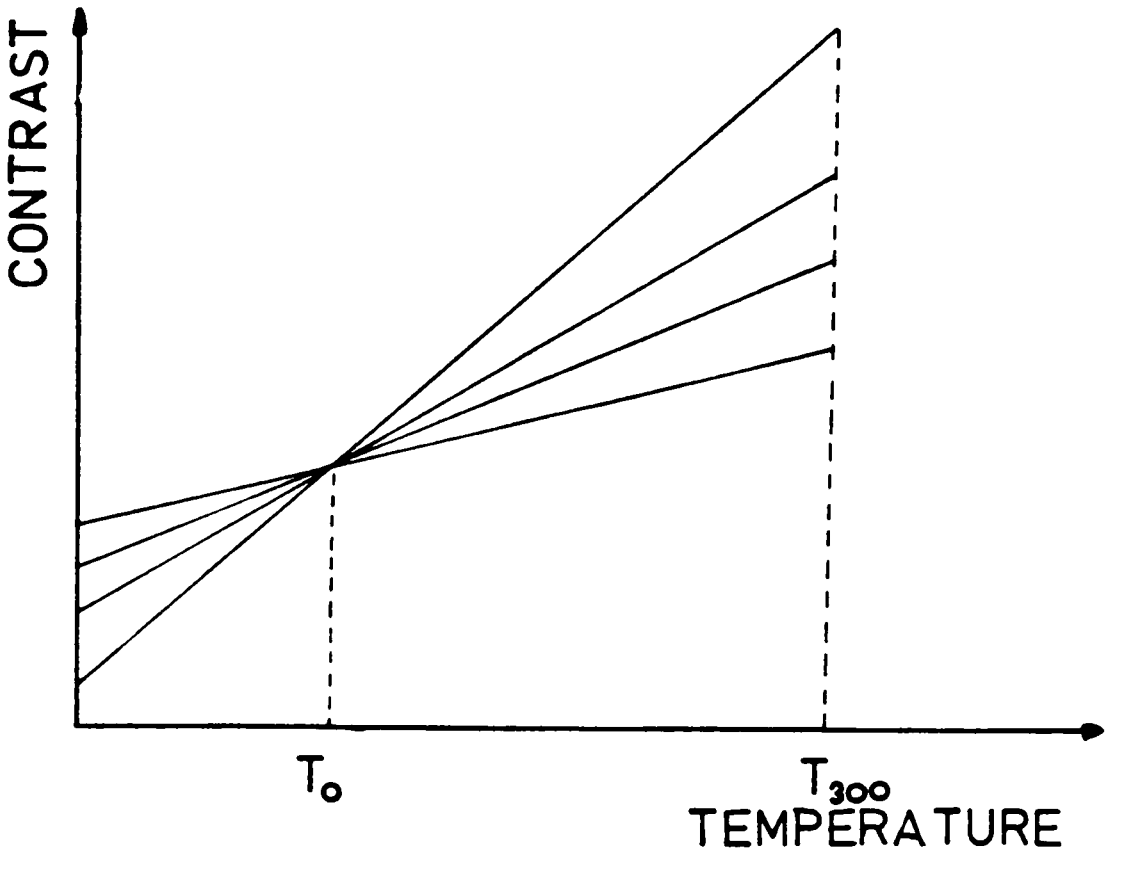


Figure 7.7 Schematic plot of C vs T curves presented by Ourmazd et al (1983b)

The equation for these lines is

$$C = \frac{(C_{300}-C_o)}{(T_{300}-T_o)} T-T_o + C_o \qquad [7.24]$$

On differentiating wrt T this gives the result that

$$\frac{dc}{dT} = \alpha C_{300} + \beta$$

where α and β are constants and C_{300} is the contrast measured at 300K. In relating these results to the present work it is noted that an almost identical set of curves has been obtained for two individual dislocation segments, figures

6.13 and 6.14. In this case the value of C_{300} is now known to be dependent upon the beam current used, i.e

$$C_{300} = A - B\ln(I_{beam}) \qquad [7.25]$$

where A and B are constants. Thus for this similar set of curves equation [7.23] becomes

$$C = \left(\frac{(A - B\ln(I_{beam})) - C_o}{T_{300} - T_o} \right)\left(T - T_o \right) + C_o$$

Leading to the result presented in section 7.5 that

$$\frac{dC}{d(\ln I_{beam})} = \delta T - \epsilon \qquad [7.26]$$

where δ and ϵ are constants.

Thus the earlier measurements performed on 8 different dislocation segments show exactly the same form as the measurements made on two different segments at a variety of beam currents. This implies that the physical significance of the two sets of curves may well be the same. The earlier set of data would have been produced if the values of A and the values of B in equation [7.25] had been the same for all 8 segments so that the changes in contrast at room temperature were due solely to the different beam currents used. The experimental set up would then have been exactly the same as for the dislocations studied in this work. Unfortunately it is not possible to check whether A and B were indeed the same since the beam current at which the measurements were performed was not measured accurately. This was because the dependence of contrast on beam current was not then

appreciated. It is however likely that the dislocation pairs were at the same depth and hence A and B the same (if random variations are discounted). This is because the dislocations were chosen to give maximum contrast and therefore would have been at the optimum depth for EBIC visibility. It thus seems likely that the effect discovered in the early work is the same as that described by [7.26] and explained in section 7.5. Thus no modification is needed to the 'standard' Donolato theory of EBIC contrast as it applies to ideal defects. That this might be necessary was originally suggested by Ourmazd et al. (1983b).

7.6.2 EBIC Work On Different Specimens

Most of the previous EBIC work on dislocations has been phenomenological and the observations made will not be commented on in great detail in relation to the present investigation. Just three specific points will be made.

1. Kittler and Seifert (see for example Kittler and Seifert (1981) and Kittler and Seifert (1983)) state that it is impossible to detect the EBIC contrast from a clean dislocation and use the EBIC contrast they measure as an indication of the impurity concentration at the dislocation. Whilst their dislocations, which are process induced, are indeed likely to be decorated the analysis they use to deduce this is flawed. They associate with a clean dislocation a maximum concentration of defect states equal to a maximum concentration of dangling bonds and with each of these states a minority carrier capture cross-section of $\sim 10^{-16} cm^2$, which

thus gives rise to an EBIC contrast below 0.5%, the detection limit. However, of the three sets of data they quote giving values of capture cross-sections, (Kittler and Seifert (1981)) two relate to the capture cross-section of electrons in n-type material and the other to holes in p-type material. In no case is the minority carrier cross-section at a charged defect given or used. Also as sections 7.3 and 7.4 show, minority carrier capture is determined by the charge on the dislocation and except at very small beam currents and large f, is only weakly dependent on N_d. Thus dislocations with very small concentrations of states, for example $\lesssim 3 \times 10^6 cm^{-1}$ as in this work, can give rise to a large contrast. The weak dependence on N_d is due to the fact that the value of N_d only directly affects the majority carrier capture over the potential barrier. N_d must be increased by a factor of ~ 50[1] at 300K to alter the barrier height ϕ (in régime 1) and hence the contrast of a dislocation by a factor of ~ 2 or 3. Thus a linear relation between N_d, the assumed concentration of impurities, and the contrast cannot be used for high beam currents where régime 1 applies. For much larger concentrations of impurities it is likely that if the contrast is measured at low beam currents where régime 3 applies N_d will be sufficiently large that the dislocation level is at or close to the Fermi level ($f \ll 1$). Under such conditions the dislocation contrast is totally independent of N_d and determined instead by ϕ_o for the impurities generating the defect level.

1 At a barrier height of 0.15eV.

2. In some EBIC work quantitative measurements of EBIC contrast from dislocations at p-n junctions are made (see for example Heydenreich et al. (1981)). Equation [7.10] shows that the EBIC contrast of dislocations is inversely proportional to the doping concentration for all beam currents and thus if this concentration changes with position relative to the junction, different values of contrast will be obtained at different positions. This effect will be found in addition to any geometrical effects predicted by Donolato's theory for dislocations and should be taken into account when comparing the contrast of different dislocations in such specimens.

3. Finally, it should be noted that in most cases beam currents of 10^{-10}A or larger, are used for EBIC contrast measurements of dislocations. In one instance 7.10^{-8}A was used for an EBIC measurement though not of a dislocation (Pasemann et al (1982)). It is thus likely that for most results in the literature recombination will be in régime 1 and thus the EBIC contrast measurements will give no information concerning ϕ_0.

7.7 Summary

1. In this chapter a new theory describing recombination at charged dislocations has been developed.

This theory correctly describes all observed aspects of the EBIC contrast of dislocations presented in chapter 6 for high beam currents and low temperatures. At high temperatures and low beam currents two different approximations are

considered. In the first $f \ll 1$ is assumed whilst in the second $f \simeq 1$ is used. The two different approximations yield different predictions for the temperature dependence of C for small beam currents and high temperatures. These are compared with the results obtained experimentally (see below).

The theory derived should be directly applicable to cathodoluminiscence experiments, where dislocations give dark contrast due to non-radiative recombination via the dislocation level, and act only as 'weak' recombination centres. With modification the theory might be applicable to photoconductivity measurements where recombination is the controlling factor.

The theory shows that for most experimental conditions recombination is determined by the height of the potential barrier surrounding the dislocation. This is independent of the position of the dislocation energy level ϕ and only weakly dependent on the density of defect states N_d.

The contrast of a dislocation is found to be inversely proportional to the doping concentration.

In deriving the theory a new insight is gained into recombination at dislocations. This together with experimental data is used to deduce that bound holes at a dislocation are stored at the dislocation level and that thermal emission of bound holes is not significant unless the excess hole concentration is of the same order as the equilibrium hole concentration in the valence band.

2. The experimental data presented in chapter 6 is analysed to deduce values for γ and minority and majority capture cross-sections per unit dislocation length.

A method is developed which allows each value of the measured contrast to be related to the dislocation barrier height ϕ. This allows $\phi_o > 0.49$eV and > 0.52eV at 350K and $N_d \gtrsim 2.16 \times 10^6 cm^{-1}$ and $\gtrsim 2.4 \times 10^6$ to be deduced for the screw and 60° dislocation respectively.

If the assumption $f \ll 1$ is used ϕ_o can be calculated exactly and is found to increase with increasing temperature. This seems unlikely and the observed behaviour can instead be simply explained by postulating $f \underset{\sim}{} 1$ for the dislocations studied when using low beam currents and high temperatures. This yields values for N_d of $2.16 \times 10^6 cm^{-1}$ and $2.4 \times 10^6 cm^{-1}$ for the screw and 60° dislocation. The theory then describes all observed EBIC results. It is the author's belief that this description is appropriate for the clean dislocations studied in this work but that the assumption that $f \ll 1$ and the resultant theory are more likely to be correct for heavily decorated dislocations.

3. The results presented indicate that neither dangling bonds nor solitons (APD's) are responsible for the observed dislocation level. And although kinks may be responsible it seems more likely that a low concentration ($\sim 2 \times 10^6 cm^{-1}$) of impurities or point defects at the dislocation generate the observed level.

4. A brief comparison with other EBIC work is made and points arising are discussed.

Chapter 8

Suggestions for Further Work and Concluding Remarks

Chapter 8 Suggestions for Further Work and Concluding Remarks

8.1 Suggestions for Further Work

In this thesis it has been shown how an EBIC system has been developed to obtain high accuracy measurements of the contrast of individual dislocations. Experiments have been performed and an analysis of the electrical characteristics of specimens deformed at 850°C and then 420°C has been made which allows the measured EBIC contrast to be directly related to the electrical activity of the dislocations themselves. The EBIC contrast of the straight screw and 60° dislocations in these specimens, which are considered to be the most nearly ideal dislocations available, have been studied as a function of various experimental parameters. A theory has been developed which describes recombination at dislocations and this has been applied to the experimental data to deduce certain characteristics of the electronic properties of the dislocations themselves.

Most of the above is new and original and so an obvious extension of the work is simply to perform the same experiments on;

i) specimens deformed at different temperatures

ii) p-type material and

iii) different semiconductors, so that the behaviour of the EBIC contrast can then be compared and possibly correlated to other electrical measurements.

One immediate improvement to the experimental technique would be to fabricate an array of smaller Schottky barriers ($0.2mm^2$ would be feasible) instead of the single large barrier $3mm^2$. Each barrier could then be connected separately within the SEM using a micro-manipulator. The reduction in area of the barrier so achieved would lead to a proportional reduction in noise generated by the specimen and so allow accurate EBIC contrast measurements to be performed at beam currents more than ten times smaller than those now possible. This would greatly extend the range over which régime 3 type EBIC recombination could be studied.

In the following it is intended to leave aside such general extensions of the techniques developed here and instead look more closely at the detailed nature of the results obtained from the one set of specimens studied (n-type 850°C/420°C) to see whether further experiments could extend the results presented in the previous chapters. The results obtained here generally fall into two categories. In the first are the measurements where régime 1 applies and for which the contrast is independent of the position of the dislocation energy level and only weakly dependent on the concentration of dislocation states. Many different dislocations have been studied and in most cases experiments have been performed on specimens deriving from ingots deformed at different times. In all aspects the observed behaviour has been reasonably consistent from specimen to specimen and from dislocation to dislocation. It is likely that such results are representative of the form of the EBIC contrast that would be obtained within this régime from straight screw and 60° dislocations generated by deformation at 850°C and 420°C.

Thus further experiments of this type on similar dislocations are unlikely to produce new results.

The second set of measurements are those made at small beam currents and high temperatures for which some aspects of the detailed properties of the dislocations structure become observable. It is perhaps one of the main results of this thesis that only under such conditions, which are very hard to obtain experimentally, is the effect of the detailed electronic structure of the dislocations studied here apparent. To deduce these detailed properties a complete set of contrast measurements at very many different temperatures and beam currents is required. In this work this has only been performed for two individual dislocation segments, one screw and one 60°. It is thus not clear whether the data gained from these two segments is representative of other screw and 60° dislocations present in the specimens. From the theory applied it appears that the equilibrium barrier height may be fixed by a low concentration of deep (0.5eV) states. If these states were due to impurities it might be expected that their concentration and hence the dislocation barrier height may change from region to region within the specimen, whereas if they are intrinsic to the dislocations themselves their concentration is more likely to be uniform. Thus it is the author's opinion that the first extension of this work should be to examine other similar dislocations at high temperatures and low beam currents to deduce the uniformity of the concentration of charged states at the dislocation band.

8.2 Concluding Remarks

From the results of two individual dislocation segments it is not possible to infer that all the dislocations in the specimens would behave in exactly the same way. However, it is unlikely that the two dislocations studied were "special" and so the general results, i.e. a deep, fully occupied state whose concentration determines the barrier height, will be assumed widely applicable to the straight dislocations in the specimens studied. In the following the findings of other experimental techniques are discussed in relation to the above description.

The first feature is that the dislocation level is very nearly full and should therefore contain few unpaired electrons and so generate only a very small EPR signal. This result is in good agreement with the experimental findings of Weber and Alexander (1983) who detect only a very small EPR signal from similar specimens.

The second point is that any other shallow energy levels present at the dislocation will be uncharged if the band bending ϕ, is sufficient to raise them above the Fermi level. Thus in this work for $\phi \simeq 0.2$eV and the Fermi level 0.25eV below the conduction band edge at 300K, any level shallower than 0.45eV would not be charged and thus would not affect the equilibrium barrier height. It is the barrier height that determines EBIC contrast and so these states would not be detected by EBIC at 300K. Thus the states E(0.19), E(0.29) and E($\sim$0.4) found by Weber and Alexander (1983) using DLTS would not be expected to be detected and no comment can be made as to whether they are located at straight dislocations. It is interesting to note that in transient

photoconductivity of specimens containing dislocations, the activation energy for photoconductivity decay is normally observed to change at about 250K. For example Mergel (1983) when investigating 10^{15} cm^{-3} n-type silicon, deformed along [213] at 800°C, obtains a value of 0.7eV above 250K and 0.15eV below. He deduces that above 250K the recombination is associated with a level 0.65eV below the conduction band edge and that at 250K the mechanism of recombination changes. However neither Mergel nor any other worker, to this author's knowledge, has presented details of why this might be the case. It is possible that the situation at the dislocations when the temperature is above 250K is as described above. That is to say there is a deep level which is almost full and which determines the amount of band bending and a shallow level which is empty because it lies above the Fermi level. As the temperature is reduced the Fermi level gets closer to the conduction band edge but the amount of band bending is unchanged, eventually the Fermi level reaches the shallower level (in this case at ~250K) which thus also becomes charged so changing the recombination mechanism. Because the level is shallower the recombination activation energy is reduced. Although such an explanation is very speculative it does seem to follow quite simply from the model outlined above.

The last point noted here in relation to the work of others is that the only DLTS measurements performed on similar specimens (Weber and Alexander(1983)) do not specifically detect any states deeper than 0.5eV. It was a deduction of this work that levels deeper than 0.5eV should be present.

As yet the author knows of no plausible explanation of this discrepancy between the EBIC and DLTS results.

Finally it is noted that the theory applied to these dislocations, which are thought to be clean and free from surrounding point defects would not apply to dislocations with a larger concentration of defect states, N_d. In this case the theory based on the approximation of a small occupation of the dislocation level as outlined in section 7.3 should be applied. For very large concentrations of recombination centres surrounding the dislocation over a region of ~1μm it is expected that the dislocation will cease to behave as a "weak" recombination centre according to the theory of Donolato. Under such circumstances the theory of recombination at "strong" defects due to Wight et al (1981) may be more applicable.

REFERENCES

A

Alexander H., Kisielowski-Kemmerich C., Weber E.R.; Physica 116 B, 583, (1983).

Anstis G.R., Hirsch P.B., Humphreys C.J., Ourmazd A.; Inst. Phys. Conf. Ser. 60, 15 (1981).

B

Baraff G.A., Kane E.O., Schluter M.; Phys. Rev. B 21, 5662 (1980).

Baumann F.H., Schroter W.; Phil. Mag. B 48, 55 (1983).

Blumtritt H., Gleichmann R., Heydenreich J., Johansen H.; Phys. Stat. Sol. (a) 55, 611 (1979).

Bourret A., Desseaux-Thibault J., Lancon F.; J. Physique 44, C4-15 (1983).

Boyes E.D., Dixon-Brown G., Ourmazd A.; Inst. Phys. Conf. Ser. 61, 517 (1981).

Breitenstein O., Heydenreich J.; J. Physique 44, C4-207 (1983).

C

Castaldini A., Cavallini A., Gondi P.; J. Physique 44, C4-305 (1983).

Chang C.Y., Sze S.M.; Solid State Electron. 13, 727 (1970).

Claesson J.; J. Physique 40, C6-41 (1979).

Cockayne D.J.H., Ray I.L.F., Whelan H.J.; Phil. Mag. 20, 1265 (1969).

Cohn A., Caledonia G.; J. Appl. Phys. 41, 3767 (1970).

D

Donolato C.; Optik 52, 19 (1978).

Donolato C., Venturi P., Tkachev V.D.; Sov. Phys. JETP Lett. 23, 597 (1976).

Drozdov N.A., Patrin A.A., Tkachev V.D.; Sov. Phys. JETP Lett. 23, 597 (1976).

E

Everhart T.E., Hoff P.H.; J. Appl. Phys. 42, 5837 (1971).

F

Figielski T.; Solid State Electron. 21, 1403 (1978).

Fraser D.A.; The Physics of Semiconductor Devices, 2nd Ed., O.U.P. (1979).

Fuyuki T., Matsunami H., Tanaka T.; J. Phys. D. 13, 1093 (1980).

Fuyuki T., Matsunami H.; Jap. J. Appl. Phys. 20, 745 (1981).

G

Gibb R.M., Rees G.J., Thomas B.W., Wilson B.L.H., Hamilton B., Wight D.R., Mott., N.F.; Phil. Mag. 36, 1021 (1977).

Gomez A., Cockayne D.J.H., Hirsch P.B., Vitek V.; Phil. Mag. 31, 105 (1975).

Gottschalk H.; J. Physique 40, C6-127 (1979).

Gottschalk H.; J. Physique 44, C4-69 (1983).

Grazhulis V.A., Kveder V.V., Osipyan Y.A.; Phys. Stat. Sol. (b) 103, 519 (1981).

H

Heggie M.I., Jones R.; J. Physique 44, C4-43 (1983).

Heydenreich J., Blumtritt H., Gleichmann R., Johansen H.; Scanning Electron Microscopy 1981, 1, 351 (SEM.Inc.AMF O'Hare, Ill.).

Hirsch P.B.; J. Physique 40, C6-27 (1979).

Hirsch P.B.; J. Mocrosc. 118, 3 (1980).

Hornstra J.; J. Phys. Chem. Solids 5, 129 (1958).

Hutchinson J.L.; J. Physique 44, C4-3 (1983).

J

Jacoboni C., Canali C., Ottaviani G., Quaranta A.A.; Solid State Electron. 20, 77 (1977).

Jones R.; J. Physique 40, C6-33 (1979).

Jones R.; Inst. Phys. Conf. Ser. 60, 45 (1981).

Jones R.; J. Physique 44, C4-61 (1983).

K

Keating P.N.; Phys. Rev. 145, 637 (1966).

Kimmerling L.C., Leamy H.J., Patel J.R.; Appl. Phys. Lett. 30, 217 (1977).

Kimmerling L.C., Patel J.R.; Appl. Phys. Lett. 34, 73 (1978).

Kimmerling L.C., Patel J.R., Benton J.L., Freeland P.E.; Inst. Phys. Conf. Ser. 59, 401 (1981).

Kimmerling L.C.; Physica 116 B, 1 (1983).

Kittler M., Seifert W.; Phys. Stat. Sol. (a) 66, 573 (1981).

Kittler M., Seifert W., Bugeil E., Richter H.; J. Physique 44, C4-437 (1983).

Klein C.A.; J. Appl. Phys. 39, 2029 (1968).

Kveder V.V., Ossipyan Y.A., Schröter W., Zoth G.; Phys. Stat. Sol. (a) 72, 701 (1982).

L

Labusch R.; J. Physique 40, C6-81 (1979).

Labusch R.; Physica 117b, 203 (1983).

Lapiccirella A., Lodge K.W.; Inst. Phys. Conf. Ser. 60, 51 (1981).

Leamy H.J.; J. Appl. Phys. 53, R51 (1982).

Lifson S., Warshel A; J. Chem. Phys. 49, 5116 (1968).

Lodge K.W., Altmann S.L., Lapiccirella A., Tomassini N.; Phil. Mag. B 49, 41 (1984).

Louchet F., George A.; J. Physique 44, C4-51 (1983).

M

Makosa A.; Cryst. Res. Techn. 16, 225 (1981).

Marcus R.B., Robinson M., Sheng T.T., Haszko S.E., Muraka S.P., Katz L.E.; J. Electrochem. Soc. 124, 425 (1977).

Marklund S.; Phys. Stat. Sol. (b) 92, 83 (1979).

Marklund S.; J. Physique 44, C4-25 (1983).

Menninger H., Raidt H., Gleichmann R.; Phys. Stat. Sol. (a) 58, 173 (1980).

Mergel D., Labusch R.; Phys. Stat. Sol. (a) 69, 151 (1982).

Mergel D.; Phys. Stat. Sol. (a) 75, 255 (1983).

Miller G.L., Lang D.V., Kimmerling L.C.; Ann. Rev. Mater. Sci. 1977, 377.

Mimkes J.; J. Physique 40, C6-181 (1979).

O

Olsen A., Spence J.C.H.; Phil. Mag. A 43, 945 (1981).

Ossipyan Y.A.; Cryst. Res. Techn. 16, 239 (1981).

Ourmazd A., Darby D.B., Booker G.R.; Inst. Phys. Conf. Ser. 36, 251 (1977).

Ourmazd A., Booker G.R.; Phys. Stat. Sol (a) 55, 771 (1979).

Ourmazd A.; Cryst. Res. Techn. 16, 137 (1981).

Ourmazd A., Weber E., Gottschalk H., Booker G.R., Alexander H.; Inst. Phys. Conf. Ser. 60, 63 (1981a).

Ourmazd A., Wilshaw P.R., Cripps R.M.; Inst. Phys. Conf. Ser. 61, 519 (1981b).

Ourmazd A., Wilshaw P.R., Booker G.R.; Physica 116B, 600 (1983a).

Ourmazd A., Wilshaw P.R., Booker G.R.; J. Physique 44, C4-289 (1983b).

P

Pasemann L.; Ultramicroscopy 6, 649 (1981).

Pasemann L.; Blumtritt H., Gleichmann R.; Phys. Stat. Sol. (a) 70, 197 (1982).

Patel J.R., Kimmerling L.C.; Cryst. Res. Techn. 16, 197 (1981).

Pearton S.J., Tavendale A.J.; Appl. Phys. Lett. 41, 1148 (1982).

Petroff P.M., Lang D.V.; Appl. Phys. Lett. 31, 60 (1977).

Pfann W.G., van Roosbroek W.; J. Appl Phys. 25, 1422 (1954).

Pohoryles B.; Phys. Stat. Sol. (a) 67, 75 (1981).

R

Read W.T.; Phil. Mag. 45, 775 (1954).

Riotte H.G., Herpers U., Weber E.; Radiochem. Radioanal. Lett. 30 (4), 311 (1977).

S

Schröter W., Labusch R.; Phys. Stat. Sol. 36, 359 (1969).

Schröter W., Scheibe E., Schoen H.; J. Microsc. 118, 23 (1980).

Schimizu R., Murata K.; J. Appl. Phys. 42, 387 (1971).

Shockley W.; Phys. Rev. 91, 228 (1953).

Sieber B., Dupuy M.; J. Physique 44, C4-297 (1983).

Sokolova E.B.; Sov. Phys. Semiconductors 3, 1266 (1970).

Suezawa M., Sumino K., Iwaizumi M.; Inst. Phys. Conf. Ser. 59, 407 (1981).

Suezawa M., Sumino K.; J. Physique 44, C4-133 (1983).

Sze S.M.; Physics of Semiconductor Devices 2nd Ed., Wiley (1981).

T

Teichler H., Veth H.; J. Physique 44, C4-93 (1983).

Thornton P.R.; Scanning Electron Microscopy, Chapman and Hall Ltd., London (1968).

Tóth A.L.; Inst. Phys. Conf. Ser. 60, 221 (1981).

V

Veth H., Teichler H.; Phil. Mag. B 49, 371 (1984).

W

Weber E., Alexander H.; J. Physique 40, C6-101 (1979).

Weber E.R., Alexander H.; J. Physique 44, C4-319 (1983).

Wessel K., Alexander H.; Phil. Mag., 35, 1523 (1977).

Wight D.R., Blenkinsop I.D., Harding W., Hamilton B.; Phys. Rev. B. 23, 5495 (1981).

Wilshaw P.R., Ourmazd A., Booker G.R.; J. Physique 44, C4-445 (1983).

Winter S.; Phys. Stat. Sol. (b) 85, 95 (1978).

Wu C.J., Wittry D.B.; J. Appl. Phys. 49 (5), 2827 (1978).